Aristotle University of Thessaloniki
Faculty of Sciences
School of Informatics

Mathematical Analysis of Interactions between a Layered Medium and a Distribution of Point Sources

A dissertation submitted in partial fulfillment of the requirements for the degree of Doctor of Philosophy

By

Andreas Kalogeropoulos

Thessaloniki, June 2022

Aristotle University of Thessaloniki
Faculty of Sciences
School of Informatics

Mathematical Analysis of Interactions between a Layered Medium and a Distribution of Point Sources

By

Andreas Kalogeropoulos

Members of the Committee

Nikolaos L. Tsitsas (Supervisor), Associate Professor, School of Informatics, Aristotle University of Thessaloniki

Eleftherios Angelis, Professor, School of Informatics, Aristotle University of Thessaloniki

Foteini Kariotou, Assistant Professor, School of Technology and Science, Hellenic Open University

Nikolaos Konofaos, Professor, School of Informatics, Aristotle University of Thessaloniki

Drossos Gintides, Professor, School of Applied Mathematical and Physical Sciences, National Technical University of Athens

Nikolaos Karachalios, Professor, Department of Mathematics, University of Thessaly

Antonios Charalambopoulos, Professor, School of Applied Mathematical and Physical Sciences, National Technical University of Athens

The realization of the doctoral thesis was co-financed by Greece and the European Union (European Social Fund) through the Operational Program "Human Resource Development, Education and Lifelong Learning", 2014-2020, in the context of the Action "Strengthening human resources through the implementation of Ph.D. Research Sub-Action 2: IKY Scholarship Program for Ph.D. Candidates at Greek Universities

Publications

Journals

[J1] A. Kalogeropoulos and N. L. Tsitsas, "Excitation of a Layered Medium by N Sources: Scattering relations, Interaction Cross Sections and Physical Bounds," *Quarterly of Applied Mathematics*, vol. 79, no. 2, pp. 335-356, 2020.
[J2] A. Kalogeropoulos and N. L. Tsitsas, "Analysis of Interaction Scattering Cross Sections and their Physical Bounds for Multiple-Dipole Stimulation of a Three-Dimensional Layered Medium," *IEEE Open Journal of Antennas and Propagation*, vol. 2, pp. 506-520, 2021.
[J3] A. Kalogeropoulos and N. L. Tsitsas, "Electromagnetic interactions of dipole distributions with a stratified medium: power fluxes and scattering cross sections", *Studies in Applied Mathematics*, vol. 140, no. 3, pp.1040-1068, 2022.
[J4] A. Kalogeropoulos and N. L. Tsitsas, "Inverse Problems Pertaining to a Layered Sphere Excited by N Point Sources", *submitted*, 2022.

Conferences

[C1] A. Kalogeropoulos and N. L. Tsitsas, "Excitation of a Layered Medium by N Internal Point Sources", *Proceedings of the 14th International Conference on Numerical and Mathematical Aspects of Wave Propagation - WAVES 2019*, pp. 424-425, 2019.
[C2] A. Kalogeropoulos and N. L. Tsitsas, "Excitation of a Layered Medium by N magnetic dipoles", *14th European Conference on Antennas and Propagation - EuCAP 2020*, pp. 4, 2020.

[C3] A. Kalogeropoulos and N. L. Tsitsas, "Excitation of a Layered Sphere by Multiple Point-generated Primary Fields", *XVII General Assembly and Scientific Symposium of the Internation Union of Radio Science - URSI-GASS 2020*, 2020.
[C4] A. Kalogeropoulos and N. L. Tsitsas, "Stimulation of a Layered Medium by N dipoles", *XVIII General Assembly and Scientific Symposium of the Internation Union of Radio Science - URSI-GASS 2021*, 2021.
[C5] A. Kalogeropoulos and N. L. Tsitsas, "Electromagnetic stimulation by a group of dipoles enclosed in a stratified sphere", *Bremen Workshop on Light Scattering 2022*, pp. 33–36, 2022.

Abstract

The problem of exciting a layered medium with an arbitrary distribution of (acoustic) point sources or (electric/magnetic) dipoles is considered in this dissertation. A mathematical formulation based on the topology of the distribution of the sources/dipoles and their number is employed.

The energy transfer process is investigated by adopting the complex form of the energy functionals. Energy Conservation Laws that relate the real part of the power flux with the corresponding scattering cross sections and the imaginary part of the power flux with the Lagrangian density in the propagating medium are derived.

The notions of Interaction Scattering Cross Sections (ISCS) and Interaction Power Fluxes (IPF) that quantify the effects of interaction between point sources/dipoles are developed and relevant optical theorems are established. Physical bounds for the ISCS ratios, the number of point sources/dipoles and the number of excitation layers are derived as well.

The exact solution of the direct problem in spherical geometry is determined by devising an overall superposition method that combines the T-Matrix, Sommerfeld's and Green's Functions methods. In particular, by formulating the superposition of the individual fields into an overall field, exact expressions for the coefficients of the scattered fields are obtained. An extensive parametric numerical analysis for the behaviour of the energy functionals and the ISCS ratios is presented.

Finally, the behaviour of the involved fields is further investigated in the so-called low frequency zone by utilizing tools of asymptotic analysis. Several inverse problems concerning the number of sources/dipoles, the physical parameters of the scatterer and/or its geometrical characteristics

are formulated and solved analytically for the spherical geometry.

Keywords: Scattering, Acoustics, Electromagnetics, Cross Sections, Energy Conservation, Inverse Problems, Interactions, Layered Medium, Dipoles, Point Sources, Spherical Waves, Partial Differential Equations

Περίληψη

Το πρόβλημα διέγερσης ενός πολυστρωματικού μέσου από μια αυθαίρετη κατανομή (ακουστικών) σημειακών πηγών ή (ηλεκτρικών / μαγνητικών) διπόλων αποτελεί το βασικό αντικείμενο αυτής της διατριβής. Το προτεινόμενο μαθηματικό μοντέλο βασίστηκε στην τοπολογία της κατανομής των πηγών καθώς και στο πλήθος τους. Συγκεκριμένα, τα εμπλεκόμενα πεδία ομαδοποιήθηκαν με βάση το στρώμα του σκεδαστή στο οποίο βρίσκονται οι πηγές/δίπολα στα οποία οφείλονται (q-διεγειρόμενα πεδία) και χαρακτηρίστηκαν ως μεμονωμένα πεδία, q-μερικά πεδία ή καθολικά πεδία ανάλογα με το αν οφείλονται σε διέγερση από μία πηγή/δίπολο, από ορισμένες πηγές ή από όλες τις πηγές που διεγείρουν τον σκεδαστή. Τα στρώματα του σκεδαστή χωρίστηκαν με βάση το αν περιέχουν πηγές/δίπολα (διεγείροντα στρώματα) ή όχι (μη διεγείροντα στρώματα).

Υιοθετόντας μια προσέγγιση όπου τα ενεργειακά συναρτησοειδή και τα ενεργειακά διανύσματα ροής θεωρήθηκαν μιγαδικές συναρτήσεις, μελετήθηκε η διαδικασία μεταφοράς ενέργειας, από τα διεγείροντα στρώματα του σκεδαστή, στο εξωτερικό του έως και την ζώνη μακρινού πεδίου. Μέσω αυτής της προσέγγισης, αποδείχθηκαν Νόμοι Διατήρησης της Ενέργειας, οι οποίοι συνδέουν ευθέως την καθολική διατομή σκέδασης με την ενεργό ροή (πραγματικό μέρος των διανυσμάτων ροής) στο εσωτερικό των διεγειρόντων στρωμάτων. Επιπλέον, η Λαγκραντζιανή πυκνότητα στο μέσο διάδοσης (εξωτερικό) και τον σκεδαστή συνδέθηκε άμεσα με την άεργο ισχύ (φανταστικό μέρος των διανυσμάτων ροής) στα διεγείροντα στρώματα.

Η εισαγωγή των εννοιών των Διατομών Αλληλεπίδρασης και των Ροών Αλληλεπίδρασης, βοήθησε στην ποσοτικοποίηση της ενέργειας και της ροής που οφείλεται στην αλληλεπίδραση μεταξύ των εμπλεκόμενων μεμονωμένων

πεδίων. Συγκεκριμένα, αποδείχθηκαν οπτικά θεωρήματα που συνδέουν τις Διατομές Αλληλεπίδρασης με τα q-μερικά πεδία, ενώ αποδείχθηκε ότι τα εν λόγω θεωρήματα, αποτελούν γενίκευση του Γενικού Θεωρήματος Σκέδασης. Με χρήση κατάλληλων τεχνικών Συναρτησιακής Ανάλυσης, αποδείχθηκαν φυσικά φράγματα για το ποσοστό των Διατομών Αλληλεπίδρασης επί της καθολικής διατομής σκέδασης και για το πλήθος των πηγών που διεγείρουν τον σκεδαστή και των διεγειρόντων στρωμάτων του σκεδαστή. Μέσω ανάλυσης των εμπλεκόμενων διανυσμάτων ροής, συσχετίστηκαν οι Ροές Αλληλεπίδρασης με τις Διατομές Αλληλεπίδρασης και τα q-μερικά πεδία.

Η ακριβής, αναλυτική λύση του ευθέος προβλήματος σκέδασης για την σφαιρική γεωμετρία επιτυγχάνεται μέσω μιας μεθόδου καθολικής υπέρθεσης, η οποία συνδυάζει στοιχεία από την μέθοδο Sommerfeld, την T-Matrix μέθοδο και μεθόδους των Συναρτήσεων Green. Συγκεκριμένα, με την εισαγωγή τελεστών διέγερσης και συναρτήσεων παρατήρησης, η υπέρθεση των μεμονωμένων πεδίων ομαδοποιείται σε ένα καθολικό πεδίο του οποίου το ανάπτυγμα περιέχει τους ζητούμενους συντελεστές σκέδασης. Μέσω της T-Matrix μεθόδου, οι συντελεστές του καθολικού πεδίου σε κάθε στρώμα του σκεδαστή εκφράζονται συναρτήσει των συντελεστών του καθολικού πεδίου στο εξωτερικό του σκεδαστή και οι οποίοι με τη σειρά τους, ευρίσκονται με την βοήθεια των τελεστών διέγερσης. Οι συντελεστές των μεμονωμένων πεδίων, βρίσκονται (χωρίς επανάληψη της αλγοριθμικής διαδικασίας) μέσω κατάλληλης αντικατάστασης.

Μέσω κατάλληλης υλοποίησης σε προγραμματιστικό περιβάλλον της ακριβούς λύσης του ευθέος προβλήματος για τη σφαιρική γεωμετρία διενεργείται εκτενής παραμετρική ανάλυση που εξετάζει την συμπεριφορά των ενεργειακών ποσοτήτων (διατομές σκέδασης και διατομές αλληλεπίδρασης) σε σύγκριση με τις μεταβολές των γεωμετρικών χαρακτηριστικών των σκεδαστών, των φυσικών τους παραμέτρων καθώς του πλήθους ή/και της τοπολογίας των πηγών/διπόλων που διεγείρουν τον σκεδαστή.

Τέλος, η συμπεριφορά των εμπλεκόμενων πεδίων ερευνάται περαιτέρω στη λεγόμενη ζώνη χαμηλών συχνοτήτων. Με χρήση εργαλείων και τεχνικών Ασυμπτωτικής Ανάλυσης, η μορφή των τύπων για αυτήν την κατηγορία προβλημάτων απλοποιείται και μια πληθώρα αντιστρόφων προβλημάτων διατυπώνε-

ται και επιλύεται αναλυτικά. Τα αντίστροφα προβλήματα αφορούν - μεταξύ άλλων - τον εντοπισμό πηγών / διπόλων που διεγείρουν τον σκεδαστή, την εύρεση των φυσικών παραμέτρων του σκεδαστή, ενώ ερευνώνται και μικτά προβλήματα, όπως π.χ. η εύρεση των φυσικών παραμέτρων μιας σφαίρας που περιέχει πηγή/δίπολο σε άγνωστη θέση στο εσωτερικό της.

Λέξεις κλειδιά: Σκέδαση, Ακουστική, Ηλεκτρομαγνητισμός, Διατομές Σκέδασης, Διατήρηση της Ενέργειας, Αντίστροφα Προβλήματα, Αλληλεπιδράσεις, Πολυστρωματικό Μέσο, Δίπολα, Σημειακές Πηγές, Σφαιρικά Κύματα, Μερικές Διαφορικές Εξισώσεις

Dedication

To my wife Georgia, to our kids Giorgos and Dimitris and to my father Giorgos who inculcated me the love for science.

Acknowledgements

I express my deep and sincere gratitude to my supervisor Nikolaos L. Tsitsas for his enduring, caring and illuminating support and the opportunities he gracefully provided me, all the years of our collaboration. My everlasting thanks to Foteini Kariotou for the great, discrete and decisive impact her presence had in my academic course. And finally, to my mother Vicki for her endless belief in my abilities.

This labour was accomplished through running. Running, and running again, and running only. So the Hind ran, faster than the hunters' arrows. Hercules ran after her. He kept running, tirelessly, like no man had run before. So should run those who wish to tell the tale. And so should run—and even more so—those who desire to hear it. Fortunately, running is done step by step. Even the fastest, the as-swift-as-lightning run, or the longest, never-ending run, is done, too, step by step. And so, step by step, shall Hercules run after the Hind of Ceryneia. And step by step he shall find the way to capture her.

Maria Aggelidou, The Labours of Hercules, Vol. I
translated by Nefelie Kalogeropoulou.

Contents

Introduction

The propagation and scattering of waves has been one of the most fundamental scientific fields, even from the early years of science. The elastic-wave behaviour was studied both theoretically and analytically by many famous scientists, even from the 19-th century. Well-known and still used today is the volume-integral formulation devised and analyzed by G. Mie in his famous paper [1]. However, Mie was not the first to derive a mathematical formulation suitable for the study of waves, [2]. In particular, many years before him, Clebsch had developed an analytical method for computing the exact solution for elastic-wave scattering by a sphere in [3], while the famous Maxwell's electromagnetic theory had been already published [4]. Nicholson addressed in a series of papers the physical and mathematical aspects of propagation and scattering waves in spherical geometry, [5], [6], [7], while other scientists like Debye [8], Watson [9], [10] and Walker [11] provided a rigorous mathematical framework for addressing scattering and diffraction problems. Furthermore, wave propagation and scattering, were the major subjects of Lord Rayleigh's scientific work, [12], [13], [14], where he studied specific physical problems like Rayleigh scattering and thoroughly investigated the use of Bessel functions in the mathematical formulation of wave problems. Ludvig Lorenz - not to be confused with Hendrik Lorentz - was also a pioneer of electromagnetics and dedicated most of his scientific work in propagation and scattering of waves, [15], [16], [17]. Finally, one cannot talk about the history of waves without mentioning the work of Heaviside and Green. Both scientists, in their efforts to deepen the study of mathematical physics, created scientific tools and concepts like Green's theorem and the use of potentials [18], [19], [20]

or invented new operators (curl, divergence) [21], [22], [23] that acquired global importance over the years. Furthermore, the necessity of using such tools in wave-related problems advocated and promoted the use of vector calculus in other fields of science. In more recent years, technological advances and the need for even deeper understanding of wave phenomena has motivated scientists [24], [25], [26] to re-invigorate the interest for analytical and numerical solutions of scattering problems.

In modern-day real-world applications, the presence of more than one sources that excite a scatterer is quite custom. In such a case, greater complexity of both the direct and inverse scattering problem occurs, especially when inhomogeneous media are involved. In the literature, boundary-value problems concerning the excitation of a layered medium by N sources, are motivated by important scattering and radiation applications that occur in diversity and abundance for both acoustic and electromagnetic waves. Such applications include the stimulation of the brain by the neurons currents [27], [28], optical diffusion [29], antenna-type scatterers radiating in a layered background [30], microstrip antennas [31], radiation by multiple antennas in inhomogeneous backgrounds [32], and techniques for cancer treatment [33].

Besides, techniques for inverse scattering problems, like field-splitting decompositions [34], reconstruction of obstacles buried in layered media [35], beamforming techniques for source localization [36], [37], microphone array methods [38], [39] and axial fans' measurements in aeroacoustics [40] often rely on the corresponding direct problems that involve excitation by a number of sources. We note that inverse schemes for the identification of individual fields on spherically-symmetric conductors are investigated in [41], issues regarding the inverse magneto-electro-encephalography (MEG) problem are addressed in [42], while point source decomposition is used for inverse schemes in [43].

When more than one radiation sources emit waves in the same volume, the various primary and secondary (scattered) generated fields interact, evidently, with each other. In the excitation of a three-dimensional, bounded, layered scatterer by a distribution of sources that generate spherical waves

(like a dipole distribution in electromagnetics or a point source distribution in acoustics), these interactions lead to the generation of interaction-induced flux, [44], [45]. This fact is demonstrated by the "extra" power flux that is present but can not be attributed to any specific field, [46].

In this dissertation, we investigate the excitation problem of a layered medium by an arbitrary number N of sources generating spherical waves. The sources are arbitrarily distributed inside or outside the medium, for both acoustic and electromagnetic waves. A layered medium is the type of scatterer that consists of an arbitrary number P of homogeneous, disjoint domains that are called *layers*. The innermost layer is called *core* while the domain in which the entire medium lies, is called *exterior*. Due to physical limitations, the layers preceding the core, usually satisfy the *transmission boundary conditions* and they are called *penetrable* (acoustic fields) or *dielectric* (electromagnetic fields), while the core can satisfy a wider range of boundary conditions. For $P = 1$, we have the simpler, yet quite common case of a *homogeneous scatterer*.

We note that for electromagnetic waves, we address the case where the dipole distribution consists of either electric dipoles only or magnetic dipoles only. This is due to the fact that, when a magnetic dipole radiates at close proximity with an electric dipole, the radiation pattern is highly assymetric and thus, not uniform propagation is present, see [47]. To address the complexity of these interactions, we adopted a formulation where we grouped the participating fields with respect to their locations (q-excitation fields), their type (primary, secondary, total) and their multitude (individual, overall). In a similar manner, we define also the corresponding power fluxes and energy functionals. We divided our investigation in two parts: Part I concerns our findings for acoustic waves, while Part II for electromagnetic waves.

By utilizing the above-mentioned formulation, in the first section of each part (sections 1 and 4) we investigated the *energy transfer process* that describes the way the power flux "travels" from the source of radiation, through the scatterer's layers to the far-field zone. In particular, we extracted energy conservation laws for both acoustic and electromagnetic

waves and proved several scattering relations, like the optical theorem. To extract these laws we introduced *interaction scattering cross sections* (ISCS) and *interaction power fluxes* (IPF) that quantify the power flux produced by the interaction between participating fields and we adopted the complex-quantity approach for the energy functionals which enables the connection between the IPF with the *Lagrangian density*, [48], [49]. We note that the complex form of the Poynting vector is not something entirely new in electromagnetics, since it is usually related to the *reactive power*, [50]. In acoustics however, despite some preliminary efforts to utilize the complex form of the energy functionals, [51], [52], its potential use in measurement techniques [53] and its physical relation with *reactive intensity* [54], [55] came into light in recent years.

Scattering relations for point-generated spherical acoustic and electromagnetic waves were investigated in [56], [57], for a homogeneous scatterer excited by external sources and in [58], [59] for a layered obstacle excited by internal sources. Volume-integral formulations were also discussed for layered particles in [60], while generalizations of the optical theorem for multipoles have been investigated in [61]. Physical bounds for the bistatic-radar *scattering cross section* (SCS) were presented in [62], while physical bounds for the ISCS were presented in [63] for electromagnetic waves and in [64] for acoustic waves.

For the solution of the direct scattering problem in the spherical geometry, several techniques have been developed over the years and the issue has been addressed in different analytical and numerical ways depending on the specifics of each problem, [65], [66], [67], [68], [69], [70], [71], including problems that involve coated objects [72], [73], [74]. We note that the spherical geometry has evolved into a "powerhouse" for several physical problems, where implementing analytical procedures leads to bench-marking conclusions with the ability to be modified easily for more complicated geometries. The sphere has been used as a realistic model in many applications such as the the ultrasonic spectrometry for particle sizing [75], the shear-acoustic interactions for systems of particles [76] and the excitation of a spherical shell immersed in an acoustic waveguide [77].

In this dissertation, we chose a method that is based on the decomposition of the Green's Function and is combined with the Sommerfeld's method and the T-Matrix approach. This method is developed in section 2 (acoustics) and section 5 (electromagnetics). The novelty of our proposed method is the use of *excitation operators* and *observation functions* that allow the grouping of the unknown coefficients in a simplified form and allow the extraction of the individual fields without additional calculations or re-runs of the same computational algorithm. The behaviour of the various energy quantities and the physical bounds of ISCS, is thoroughly analyzed for the spherical geometry. In particular, subsections 2.4 (acoustics) and 5.4 (electromagnetics) contain an extensive parametric analysis for the spherical geometry. This analysis, addresses various aspects of the scattering phenomena like the variations of the ISCS ratios to the overall SCS, the behaviour of the values of ISCS and SCS for different core sizes and/or varying distributions. Additionally, the form of the point source/dipole distribution affects the behaviour of the involved quantities was examined for all possible types of excitation: *external excitation* where all sources lie in the exterior of the scatterer, *internal excitation* where all sources lie in the interior of a scatterer's shell and *mixed excitation* where the sources lie in both the exterior and the interior of the scatterer.

In the final section of each part (section 3 - acoustics and section 6 - electromagnetics), we address a set of inverse problems, with our main focus being the so-called *low-frequency zone*, i.e. $k_0 a_1 << 1$. Utilizing techniques of asymptotic analysis, we are able to construct simple approximations of the exact fields, with high accuracy in the low-frequency zone. Furthermore, these approximations in many occasions remain accurate even as we deviate from the low-frequency zone. Utilizing the above mentioned approximations, we formulate and solve a set of inverse problems: identification of the number of sources exciting a scatterer, which has been proved a significant difficulty in beamforming techniques [78], analytical source localization schemes for the case where 2 and 3 sources excite the sphere, extraction of the geometrical characteristics of the sphere and determination of its physical parameters, and finally some combined problems, e.g.,

the problem of a sphere with unknown physical parameters and geometrical characteristics emitting a wave from an unknown source located in its interior.

Part I:
Acoustic Waves

Chapter 1

Energy Transfer Process

1.1 Mathematical Formulation of the Excitation Problem due to N Point Sources

The layered scatterer V is identified as a bounded and closed subset of $\mathbb{R}^3$ with $\mathcal{C}^2$ boundary S_1, whose interior is divided by $P-1$ $\mathcal{C}^2$ surfaces S_p ($p = 2, \ldots, P$) into P nested, annuli-like layers V_p ($p = 1, \ldots, P$), see Fig. 4.1. Each surface S_{p+1} is enclosed by the surface S_p, with $\mathrm{dist}(S_p, S_{p+1})>0$, and is oriented by the outward normal unit vector $\hat{\mathbf{n}}$. The scatterer's layers V_p, for $p = 1, \ldots, P-1$, are homogeneous and isotropic and are characterized by real wavenumbers k_p, mean compressibilities γ_p, and mass densities ρ_p. The scatterer's core V_P can be soft, hard, resistive or penetrable with wavenumber k_P, mean compressibility γ_P, and mass density ρ_P. The exterior V_0 of V has wavenumber k_0, mean compressibility γ_0, and mass density ρ_0.

A distribution of N point sources - which can be internal or external - excite the scatterer V. Each point source is located at $\mathbf{r}^i$. These sources, are distributed inside Q *excitation layers* V_q^{ex}, with $q = 1, \ldots, Q$ and $Q \leq P+1$. In the case where the exterior V_0 of the scatterer contains sources, then V_1^{ex} coincides with V_0. If no sources are contained in V_0, then V_1^{ex} is the outermost layer containing sources. Excitation layer V_q^{ex} contains n_q sources each one of strength $A_{q,j}$ and position vector $\mathbf{r}_{q,j}$, for $j = 1, \ldots, n_q$. Evidently, it holds that $n_1 + n_2 + \cdots + n_Q = N$.

The first-order (linearized) equations of sound propagation in a lossless

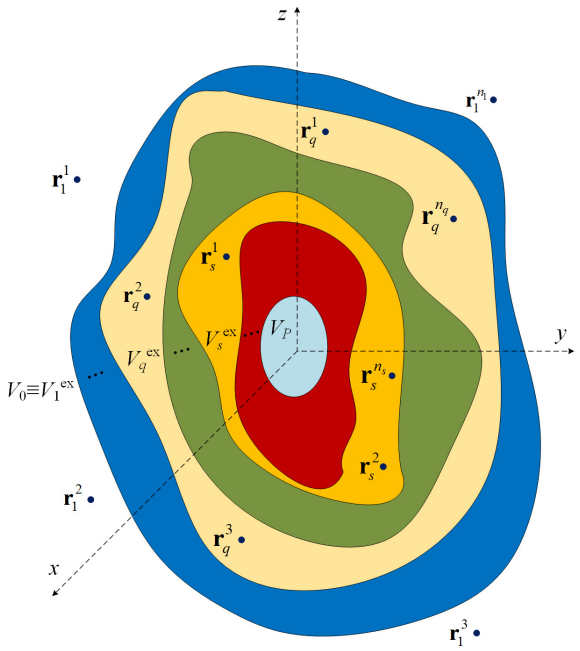

Figure 1.1: The considered layered scatterer V excited by multiple external and internal point sources

medium take the following form [79]:

$$\gamma P_t(\mathbf{r},t) + \nabla \cdot \mathbf{V}(\mathbf{r},t) = 0 \tag{1.1}$$

$$\rho \mathbf{V}_t(\mathbf{r},t) + \nabla P(\mathbf{r},t) = 0 \tag{1.2}$$

with $P(\mathbf{r},t)$ denoting the *acoustic pressure* and with $\mathbf{V}(\mathbf{r},t)$ denoting the *acoustic velocity* inside the propagating medium. For time-harmonic fields, the acoustic pressure is of the form

$$P(\mathbf{r},t) = e^{-\mathrm{i}\omega t} u(\mathbf{r}) \tag{1.3}$$

with $u(\mathbf{r})$ the *spatial acoustic pressure*. On the other hand, for time-harmonic dependence, by taking the rotation of equation (1.2) we readily prove that the acoustic velocity is irrotational and hence, a spatial, scalar potential $\phi(\mathbf{r})$ exists such as to hold

$$\mathbf{V}(\mathbf{r},t) = e^{-\mathrm{i}\omega t} \nabla \phi(\mathbf{r}) \tag{1.4}$$

Substituting (1.3), (1.4) to (1.1) and (1.2), we respectively arrive at

$$u(\mathbf{r}) = \mathrm{i}\omega\rho\phi(\mathbf{r}) \tag{1.5}$$

$$\nabla u(\mathbf{r}) = \mathrm{i}\omega\rho\nabla\phi(\mathbf{r}) \tag{1.6}$$

Since (1.6) is a direct consequence of (1.5), we derived that equation (1.5) constitutes the *fundamental equation* of time-harmonic sound propagation in a lossless medium. In the rest of the text, we will restrict the definitions - unless there is risk of confusion - to the spatial acoustic pressure. Furthermore, we will use the term "fields" when we refer collectively to both the spatial acoustic pressure and the spatial acoustic velocity potential.

The spatial primary acoustic pressure induced by the point source at $\mathbf{r}_{q,j}$ is given by

$$u^{\mathrm{pr}}_{q,j}(\mathbf{r}) = A_{q,j}\left(\frac{\exp(\mathrm{i}k_q|\mathbf{r}-\mathbf{r}_{q,j}|)}{|\mathbf{r}-\mathbf{r}_{q,j}|}\right), \quad \mathbf{r} \neq \mathbf{r}_{q,j}, \tag{1.7}$$

where $j = 1, \ldots, n_q$ and $q = 1, \ldots, Q$, which is a variation of the fundamental solution of the Helmholtz equation, see [80].

If V_p is not an excitation layer, the secondary pressure generated in V_p by a source at $\mathbf{r}_{q,j}$ coincides with the total pressure in V_p and will be denoted by $u^p_{q,j}$. Following Sommerfeld's method [81], the total pressure induced in the excitation layer V^{ex}_q due to a single source at $\mathbf{r}_{q,j} \in V^{\mathrm{ex}}_q$ has the decomposition

$$u^q_{q,j}(\mathbf{r}) = u^{\mathrm{pr}}_{q,j}(\mathbf{r}) + u^{\mathrm{sec}}_{q,j}(\mathbf{r}), \quad \mathbf{r} \in V^{\mathrm{ex}}_q \setminus \{\mathbf{r}_{q,j}\}. \tag{1.8}$$

Fields due to a single source will be referred to as *individual fields*. Moreover, the *total q-excitation pressure* u^p_q of V_p is the superposition of the total individual fields in V_p due to all sources in V^{ex}_q, i.e.

$$u^p_q(\mathbf{r}) = \sum_{j=1}^{n_q} u^p_{q,j}(\mathbf{r}). \tag{1.9}$$

For excitation layers V^{ex}_q, the *primary q-excitation pressure* u^{pr}_q and the *secondary q-excitation pressure* u^{sec}_q are defined as the superpositions of the

corresponding individual pressures due to all sources in $V_q^{\rm ex}$, i.e.

$$u_q^\ell(\mathbf{r}) = \sum_{j=1}^{n_q} u_{q,j}^\ell(\mathbf{r}), \tag{1.10}$$

where $\ell \in \{\mathrm{pr}, \mathrm{sec}\}$. Then, the *total q-excitation pressure* of V_q is given by

$$u_q^q(\mathbf{r}) = u_q^{\rm pr}(\mathbf{r}) + u_q^{\rm sec}(\mathbf{r}), \quad \mathbf{r} \in V_q^{\rm ex} \setminus \{\mathbf{r}_{q,1}, \ldots, \mathbf{r}_{q,n_q}\}. \tag{1.11}$$

Besides, the *overall pressure* u^p of V_p is defined as the superposition of all individual pressures of V_p, i.e.

$$u^p(\mathbf{r}) = \sum_{q=1}^{Q} \sum_{j=1}^{n_q} u_{q,j}^p(\mathbf{r}) = \sum_{q=1}^{Q} u_q^p(\mathbf{r}). \tag{1.12}$$

If V_q coincides with an excitation layer, the *overall secondary pressure* of V_q is the superposition of all individual secondary pressures of V_q, whereas the *overall pressure* of V_q is defined as

$$u^q(\mathbf{r}) = u_q^{\rm pr}(\mathbf{r}) + u_q^{\rm sec}(\mathbf{r}) + \sum_{s \neq q} u_s^q(\mathbf{r}). \tag{1.13}$$

Individual, q-excitation, and overall pressures satisfy the scalar Helmholtz equations; e.g. for the total q-excitation field of V_p, it holds

$$\nabla^2 u_q^p(\mathbf{r}) + k_p^2 u_q^p(\mathbf{r}) = \mathbf{0}, \tag{1.14}$$

in V_p, if V_p is not an excitation layer, and in $V_q^{\rm ex} \setminus \{\mathbf{r}_{q,1}, \ldots, \mathbf{r}_{q,n_q}\}$ if V_p is an excitation layer $V_q^{\rm ex}$.

The (total) individual, q-excitation and overall fields satisfy the transmission conditions

$$u^{p-1}(\mathbf{r}) = u^p(\mathbf{r}), \tag{1.15}$$

$$\frac{\partial \phi^{p-1}(\mathbf{r})}{\partial n} = \frac{\partial \phi^p(\mathbf{r})}{\partial n}, \tag{1.16}$$

on the boundaries of each layer V_p ($p = 1, \ldots, P-1$). For a penetrable core V_P, conditions (1.15) and (1.16) hold also for $p = P$. For soft, hard or resistive core, the following conditions hold on its boundary S_P [79]

$$u^{P-1}(\mathbf{r}) = 0, \tag{1.17}$$

$$\frac{\partial \phi^{P-1}(\mathbf{r})}{\partial n} = 0, \tag{1.18}$$

$$\frac{\partial \phi^{P-1}(\mathbf{r})}{\partial n} + \frac{u^{P-1}(\mathbf{r})}{Z_{P-1}} = 0. \tag{1.19}$$

with Z_{P-1} the acoustic impedance of V_{P-1}. Moreover, the total (individual) fields in V_0 satisfy the Sommerfeld radiation condition [79], [82]

$$\lim_{r\to\infty} \left(\frac{\partial \phi^0_{q,j}(\mathbf{r})}{\partial r} + \frac{u^0_{q,j}(\mathbf{r})}{\zeta_0} \right) = 0, \tag{1.20}$$

uniformly over all directions $\hat{\mathbf{r}} = \mathbf{r}/r$, with ζ_0 denoting the *medium admittance* of the exterior V_0 which is given by

$$\zeta_0 = \sqrt{\frac{\rho_0}{\gamma_0}}.$$

Remark 1.1.1 *Another form of (1.19) is (see [79], [83])*

$$\frac{\partial u^{P-1}(\mathbf{r})}{\partial n} + \mathrm{i}k_{P-1}\lambda u^{P-1}(\mathbf{r}) = 0 \tag{1.21}$$

which utilizes the dimensionless constant λ, known as characteristic admittance *which is given by*

$$\lambda = \frac{\zeta_{P-1}}{Z_{P-1}} \tag{1.22}$$

with ζ_{P-1} the medium admittance *of V_{P-1}. Equation (1.19) offers the physical explanation of acoustic impedance: it constitutes the constant ratio between the loss in pressure and the gain in speed over the direction of the outward normal.*

Evidently, q-excitation and overall fields satisfy condition (1.20) as well. Additionally, the acoustic pressure has the following asymptotic expression

$$u^0_{q,j}(\mathbf{r}) = g_{q,j}(\hat{\mathbf{r}})h_0(k_0 r) + \mathcal{O}(r^{-2}), \quad r = |\mathbf{r}| \to \infty, \tag{1.23}$$

where h_0 is the zero-th order spherical Hankel function of the first kind. The function $g_{q,j}(\hat{\mathbf{r}})$ is the *individual far-field* in the direction of observation $\hat{\mathbf{r}}$ due to the source at $\mathbf{r}_{q,j} \in V_q^{\text{ex}}$. Next, the *q-excitation far-field* $g_q(\hat{\mathbf{r}})$ and the *overall far-field* $g(\hat{\mathbf{r}})$ are defined as the superpositions of the individual far-fields due to all sources within V_q^{ex} and due to all N sources, respectively; namely it holds

$$g_q(\hat{\mathbf{r}}) = \sum_{j=1}^{n_q} g_{q,j}(\hat{\mathbf{r}}), \tag{1.24}$$

$$g(\hat{\mathbf{r}}) = \sum_{q=1}^{Q} g_q(\hat{\mathbf{r}}). \tag{1.25}$$

Similarly, the *individual cross section* $\sigma_{q,j}$, *q-excitation cross section* σ_q, and *overall cross section* σ are the scattering cross sections due to a source at $\mathbf{r}_{q,j} \in V_q^{\text{ex}}$, all sources in V_q^{ex}, and all N sources, and are, respectively, given by

$$\sigma_{q,j} = \frac{1}{k_0^2} \int_{S^2} |g_{q,j}(\hat{\mathbf{r}})|^2 \mathrm{d}s(\hat{\mathbf{r}}), \tag{1.26}$$

$$\sigma_q = \frac{1}{k_0^2} \int_{S^2} |g_q(\hat{\mathbf{r}})|^2 \mathrm{d}s(\hat{\mathbf{r}}), \tag{1.27}$$

$$\sigma = \frac{1}{k_0^2} \int_{S^2} |g(\hat{\mathbf{r}})|^2 \mathrm{d}s(\hat{\mathbf{r}}), \tag{1.28}$$

where S^2 is the unit sphere of $\mathbb{R}^3$.

The sum of the individual scattering cross sections due to the excitation by all dipoles and the overall scattering cross section are (in general) different. For acoustic fields, this was elaborated in [64] for point-source excitation of a layered medium, and in [84] for multiple scattering due to plane incident waves. This fact, implies the existence of physical quantities that remain in quadrature such as reactive sound fields [54] and is mathematically explained by the quadratic form of the scattering cross sections, [85]. Their presence can be unveiled through examination of the non-linear nature of the energy functionals and their importance is highlighted by their connection with active and reactive sound intensity [53].

For $N > 2$, we notice that this interaction scattering cross section can be zero without the involved far-fields being orthogonal.

Now, by means of (1.26)-(1.28), we define the *interaction scattering cross sections (ISCS)* and present their basic properties.

Definition 1.1.2 *The q-ISCS, $\tilde{\sigma}_q$, is the difference between the q-excitation cross section σ_q and the sum of the individual cross sections due to all dipoles in V_q^{ex}*

$$\tilde{\sigma}_q = \sigma_q - \sum_{j=1}^{n_q} \sigma_{q,j}. \tag{1.29}$$

The indirect ISCS, σ^{I}, is the difference between the overall cross section σ and the sum of the q-excitation cross sections

$$\sigma^{\mathrm{I}} = \sigma - \sum_{q=1}^{Q} \sigma_q. \tag{1.30}$$

The total ISCS, σ^{T}, is the difference between the overall cross section σ and the sum of the individual cross sections due to all N dipoles

$$\sigma^{\mathrm{T}} = \sigma - \sum_{q=1}^{Q} \sum_{j=1}^{n_q} \sigma_{q,j}. \tag{1.31}$$

By taking into account (1.26)-(1.28), we also derive the following expressions of the above-defined ISCS

$$\tilde{\sigma}_q = \frac{2}{k_0^2} \mathrm{Re} \left[\sum_{j=1}^{n_q-1} \sum_{\nu=j+1}^{n_q} \int_{S^2} g_{q,j}(\hat{\mathbf{r}}) \overline{g_{q,\nu}(\hat{\mathbf{r}})} \mathrm{d}s(\hat{\mathbf{r}}) \right], \tag{1.32}$$

$$\sigma^{\mathrm{I}} = \frac{2}{k_0^2} \mathrm{Re} \left[\sum_{q=1}^{Q-1} \sum_{s=q+1}^{Q} \int_{S^2} g_q(\hat{\mathbf{r}}) \overline{g_s(\hat{\mathbf{r}})} \mathrm{d}s(\hat{\mathbf{r}}) \right], \tag{1.33}$$

$$\sigma^{\mathrm{T}} = \frac{2}{k_0^2} \mathrm{Re} \left[\sum_{\nu=1}^{N-1} \sum_{j=\nu+1}^{N} \int_{S^2} g^{\nu}(\hat{\mathbf{r}}) \overline{g^{j}(\hat{\mathbf{r}})} \mathrm{d}s(\hat{\mathbf{r}}) \right], \tag{1.34}$$

where $g^{\nu}(\hat{\mathbf{r}})$ is the individual far field due to a source at $\mathbf{r}^{\nu}$.

1.2 Energy Conservation

1.2.1 Acoustic Intensity and Energy Functionals

The complex acoustic intensity $\mathcal{I}(\mathbf{r},t)$ is a measure of the acoustic power flux [86] and is defined as follows:

$$\mathcal{I}(\mathbf{r},t) = P(\mathbf{r},t)\overline{\mathbf{V}}(\mathbf{r},t). \tag{1.35}$$

For time-harmonic fields, the complex acoustic intensity coincides with its spatial part $\mathbf{I}(\mathbf{r})$ given by

$$\mathcal{I}(\mathbf{r},t) = u(\mathbf{r})\nabla\overline{\phi}(\mathbf{r}) = \mathbf{I}(\mathbf{r}). \tag{1.36}$$

Hereafter, for the real part of the acoustic intensity we use the term *active intensity* and for the imaginary part the term *reactive intensity* [52], [53].

Additionally, the *kinetic energy density* $\mathcal{K}$ and the *potential energy density* $\mathcal{U}$ are defined as follows:

$$\mathcal{K}(\mathbf{r},t) = \frac{\rho}{2}|\mathbf{V}(\mathbf{r},t)|^2, \qquad \mathcal{U}(\mathbf{r},t) = \frac{\gamma}{2}|P(\mathbf{r},t)|^2. \tag{1.37}$$

Under harmonic time dependence, they are real functions that do not depend on time and are given by

$$K(\mathbf{r}) = \frac{\rho}{2}|\nabla\phi(\mathbf{r})|^2, \qquad U(\mathbf{r}) = \frac{\gamma}{2}|u(\mathbf{r})|^2. \tag{1.38}$$

An important quantity in the energy transfer process is the *Lagrangian density* $L(\mathbf{r})$, which is the difference between the kinetic and potential energy densities, i.e. [87]

$$L(\mathbf{r}) = K(\mathbf{r}) - U(\mathbf{r}) = \frac{1}{2}\left(\rho|\nabla\phi(\mathbf{r})|^2 - \gamma|u(\mathbf{r})|^2\right). \tag{1.39}$$

The above discussed energy functionals are –by definition– quadratic quantities. Hence, the overall acoustic intensity and its corresponding energy densities is not simply a sum of the corresponding "individual" quantities. As we will elaborate later on, this fact implies that there is flux–and subsequently, energy–that is induced by the interaction between the "individual" fields. That was proven for multiple acoustic scattering from

point-like scatterers [84] and scattering of spherical waves by a layered medium [64], while the specifics of the behaviur of the power flux is used in numerical inverse methods, [88]. The induced energy flux or intensity, might seem evident for q-excitation and overall acoustic fields but we stress the fact that the quadratic nature of the energy functionals occurs even for individual acoustic intensities; something discussed for scattering of an individually-induced acoustic wave by an impenetrable cluster in [89].

In particular, the acoustic intensity in layer V_q due to the source at $\mathbf{r}_{q,j}$ is denoted in accordance with our formulation by $\mathbf{I}^q_{q,j}(\mathbf{r})$ and it will hold for it:

$$\begin{aligned}\mathbf{I}^q_{q,j}(\mathbf{r}) = u^{\mathrm{pr}}_{q,j}(\mathbf{r})\nabla\overline{\phi^{\mathrm{pr}}_{q,j}}(\mathbf{r}) + u^{\mathrm{sec}}_{q,j}(\mathbf{r})\nabla\overline{\phi^{\mathrm{sec}}_{q,j}}(\mathbf{r}) + \\ u^{\mathrm{pr}}_{q,j}(\mathbf{r})\nabla\overline{\phi^{\mathrm{sec}}_{q,j}}(\mathbf{r}) + u^{\mathrm{sec}}_{q,j}(\mathbf{r})\nabla\overline{\phi^{\mathrm{pr}}_{q,j}}(\mathbf{r}).\end{aligned} \tag{1.40}$$

Evidently, the individual *primary acoustic intensity* induced by the individual primary acoustic wave due to the source at $\mathbf{r}_{q,j}$ and the individual *secondary acoustic intensity* induced by the corresponding individual secondary wave due to the source at $\mathbf{r}_{q,j}$ are defined by

$$\mathbf{I}^{\mathrm{pr}}_{q,j}(\mathbf{r}) = u^{\mathrm{pr}}_{q,j}(\mathbf{r})\nabla\overline{\phi^{\mathrm{pr}}_{q,j}}(\mathbf{r}), \tag{1.41}$$

$$\mathbf{I}^{\mathrm{sec}}_{q,j}(\mathbf{r}) = u^{\mathrm{sec}}_{q,j}(\mathbf{r})\nabla\overline{\phi^{\mathrm{sec}}_{q,j}}(\mathbf{r}). \tag{1.42}$$

Equation (1.41) holds for $\mathbf{r} \in V_q \setminus \{\mathbf{r}_{q,j}\}$, while (1.42) holds for $\mathbf{r} \in V_q$. However, inside the layer V_q due to the fact that both the primary and secondary fields propagate uniformly over all directions, interaction between the primary field with its own secondary field will occur. This interaction results in an "extra" acoustic intensity which stems from precisely that interaction and it will given by:

$$\mathbf{I}^{\mathrm{ext}}_{q,j}(\mathbf{r}) = u^{\mathrm{pr}}_{q,j}(\mathbf{r})\nabla\overline{\phi^{\mathrm{sec}}_{q,j}}(\mathbf{r}) + u^{\mathrm{sec}}_{q,j}(\mathbf{r})\nabla\overline{\phi^{\mathrm{pr}}_{q,j}}(\mathbf{r}). \tag{1.43}$$

Therefore, the *individual acoustic intensity* in the excitation layer V_q due to the point source at $\mathbf{r}_{q,j}$ is decomposed as follows:

$$\mathbf{I}^q_{q,j}(\mathbf{r}) = \mathbf{I}^{\mathrm{pr}}_{q,j}(\mathbf{r}) + \mathbf{I}^{\mathrm{sec}}_{q,j}(\mathbf{r}) + \mathbf{I}^{\mathrm{ext}}_{q,j}(\mathbf{r}) \tag{1.44}$$

the q-*excitation* intensity in the excitation layer V_q is denoted by $\mathbf{I}_q^q$ and it holds

$$\mathbf{I}_q^q(\mathbf{r}) = \mathbf{I}_q^{\mathrm{pr}}(\mathbf{r}) + \mathbf{I}_q^{\mathrm{sec}}(\mathbf{r}) + \mathbf{I}_q^{\mathrm{ext}}(\mathbf{r}) \tag{1.45}$$

with $\mathbf{r} \in V_q \setminus \{\mathbf{r}_{q,1}, \mathbf{r}_{q,2}, \ldots, \mathbf{r}_{q,n_q}\}$. With $\mathbf{I}_q^\ell$, for $\ell \in \{\mathrm{pr}, \mathrm{sec}, \mathrm{ext}\}$ we denote the acoustic intensity in V_q that is caused by the q-excitation primary fields, the q-excitation secondary fields and the interaction between them, respectively. In the same spirit the *overall intensity* in V_q is decomposed as follows

$$\mathbf{I}^q(\mathbf{r}) = \mathbf{I}_q^{\mathrm{pr}}(\mathbf{r}) + \mathbf{I}^{\mathrm{sec}}(\mathbf{r}) + \mathbf{I}^{\mathrm{ext}}(\mathbf{r}) \tag{1.46}$$

for $\mathbf{r} \in V_q \setminus \{\mathbf{r}_{q,1}, \mathbf{r}_{q,2}, \ldots, \mathbf{r}_{q,n_q}\}$, with $\mathbf{I}^\nu$ for $\nu \in \{\mathrm{sec}, \mathrm{ext}\}$ the intensity in V_q caused by the overall secondary field in V_q and the intensity caused by the interaction between the primary q-excitation field in V_q with the overall secondary field in V_q, respectively. We note that the individual, q-excitation and overall intensities in non-excitation layers V_p, coincide with the intensities caused by the secondary fields "operating" in V_p. For simplicity they will be denoted by $\mathbf{I}_{q,j}^p, \mathbf{I}_q^p, \mathbf{I}^p$, respectively.

In the previous section we discussed about the different types of scattering cross sections that measure the intensity radiating in the far-field due to the interaction between the individual and/or q-excitation fields. These interactions stem from their corresponding acoustic intensity in the excitation layers - as we will prove later on. This fact, yields another decomposition for the q-excitation and overall acoustic intensities in V_p. In particular, we denote the sum of the individual intensities in V_p with $\hat{\mathbf{I}}_q^p$ and with $\tilde{\mathbf{I}}_q^p$ the q-*interaction intensity* of V_p. Evidently it holds:

$$\hat{\mathbf{I}}_q^p(\mathbf{r}) + \tilde{\mathbf{I}}_q^p(\mathbf{r}) = \mathbf{I}_q^{\mathrm{pr}}(\mathbf{r}) + \mathbf{I}_q^{\mathrm{sec}}(\mathbf{r}) + \mathbf{I}_q^{\mathrm{ext}}(\mathbf{r}) = \mathbf{I}_q^p(\mathbf{r}) \tag{1.47}$$

If V_p is a non-excitation layer, then it holds $\mathbf{I}_q^{\mathrm{pr}}(\mathbf{r}) = \mathbf{I}_q^{\mathrm{ext}}(\mathbf{r}) = 0$ in V_p. In a similar spirit, we denote with $\mathbf{I}_{\mathrm{T}}^p$ the *total interaction intensity* of V_p, with $\mathbf{I}_{\mathrm{I}}^p$ the *indirect interaction intensity* of V_p and with $\mathbf{I}_{\mathrm{D}}^p$ the *direct interaction*

intensity of V_p which are given by

$$\mathbf{I}_{\mathrm{T}}^{p} = \mathbf{I}^{p} - \sum_{q=1}^{Q} \sum_{j=1}^{n_q} \mathbf{I}_{q,j}^{p} \tag{1.48}$$

$$\mathbf{I}_{\mathrm{I}}^{p} = \mathbf{I}^{p} - \sum_{q=1}^{Q} \mathbf{I}_{q}^{p} \tag{1.49}$$

$$\mathbf{I}_{\mathrm{D}}^{p} = \sum_{q=1}^{Q} \tilde{\mathbf{I}}_{q}^{p} \tag{1.50}$$

By definition, in each layer V_p, it holds

$$\mathbf{I}_{\mathrm{T}}^{p} = \mathbf{I}_{\mathrm{I}}^{p} + \mathbf{I}_{\mathrm{D}}^{p} \tag{1.51}$$

1.2.2 Energy Conservation Laws

At this point we will prove a series of theorems that lead to a better understanding of the process that is involved in "transferring" the energy from the excitation layers, through the rest of the scatterer's layers and its exterior, until it is radiated in the far-field zone. The main mathematical tool is Green's first scalar identity combined with appropriate geometrical manipulation. First, we provide a theorem relating the q-excitation scattering cross section with its corresponding Lagrangian density and intensity through an excitation layer's surface. This theorem constitutes the complex form of the energy conservation law for the scattering problem of a multiple-source induced acoustic wave by a layered scatterer in the case where all sources lie in the same layer V_q.

Theorem 1.2.1 *The q-excitation scattering cross section σ_q, the Lagrangian densities L_q^p of a distribution of point sources within a single-excitation layer V_q and the acoustic intensity $\mathbf{I}_q^q$ of V_q due to all dipoles in V_q are connected as follows:*

$$\sigma_q = \zeta_0 \left(2\mathrm{i}\omega \sum_{p=0}^{q-1} \int_{V_p} L_q^p(\mathbf{r}) \mathrm{d}v(\mathbf{r}) + \int_{S_q} \hat{\mathbf{n}} \cdot \mathbf{I}_q^q(\mathbf{r}) \mathrm{d}s(\mathbf{r}) \right) \tag{1.52}$$

Proof. Let Ω the domain of $\mathbb{R}^3$ that is bounded by the scatterer's external surface S_1 and the sphere S_R of radius R; see Fig. 1.2. Applying Green's

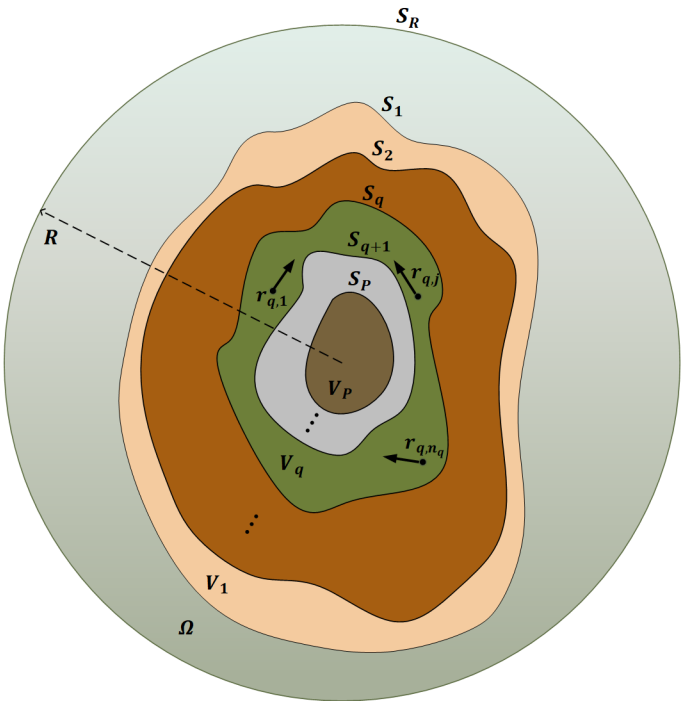

Figure 1.2: A layered scatterer V with a single excitation layer V_q, surrounded by a sphere of radius R.

first scalar identity in Ω for the intensity vector $\mathbf{I}_q^0$ of V_0 due to the sources in V_q, yields

$$\int_{S_R} \hat{\mathbf{r}} \cdot \mathbf{I}_q^0(\mathbf{r}) \mathrm{d}s(\mathbf{r}) - \int_{S_1} \hat{\mathbf{n}} \cdot \mathbf{I}_q^0(\mathbf{r}) \mathrm{d}s(\mathbf{r}) = \int_{\Omega} \left(u_q^0(\mathbf{r}) \nabla \overline{\phi_q^0(\mathbf{r})} - \nabla u_q^0(\mathbf{r}) \cdot \nabla \overline{\phi_q^0(\mathbf{r})} \right) \mathrm{d}v(\mathbf{r}), \tag{1.53}$$

Last relation by means of (1.5) takes the form

$$\int_{S_R} \hat{\mathbf{r}} \cdot \mathbf{I}_q^0(\mathbf{r}) \mathrm{d}s(\mathbf{r}) = \int_{S_1} \hat{\mathbf{n}} \cdot \mathbf{I}_q^0(\mathbf{r}) \mathrm{d}s(\mathbf{r}) + 2\mathrm{i}\omega \int_{\Omega} L_q^0(\mathbf{r}) \mathrm{d}v(\mathbf{r}), \tag{1.54}$$

where L_q^0 denotes the Lagrangian density in V_0 due to all sources of V_q. Letting $r \to \infty$ we are transferred in the far-field zone. Applying Sommerfeld

radiation condition (1.20) we arrive at

$$\hat{\mathbf{r}} \cdot \mathbf{I}_q^0(\mathbf{r}) = \frac{1}{\zeta_0 k_0^2 r^2} |g_q(\hat{\mathbf{r}})|^2 + \mathcal{O}(r^{-3}), \tag{1.55}$$

Last relation, in conjunction with (1.54) for $R \to \infty$, yields

$$\lim_{R\to\infty} \left(\frac{1}{\zeta_0 k_0^2 r^2} \int_{S_R} |g_q(\hat{\mathbf{r}})|^2 \mathrm{d}s(\mathbf{r}) \right) = \int_{S_1} \hat{\mathbf{n}} \cdot \mathbf{I}_q^0(\mathbf{r}) \mathrm{d}s(\mathbf{r}) + 2\mathrm{i}\omega \int_{V_0} L_q^0(\mathbf{r}) \mathrm{d}v(\mathbf{r}). \tag{1.56}$$

Taking into account (1.27) we obtain

$$\frac{\sigma_q}{\zeta_0} = \int_{S_1} \hat{\mathbf{n}} \cdot \mathbf{I}_q^0(\mathbf{r}) \mathrm{d}s(\mathbf{r}) + 2\mathrm{i}\omega \int_{V_0} L_q^0(\mathbf{r}) \mathrm{d}v(\mathbf{r}). \tag{1.57}$$

Successive implementation of Green's first scalar identity in layer V_p, for $p = 1, \ldots, q-1$, yields

$$\int_{S_p} \hat{\mathbf{n}} \cdot \mathbf{I}_q^p(\mathbf{r}) \mathrm{d}s(\mathbf{r}) = \int_{S_{p+1}} \hat{\mathbf{n}} \cdot \mathbf{I}_q^p(\mathbf{r}) \mathrm{d}s(\mathbf{r}) + 2\mathrm{i}\omega \int_{V_p} L_q^p(\mathbf{r}) \mathrm{d}v(\mathbf{r}) \tag{1.58}$$

Imposing boundary conditions on the acoustically penetrable surface S_{p+1}, leads to

$$\hat{\mathbf{n}} \cdot \mathbf{I}_q^p(\mathbf{r}) = u_q^p(\mathbf{r}) \nabla \overline{\phi_q^p}(\mathbf{r}) = u_q^{p+1}(\mathbf{r}) \nabla \overline{\phi_q^{p+1}}(\mathbf{r}) = \hat{\mathbf{n}} \cdot \mathbf{I}_q^{p+1}(\mathbf{r}). \tag{1.59}$$

Applying again Green's first scalar identity, for $p = 1, \ldots, q-1$ and taking into consideration (1.58) and (1.59) we get

$$\int_{S_1} \hat{\mathbf{n}} \cdot \mathbf{I}_q^0(\mathbf{r}) \mathrm{d}s(\mathbf{r}) = 2\mathrm{i}\omega \sum_{p=1}^{q-1} \int_{V_p} L_q^p(\mathbf{r}) \mathrm{d}v(\mathbf{r}) + \int_{S_q} \hat{\mathbf{n}} \cdot \mathbf{I}_q^q(\mathbf{r}) \mathrm{d}s(\mathbf{r}) \tag{1.60}$$

Relation (1.52) is obtained through (1.57) and (1.60).

□

Taking the real part of (1.52), we obtain a generic form of the optical theorem

Corollary 1.2.2 *The individual scattering cross section and the average active intensity per unit area out of the excitation layer V_q, are connected by the relation:*

$$\sigma_q = \zeta_0 \mathrm{Re}\left(\int_{S_q} \hat{\mathbf{n}} \cdot \mathbf{I}_q^q(\mathbf{r}) \mathrm{d}s(\mathbf{r})\right). \tag{1.61}$$

Taking the imaginary parts in (1.52) reveals the role of the reactive power. In particular, it holds:

Corollary 1.2.3 *The reactive intensity directed into the excitation layer V_q is related with stored energy in all layers of the scatterer prior to V_q by the relation:*

$$2\omega \sum_{p=0}^{q-1} \int_{V_p} L_q^p(\mathbf{r}) \mathrm{d}v(\mathbf{r}) = -\mathrm{Im}\left(\int_{S_q} \hat{\mathbf{n}} \cdot \mathbf{I}_q^q(\mathbf{r}) \mathrm{d}s(\mathbf{r})\right). \tag{1.62}$$

For $n_q = 1$, we obtain the corresponding results for the individual quantities. Equation (1.61) demonstrates that the average active intensity through an excitation layer's surface is "transferred" directly to the far-field as intensity manifested by the q-excitation cross section. On the other hand, Eq. (1.62) states that the reactive intensity is not "transferred" in the far field. Instead, it is stored as difference between the kinetic energy and potential energy in the scatterer's layers enclosing the excitation layer and allows us to conclude that it acts as an "intensity carrier" that enables the transfer from the excitation layer to the far-field. The term "energy transfer process" is clearly explained by relation (1.52). It contains three terms: A term that concerns the intensity in the excitation layer, a term that concerns the layers that enclose the excitation layer and finally, a term that concerns the far-field.

We continue with the investigation of the energy conservation mechanism and in particular, with the energy transfer "below" an excitation layer, i.e. for $p > q$. The following theorem provides a more detailed insight to the intensity induced in an excitation layer.

Theorem 1.2.4 *The acoustic intensity through the surface S_q of excitation layer V_q is connected with the interaction intensities in the interior of*

V_q as follows:

$$\int_{S_q} \hat{\mathbf{n}} \cdot \mathbf{I}_q^q(\mathbf{r}) \mathrm{d}s(\mathbf{r}) = \int_{\partial V_q} \hat{\mathbf{n}} \cdot \left(\mathbf{I}_q^{\mathrm{pr}}(\mathbf{r}) + \mathbf{I}_q^{\mathrm{ext}}(\mathbf{r}) \right) \mathrm{d}s(\mathbf{r}) + 2\mathrm{i}\omega \sum_{p=q}^{P} \int_{V_p} L_q^p(\mathbf{r}) \mathrm{d}v(\mathbf{r}) \tag{1.63}$$

Proof. Applying Green's first scalar identity in V_q for the q-excitation secondary intensity, we get

$$\int_{S_q} \hat{\mathbf{n}} \cdot \mathbf{I}_q^{\mathrm{sec}}(\mathbf{r}) \mathrm{d}s(\mathbf{r}) = 2\mathrm{i}\omega \int_{V_q} L_q^{\mathrm{sec}}(\mathbf{r}) \mathrm{d}v(\mathbf{r}) + \int_{S_{q+1}} \hat{\mathbf{n}} \cdot \mathbf{I}_q^{\mathrm{sec}}(\mathbf{r}) \mathrm{d}s(\mathbf{r}) \tag{1.64}$$

with L_q^{sec} denoting the Lagrangian density of the secondary fields in V_q. Imposing boundary conditions on S_{q+1} for u_q^q, ϕ_q^q, we have

$$\int_{S_{q+1}} \hat{\mathbf{n}} \cdot \mathbf{I}_q^{\mathrm{sec}}(\mathbf{r}) \mathrm{d}s(\mathbf{r}) = \int_{S_{q+1}} \hat{\mathbf{n}} \cdot \mathbf{I}_q^{q+1}(\mathbf{r}) \mathrm{d}s(\mathbf{r}) - \int_{S_{q+1}} u_q^{\mathrm{pr}}(\mathbf{r}) \frac{\phi_q^{q+1}(\mathbf{r})}{\partial n} \mathrm{d}s(\mathbf{r}) + \int_{S_{q+1}} \hat{\mathbf{n}} \cdot \mathbf{I}_q^{\mathrm{pr}}(\mathbf{r}) \mathrm{d}s(\mathbf{r}) - \int_{S_{q+1}} u_q^{q+1}(\mathbf{r}) \frac{\phi_q^{\mathrm{pr}}(\mathbf{r})}{\partial n} \mathrm{d}s(\mathbf{r}) \tag{1.65}$$

Imposing again the boundary conditions on S_{q+1}, this time for the fields u_q^{q+1}, ϕ_q^{q+1}, relation (1.65) yields

$$\int_{S_{q+1}} \hat{\mathbf{n}} \cdot \mathbf{I}_q^{\mathrm{sec}}(\mathbf{r}) \mathrm{d}s(\mathbf{r}) = \int_{S_{q+1}} \hat{\mathbf{n}} \cdot \mathbf{I}_q^{q+1}(\mathbf{r}) \mathrm{d}s(\mathbf{r}) - \int_{S_{q+1}} \hat{\mathbf{n}} \cdot \mathbf{I}_q^{\mathrm{pr}}(\mathbf{r}) \mathrm{d}s(\mathbf{r}) - \int_{S_{q+1}} \hat{\mathbf{n}} \cdot \mathbf{I}_q^{\mathrm{ext}}(\mathbf{r}) \mathrm{d}s(\mathbf{r}). \tag{1.66}$$

On the other hand, a successive application of Green's first scalar identity in V_p for $p = q+1, q+2, \ldots, P$ yields

$$\int_{S_{q+1}} \hat{\mathbf{n}} \cdot \mathbf{I}_q^q(\mathbf{r}) \mathrm{d}s(\mathbf{r}) = 2\mathrm{i}\omega \sum_{p=q+1}^{P} \int_{V_p} L_q^p(\mathbf{r}) \mathrm{d}v(\mathbf{r}), \tag{1.67}$$

Relation (1.63) is obtained from (1.64), (1.66) and (1.67) with the help of (1.46).

□

Taking the real parts of (1.63) we readily conclude that the average active intensity through the excitation layer's surface equals the average active intensity through the excitation layer's boundary, that is induced by the interaction between the individual primary and all other individual fields in V_q. Equation (1.63) in conjunction with (1.52) yields an alternative form of Theorem 1.2.1

$$\sigma_q = \zeta_0 \left(2\mathrm{i}\omega \sum_{p=0}^{P} \int_{V_p} L_q^p(\mathbf{r}) \mathrm{d}v(\mathbf{r}) + \int_{\partial V_q} \hat{\mathbf{n}} \cdot \left(\mathbf{I}_q^{\mathrm{pr}}(\mathbf{r}) + \mathbf{I}_q^{\mathrm{ext}}(\mathbf{r}) \right) \mathrm{d}s(\mathbf{r}) \right), \tag{1.68}$$

implying that only the interactions related with the primary fields induce active intensity. The interaction between secondary fields concerns the reactive intensity which seems to operate as an "intensity-carrier" that "transfers" the induced energy flow from the excitation layer, through the scatterer's layers, to the far-field. Finally, the secondary intensity in all layers and the q-primary intensity in the excitation layer V_q is manifested through the difference between kinetic and potential energy in the scatterer's layers. Similar results can be obtained for the overall Lagrangian densities, scattering cross sections and intensities in the case of mixed excitation, see Chapter 4 of Part II of this dissertation.

1.3 Scattering Relations and Physical Bounds

1.3.1 Scattering Relations

For a layered scatterer, excited by sources in different layers, two types of interactions occur: *direct* interaction due to sources contained in the same excitation layer, and *indirect* interaction due to sources contained in different layers. By means of (1.29)-(1.31), we derive the following theorem,

which concerns a decomposition of the total ISCS into the direct (sum of the q-interaction cross sections) and indirect ISCS.

Theorem 1.3.1 *Interaction cross sections σ^{T}, σ^{I}, and $\tilde{\sigma}_q$ are related as follows*

$$\sigma^{\mathrm{T}} = \sigma^{\mathrm{D}} + \sigma^{\mathrm{I}}, \tag{1.69}$$

where

$$\sigma^{\mathrm{D}} = \sum_{q=1}^{Q} \tilde{\sigma}_q \tag{1.70}$$

is the direct interaction cross section.

We observe that ISCS follow the same decomposition property as their corresponding intensities, see (1.51). Next, we establish scattering relations between the individual, the q-excitation fields and far-field patterns as well as the respective individual and overall cross sections. Scattering relations have been used as an important theoretical tool for the physical understanding in scattering phenomena like single- and multiple-scattering configurations [24], [90]. First, we give a reciprocity theorem, relating the total fields in layers V_q^{ex} and V_s^{ex} due to the sources at V_s^{ex} and V_q^{ex}, respectively.

Theorem 1.3.2 *The s-excitation field of V_q^{ex} and the q-excitation field of V_s^{ex} are related by*

$$\sum_{j=1}^{n_q} A_{q,j} u_s^q(\mathbf{r}_{q,j}) = \sum_{\nu=1}^{n_s} A_{s,\nu} u_q^s(\mathbf{r}_{s,\nu}). \tag{1.71}$$

Proof. Adapting Theorem 1 of [59] to the present formulation, we conclude that for any pair of sources lying at different layers it holds

$$A_{q,j} u_{s,\nu}^q(\mathbf{r}_{q,j}) = A_{s,\nu} u_{q,j}^s(\mathbf{r}_{s,\nu}). \tag{1.72}$$

Relation (1.72) holds for all locations $\mathbf{r}_{s,\nu}$. Fixing $\mathbf{r}_{q,j}$ and summing for $\nu = 1, \ldots, n_s$, we get

$$A_{q,j} u_s^q(\mathbf{r}_{q,j}) = \sum_{\nu=1}^{n_s} A_{s,\nu} u_{q,j}^s(\mathbf{r}_{s,\nu}),$$

which, summing for all $j = 1 \ldots, n_q$, yields

$$\sum_{j=1}^{n_q} A_{q,j} u_s^q(\mathbf{r}_{q,j}) = \sum_{j=1}^{n_q} \sum_{\nu=1}^{n_s} A_{s,\nu} u_{q,j}^s(\mathbf{r}_{s,\nu}). \tag{1.73}$$

Changing the summation order in (1.73) and taking into account (1.9), we arrive at (1.71).

□

Remark 1.3.3 For $Q = 2$ and $n_1 = n_2 = 1$ (i.e. $N = 2$ dipoles located in two different excitation layers), Theorem 1.3.2 reduces to Theorem 1 of [59]. For $Q = 1$ with $V_1^{\text{ex}} \equiv V_0$ and $N = 2$, Theorem 1.3.2 recovers Theorem 1.3.6 of [56].

Moreover, we define the *individual primary cross section* $\sigma_{q,j}^{\text{pr}}$, *q-primary cross section* σ_q^{pr}, and *primary interaction cross section*, $\tilde{\sigma}_q^{\text{pr}}$, as follows:

$$\sigma_{q,j}^{\text{pr}} = \frac{1}{k_q^2} \int_{S^2} |g_{q,j}^{\text{pr}}(\hat{\mathbf{r}})|^2 \mathrm{d}s(\hat{\mathbf{r}}) = 4\pi |A_{q,j}|^2, \tag{1.74}$$

$$\sigma_q^{\text{pr}} = \frac{1}{k_q^2} \int_{S^2} |g_q^{\text{pr}}(\hat{\mathbf{r}})|^2 \mathrm{d}s(\hat{\mathbf{r}}), \tag{1.75}$$

$$\tilde{\sigma}_q^{\text{pr}} = \frac{2}{k_q^2} \sum_{j=1}^{n_q-1} \sum_{\nu=j+1}^{n_q} \mathrm{Re}\left(\int_{S^2} \overline{g_{q,j}^{\text{pr}}(\hat{\mathbf{r}})} g_{q,\nu}^{\text{pr}}(\hat{\mathbf{r}}) \mathrm{d}s(\hat{\mathbf{r}}) \right), \tag{1.76}$$

where $g_{q,j}^{\text{pr}}$ is the primary far-field pattern (for a source at $\mathbf{r}_{q,j}$) defined by

$$u_{q,j}^{\text{pr}}(\mathbf{r}) = g_{q,j}^{\text{pr}}(\hat{\mathbf{r}}) h_0(k_q r) + \mathcal{O}(r^{-2}), \quad r \to \infty. \tag{1.77}$$

For the primary field (1.7), the primary far-field pattern is given by

$$g_{q,j}^{\text{pr}}(\hat{\mathbf{r}}) = \mathrm{i} k_q A_{q,j} \exp\left(-\mathrm{i} k_q \mathbf{r}_{q,j}\right). \tag{1.78}$$

Physically, $\tilde{\sigma}_{q,j,\nu}^{\text{pr}}$ represents the average rate of the acoustic intensity per surface unit area, induced by the interaction between fields generated by the sources at $\mathbf{r}_{q,j}$ and $\mathbf{r}_{q,\nu}$ under the absence of the scatterer. Note that unless $V_q^{\text{ex}} \equiv V_0$, the primary cross sections are not part of the overall scattering cross section.

We, now, prove optical theorems for the overall scattering cross section and the direct and indirect ISCS.

Theorem 1.3.4 *The overall scattering cross section σ due to the excitation of the layered scatterer V by N point sources is given by*

$$\sigma = 4\pi\zeta_0 \mathrm{Re}\left(\sum_{q=1}^{Q}\sum_{j=1}^{n_q}\overline{A_{q,j}}\phi_q^{\mathrm{sec}}(\mathbf{r}_{q,j})\right) + \frac{\zeta_0}{\zeta_q}\sum_{q=1}^{Q}\sigma_q^{\mathrm{pr}}. \tag{1.79}$$

The direct ISCS σ^{D} and indirect ISCS σ^{I} are expressed, respectively, by

$$\sigma^{\mathrm{D}} = 4\pi\zeta_0 \mathrm{Re}\left(\sum_{q=1}^{Q}\sum_{j=1}^{n_q}\overline{A_{q,j}}\tilde{\phi}_{q,j}^{\mathrm{sec}}(\mathbf{r}_{q,j})\right) + \frac{\zeta_0}{\zeta_q}\sum_{q=1}^{Q}\tilde{\sigma}_q^{\mathrm{pr}} \tag{1.80}$$

and

$$\sigma^{\mathrm{I}} = 4\pi\zeta_0 \mathrm{Re}\left(\sum_{q=1}^{Q}\sum_{j=1}^{n_q}\overline{A_{q,j}}\tilde{\phi}_{q}^{\mathrm{sec}}(\mathbf{r}_{q,j})\right), \tag{1.81}$$

where $\tilde{\phi}_{q,j}^{\mathrm{sec}}$ denotes the sum of all individual secondary fields of V_q^{ex} except the field due to the source at $\mathbf{r}_{q,j}$. $\tilde{\phi}_q^{\mathrm{sec}}$ denotes the sum of all q-excitation secondary fields radiating in V_q^{ex}, except the fields due to the sources of V_q^{ex}.

Proof. Adapting Theorem 2 of [59], to the present formulation we get that for any two sources $\mathbf{r}_{q,j} \in V_q^{\mathrm{ex}}$ and $\mathbf{r}_{s,\nu} \in V_s^{\mathrm{ex}}$, it holds

$$k_0^2\zeta_0\left(\overline{A_{q,j}}\phi_{s,\nu}^{q}(\mathbf{r}_{q,j}) + A_{s,\nu}\overline{\phi_{q,j}^{s}(\mathbf{r}_{s,\nu})}\right) = \frac{1}{2\pi}\int_{S^2}\overline{g_{q,j}(\hat{\mathbf{r}})}g_{s,\nu}(\hat{\mathbf{r}})\mathrm{d}s(\hat{\mathbf{r}}). \tag{1.82}$$

Summing with respect to ν (i.e. for all dipoles in V_s^{ex}), and then with respect to j (i.e. for all dipoles in V_q^{ex}), and using (1.9), we find that the

velocity potentials in any two layers $V_q^{\rm ex}$ and $V_s^{\rm ex}$ are connected as follows:

$$k_0^2\zeta_0\left(\sum_{j=1}^{n_q}\overline{A_{q,j}}\phi_s^q(\mathbf{r}_{q,j})+\sum_{\nu=1}^{n_s}A_{s,\nu}\overline{\phi_q^s(\mathbf{r}_{s,\nu})}\right)= \frac{1}{2\pi}\int_{S^2}\overline{g_q(\hat{\mathbf{r}})}g_s(\hat{\mathbf{r}})\mathrm{d}s(\hat{\mathbf{r}}). \tag{1.83}$$

On the other hand, by Theorem 4 of [59], we find that for every two individual secondary fields of $V_q^{\rm ex}$, due to sources at $\mathbf{r}_{q,j}$ and $\mathbf{r}_{q,\nu}$, holds

$$k_0^2\zeta_0\left(\overline{A_{q,j}}\phi_{q,\nu}^{\rm sec}(\mathbf{r}_{q,j})+A_{q,\nu}\overline{\phi_{q,j}^{\rm sec}(\mathbf{r}_{q,\nu})}+ \frac{2}{\zeta_q}\overline{A_{q,j}}A_{q,\nu}\mathrm{sinc}(k_q|\mathbf{r}_{q,j}-\mathbf{r}_{q,\nu}|)\right)= \frac{1}{2\pi}\int_{S^2}\overline{g_{q,j}(\hat{\mathbf{r}})}g_{q,\nu}(\hat{\mathbf{r}})\mathrm{d}s(\hat{\mathbf{r}}). \tag{1.84}$$

Using the definition (1.27) of σ_q, and summing (1.84) for all $\nu, j = 1,\ldots,n_q$, we obtain

$$\sigma_q = 4\pi\zeta_0\mathrm{Re}\left(\sum_{j=1}^{n_q}\overline{A_{q,j}}\phi_q^{\rm sec}(\mathbf{r}_{q,j})\right)+\frac{\zeta_0}{\zeta_q}\sigma_q^{\rm pr}. \tag{1.85}$$

Summing (1.83) for both indices q, s by implementation of (1.85) for $V_q^{\rm ex}\equiv V_s^{\rm ex}$ and taking into account definition (1.28) of σ relation (1.79) is obtained. Adapting Theorem 5 of [59] to the present formulation, we arrive at

$$\sigma_{q,j} = 4\pi\zeta_0\mathrm{Re}\left(\overline{A_{q,j}}\phi_{q,j}^{\rm sec}(\mathbf{r}_{q,j})\right)+\frac{\zeta_0}{\zeta_q}\sigma_{q,j}^{\rm pr}. \tag{1.86}$$

Equation (1.80) is derived by (1.85) and (1.86) after considering the definitions (1.29) and (1.70). A summation of (1.85) for all $q = 1,\ldots,Q$ with the help of (1.79) and the definition (1.30), derives (1.81).

□

Remark 1.3.5 *The corresponding formula for $\sigma^{\rm T}$ can be obtained by (3.14), (1.80), and (1.81).*

1.3.2 Physical Bounds on Interaction Scattering Cross Sections

In this section, physical bounds for the ratios of ISCS over the corresponding scattering cross sections are established. The ISCS ratios are a key factor in determining the additivity of the scattering cross sections. Then, the behaviors of these ratios as the multitude N of the point sources increases, is investigated.

Theorem 1.3.6 *The total ISCS, σ^{T}, satisfies*

$$1 - N\frac{\sigma^{\max}}{\sigma} \leq \frac{\sigma^{\mathrm{T}}}{\sigma} \leq \min\left\{1 - N\frac{\sigma^{\min}}{\sigma}, 1 - \frac{1}{N}\right\}, \tag{1.87}$$

where $\sigma^{\min}$ and $\sigma^{\max}$ are the minimum and maximum individual cross sections of all sources. For

$$N^2\sigma^{\min} \leq \sigma, \tag{1.88}$$

the minimum involved in (1.87) is $1 - \frac{1}{N}$.

Proof. For $\sigma^{\min}$ and $\sigma^{\max}$, we have

$$-N\sigma^{\max} \leq -\sum_{j=1}^{N}\sigma^j \leq -N\sigma^{\min}, \tag{1.89}$$

with σ^j the individual scattering cross section due to a dipole at $\mathbf{r}^j$. Then, by (1.31), we get

$$1 - N\frac{\sigma^{\max}}{\sigma} \leq \frac{\sigma^{\mathrm{T}}}{\sigma} \leq 1 - N\frac{\sigma^{\min}}{\sigma}. \tag{1.90}$$

By the definition (1.28) of the overall cross section, we find

$$\sigma \leq \frac{1}{k_0^2}\left[\sum_{j=1}^{N}\int_{S^2}|g^j(\hat{\mathbf{r}})|^2\mathrm{d}s(\hat{\mathbf{r}})\right] + \frac{2}{k_0^2}\left[\sum_{j=1}^{N-1}\sum_{\nu=j+1}^{N}\left|\int_{S^2}g^j(\hat{\mathbf{r}})\overline{g^{\nu}(\hat{\mathbf{r}})}\mathrm{d}s(\hat{\mathbf{r}})\right|\right]. \tag{1.91}$$

By Hölder's inequality, the last relation takes the form

$$\sigma \leq \sum_{j=1}^{N} \sigma^j + 2 \sum_{j=1}^{N-1} \sum_{\nu=j+1}^{N} \left(\sigma^j\right)^{1/2} \left(\sigma^\nu\right)^{1/2}. \tag{1.92}$$

Since

$$2\left(\sigma^j\right)^{1/2} \left(\sigma^\nu\right)^{1/2} \leq \sigma^j + \sigma^\nu, \tag{1.93}$$

from (1.92), we have

$$\sigma \leq \sum_{j=1}^{N} \sigma^j + \sum_{j=1}^{N-1} \sigma^j (N-j) + \sum_{j=2}^{N} \sigma^j (j-1) = N \sum_{j=1}^{N} \sigma^j. \tag{1.94}$$

The last inequality in conjunction with the definition (1.31) imply that

$$\frac{\sigma^{\mathrm{T}}}{\sigma} \leq 1 - \frac{1}{N}. \tag{1.95}$$

Eq. (1.87) is derived from (1.90) and (1.95). Implication (1.88) is obvious.

□

Moreover, since $\sigma^j \leq \sigma^{\max}$, for $j = 1, \ldots, N$, Eq. (1.92) implies

$$\sigma \leq N\sigma^{\max} + 2 \sum_{j=1}^{N-1} \sum_{\nu=j+1}^{N} \sigma^{\max} = N^2 \sigma^{\max}. \tag{1.96}$$

By combining (1.96) with (1.88), we verify the following

Corollary 1.3.7 *Condition (1.88) holds if and only if*

$$\sqrt{\frac{\sigma}{\sigma^{\max}}} \leq N \leq \sqrt{\frac{\sigma}{\sigma^{\min}}}. \tag{1.97}$$

Remark 1.3.8 *Inequalities similar to (1.87) and (1.97) can be proved in the same way for the number n_q of the dipoles inside an excitation layer V_q^{ex} and the ratio of the corresponding q-interaction cross section $\tilde{\sigma}_q$ over the q-excitation cross section σ_q as well as for the number Q of excitation layers and the ratio of the corresponding indirect ISCS σ^{I} over the overall cross section σ; see [64]. Additionally, we note that if each layer contains only one point source, then $\tilde{\sigma}_q = 0$, whereas if there is only one excitation layer, then $\sigma^{\mathrm{I}} = 0$.*

Remark 1.3.9 *If inequality (1.88) is reversed, then the upper bound of Corollary 1.3.7, becomes a lower bound for N.*

1.3.3 Large-N Behavior of Scattering Cross-Sections Ratios

Our main tool for investigating the large-N behavior of the ISCS ratios is provided from the physical bounds indicated by Theorem 1.3.6. First we define in a rigorous way the ratios of the individual cross sections and the total ISCS the overall cross section, respectively, as

$$R_N^j = \sigma_N^j/\sigma_N, \;\; j = 1, \ldots, N, \quad \text{and} \quad R_N^{\mathrm{T}} = \sigma_N^{\mathrm{T}}/\sigma_N, \tag{1.98}$$

The subscript N is included in all the involved cross sections for clarity. The minimum and maximum ratios R_N^j, for each N, are denoted by $R_N^{\min}$ and $R_N^{\max}$. By (1.31), we have

$$R_N^{\mathrm{T}} + \sum_{j=1}^{N} R_N^j = 1. \tag{1.99}$$

When $\sigma_N^{\mathrm{T}} > 0$, then $R_N^j \in (0, 1)$. The positive sign of σ_N^{T} accounts for the case where the interactions between fields in excitation layers accelerate the flow of active intensity. Taking under consideration the physical interpretation of the energy conservation law (1.63), we conclude that in such a case, the active intensity is directed towards the excitation layer. When a new source is placed sufficiently close to a group of existing N sources, the individual cross sections remain the same, but the ISCS will - in general - change. This fact can be explained by the physical meaning of the non-linear nature of the ISCS: The total ISCS $\sigma_{N+1}^{\mathrm{T}}$ for $N+1$ sources is the total ISCS σ_N^{T} for N sources plus the ISCS that is induced by the interaction of the new source with the existing N sources, i.e.

$$\sigma_{N+1}^{\mathrm{T}} = \sigma_N^{\mathrm{T}} + \sum_{j=1}^{N} \tilde{\sigma}_{N+1,j} \tag{1.100}$$

with

$$\tilde{\sigma}_{N+1,j} = \frac{2}{k_0^2} \mathrm{Re} \int_{S^2} g^{N+1}(\hat{\mathbf{r}}) \overline{g^j(\hat{\mathbf{r}})} \mathrm{d}s(\hat{\mathbf{r}})$$

We will show that under certain conditions, the cross-section ratios approach limiting values when N exceeds a certain threshold N_0. Below, $R_N^j \to 0$, for $N \to \infty$, is used to describe that $\sigma_N^j << \sigma_N$, for $N > N_0$. Similarly, $R_N^{\mathrm{T}} \to 1$, for $N \to \infty$, refers to that $\sigma_N^{\mathrm{T}} \simeq \sigma_N$, for $N > N_0$. The use of ratios instead of the actual values is justified by the fact that actual values change with each new added source. Total ISCS values might not stabilize as we keep adding new sources, but their ratios, in some cases, are stabilized. The following corollary presents certain consequences of (1.87) that connect the sign of the total ISCS with the behavior of specific individual cross sections.

Corollary 1.3.10 *If $\sigma_N^{\mathrm{T}} > 0$, for $N \geq N_0$, with N_0 a certain number of sources, then*

$$R_N^{\min} \to 0, \quad for \quad N \to \infty. \tag{1.101}$$

If $\sigma_N^{\mathrm{T}} < 0$ for a fixed number N of sources, then

$$R_N^{\max} > \frac{1}{N}. \tag{1.102}$$

If $R_N^{\min} > \frac{1}{N}$ for a fixed number N of sources, then

$$\sigma_N^{\mathrm{T}} < 0. \tag{1.103}$$

If $1 - R_{N(\delta)}^{\mathrm{T}} = \delta$, for a fixed $\delta > 0$ and a number $N(\delta)$ of sources, then

$$N(\delta) > \frac{1}{\delta}. \tag{1.104}$$

□

Remark 1.3.11 *The first three relations connect the sign of the total ISCS with the contribution of individual cross sections. The last relation however, connects the number of sources with the "distance" δ between total ISCS and the overall scattering cross section. In particular, implies that each total ISCS ratio has a corresponding minimum number of sources required for its appearance.*

Next, we show that even if the maximum cross section ratio increases with N, there is an upper bound depending on the maximum individual cross section ratio for a certain N_0.

Theorem 1.3.12 *If there is a number N_0 of sources such that $R_N^{\max}$ increases for all $N \geq N_0$, and $\sigma_N^{\mathrm{T}} > 0$ for all $N \geq N_0$, then*

$$R_N^{\max} \to a R_{N_0}^{\max}, \quad for \quad N \to \infty, \tag{1.105}$$

where $a \in [1, N_0^2]$, and $R_{N_0}^{\max}$ is the maximum cross section ratio for N_0 sources.

Proof. Our hypothesis implies that

$$R_{N+1}^{\max} = a_N \, R_N^{\max}, \quad N \geq N_0 \tag{1.106}$$

with $a_N > 1$. A successive implementation of (1.106) for $k = N_0, N_0 + 1, \ldots, N + 1$ yields

$$R_{N+1}^{\max} = \left(\prod_{k=N_0}^{N} a_k \right) R_{N_0}^{\max}. \tag{1.107}$$

Eq. (1.99), for $\sigma_N^{\mathrm{T}} > 0$, implies that $R_{N+1}^{\max} \leq 1$. This fact in conjunction with (1.107) leads to

$$\prod_{k=N_0}^{N} a_k \leq \frac{1}{R_{N_0}^{\max}}. \tag{1.108}$$

Thus, sequence $\prod_{k=N_0}^{N} a_k$ is increasing and upper bounded, and, therefore, convergent. Let a be its limit. Evidently, it holds $a \geq 1$. Relation (1.105) is obtained by combining (1.107) and (1.108). The fact that $a \leq N_0^2$ stems from (1.96) and (1.108). The above proof holds even for $a = 1$, which corresponds to the case where $R_N^{\max}$ is constant after N_0 sources.

□

Remark 1.3.13 *The maximum individual cross section ratio $R_N^{\max}$ can increase with N, when we add a "stronger" source than the existing ones. Theorem 1.3.12 states that even then, $R_N^{\max}$ will eventually be stabilized, if the number N_0 of sources exceeds a certain threshold.*

Finally, relation (1.87) can be used to extract a set of conditions regarding the approximation of the overall cross section by the total ISCS. In particular, the following conditions hold:

Corollary 1.3.14 ***Condition 1*** *If for the maximum individual cross section ratio there exists an N_0, such that*

$$R_N^{\max} < \frac{1}{N} \tag{1.109}$$

for all N with $N \geq N_0$, then

$$R_N^{\mathrm{T}} \to 1, \quad as \quad N \to \infty. \tag{1.110}$$

Condition 2 *The following assertions are equivalent*

$$R_N^{\mathrm{T}} \to 1, \quad \text{for} \quad N \to \infty \tag{1.111}$$

$$R_N^j \to 0, \quad \text{for} \quad N \to \infty, \quad \text{with} \quad j = 1, \ldots, N. \tag{1.112}$$

□

Remark 1.3.15 *Results for the ratios of $\tilde{\sigma}_q$ and σ^{I} corresponding to those of Corollary 1.3.14 can be readily obtained by replacing N with n_q and Q, respectively.*

Chapter 2

The Layered Sphere Excited by N Point Sources

2.1 Geometry Setting

We consider a spherical scatterer of radius a_1, divided into P nested, concentric spherical layers V_p $(p = 1, \ldots, P)$ by $P - 1$ spherical surfaces S_p, each of radius a_p $(p = 2, \ldots, P)$; see Fig. 5.1. Each layer V_p, defined by $a_{p+1} < r < a_p$, is characterized by wavenumbers k_p, mass densities ρ_p and mean compressibilities γ_p for $(p = 1, \ldots, P - 1)$. The exterior V_0 of the scatterer has wavenumber k_0 and mass density ρ_0. Of all P layers of the scatterer, Q of them, with $Q \leq P + 1$, host N point sources arbitrarily located at $\mathbf{r}_{q,j} \in V_q$ for $j = 1, \ldots, n_q$ and $q = 1, \ldots, Q$ with n_q the sources contained in excitation layer V_q. These point sources emanate spherical waves, with their *individual primary fields* given by (1.7). On the boundaries of each layer V_p, all total individual and overall fields satisfy for $p = 1, \ldots, P - 1$ the transmission boundary conditions:

$$u^{p-1}(\mathbf{r}) = u_p^{\mathrm{t}}(\mathbf{r}), \qquad r = a_p \tag{2.1}$$

$$\frac{\partial \phi^{p-1}(\mathbf{r})}{\partial n} = \frac{\partial \phi^{p}(\mathbf{r})}{\partial n}, \qquad r = a_p. \tag{2.2}$$

Evidently, the overall field of V_0 will also satisfy the Sommerfeld's radiation condition. The medium's core V_P can be soft, hard, resistive or penetrable.

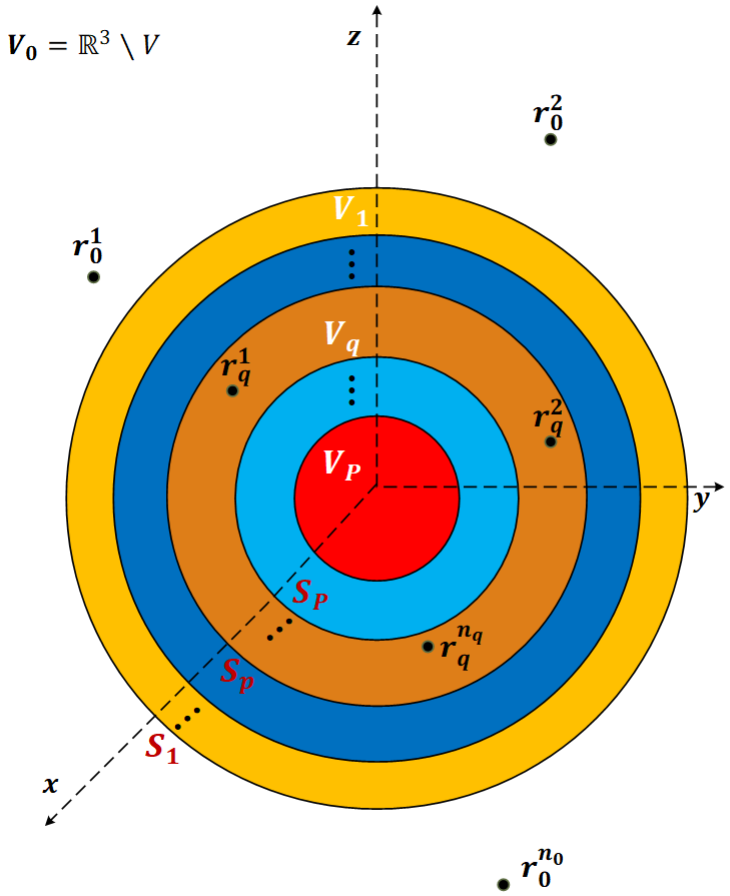

Figure 2.1: Layered spherical medium excited by N arbitrarily-located point sources

For a soft, hard or resistive core, the respective boundary conditions are

$$u^{P-1}(\mathbf{r}) = 0, \qquad r = a_P \tag{2.3}$$

$$\frac{\partial \phi^{P-1}(\mathbf{r})}{\partial n} = 0, \qquad r = a_P, \tag{2.4}$$

$$\frac{\partial \phi^{P-1}(\mathbf{r})}{\partial n} + \frac{u^{P-1}(\mathbf{r})}{Z_{P-1}} = 0 \qquad r = a_P. \tag{2.5}$$

whereas for a penetrable core, conditions (5.3)-(5.4) hold for V_P as well.

2.2 Excitation Operators and Observation Functions

We choose a spherical coordinate system (r, θ, ϕ) with the sphere's center O at the origin. Then, the position vector of each point source will be given by

$$\mathbf{r}_{q,j} = r_{q,j}\hat{\mathbf{r}} + \theta_{q,j}\hat{\boldsymbol{\theta}} + \phi_{q,j}\hat{\boldsymbol{\phi}}$$

with $r_{q,j} \in (a_{q+1}, a_q)$, $\theta_{q,j} \in [0, \pi]$ and $\phi_{q,j} \in [0, 2\pi)$ for $j = 1, \ldots, n_q$. The individual primary fields have the following expansion [67]

$$u^{\mathrm{pr}}_{q,j}(\mathbf{r}) = 4\pi \mathrm{i} k_q A_{q,j} \begin{cases} \sum_{n,m}(-1)^m Y_n^{-m}(\hat{\mathbf{r}}_{q,j}) Y_n^m(\hat{\mathbf{r}}) \times \\ h_n(k_q r) j_n(k_q r_{q,j}), \qquad r > r_{q,j} \\ \sum_{n,m}(-1)^m Y_n^{m}(\hat{\mathbf{r}}_{q,j}) Y_n^{-m}(\hat{\mathbf{r}}) \times \\ j_n(k_q r) h_n(k_q r_{q,j}), \qquad r < r_{q,j}, \end{cases} \tag{2.6}$$

with

$$\sum_{n,m} \equiv \sum_{n=0}^{\infty} \sum_{m=-n}^{m=n}$$

On the other hand, the individual secondary fields in V_p can be expanded as

$$u^{p}_{q,j}(\mathbf{r}) = 4\pi \mathrm{i} k_q A_{q,j} \sum_{n,m} (-1)^m Y_n^{-m}(\hat{\mathbf{r}}_{q,j}) Y_n^m(\hat{\mathbf{r}}) \times \\ h_n(k_q r_{q,j}) \left(a^{n,p}_{q,j} j_n(k_p r) + b^{n,p}_{q,j} h_n(k_p r) \right) \tag{2.7}$$

with j_n and h_n denoting the n-th order spherical Bessel and Hankel functions, while Y_n^m, Y_n^{-m} denote the spherical harmonic functions.

To simplify the expressions of the fields involved, in a way that will reduce the anticipated workload, we first define the following *observation functions* of V_p:

$$\mathscr{J}^{p}_{n,m}(\mathbf{r}) = Y_n^m(\hat{\mathbf{r}}) j_n(k_p r) \tag{2.8}$$

$$\mathscr{H}^{p}_{n,m}(\mathbf{r}) = Y_n^m(\hat{\mathbf{r}}) h_n(k_p r) \tag{2.9}$$

Using the observation function of excitation layer V_q we define the following

q-excitation vector of V_q:

$$\mathbf{j}_{n,m,q} = (-1)^m \mathrm{i}k_q \left(A_{q,1}\mathscr{J}^q_{n,-m}(\mathbf{r}_{q,1}), \ldots, A_{q,n_q}\mathscr{J}^q_{n,-m}(\mathbf{r}_{q,n_q})\right) \tag{2.10}$$

$$\mathbf{h}_{n,m,q} = (-1)^m \mathrm{i}k_q \left(A_{q,1}\mathscr{H}^q_{n,-m}(\mathbf{r}_{q,1}), \ldots, A_{q,n_q}\mathscr{H}^q_{n,-m}(\mathbf{r}_{q,n_q})\right) \tag{2.11}$$

Finally, we define the *q-excitation operators* which constitute our basic tool:

$$\mathcal{J}_{n,m,q}(\mathbf{x}_q) = \mathbf{j}_{n,m,q} \cdot \mathbf{x}_q = \mathrm{i}k_q A_{q,j} \sum_{j=1}^{n_q} (-1)^m Y_n^{-m}(\hat{\mathbf{r}}_{q,j}) j_n(k_q r_{q,j}) x_{q,j} \tag{2.12}$$

$$\mathcal{H}_{n,m,q}(\mathbf{x}_q) = \mathbf{h}_{n,m,q} \cdot \mathbf{x}_q = \mathrm{i}k_q A_{q,j} \sum_{j=1}^{n_q} (-1)^m Y_n^{-m}(\hat{\mathbf{r}}_{q,j}) h_n(k_q r_{q,j}) x_{q,j} \tag{2.13}$$

with $\mathbf{x}_q = (x_{q,1}, \ldots, x_{q,n_q}) \in \mathbb{C}^{n_q}$and $\mathcal{J}, \mathcal{H} : \mathbb{C}^3 \to \mathbb{C}$.

Excitation operators contain the information about the point source distribution, since each of their terms is related to a specific point source. In particular, every term is a product of a spherical harmonic that contains the information about the angle and azimuth of the point source, with a spherical Bessel or Hankel function that contains the information about the distance and the layer enclosing the point source.

The unknown scattering coefficients of the overall fields can be expressed in a closed form with the help of the excitation operators as follows

$$\mathcal{A}^p_{n,m,q} = \mathcal{H}_{n,m,q}(\mathbf{a}^{n,p}_q) = \mathbf{h}_{n,m,q} \cdot \mathbf{a}^{n,p}_q \tag{2.14}$$

$$\mathcal{B}^p_{n,m,q} = \mathcal{H}_{n,m,q}(\mathbf{b}^{n,p}_q) = \mathbf{h}_{n,m,q} \cdot \mathbf{b}^{n,p}_q \tag{2.15}$$

with $\mathbf{a}^{n,p}_q = (a^{n,p}_{q,1}, \ldots, a^{n,p}_{q,n_q})$ and $\mathbf{b}^{n,p}_q = (b^{n,p}_{q,1}, \ldots, b^{n,p}_{q,n_q})$ denoting the vectors containing the scattering coefficients of individual fields. By utilizing excitation operators we see that the q-excitation secondary field of V_p and the overall secondary field of V_p take, respectively, the following form:

$$u^p_q(\mathbf{r}) = \sum_{n,m} \left(\mathscr{J}^p_{n,m}(\mathbf{r})\mathcal{A}^p_{n,m,q} + \mathscr{H}^p_{n,m}(\mathbf{r})\mathcal{B}^p_{n,m,q}\right) \tag{2.16}$$

$$u^p(\mathbf{r}) = \sum_{n,m} \left(\mathscr{J}^p_{n,m}(\mathbf{r})\mathcal{A}^p_{n,m} + \mathscr{H}^p_{n,m}(\mathbf{r})\mathcal{B}^p_{n,m}\right) \tag{2.17}$$

with $\mathcal{X}^p_{n,m} = \sum_{q=1}^{Q} \mathcal{X}^p_{n,m,q}$ for $\mathcal{X} \in \{\mathcal{A}, \mathcal{B}\}$. The q-excitation primary field of V_q takes the following form:

$$u_q^{\mathrm{pr}}(\mathbf{r}) = 4\pi \begin{cases} \sum_{n,m} \mathscr{H}^q_{n,m}(\mathbf{r}) \mathcal{J}_{n,m,q}(\mathbf{u}_q), & r > \max\{r_{q,1}, \ldots, r_{q,n_q}\} \\ \sum_{n,m} \mathscr{J}^q_{n,-m}(\mathbf{r}) \mathcal{H}_{n,m,q}(\mathbf{u}_q), & r < \min\{r_{q,1}, \ldots, r_{q,n_q}\} \end{cases} \tag{2.18}$$

with $\mathbf{u}_q$ denoting vector $(1, 1, \ldots, 1)$ of $\mathbb{R}^{n_q}$. In the single-layer excitation case, i.e. $Q = 1$ we note that q-excitation fields coincide with the overall fields.

2.3 Solution of the Direct Problem

To facilitate the text flow we will suppose that the outermost excitation layer is the layer V_q, with $q \geq 0$. We impose the transmission boundary conditions on the surface V_1, i.e. for $r = a_1$ and by taking into account the orthogonality of the spherical harmonics, we readily arrive at:

$$\begin{bmatrix} \mathcal{A}^1_{n,m} \\ \mathcal{B}^1_{n,m} \end{bmatrix} = \mathbf{T}^1_n \cdot \begin{bmatrix} 0 \\ \mathcal{B}^0_{n,m} \end{bmatrix} \tag{2.19}$$

where $\mathbf{T}^1_n$ denotes *transition matrix* from the exterior V_0 to layer V_1. In general, with $\mathbf{T}^p_n$ we will denote the *transition matrix* from layer V_{p-1} to layer V_p. The exact form of the matrix is given in [59]. We will re-write here for convenience with the help of functional $\mathcal{T}_p$:

$$\mathbf{T}^p_n = -\mathrm{i}x_p^2 \begin{bmatrix} \mathcal{T}_p(h_n, j_n) & \mathcal{T}_p(h_n, h_n) \\ -\mathcal{T}_p(j_n, j_n) & -\mathcal{T}_p(j_n, h_n) \end{bmatrix}$$

Functional $\mathcal{T}_p : \mathbb{C}^3 \to \mathbb{C}$ is defined as:

$$\mathcal{T}_p(f, g)(x_p, y_p) = f'(x_p)g(y_p) - w_p f(x_p)g'(y_p)$$

The quantities x_p, y_p, w_p depend solely on the physical parameters of the scatterer, i.e.

$$x_p = k_p a_p, \quad y_p = k_{p-1} a_p, \quad w_p = \frac{k_{p-1}\rho_p}{k_p \rho_{p-1}} = \frac{\varrho_p}{\eta_p}$$

with η_p the relative refractive index of V_p and ϱ_p the relative mass density index of V_p.

Keeping in mind that in every layer V_p the spherical harmonics consitute a complete orthonormal system, a successive implementation of the boundary conditions in the surfaces S_p, i.e. $r = a_p$ for $p = 2, \ldots, q_1$ leads to the following relation:

$$\begin{bmatrix} \mathcal{A}_{n,m}^{q-1} \\ \mathcal{B}_{n,m}^{q-1} \end{bmatrix} = \mathbf{T}_n^{(0\to q-1)} \cdot \begin{bmatrix} 0 \\ \mathcal{B}_{n,m}^{0} \end{bmatrix}, \tag{2.20}$$

with $\mathbf{T}_n^{(0\to q-1)}$ denoting the transition matrix from the exterior V_0 to layer V_{q-1}. In general, with $\mathbf{T}_n^{(0\to p)}$ we will denote the transition matrix from the exterior V_0 to layer V_p, which is given by

$$\mathbf{T}_n^{(0\to p)} = \mathbf{T}_n^p \, \mathbf{T}_n^{p-1} \ldots \mathbf{T}_n^1$$

Implementing boundary conditions in the "outer" surface S_q of the outermost excitation layer V_q, in conjunction with (2.20) yields:

$$\begin{bmatrix} \mathcal{A}_{n,m}^{q} \\ \mathcal{B}_{n,m}^{q} + \mathcal{J}_{n,m,q}(\mathbf{u}_q) \end{bmatrix} = \mathbf{T}_n^{(0\to q)} \cdot \begin{bmatrix} 0 \\ \mathcal{B}_{n,m}^{0} \end{bmatrix}. \tag{2.21}$$

On the other hand, transmission boundary conditions at the "inner" surface S_{q+1} of the outermost excitation layer V_q lead to:

$$\begin{bmatrix} \mathcal{A}_{n,m}^{q+1} \\ \mathcal{B}_{n,m}^{q+1} \end{bmatrix} = \mathbf{T}_n^{q+1} \cdot \begin{bmatrix} \mathcal{A}_{n,m}^{q} + \mathcal{H}_{n,m,q}(\mathbf{u}_q) \\ \mathcal{B}_{n,m}^{q} \end{bmatrix} \tag{2.22}$$

A combination of (2.21) and (2.22) results in the following relation:

$$\begin{bmatrix} \mathcal{A}_{n,m}^{q+1} \\ \mathcal{B}_{n,m}^{q+1} \end{bmatrix} = \mathbf{T}_n^{(0\to q+1)} \cdot \begin{bmatrix} 0 \\ \mathcal{B}_{n,m}^{0} \end{bmatrix} + \mathbf{T}_n^{q+1} \cdot \begin{bmatrix} \mathcal{H}_{n,m,q}(\mathbf{u}_q) \\ -\mathcal{J}_{n,m,q}(\mathbf{u}_q) \end{bmatrix} \tag{2.23}$$

Now, let V_s be the next (closer to V_q) excitation layer. Then all layers V_p for $p = q+1, \ldots, s-1$ do not contain sources. Thus, a successive implementation of the boundary conditions in surfaces $S_{q+2}, \ldots, S_s$, yields the following:

$$\begin{bmatrix} \mathcal{A}_{n,m}^{s} \\ \mathcal{B}_{n,m}^{s} + \mathcal{J}_{n,m,s}(\mathbf{u}_s) \end{bmatrix} = \mathbf{T}_n^{(q\to s)} \cdot \begin{bmatrix} \mathcal{A}_{n,m}^{q+1} \\ \mathcal{B}_{n,m}^{q+1} \end{bmatrix} \tag{2.24}$$

with $\mathbf{T}_n^{(q\to s)}$ denoting the transition matrix from layer V_q to layer V_s.

In general, the transition matrices satisfy the following relations:

$$\mathbf{T}_n^{(q\to q)} = \mathbb{I}_2 \tag{2.25}$$

$$\mathbf{T}_n^{(q-1\to q)} = \mathbf{T}_n^q \tag{2.26}$$

$$\mathbf{T}_n^{(q\to s)} = [\mathbf{T}_n^{(s\to q)}]^{-1} \tag{2.27}$$

$$\mathbf{T}_n^{(q\to s)} = \mathbf{T}_n^{(p\to s)} \cdot \mathbf{T}_n^{(q\to p)} \tag{2.28}$$

with $\mathbb{I}_2$ denoting the 2×2 unit matrix.

To continue with the solution of the direct problem, by imposing the boundary conditions in the "inner" surface S_{s+1} of excitation layer V_s we arrive at:

$$\begin{bmatrix} \mathcal{A}_{n,m}^{s+1} \\ \mathcal{B}_{n,m}^{s+1} \end{bmatrix} = \mathbf{T}_n^{s+1} \cdot \begin{bmatrix} \mathcal{A}_{n,m}^{s} + \mathcal{H}_{n,m,s}(\mathbf{u}_s) \\ \mathcal{B}_{n,m}^{s} \end{bmatrix} \tag{2.29}$$

If we combine (2.24),(2.29) with (2.23), we obtain:

$$\begin{bmatrix} \mathcal{A}_{n,m}^{s+1} \\ \mathcal{B}_{n,m}^{s+1} \end{bmatrix} = \mathbf{T}_n^{(0\to s+1)} \cdot \begin{bmatrix} 0 \\ \mathcal{B}_{n,m}^{0} \end{bmatrix} + \mathbf{T}_n^{(q\to s)} \cdot \begin{bmatrix} \mathcal{H}_{n,m,q}(\mathbf{u}_q) \\ -\mathcal{J}_{n,m,q}(\mathbf{u}_q) \end{bmatrix} + \mathbf{T}_n^{s+1} \cdot \begin{bmatrix} \mathcal{H}_{n,m,s}(\mathbf{u}_s) \\ -\mathcal{J}_{n,m,s}(\mathbf{u}_s) \end{bmatrix} \tag{2.30}$$

Implementing the preceded procedure for all excitation layers V_q^{ex} we obtain:

$$\begin{bmatrix} \mathcal{A}_{n,m}^{P-1} \\ \mathcal{B}_{n,m}^{P-1} \end{bmatrix} = \mathbf{T}_n^{(0\to P-1)} \cdot \begin{bmatrix} 0 \\ \mathcal{B}_{n,m}^{0} \end{bmatrix} + \sum_{q=1}^{Q} \mathbf{T}_n^{(q\to P-1)} \cdot \begin{bmatrix} \mathcal{H}_{n,m,q}(\mathbf{u}_q) \\ -\mathcal{J}_{n,m,q}(\mathbf{u}_q) \end{bmatrix} \tag{2.31}$$

where q is used in reference to the V_q^{ex} layer.

Depending on the type of the core, we can extract the unknown coefficients of the overall secondary field. For a soft, hard or resistive core, we obtain

$$\mathcal{B}_{n,m}^{0} = \sum_{q=1}^{Q} \left(\frac{\Psi_{n,q}^{2}(k_q a_{q+1})}{\Psi_{n,0}^{2}(k_{P-1} a_P)} \mathcal{J}_{n,m,q}(\mathbf{u}_q) - \quad \frac{\Psi_{n,q}^{1}(k_q a_{q+1})}{\Psi_{n,0}^{2}(k_{P-1} a_P)} \mathcal{H}_{n,m,q}(\mathbf{u}_q) \right) \tag{2.32}$$

where $\Psi^i_{n,q}(x)$ with $i = 1, 2$ denotes the i component of the *q-boundary transition vector*

$$\mathbf{\Psi}_{n,q}(x) = \left(\mathbf{T}_n^{(q\to P-1)}\right)^{\mathrm{T}} \cdot \begin{bmatrix} f_n(x) \\ g_n(x) \end{bmatrix} \tag{2.33}$$

with $\left(\mathbf{T}_n^{(q\to P-1)}\right)^{\mathrm{T}}$ denote the transverse matrix of $\mathbf{T}_n^{(q\to P-1)}$. The exact form of f_n, g_n depends on the boundary conditions, e.g.

$$f_n(x) = \begin{cases} j_n(x), & \textit{soft} \quad \textit{core} \\ j_n^{'}(x), & \textit{hard} \quad \textit{core} \\ j_n^{'}(x) + \mathrm{i}\lambda j_n(x), & \textit{resistive} \quad \textit{core} \end{cases} \tag{2.34}$$

$$g_n(x) = \begin{cases} h_n(x), & \textit{soft} \quad \textit{core} \\ h_n^{'}(x), & \textit{hard} \quad \textit{core} \\ h_n^{'}(x) + \mathrm{i}\lambda h_n(x), & \textit{resistive} \quad \textit{core} \end{cases} \tag{2.35}$$

with λ given by (1.22). In the case of a penetrable core, the overall scattering coefficients of the external field are given by

$$\mathcal{B}^0_{n,m} = \sum_{q=1}^{Q} \left(\frac{T^{(q\to P)}_{22,n}}{T^{(0\to P)}_{22,n}} \mathcal{J}_{n,m,q}(\mathbf{u}_q) - \frac{T^{(q\to P)}_{21,n}}{T^{(0\to P)}_{22,n}} \mathcal{H}_{n,m,q}(\mathbf{u}_q) \right) \tag{2.36}$$

where $T^{(q\to P)}_{ij,n}$ denotes the ij element of transition matrix $\mathbf{T}_n^{(q\to P)}$. In the cases where the exterior V_0 or the core V_P of the scatterer contain point sources, formulas (2.32) and (2.36) hold as well by omitting the terms containing $\mathcal{J}_{n,m,0}$ and $\mathcal{H}_{n,m,P}$, respectively.

One of the advantages of using excitation operators, is that the coefficients for the individual secondary fields can be obtained directly from (2.32), (2.36) as follows for the soft, hard and resistive core

$$b^{n,0}_{q,j} = \frac{\Psi^2_n(k_q a_{q+1})}{\Psi^2_n(k_{P-1} a_P)} \mathcal{J}_{n,m,q}(\mathbf{w}_{q,j}) - \frac{\Psi^1_n(k_q a_{q+1})}{\Psi^2_n(k_{P-1} a_P)} \mathcal{H}_{n,m,q}(\mathbf{v}_{q,j}), \tag{2.37}$$

and for the penetrable core

$$b^{n,0}_{q,j} = \frac{T^{(q\to P)}_{22,n}}{T^{(0\to P)}_{22,n}} \mathcal{J}_{n,m,q}(\mathbf{w}_{q,j}) - \frac{T^{(q\to P)}_{21,n}}{T^{(0\to P)}_{22,n}} \mathcal{H}_{n,m,q}(\mathbf{v}_{q,j}), \tag{2.38}$$

with vectors $\mathbf{v}_{q,j}$, $\mathbf{w}_{q,j}$ given by

$$\mathbf{v}_{q,j} = \frac{\mathbf{e}_{q,j}}{A_{q,j}\mathscr{J}_{n,-m}(\mathbf{r}_{q,j})}, \quad \mathbf{w}_{q,j} = \frac{\mathbf{e}_{q,j}}{A_{q,j}\mathscr{H}_{n,-m}(\mathbf{r}_{q,j})}$$

with $\mathbf{e}_{q,j}$ for $j = 1, \ldots, n_q$, the vectors of the standard base of $\mathbb{R}^{n_q}$.

The expression for the overall far-field, $g(\hat{\mathbf{r}})$ is derived from (2.17). In particular, in V_0 the secondary fields must satisfy Sommerfeld radiation condition. Therefore for the external individual fields it holds $a_{q,j}^{n,0} = 0$ and subsequently, $\mathcal{A}_{n,m}^0 = 0$. Finally, by taking into account that $h_n(z) \simeq (-\mathrm{i})^n h_0(z)$ as $z \to \infty$ we arrive at the following expression for the overall far-field:

$$g(\hat{\mathbf{r}}) = 4\pi \sum_{n,m} (-1)^m (-\mathrm{i})^n Y_n^m(\hat{\mathbf{r}}) \mathcal{B}_{n,m}^0 \tag{2.39}$$

The expression for the overall scattering cross section σ is readily derived by considering that spherical harmonics consitute a complete orthonormal system in $L^2(S^2)$:

$$\sigma = \frac{4\pi}{k_0^2} \sum_{n,m} (2n+1) \frac{(n-m)!}{(n+m)!} \left|\mathcal{B}_{n,m}^0\right|^2 \tag{2.40}$$

Now we will address two special cases, that require a slightly different approach. Both of them have significant applications, as they are quite common in many real-life occasions: The case of *external excitation* where all sources lie in the exterior V_0 of the scatterer and the case of *core excitation* where all sources lie in the core V_P of the scatterer. For a soft, hard or resistive core the formula for the external excitation is:

$$\mathcal{B}_{n,m}^0 = -\frac{\Psi_{n,0}^1(k_{P-1}a_P)}{\Psi_{n,0}^2(k_{P-1}a_P)} \mathcal{H}_{n,m,0}(\mathbf{u}_0) \tag{2.41}$$

while for the penetrable core, we obtain:

$$\mathcal{B}_{n,m}^0 = \begin{cases} -\frac{T_{21,n}^{(0\to P)}}{T_{22,n}^{(0\to P)}} \mathcal{H}_{n,m,0}(\mathbf{u}_0), & \text{external excitation} \\ \frac{1}{T_{22,n}^{(0\to P)}} \mathcal{J}_{n,m,0}(\mathbf{u}_P), & \text{core excitation} \end{cases} \tag{2.42}$$

We note that for $N = 1$, equation (2.32) coincides with (11) of [67], while for $N = 1$ and $\theta_j = 0$, equation (2.36) reduces to (3.10) of [83].

2.4 Parametric Analysis

In this chapter, we present a parametric analysis for the behaviour of the ISCS and the corresponding cross section.

2.4.1 Single-Layer Excitation

The numerical results we present in this section, concern the case where a layered spherical scatterer V is excited by a distribution of point sources located in the sphere's exterior (*external excitation*) or in a specific layer (*internal excitation*). In particular, we considered the case where a 2-layered spherical scatterer V (i.e. $P = 2$) of external radius a_1 and core's radius a_2, is excited by either a source distribution lying in V_0 ($r > a_1$) or a source distribution lying in the spherical shell V_1 ($a_2 < r < a_1$). The core V_2 ($0 \leq r < a_2$) can soft, hard or penetrable. In most cases the sources lie on the z-axis.

In figure 2.2, we depict the variations of $\sigma^{\mathrm{T}}/\sigma$ versus $k_0 a_1$ for a distribution of $N = 4$ external point sources. We consider three dipole distributions with the dipoles' distances are given by: $r_j = (1.525 + 0.25j)a_1$, $r_j = (2.525 + 0.25j)a_1$, and $r_j = (3.525 + 0.25j)a_1$, with $j = 1, 2, 3, 4$. We notice that the ISCS ratios are oscillatory for higher frequencies when the sources lie closer to the sphere's boundary. However, the ratio remains within a 5% and a 4% margin in the hard and penetrable core case, respectively. As the sources move away from the scatterer, we notice that the oscillatory behavior remains, but the variation margin deteriorates and thus, the ISCS ratios for all examined frequencies achieve the upper bound $1 - \frac{1}{N} = 0.75$ of (4.45). In figure 2.3, we depict the ISCS ratios and their physical bounds indicated by (4.45) for a distribution of $N = 4$ point sources lying in the exterior V_0 of the sphere, at distances $r_j = (1.525 + 0.25j)a_1$, with $j = 1, 2, 3, 4$ from the sphere's origin. At first we notice that for both core types for $k_0 a_1 < 6$ the upper bound of (4.45) is $1 - 1/N$, which in turn implies that $\sigma_q^{\min} \leq \sigma/N^2$. Additionally, for all examined frequencies, the differences between the upper bound and the actual ISCS ratio are less than 1%. On the other hand, the differences

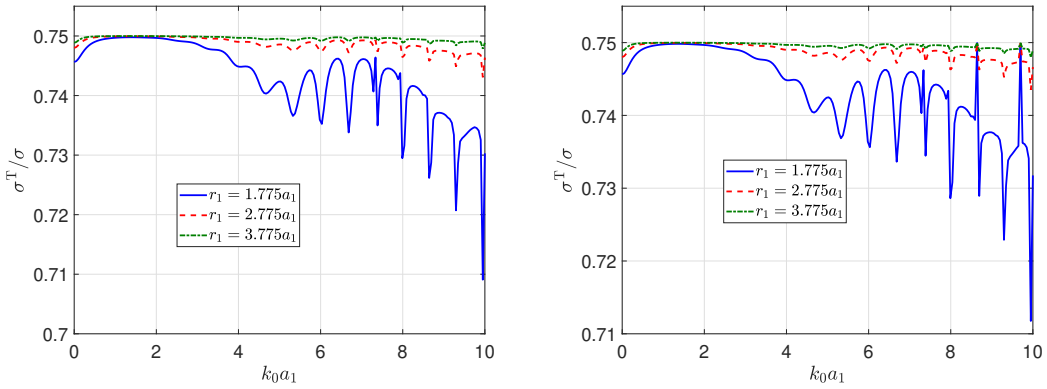

Figure 2.2: ISCS ratios $\sigma^{\mathrm{T}}/\sigma$ versus k_0a_1 for a spherical scatterer with $a_1 = 4a_2, \rho_1 = 2\rho_0, \eta_1 = 1.75\eta_0$ and a soft core (left panel) and penetrable core with $\rho_2 = 2.25\rho_2, \eta_2 = 2\eta_0$ (right panel). The scatterer is excited by three sets of $N = 4$ external sources with distances $0.25a_1$ between successive sources.

between the lower and the upper bounds of (4.45) do not exceed 4% while $k_0a_1 \geq 1$, and thus, the upper bound constitutes a more precise estimation for the ISCS ratio. On the other hand, in the low-frequency region we see that the q-ISCS ratios are close to the upper bound, whereas the difference with the lower bounds of (4.45) is substantial. This behaviour is explained by considering the minimum and maximum individual cross sections ratios over the q-excitation cross section. In the low-frequency region they differ substantially, e.g. for $k_0a_1 \leq 1$, the difference exceeds 2.5%, which leads to a 10% difference between the corresponding physical bounds. The ISCS

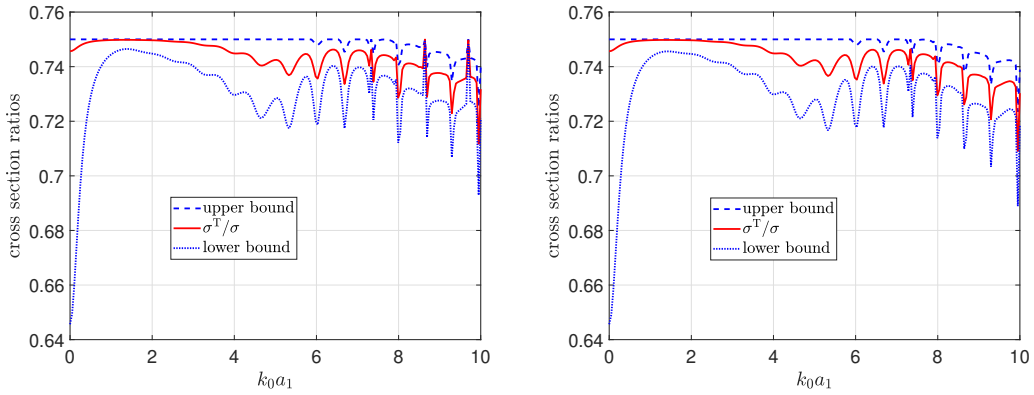

Figure 2.3: ISCS ratios $\sigma^{\mathrm{T}}/\sigma$ and their physical bounds versus k_0a_1 for the same sphere of figure 2.2

ratios for the case of $N = 4$ internal sources located at the z-axis are shown in Fig. 2.4. The sources are located $r_j = (0.25+0.05j)a_1$, with $j = 1, 2, 3, 4$ and we depict the variations of the ISCS ratio for the three core types. We notice for all core types a steep descent for the ISCS ratio in contrast to the external excitation case. Additionally, for the examined frequencies we observe that for lower frequencies, i.e. $k_0a_1 < 2.5$ the ratio does not differ substantially, whereas that changes for higher frequencies, where the penetrable core leads to smaller ISCS ratios. In figure 2.5 we demonstrate the

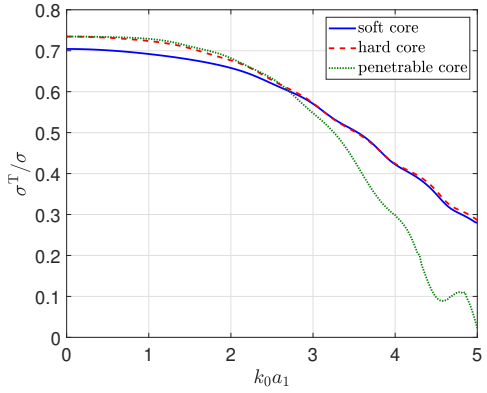

Figure 2.4: ISCS ratios $\sigma^{\mathrm{T}}/\sigma$ versus k_0a_1 for the same sphere of figure 2.2 for internal excitation by $N = 4$ point sources for a soft, hard or penetrable core.

accuracy of the physical bounds for the number N of dipoles that excite the spherical scatterer with a soft or a penetrable core. The source distribution is external, with the distance of each source from the sphere's region given by $r_j = (1.525 + 0.25j)a_1, j = 1, 2, 3, 4$. The similarity in the behavior of the physical bounds for both types of core is remarkable. Specifically, for $0.2 < k_0a_1 < 6$, the physical bounds are valid and determine accurately the number of dipoles exciting the scatterer. A very interesting observation - which have been observed in a variety of source distributions - is that in the higher frequencies ($k_0a_1 > 6$) it holds $N = [\sqrt{\sigma/\sigma^{\min}}] + 1$, where $[x]$ denotes the integer part of x. This is caused by the fact that the minimum and maximum individual cross sections do not differ substantially. We would also like to note that similar patterns with respect to the physical bounds and the estimation of the number of sources excit-

ing the sphere, have been found to be exhibited by even sparser or denser dipole distributions - as well as for the case where the sphere contains an acoustically hard core. In figure 2.6, the variations of the total ISCS $\sigma^{\mathrm{T}}/\sigma$

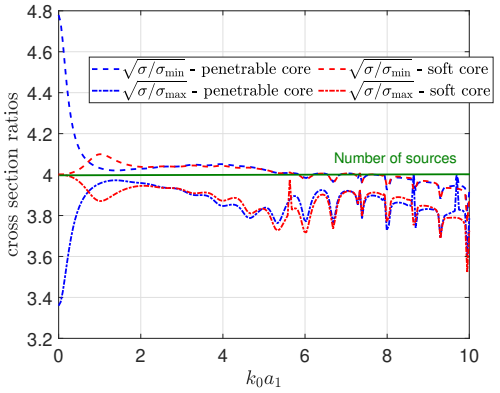

Figure 2.5: Physical bounds for the number N of sources exciting a 2-layered sphere with $a_1 = 4a_2$, $\rho_1 = 2\rho_0$, $\eta_1 = 1.75\eta_0$. The bounds for a soft core are depicted with red and the bounds for a penetrable core with blue. For the penetrable core, it also holds $\rho_2 = 2.25\rho_0$ and $\eta_2 = 2\eta_0$. The scatterer is excited by $N = 4$ external sources.

versus the relative mass density $\varrho_1 = \rho_1/\rho_0$ of the first spherical shell are depicted for two different k_0a_1, namely $k_0a_1 = 0.5$ and $k_0a_1 = 2.5$. The spherical scatterer has a penetrable core and is excited by $N = 4$ point sources located at $r_1 = (1.525 + 0.25j)a_1$ for $j = 1, 2, 3, 4$ on the z-axis of the scatterer's exterior. For the lower frequency, the total ISCS ratio seems to variate slightly more than the ISCS ratio of the higher frequency. In both cases however, the variation of the ISCS ratio as ϱ_1 increases, does not exceed 0.15% for $k_0a_1 = 0.5$ and 0.03% for $k_0a_1 = 2.5$. For both types of core, the total ISCS does not seem to oscillate, while its behaviour for a hard and penetrable core is quite similar. In particular, for the lower frequency is almost identical, while on the higher frequency for $\varrho_1 > 5$ the ISCS ratio on the hard core case seems to deviate from the corresponding ratio of the penetrable core. Similar patterns have been observed at both lower and higher frequencies, for different source distributions. In figure 2.7, we demonstrate the behavior of the values (left panel) and ratios (right panel) for the total ISCS, a source distribution consisting of $N = 4$ sources located at the first shell V_1 of the sphere, with a soft core V_2 of

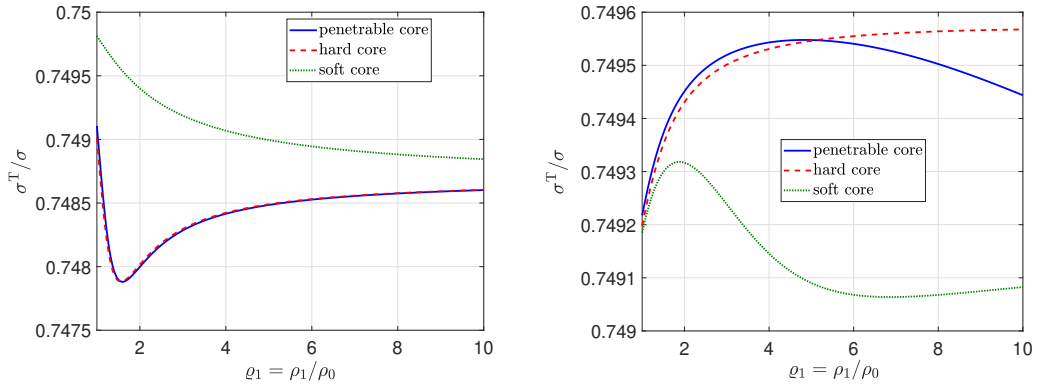

Figure 2.6: ISCS ratios $\sigma^{\mathrm{T}}/\sigma$ versus the relative mass density $\varrho_1 = \rho_1/\rho_0$ of a 2-layered spherical scatterer, with a penetrable core and $a_1 = 4a_2$, $\eta_1 = 1.75\eta_0, \eta_2 = 2\eta_0$ for two fixed frequencies $k_0a_1 = 0.5$ (left panel) or $k_0a_1 = 2.5$ (right panel). The scatterer is excited by $N = 4$ external sources.

radius $a_1 = 4a_2$ and parameters $\eta_1 = 1.75\eta_0, \rho_1 = 2\rho_0$. In the right subfigure, we consider three different placements for the source distribution. In the "core side" the sources are placed near the sphere's core at distances $r_j = (0.25 + 0.05j)a_1$ for $j = 1, 2, 3, 4$ from the sphere's origin. In the "middle side" the sources are placed at distances $r_j = (0.45 + 0.05j)a_1$ for $j = 1, 2, 3, 4$, while in the "boundary side" are placed at distances $r_j = (0.75 + 0.05j)a_1$ for $j = 1, 2, 3, 4$. We notice, that the "boundary side" placement leads to an oscillating behaviour for $k_0a_1 > 3$, while "core" and "middle" placements lead to smoother behaviours. In all cases, we observe a small variation in the ISCS ratios as k_0a_1 rises for all placements, which can be attributed to the dense nature of the distribution. Finally, in the bottom panel, we depict the variations of the ISCS values for the same setup of the upper right panel. As we observe, the similarity between the ISCS ratios is not a product of the similarity between the corresponding ISCS values. As we notice, the "boundary side" and "middle side" placements follow a similar, oscillatory pattern for $k_0a_1 > 2.5$, with the oscillations for the "boundary side" placement being steeper compared to the "middle side" placement. On the other hand, the "core side" placement follows a smooth, slightly ascending behaviour for all examined frequencies but with its values significantly smaller than the rest of the examined placements. For $k_0a_1 < 2.5$ all placements ascend smoothly, with

the "boundary side" placement having the greatest values and the "core side" placement having the lowest values. In figure 2.8, we compare the

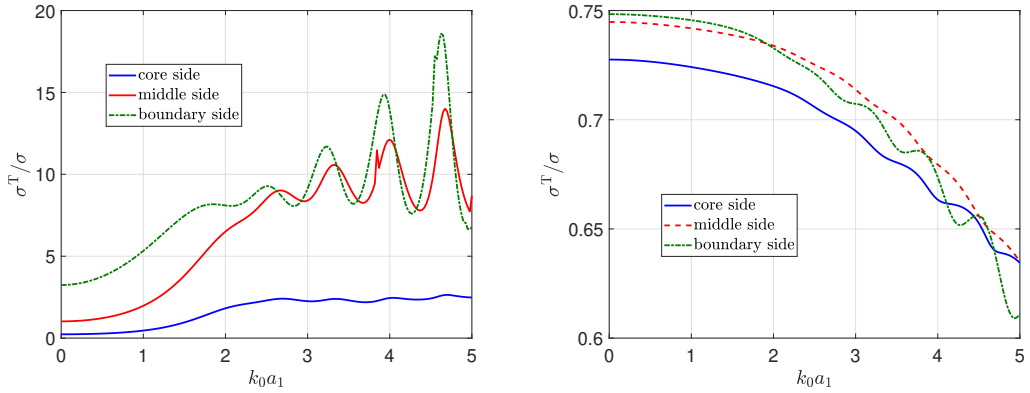

Figure 2.7: ISCS values (left panel) and ratios (right panel) for a 2-layered sphere with a soft core of radius $a_2 = a_1/4$. The sphere is excited by $N = 4$ sources lying in the first shell at three different placements: "core side", "middle side" and "boundary side".

behavior of the total ISCS ratio $\sigma^{\mathrm{T}}/\sigma$ versus the radius k_0a_1 for different core radii. The sphere in this case, has a penetrable core and is excited by a distribution of $N = 4$ external sources that lie in the exterior V_0 at locations $r_j = (1.525+0.25j)a_1$ for $j = 1, 2, 3, 4$. The sphere's mass densities are $\rho_1 = 2\rho_0, \rho_2 = 2.25\rho_0$ and the corresponding refractive indices are $\eta_1 = 1.75\eta_0, \eta_2 = 2\eta_0$. For all examined frequencies, we observe that for larger cores $a_2 = 0.9a_1, a_2 = 0.67a_1$ the ISCS ratio variates slightly as k_0a_1 ascends. For smaller cores, the ISCS ratio does not change significantly, but oscillates in a mild way. Finally, in figure 2.9 we depict the behavior of the total ISCS values for a spherical scatterer with a soft core for external excitation for different point source distributions. In particular the sources are located for $N = 5$ at distances $r_j = (0.25 + j)a_1$, for $j = 1, \ldots, 5$, for $N = 10$ at distances $r_j = (0.75 + j)a_1$, for $j = 1, \ldots, 10$, for $N = 20$ at distances $r_j = (1 + 0.25j)a_1$, for $j = 1, \ldots, 20$, for $N = 50$ at distances $r_J = (1.15 + 0.1j)a_1$, for $j = 1, \ldots, 50$. We notice that the ratios follow a descending pattern as k_0a_1 grows, with the oscillations occuring for greater frequencies. On the other hand, as the number N of sources grows - which leads inevitably to denser source distributions - we observe that the total ISCS ratio reaches the threshold $1 - 1/N$, e.g. for $N = 50$ the ISCS ratio

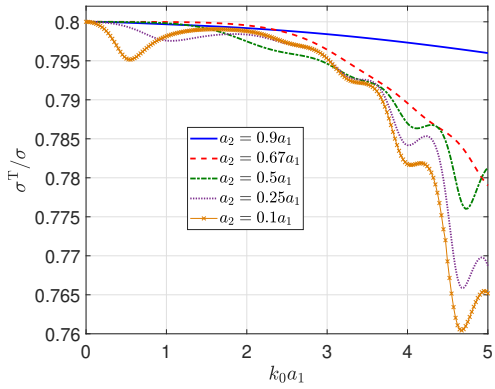

Figure 2.8: Total ISCS ratios $\sigma^{\mathrm{T}}/\sigma$ versus the radius k_0a_1 for different core radii of a sphere with a penetrable core, excited by $N = 4$ external point sources.

is greater than 97.75% in all examined frequencies.

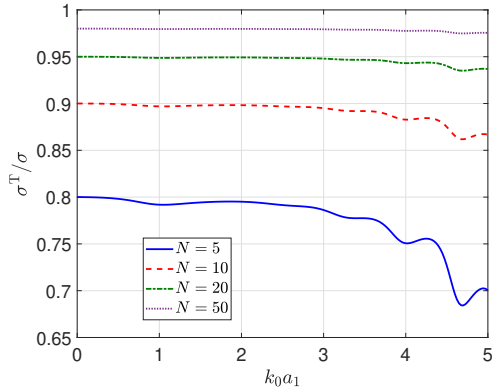

Figure 2.9: Total ISCS σ^{T} of a 2-layered scatterer for source distributions of varying N number of sources.

2.4.2 Mixed Excitation

Now, we consider that the scatterer V is excited by a point source distribution with the some of the sources lying in the external region V_0 $(r > a_1)$ and the rest of the sources lying in the first spherical shell V_1 $(a_2 < r < a_1)$; hence we have $Q = 2$ excitation layers.

In Fig. 2.10, we depict the variations of the total $\sigma^{\mathrm{T}}/\sigma$, indirect $\sigma^{\mathrm{I}}/\sigma$, and direct $\sigma^{\mathrm{D}}/\sigma$ ISCS ratios (left panel) and the values of $\sigma, \sigma^{\mathrm{T}}$ and σ^{I} (right panel) for a soft and a hard core. We considered a distribution

of $N = 8$ sources, with $n_0 = 4$ of them in the exterior V_0 at distances $r_j^0 = (1 + 0.25j)a_1$ and $n_1 = 4$ of them in the interior V_1 at distances $r_j^1 = (0.75 + 0.05j)a_1$ from the sphere's origin. For both cores we assumed $a_1 = 4a_2$, $\rho_1 = 2\rho_0$ and $\eta_1 = 1.75\eta_0$. As we observe, for $k_0a_1 > 1$ the variations of the ISCS ratios do not seem to be affected much by the core type, for the total ISCS. The same holds for the direct ISCS and the indirect ISCS but for $k_0a_1 > 3$, while for $k_0a_1 < 3$ there are notable changes between the soft and the hard core. However, the most notable fact observed, is the negativity of the indirect ISCS for most of the examined k_0a_1. This fact is - naturally - accompanied by large ratios of the direct ISCS. Thus, by the discussion of 1.2.2, we assume that in this setup the cumulative interaction between the sources produces energy flux that is directed towards the sphere's exterior while the interaction between the fields produced in different layers - V_0 and V_1 in our setup - produces energy flux directed towards the interior of the sphere. Fig. 2.11 depicts the variations of the ISCS ratios (left panel) as well as the corresponding ISCS values (right panel) for the case of a penetrable core. We considered two different material settings: the "weak" material setting has parameters $\eta_1 = 1.75\eta_0, \eta_2 = 2\eta_0$ and the "strong" material setting has parameters $\eta_1 = 2.25\eta_0, \eta_2 = 2.75\eta_0$. As we observe for $k_0a_1 < 1$ the parameters do not significantly affect the ISCS ratios, while for $1 < k_0a_1 < 4$ the parameters affect to some extent the ISCS ratios (less than 15% variation). However, for $k_0a_1 > 4$ we observe the strong oscillatory behaviour for the stronger material setting, while the weaker material setting offers a smoother ISCS ratio behaviour, while the indirect ISCS takes negative values.

Fig. 2.12 shows the variations for the values of σ, σ^{T} and σ^{I}, and the direct $\sigma^{\mathrm{D}}/$ versus the core size a_2 of a 2-layered sphere with $k_0a_1 = 1.5$ and a soft core. The core size is expressed as the portion $\xi = a_1/a_2$. We notice that while the core occupies the larger part of the sphere, i.e. for $\xi \leq 2$, σ rises as the core shrinks, while σ^{I} descends. The values of σ^{T} do not seem to be greatly affected. For $\xi > 2$ all values seem to stabilize, and especially for $\xi > 4$ we practically see no change in the values of σ, σ^{T} and σ^{I}, while for σ^{I} the values remain negative for $\xi > 2$

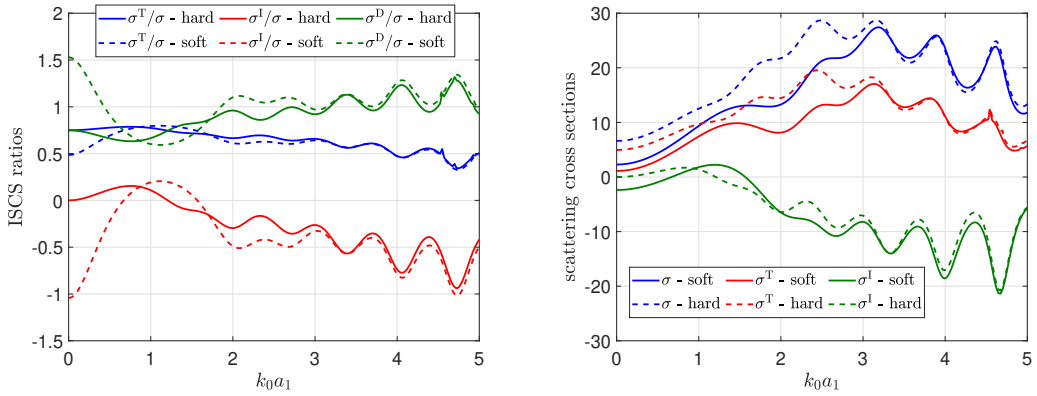

Figure 2.10: ISCS ratios (left panel) and values (right panel) versus radius k_0a_1 of a 2-layered sphere V with a soft or a hard core with $\rho_1 = 2\rho_0, \eta_1 = 1.75\eta_0$ excited by $N = 8$ sources, with $n_0 = 4$ dipoles in V_0 and $n_1 = 4$ in V_1.

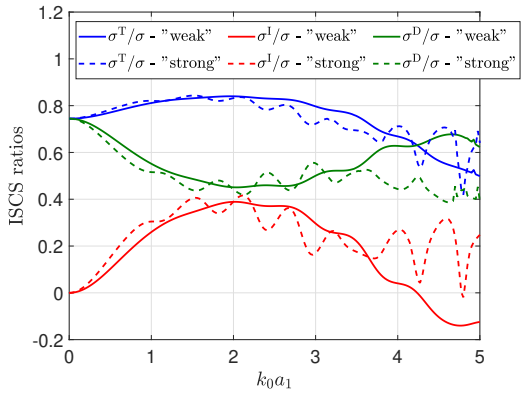

Figure 2.11: ISCS ratios versus k_0a_1 for a 2-layered sphere with a penetrable core for two different material settings, excited by the same distribution of figure 2.10.

for this particular setup. We note, that at different k_0a_1 similar patterns are observed for the same point source distribution. In Fig. 2.13, we depict the physical bounds for the number Q of excitation layers indicated by (4.50) for a point source distribution consisting of $N = 8$ point sources, with $n_0 = 4$ of them in V_0 at $r_j^0 = (1 + 0.25j)a_1$ and $n_1 = 4$ of them in V_1 at distances $r_j = (0.2 + 0.1j)a_1$ with $\eta_1 = 1.75\eta_0$ and $\rho_1 = 2\rho_0$ and $\xi = a_1/a_2 = 4$. We note that the sphere can have a soft or a hard core. The considered number $Q = 2$ is depicted with a straight red line. First of all we observe the remarkable similarity for both types of core, for

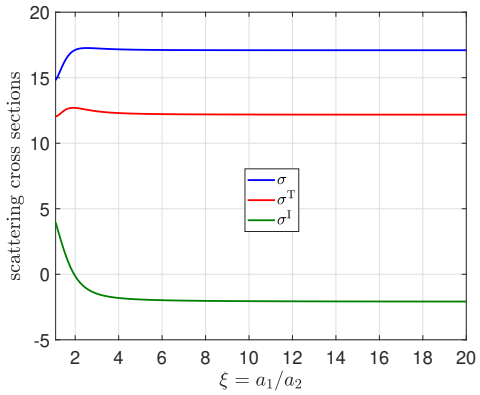

Figure 2.12: Values of σ, σ^{T} and σ^{I} versus the portion $\xi = a_1/a_2$ for a 2-layered scatterer with $k_0 a_1 = 1.5$ and a soft core. The sphere is excited by $N = 8$ sources with $n_0 = 4$ in V_0 and $n_1 = 4$ in the first shell V_1.

$k_0 a_1 > 1$. We note that the physical bounds can be used to determine accurately Q for most all the examined frequencies. This does not hold for $k_0 a_1 \in (1.4 - 1.7)$ for the soft core and $k_0 a_1 \in (1.2 - 1.6)$ for the hard core; in these cases however, we note that the upper physical bound remains very close to the number Q of excitation layers. In fact, we observe that it holds $Q = [\sqrt{\sigma/\sigma_{\mathrm{ex}}^{\max}}] + 1$. In the inset figure, we demonstrate the same physical bounds in the low-frequency region, i.e. for $k_0 a_1 \leq 1$. In the hard core, we observe that the bounds remain valid, but for $k_0 a_1 \leq 0.75$ they cannot be safely used for the determination of Q, since the minimum q-excitation cross section–σ_1 in this case–is significantly smaller than the overall cross section. For the soft core, the physical bounds remain valid for $k_0 a_1 < 0.75$. Finally, for both types of cores we observe a change in the minimum and maximum q-excitation cross sections at $k_0 a_1 = 1.6$ for the soft core and at $k_0 a_1 = 1.35$ for the hard core. In particular, for both types of core, we see that $\sigma_0 < \sigma_1$ in the lower frequencies, while $\sigma_0 > \sigma_1$ in the greater frequencies. Fig. 2.14 depicts the variations of σ,σ^{T} and σ^{I} for $k_0 a_1 = 1.5$ versus the relative mass density $\varrho_1 = \rho_1/\rho_0$ of layer V_1, $\rho_2 = 1.125\rho_1$ for 2-layered sphere with a penetrable core, excited by $N = 8$ sources with $n_0 = 4$ and $n_1 = 4$. The left panel depicts, the behaviour of σ,σ^{T} and σ^{I} for three different kinds of external distribution: "Dense" with $r_j^0 = (1.2 + 0.05j)a_1$, "medium" with $r_j^0 = (1 + 0.25j)a_1$ and "sparse" with

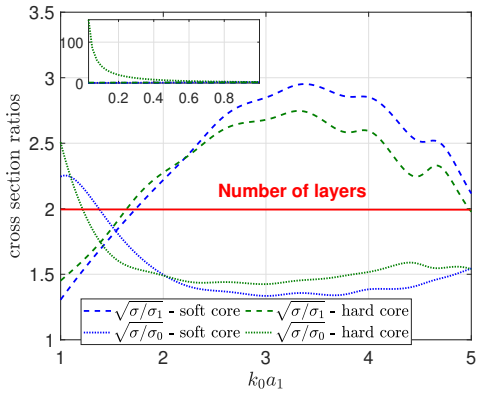

Figure 2.13: Physical bounds for the number Q of excitation layers versus k_0a_1 of a 2-layered sphere with $a_1 = 4a_2$, $\eta_1 = 1.75\eta_0$, $\rho_1 = 2\rho$ with a soft (blue lines) or a hard core (green lines). The scatterer is excited by $N = 8$ sources, 4 of the lying in the exterior of the sphere and 4 of them first spherical shell.

$r_j^0 = (0.25 + j)a_1$. The sources in V_1 are at distances $r_j^1 = (0.25 + 0.05j)a_1$ for all external distributions, while it holds $\eta_1 = 1.75\eta_0, \eta_2 = 2\eta_0$. First, we observe the notable similarity in the behaviour of all quantities examined with the "dense" external distribution leading to greater values, contrary to the "sparse" external distribution. We also note that for all relative mass densities examined, the total and indirect ISCS remain positive. In the right panel, we depict the behaviour of σ,σ^{T} and σ^{I} for three different internal distributions: "Dense" with $r_j^1 = (0.25 + 0.05j)a_1$, "medium" with $r_j^1 = (0.175 + 0.125j)a_1$ and "sparse" with $r_j^0 = (0.075 + 0.225j)a_1$. The sources in V_0 are at distances $r_j^1 = (1.25 + 0.05j)a_1$ for all external distributions. We note the significantly lesser values of σ, $\sigma^{\mathrm{T}} and \sigma^{\mathrm{I}}$ for the "sparse" distribution, compared to the ones for the "dense" distribution. Finally, we note that for $\varrho_1 > 10$ it holds $\sigma^{\mathrm{T}} > \sigma^{\mathrm{I}}$, which implies that $\sigma^{\mathrm{D}} < 0$. Thus, the power flux induced by the interaction between the sources, is directed towards the sphere's core. Qualitatively similar results were drawn for the soft and hard core cases as well, which leads us to estimate that the topological density of the point sources plays an important role in the values of the cross sections, in contrast to the density of the point source distribution in the exterior of the sphere. Finally, we see that as relative mass density rises, the values of ISCS and SCS follow a descending pattern, without their corresponding ratios necessarily affected.

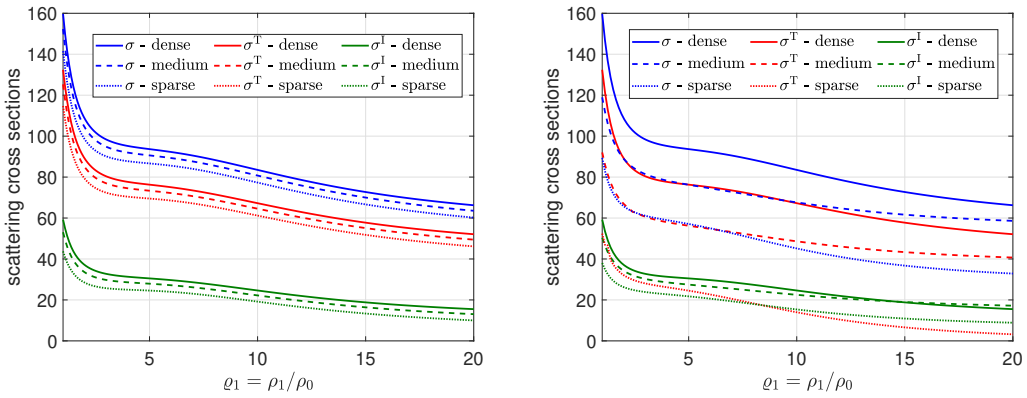

Figure 2.14: Variations of σ, σ^{T} and σ^{I} versus the relative mass density index of V_1, $\varrho_1 = \rho_1/\rho_0$ at $k_0 a_1 = 2.5$, for a 2-layered scatterer with a penetrable core for different types of external point source distributions (left panel) and internal point source distributions (right panel). The sphere is excited by $N = 8$ sources, with $n_0 = 4$ and $n_1 = 4$.

Chapter 3

Inverse Problems

3.1 Low-Frequency Approximations

Now, we steer our focus in the so-called *low frequency zone*, which refers to the case where the wavelength is significantly larger than the scatterer's size, i.e. $k_0 a_1 << 1$. Results in the low-frequency region were obtained by various authors in the past that utilized different techniques, [79] [91], [92], [93]. We limit our investigation in the case of a 2-layered sphere, since the presence of more than 2 layers does not offer significant qualitative differences - only on the algebraic complexity of the analytical procedures. This is due to the fact that the extraction of the fields' coefficients follow a recursive rule, see (3.11) of [83].

First we introduce the following parameters

$$\xi = \frac{a_1}{a_2}, \qquad \eta_p = \frac{k_p}{k_0}, \qquad d_{q,j} = \frac{r_{q,j}}{a_2}, \qquad \tau_j = \frac{a_1}{r_j},$$

and let the power constant be of the form

$$A_{q,j} = r_{q,j} e^{-ik_q r_{q,j}}.$$

Primary spherical waves with the above constant, reduce to plane waves as $r \to \infty$ and transfer the same amount of energy from the source's location $\mathbf{r}_{q,j}$ to the origin, as a plane wave propagating in the direction of $-\mathbf{r}_{q,j}$, see [65].

By the asymptotic properties of the spherical Bessel and Hankel functions for small argument, see (10.1.4)-(10.1.5) of [94] in combination with

Legendre's addition theorem, see (12.178) of [95] the following expression for the overall far-field is derived

$$g(\hat{\mathbf{r}}) = \sum_{q=1}^{Q}\sum_{j=1}^{n_q}\left[\kappa\mu_1 + \kappa^2\mu_2(\theta,\phi) + \kappa^3\mu_3(\theta,\phi)\right] + \mathcal{O}(\kappa^4) \tag{3.1}$$

with

$$\mu_1 = \sum_{q=1}^{Q}\sum_{j=1}^{n_q} C_1^{q,j} \tag{3.2a}$$

$$\mu_2(\theta,\phi) = \sum_{q=1}^{Q}\sum_{j=1}^{n_q}\left(C_2^{q,j} + C_3^{q,j}\tau_{q,j}P_1(\hat{\mathbf{r}}_{q,j}\cdot\hat{\mathbf{r}})\right) \tag{3.2b}$$

$$\mu_3(\theta,\phi) = \sum_{q=1}^{Q}\sum_{j=1}^{n_q}\left(C_4^{q,j} + C_5^{q,j}P_1(\hat{\mathbf{r}}_{q,j}\cdot\hat{\mathbf{r}}) + \quad \frac{C_6^{q,j}}{4}(\tau_{q,j})^2 P_2(\hat{\mathbf{r}}_{q,j}\cdot\hat{\mathbf{r}})\right) \tag{3.2c}$$

Quantities $C_\nu^{q,j}$ for $\nu = 1,\ldots,6$ depend - in general - on the geometrical and physical characteristics of the spherical scatterer as well as on the point source's location. For detailed expressions of these quantities, see appendix. We stress that in the external excitation case, quantities $S_\nu^{q,j}$ depend solely on the physical and geometrical characteristics of the scatterer and have no dependence on the sources' location.

Functions $P_\nu(\hat{\mathbf{r}}_{q,j}\cdot\hat{\mathbf{r}})$ are the Legendre polynomials of order 1 and 2 and are given, respectively, by:

$$P_1(\hat{\mathbf{r}}_{q,j}\cdot\hat{\mathbf{r}}) = \cos\theta_{q,j}\cos\theta + \sin\theta_{q,j}\sin\theta\cos(\phi_{q,j}-\phi) \tag{3.3}$$

$$P_2(\hat{\mathbf{r}}_{q,j}\cdot\hat{\mathbf{r}}) = \sin 2\theta\sin 2\theta_{q,j}\cos(\phi_{q,j}-\phi) + \sin^2\theta\sin^2\theta_{q,j}\cos(2(\phi_{q,j}-\phi)) + (\cos^2\theta_{q,j} - \frac{1}{3})(3\cos^2\theta - 1)) \tag{3.4}$$

Quantity, $P_1(\hat{\mathbf{r}}_{q,j}\cdot\hat{\mathbf{r}})$ is the cosinus of the angle between the position vector of each point source [96], $\mathbf{r}_{q,j}$ and the position vector of observation, $\mathbf{r}$ with respect to the sphere's centre. By utilizing the techniques of [65] we can isolate the terms of the far-field, which combined with the properties

of Legendre polynomials derive the far-field low-frequency approximation coefficients:

$$\sum_{q=1}^{Q}\sum_{j=1}^{n_q} C_2^{q,j} = \frac{\mu_2(0,\phi)+\mu_2(\pi,\phi)}{2} = \mathcal{M}_1 \tag{3.5a}$$

$$\sum_{q=1}^{Q}\sum_{j=1}^{n_q} C_3^{q,j}\tau_{q,j}\cos\theta_{q,j} = \frac{\mu_2(0,\phi)-\mu_2(\pi,\phi)}{2} = \mathcal{M}_2 \tag{3.5b}$$

$$\sum_{q=1}^{Q}\sum_{j=1}^{n_q} C_3^{q,j}\tau_{q,j}\sin\theta_{q,j}\cos\phi_{q,j} = \frac{\mu_2(\frac{\pi}{2},0)-\mu_2(\frac{\pi}{2},\pi)}{2} = \mathcal{M}_3 \tag{3.5c}$$

$$\sum_{q=1}^{Q}\sum_{j=1}^{n_q} C_3^{q,j}\tau_{q,j}\sin\theta_{q,j}\sin\phi_{q,j} = \frac{\mu_2(\frac{\pi}{2},\frac{\pi}{2})-\mu_2(\frac{\pi}{2},\frac{3\pi}{2})}{2} = \mathcal{M}_4 \tag{3.5d}$$

$$\sum_{q=1}^{Q}\sum_{j=1}^{n_q} C_5^{q,j}\cos\theta_{q,j} = \frac{\mu_3(0,\phi)-\mu_3(\pi,\phi)}{2} = \mathcal{N}_1 \tag{3.5e}$$

$$\sum_{q=1}^{Q}\sum_{j=1}^{n_q} C_5^{q,j}\sin\theta_{q,j}\cos\phi_{q,j} = \frac{\mu_3(\frac{\pi}{2},0)-\mu_3(\frac{\pi}{2},\pi)}{2} = \mathcal{N}_2 \tag{3.5f}$$

$$\sum_{q=1}^{Q}\sum_{j=1}^{n_q} C_5^{q,j}\sin\theta_{q,j}\sin\phi_{q,j} = \frac{\mu_3(\frac{\pi}{2},\frac{\pi}{2})-\mu_3(\frac{\pi}{2},\frac{3\pi}{2})}{2} = \mathcal{N}_3 \tag{3.5g}$$

$$\sum_{q=1}^{Q}\sum_{j=1}^{n_q} C_4^{q,j} = \frac{2\mu_3(\frac{\pi}{2},0)+2\mu_3(\frac{\pi}{2},\pi)+\mu_3(0,\phi)+\mu_3(\pi,\phi)}{6} = \mathcal{N}_4 \tag{3.5h}$$

$$\sum_{q=1}^{Q}\sum_{j=1}^{n_q} \frac{C_6^{q,j}}{2}(\tau_{q,j})^2(3\cos^2\theta_{q,j}-1) =$$

$$\mu_3(0,\phi)+\mu_3(\pi,\phi)-\mu_3(\frac{\pi}{2},0)-\mu_3(\frac{\pi}{2},\pi) = \mathcal{N}_5 \tag{3.5i}$$

With the help of relations (3.5b)-(3.5i) we can express the overall far-field as a sum of far-field measurements:

$$g(\hat{\mathbf{r}}) = \Bigg[\kappa\mu_1 + \kappa^2\Big(\mathcal{M}_1 + \mathcal{M}_2\cos\theta + \sin\theta(\mathcal{M}_3\cos\phi - \mathcal{M}_4\sin\phi)\Big) + \\ + \kappa^3\Bigg(\mathcal{N}_4 + \mathcal{N}_1\cos\theta + \sin\theta(\mathcal{N}_2\cos\phi - \mathcal{N}_3\sin\phi) + \\ \sum_{q=1}^{Q}\sum_{j=1}^{n_q}\frac{C_6^{q,j}}{4}(\tau_{q,j})^2 P_2(\hat{\mathbf{r}}_{q,j}\cdot\hat{\mathbf{r}})\Bigg)\Bigg] + \mathcal{O}(\kappa^4) \quad (3.6)$$

Utilizing (2.40), the low-frequency approximation for the overall scattering cross section takes the generic form

$$\sigma = \gamma_1 + (k_0 a_1)^2\,(\gamma_{2,1} + \gamma_{2,2}) \quad (3.7)$$

The terms $\gamma_1, \gamma_{2,1}, \gamma_{2,2}$ depend on the geometrical characteristics of the scatterer, the physical parameters of the scatterer and on the dipole distribution. By considering the far-field measurements (3.5a)-(3.5i) we arrive at the following relations:

$$\gamma_1 = 4\pi a_1^2\mu_1^2 \quad (3.8)$$

$$\gamma_{2,1} = 4\pi a_1^2(\mathcal{M}_1^2 - 2\mathcal{N}_4\mu_1) \quad (3.9)$$

$$\gamma_{2,2} = 4\pi a_1^2(\mathcal{M}_2^2 + \mathcal{M}_3^2 + \mathcal{M}_4^2) \quad (3.10)$$

We point out, that for the external excitation case, by letting $t_{0,j} \to 0$ we obtain the coefficients for the overall far-field in the case where our spherical scatterer is excited by a group of N plane waves, with incident directions $-\mathbf{r}_{0,j}$. In this a case, it holds $\mathcal{M}_2 = \mathcal{M}_3 = \mathcal{M}_4 = \mathcal{N}_5 = 0$. Thus, the expressions of the overall far-field and the overall scattering cross section will be, respectively, simplified into the following:

$$g(\hat{\mathbf{r}}) = \sum_{j=1}^{N}\Big[\kappa C_1^{0,j} + \kappa^2 C_2^{0,j} + \kappa^3\Big(C_4^{0,j} + C_5^{0,j}P_1(\hat{\mathbf{r}}_{0,j}\cdot\hat{\mathbf{r}})\Big)\Big] + \mathcal{O}(\kappa^4)$$

$$\sigma = 4\pi N^2 a_1^2 (C_1^{0,j})^2\Big[1 + (k_0 a_1)^2 (C_1^{0,j})^2\delta(\rho,\eta,\xi)\Big] + \mathcal{O}(\kappa^4)$$

with $\delta(\rho,\eta,\xi)$ given by

$$\delta(\rho,\eta,\xi) = (\varrho_1\eta_1)^2 - \frac{\varrho_1\eta_1^2(2\xi\varrho_1+\varrho_1-1)}{3\xi}$$

3.1.1 Single-Layer Excitation

In the previous chapter, we investigated the behaviour of the total ISCS and its ratio over the overall cross section for an arbitrary layered medium. Now, we will exploit the low-frequency approximation to accurately portray the behaviour of the ISCS ratio in the case of a layered, spherical scatterer. Furthermore, we illustrate through some numerical results the strong dependence of the cross sections on the scatterer's geometrical and physical characteristics and on the number of sources N. On the other hand, we will demonstrate the rather insignificant part that the distribution of the sources on the single-layer excitation plays. This fact - which is supported by the discussion for the energy conservation of the previous chapter - leads to the conclusion that the single-layer excitation is characterized by a predictable ISCS ratio behaviour.

External Excitation

First we address the case where all N sources, are located in the scatterer exterior, V_0. It is worth noting, that the coefficients $C_\nu^{q,j}$ do not depend on the source's position vector - only on the characteristics of the scatterer.

Soft Core

For a soft core it holds:

$$\begin{array}{cc} C_1^{q,j} = S_1^0, & C_2^{q,j} = \rho\eta(S_1^0)^2 \\ C_3^{q,j} = S_2^0, & C_4^{q,j} = (S_1^0)^3\beta(\rho,\eta,\xi) \\ C_5^{q,j} = -S_2^0, & C_6^{q,j} = S_3^0 \end{array} \tag{3.11}$$

with

$$\beta(\rho,\eta,\xi) = \frac{\rho\eta^2(2\xi\rho+\rho-1)}{3\xi} \tag{3.12}$$

The overall far-field in this case can be written as

$$g(\hat{\mathbf{r}}) = \kappa N S_1^0 + \kappa^2 \left(N\rho\eta (S_1^0)^2 + S_2^0 \sum_{j=1}^{N} \tau_j P_1(\hat{\mathbf{r}}_{q,j} \cdot \hat{\mathbf{r}}) \right) + \kappa^3 \Bigg(N\beta(\rho,\xi,\eta)(S_1^0)^3 - S_2^0 \sum_{j=1}^{N} P_1(\hat{\mathbf{r}}_{q,j} \cdot \hat{\mathbf{r}}) + S_3^0 \sum_{j=1}^{N} \tau_j^2 P_2(\hat{\mathbf{r}}_{q,j} \cdot \hat{\mathbf{r}}) \Bigg) \tag{3.13}$$

with

$$\delta(\rho,\eta,\xi) = (\rho\eta)^2 - \beta(\rho,\eta,\xi) \tag{3.14}$$

The terms in the overall scattering cross section expression (3.7) in the soft core case take the following form:

$$\gamma_1 = 4\pi a_1^2 N^2 (S_1^0)^2 \tag{3.15a}$$

$$\gamma_{2,1} = 4\pi a_1^2 N^2 (S_1^0)^4 \delta(\rho,\eta,\xi) \tag{3.15b}$$

$$\gamma_{2,2} = \frac{4\pi a_1^2 (S_2^0)^2}{3} \left(\sum_{j=1}^{N} \tau_j^2 + 2 \sum_{j=1}^{N-1} \sum_{\nu=j+1}^{N} \tau_j \tau_\nu P_1(\hat{\mathbf{r}}_{q,j} \cdot \hat{\mathbf{r}}_{q,\nu}) \right) \tag{3.15c}$$

Taking a closer look at equations (3.15a)-(3.15c) we observe that the distribution of the point sources plays a limited part in the overall scattering cross section and the total ISCS. This is due to the fact that the components of the position vectors of the point sources, appear only on the second term of order $\mathcal{O}(\kappa^2)$.

In the next, we will use the hat symbol to denote quantities that refer to the sum of the individual cross sections and the tilde symbol will be used to denote quantities that refer to the ISCS. The sum of individual cross sections and the total ISCS have a similar generic form as the corresponding overall scattering cross section:

$$\sigma^{\mathrm{T}} = \tilde{\gamma}_1 + (k_0 a_1)^2 (\tilde{\gamma}_{2,1} + \tilde{\gamma}_{2,2}) \tag{3.16}$$

$$\hat{\sigma} = \hat{\gamma}_1 + (k_0 a_1)^2 (\hat{\gamma}_{2,1} + \hat{\gamma}_{2,2}) \tag{3.17}$$

with

$$\hat{\gamma}_1 = 4\pi a_1^2 N (S_1^0)^2 \tag{3.18a}$$

$$\tilde{\gamma}_1 = 4\pi a_1^2 N (N-1)(S_1^0)^2 \tag{3.18b}$$

$$\hat{\gamma}_{2,1} = 4\pi a_1^2 N (S_1^0)^4 \delta(\rho, \eta, \xi) \tag{3.18c}$$

$$\tilde{\gamma}_{2,1} = 4\pi a_1^2 N (N-1)(S_1^0)^4 \delta(\rho, \eta, \xi) \tag{3.18d}$$

$$\hat{\gamma}_{2,2} = \frac{4\pi a_1^2 (S_2^0)^2}{3} \sum_{j=1}^{N} \tau_j^2 \tag{3.18e}$$

$$\tilde{\gamma}_{2,2} = \frac{8\pi a_1^2 (S_2^0)^2}{3} \sum_{j=1}^{N-1} \sum_{\nu=j+1}^{N} \tau_j \tau_\nu P_1(\hat{\mathbf{r}}_{q,j} \cdot \hat{\mathbf{r}}) \tag{3.18f}$$

In the following theorem, we provide a lower bound for the low-frequency approximation of the total ISCS ratio. This lower bound is a sharper lower bound that the one indicated by (1.87).

Theorem 3.1.1 *For the low-frequency approximation of the total ISCS ratio induced by a distribution of N external point sources, exciting a sphere with a soft core, it holds:*

$$\frac{N-1}{N} - \frac{\mathrm{VR}(\boldsymbol{\tau})}{3N\rho^2\xi^2}(k_1 a_2)^2 \leq \frac{\sigma^{\mathrm{T}}}{\sigma} \tag{3.19}$$

where $\mathrm{VR}(\boldsymbol{\tau})$ *denotes the* variance *for the location vector* $\boldsymbol{\tau} = (\tau_1, \tau_2, \ldots, \tau_N)$.

Proof. By equations (3.15a)-(3.15c) and (3.18a) we readily obtain:

$$\frac{N-1}{N}\sigma - \sigma^{\mathrm{T}} = \frac{(k_0 a_1)^2}{N} \left(N\hat{\gamma}_{2,2} - \gamma_{2,2}\right) \tag{3.20}$$

Since $P_1(\hat{\mathbf{r}}_{q,j} \cdot \hat{\mathbf{r}}) = \cos\alpha$ with α being the angle with respect to the origin, between the source's position vector and the vector of observation, last relation can be reduced to:

$$\frac{N-1}{N}\sigma - \sigma^{\mathrm{T}} \leq (k_0 a_1)^2 \frac{4\pi a_1^2 (S_2^0)^2}{3} \left(\sum_{j=1}^{N} \tau_j^2 - \frac{1}{N} \left(\sum_{j=1}^{N} \tau_j \right)^2 \right)$$

But for the variance $\mathrm{VR}(\boldsymbol{\tau})$ of the *location vector* $\boldsymbol{\tau}$ with components the normalized distances τ_j, it holds:

$$\mathrm{VR}(\boldsymbol{\tau}) = \frac{1}{N}\left(\sum_{j=1}^{N}\tau_j^2 - \frac{1}{N}\left(\sum_{j=1}^{N}\tau_j\right)^2\right)$$

Combining the last two relations we obtain:

$$\frac{N-1}{N}\sigma - \sigma^{\mathrm{T}} \leq (k_0 a_1)^2 N \frac{4\pi a_1^2 (S_2^0)^2}{3}\mathrm{VR}(\boldsymbol{\tau}) \tag{3.21}$$

By substituting the expression of S_2^0 in (3.21), we obtain:

$$\sigma^{\mathrm{T}} \geq \frac{N-1}{N}\sigma - (k_0 a_1)^2 N \frac{4\pi a_2^2 \eta^2}{3}\mathrm{VR}(\boldsymbol{\tau})$$

Equations (3.21) and (3.7) lead to (3.19) after some algebraic manipulation.

□

Remark 3.1.2 *For the variance it holds* $\mathrm{VR}(\boldsymbol{\tau}) << 1$. *This stems from the fact that* $\tau_j < 1$. *In combination with* $k_0 a_2 << 1$ *we conclude that it holds:*

$$\sigma^{\mathrm{T}} \simeq \frac{N-1}{N}\sigma \tag{3.22}$$

Relation (3.22) is asymptotic but remains valid for a variety of point source distributions. For a spherical point source distribution we have the lowest possible variance, i.e. $\mathrm{VR}(\boldsymbol{\tau}) = 0$. This results in $\sigma^{\mathrm{T}}/\sigma = 1 - 1/N$. In contrast, the maximum possible variance occurs when all sources lie in different spheres (e.g. all sources lie in a line). Since $\tau_j \in (0,1)$ we can view the location vector $\boldsymbol{\tau}$ as a sample from the uniform distribution $\mathcal{U}(0,1)$. Therefore, we can readily conclude that for all cases, it holds $\mathrm{VR}(\boldsymbol{\tau}) < 1/12$ which is the variance of $\mathcal{U}(0,1)$. Taking this fact into account, we extract a lower bound for the low-frequency approximation that does not depend on the sources' distribution - only on their number and the sphere's parameters:

$$\frac{N-1}{N} - \frac{(k_1 a_2)^2}{36 N \rho^2} \leq \frac{\sigma^{\mathrm{T}}}{\sigma} \leq \frac{N-1}{N} \tag{3.23}$$

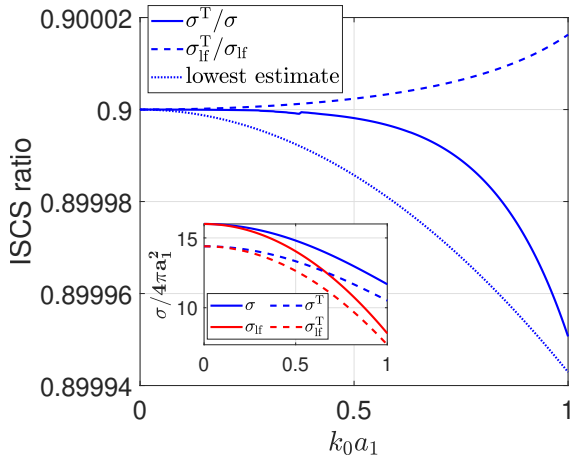

Figure 3.1: Comparison of cross section ratios and cross section values for the exact cross section and their low-frequency approximations for a 2-layered scatterer with a soft core excited by 10 external sources

Figure 3.2 demonstrates the sharpness of the estimate for the ISCS ratio, compared to the accuracy of the low-frequency approximation for the corresponding cross section values. The actual ratio lies well between the ratio of the low-frequency estimates and the lower bound indicated by (3.23) with the maximum error to be less than 0.01%. In the inset figure, we see the plots for the values of the ISCS and the overall scattering cross section, compared to their estimates. We see that despite the fact that the cross section values appear to deviate from their estimates as frequency rises, their corresponding estimated ratios do not. Finally, we restrict the greater part of our investigation in the case of $P = 2$ but as figure 3.2 indicates, the number of non-excitation layers does not affect significantly the ISCS ratio in the soft core case.

Hard or Penetrable Core

For a hard core or a penetrable core, the overall cross section will be given by:

$$\sigma = 4\pi a_1^2 \left[(k_0 a_1)^2 \frac{(C_1^0)^2}{3} \left(\sum_{j=1}^{N} \tau_j^2 + 2 \sum_{j=1}^{N-1} \sum_{\nu=j+1}^{N} \tau_j \tau_\nu P_1(\hat{\mathbf{r}}_{q,j} \cdot \hat{\mathbf{r}}) \right) \right]$$

The following theorem, gives an upper bound for the total ISCS ratio.

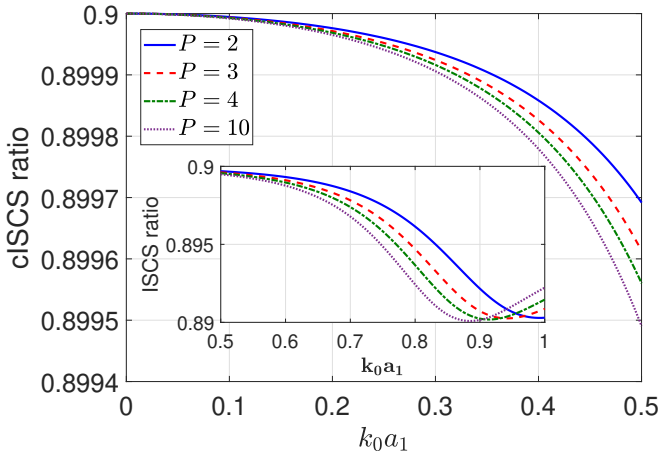

Figure 3.2: Comparison of the exact cross section ratio of a layered sphere with a soft core excited by 10 external sources for different layer numbers.

Theorem 3.1.3 *If $k_0a_1 << 1$ then for the total ISCS ratio of a group of N external sources, exciting a sphere with a hard or penetrable core, it holds*

$$\frac{\sigma^{\mathrm{T}}}{\sigma} \leq \frac{N-1}{N}\left(\frac{\overline{\boldsymbol{\tau}}^2}{\mathrm{VR}(\boldsymbol{\tau})} - \frac{1}{N-1}\right), \tag{3.24}$$

where $\overline{\boldsymbol{\tau}}$ denotes the median of location vector $\boldsymbol{\tau}$.

Proof. Considering that for all $j, \nu = 1, \ldots, N$ it holds $P_1(\hat{\mathbf{r}}_j \cdot \hat{\mathbf{r}}_\nu) \geq -1$, we get

$$\sigma \geq 4\pi a_1^2 (k_0a_1)^2 \frac{(C_3^0)^2}{3}\left[\left(\sum_{j=1}^{N}\tau_j\right)^2 - 2\sum_{j=1}^{N-1}\sum_{\nu=j+1}^{N}\tau_j\tau_\nu\right] \tag{3.25}$$

Given that

$$\mathrm{VR}(\boldsymbol{\tau}) = \frac{1}{N^2}\sum_{j=1}^{N-1}\sum_{\nu=j+1}^{N}(\tau_j - \tau_\nu)^2 = \frac{1}{N}\sum_{j=1}^{N}\tau_j^2 - \overline{\boldsymbol{\tau}}^2, \tag{3.26}$$

relation (3.25) implies

$$\sigma \geq 4\pi a_1^2 (k_0a_1)^2 N^2 \frac{(C_3^0)^2}{3}\mathrm{VR}(\boldsymbol{\tau}) \tag{3.27}$$

Since $P_1(\hat{\mathbf{r}}_j \cdot \hat{\mathbf{r}}_\nu) \leq 1$, the low-frequency approximation of the total ISCS, satisfies

$$\sigma^{\mathrm{T}} \leq 8\pi a_1^2 \left[(k_0 a_1)^2 \frac{(C_3^0)^2}{3} \left(\sum_{j=1}^{N-1} \sum_{\nu=j+1}^{N} \tau_j \tau_\nu \right) \right] \tag{3.28}$$

But, it holds

$$2 \sum_{j=1}^{N-1} \sum_{\nu=j+1}^{N} \tau_j \tau_\nu = \left(\sum_{j=1}^{N} \tau_j \right)^2 - \sum_{j=1}^{N} \tau_j^2 = N^2 \overline{\boldsymbol{\tau}}^2 - \sum_{j=1}^{N} \tau_j^2. \tag{3.29}$$

Combining equations (3.26), (3.27), and (3.29), yields (3.24).

□

Last theorem can be interpreted in the following manner: According to the low-frequency approximation the total ISCS ratio depends only on the distances from the sphere's center and not on the sphere's characteristics and physical parameters. Therefore, different distributions expect to have similar ISCS ratio behavior. As we saw on the soft core case, when all sources lie on a sphere of radius R, the total ISCS ratio will be the maximum possible: $(N-1)/N$. In contrast, the minimum possible total ISCS ratio will occur for a distribution where all sources are at different distances from the sphere's center.

Unlike the soft core case however, (3.24) implies that the total ISCS ratio might deviate significantly from its upper bound $(N-1)/N$. One such example, is a dense distribution with small variance and a large harmonic median. In the following table, we present numerical results that demonstrate these facts.

In particular, all presented distributions have the same harmonic median $\overline{\boldsymbol{\tau}} = 0.5$ and different variances. In each distribution, we present the exact total ISCS ratio, utilizing the exact solutions for the external excitation, we developed earlier, as well as the low-frequency approximation. Similar results to Figure 3.2 can be observed for the ISCS ratio and its low-frequency estimates in the hard core case. The estimation sharpness is reduced but the bound indicated by (3.24) remains very close to the actual ISCS ratio, even in the cases where the low-frequency approximation

fails to converge to the actual cross section values. This fact demonstrates the power of Theorems 3.1.1 and 3.1.3: the low-frequency estimation for the ISCS ratios remains sharp, even in the cases where the corresponding estimation for the cross section values, does not.

$\mathrm{VR}(\boldsymbol{\tau}) = 0.0205$	$k_0 a_1 = 0.025$	$k_0 a_1 = 0.1$	$k_0 a_1 = 0.25$	$k_0 a_1 = 0.5$
exact	0.74999	0.74997	0.74981	0.74883
low frequency	0.74999	0.74999	0.74999	0.74998
$\mathrm{VR}(\boldsymbol{\tau}) = 0.0566$	$k_0 a_1 = 0.025$	$k_0 a_1 = 0.1$	$k_0 a_1 = 0.25$	$k_0 a_1 = 0.5$
exact	0.74999	0.74996	0.74977	0.74866
low frequency	0.74999	0.74999	0.74995	0.74979

Table 3.1: Total ISCS ratios for a line distribution of 4 sources

$\mathrm{VR}(\boldsymbol{\tau}) = 0.0397$	$k_0 a_1 = 0.025$	$k_0 a_1 = 0.1$	$k_0 a_1 = 0.25$	$k_0 a_1 = 0.5$
exact	0.74999	0.74997	0.74982	0.74908
low frequency	0.74999	0.74997	0.74984	0.74951
$\mathrm{VR}(\boldsymbol{\tau}) = 0.0031$	$k_0 a_1 = 0.025$	$k_0 a_1 = 0.1$	$k_0 a_1 = 0.25$	$k_0 a_1 = 0.5$
exact	0.74999	0.74998	0.74988	0.74925
low frequency	0.74999	0.74998	0.74988	0.74944

Table 3.2: Total ISCS ratios for an arbitrary distribution of 4 sources

$\mathrm{VR}(\boldsymbol{\tau}) = 0.0085$	$k_0 a_1 = 0.025$	$k_0 a_1 = 0.1$	$k_0 a_1 = 0.25$	$k_0 a_1 = 0.5$
exact	0.89999	0.89999	0.89993	0.89955
low frequency	0.89999	0.89999	0.89995	0.89979
$\mathrm{VR}(\boldsymbol{\tau}) = 0.0379$	$k_0 a_1 = 0.025$	$k_0 a_1 = 0.1$	$k_0 a_1 = 0.25$	$k_0 a_1 = 0.5$
exact	0.89999	0.89999	0.89991	0.89948
low frequency	0.89999	0.89999	0.89994	0.89971

Table 3.3: Total ISCS ratios for a line distribution of 10 sources

Equivalent Source

Now, we will address the problem of finding an *equivalent source*. The statement of the problem is the following: We suppose that N sources located in the exterior V_0, stimulate a layered sphere of known physical parameters and geometrical characteristics. We seek to determine the location and the strength of a solitary point source that will radiate the

$N = 10$ sources	$k_0a_1 = 0.05$	$k_0a_1 = 0.1$	$k_0a_1 = 0.25$	$k_0a_1 = 0.5$
exact	0.00006	0.00024	0.00236	0.02268
low frequency	0.00003	0.00014	0.00087	0.00349
$N = 5$ sources	$k_0a_1 = 0.05$	$k_0a_1 = 0.1$	$k_0a_1 = 0.25$	$k_0a_1 = 0.5$
exact	0.00003	0.00012	0.00118	0.01134
low frequency	0.00002	0.00007	0.00044	0.00175

Table 3.4: Differences between overall SCS and total ISCS, $|\sigma - \sigma^{\mathrm{T}}|$

same average intensity over all directions per unit area, as the existing point source distribution.

In other words, we will determine the location

$$\tau_{\mathrm{eq}} = \frac{a_1}{r_{\mathrm{eq}}}$$

and strength

$$A_{\mathrm{eq}} = |A| r_{\mathrm{eq}} \exp(-ik_0 r_{\mathrm{eq}})$$

of a source that will lead to the same cross section as the overall cross section of the point source distribution. By [67] the individual cross section of the solitary source has the following form:

$$\sigma_{\mathrm{eq}} = 4\pi a_1^2 |A|^2 \left[(S_1^0)^2 + (k_0 a_1)^2 \left((S_1^0)^4 \delta(\rho, \eta, \xi) + \frac{(S_2^0)^2}{3} \tau_{\mathrm{eq}}^2 \right) \right] \tag{3.30}$$

Combining (3.30) with (3.7) and (3.15a)-(3.15c) we arrive that a source located at

$$\mathbf{r}_{\mathrm{eq}} = \left(\frac{a_1}{\sqrt{\gamma_{2,2}^0}}, 0, 0 \right) \tag{3.31}$$

and of strength

$$A_{\mathrm{eq}} = N \exp\left(\frac{-\mathrm{i} k_0 a_1}{\sqrt{\gamma_{2,2}^0}} \right) \tag{3.32}$$

will result in the same cross section as the distribution of the N sources. For a hard or a penetrable core, the corresponding individual cross section

is given by:

$$\sigma = 4\pi a_1^2 |A|^2 \left[(k_0 a_1)^2 \frac{(C_1^0)^2}{3} \tau_{\mathrm{eq}}^2 \right] \tag{3.33}$$

which readily results in:

$$|A_{\mathrm{eq}}|^2 \tau_{\mathrm{eq}}^2 = \gamma_{2,2}^0 \tag{3.34}$$

Last equation, implies that the solution of the problem is not unique. One of the choices for the source's location and strength is the following:

$$\mathbf{r}_{\mathrm{eq}} = \left(M \frac{a_1}{\sqrt{\gamma_{2,2}^0}}, 0, 0 \right) \tag{3.35}$$

$$A_{\mathrm{eq}} = M \exp\left(\frac{-\mathrm{i} k_0 a_1}{M \sqrt{\gamma_{2,2}^0}} \right) \tag{3.36}$$

where M is a positive number. The choice of M is not rigid, but it is important to ensure that the primary field emitted by the equivalent source, does not degenerate to a plane wave.

Remark 3.1.4 *It is important to note that equivalent sources guarantee an equity between scattering cross sections. The corresponding far-fields, however, will not - in general - be equal.*

Plane Waves

Letting $\tau_j \to 0$ in (3.15a)-(3.15c) leads to the conclusion that individual, overall and ISCS depend solely on the physical and geometrical characteristics of the spherical scatterer. In particular, it will hold

$$\sigma = 4\pi a_1^2 N^2 (S_1^0)^2 \tag{3.37}$$

Therefore, in such a case, we immediately obtain:

$$\sigma^{\mathrm{T}} = \frac{N-1}{N} \sigma, \qquad \sigma_{0,j} = \frac{\sigma}{N^2} \tag{3.38}$$

Thus, inequality (1.87) degenerates into equity in the case of excitation by a group of N plane waves. Another interesting point is that only the

scattered fields will interact with each other; the incident fields will not - in general - interact. For a hard or a penetrable core, the stimulation of the sphere by a group of incident plane waves leads to an overall scattering cross section of order $\mathcal{O}(\kappa^4)$ which is much weaker than the overall scattering cross section due to a point source distribution.

Internal Excitation

By *internal excitation* we refer to the case where all N sources lie within a layer of the sphere, i.e. $Q = 1, V_q \neq V_0$. Following a procedure similar to the external excitation case, after lengthy calculations we obtain for a soft and a hard core, respectively

$$\frac{\sigma^{\mathrm{T}}}{\sigma} \leq \frac{1}{N}\left(N - 1 - \frac{\mathrm{VR}(\mathbf{d})}{(\overline{\mathbf{d}} - 1)^2}\left(1 + (k_1 a_2)^2\right)\right), \tag{3.39}$$

$$\frac{\sigma^{\mathrm{T}}}{\sigma} \leq \frac{N-1}{N}\left(1 - \mathrm{VR}(\mathbf{d})\frac{(k_1 a_2)^2}{3\varrho_1^2}\right), \tag{3.40}$$

where $\overline{\mathbf{d}}$ and $\mathrm{VR}(\mathbf{d})$ the median and variance of location vector $\mathbf{d} = (d_{q,1}, d_{q,2}, \ldots, d_{q,N})$.

From figure 3.3, we see that the low-frequency approximation for the ISCS ratio can be safely used regardless of the corresponding low-frequency approximation accuracy to the exact SCS values. Importantly, the ratio estimate is accurate even outside the low-frequency regime. Specifically, the relative error between the exact and low-frequency ratios is smaller than 1.5% for all $k_0 a_1 < 1$.

Sources required for a given cross section value

Now we address the problem of finding the number of sources required for a given cross section value. A more detailed statement of the problem is the following: We seek to stimulate a 2-layered spherical scatterer with known physical parameters and geometrical characteristics, with a source distribution which will produce a scattered field radiating acoustic intensity in the far-field zone, at a pre-determined rate per unit area of σ_0. To

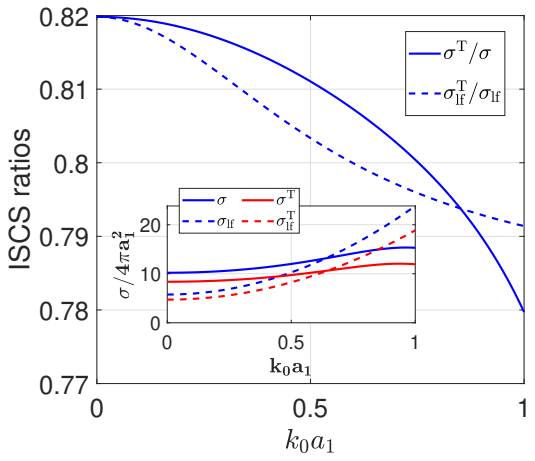

Figure 3.3: Comparison of cross section ratios and cross section values for the exact cross section and their low-frequency approximations for a 2-layered scatterer with a hard core excited by 10 external sources

simplify the procedure, we will suppose that each of the point source radiates in the far-field zone acoustic intensity at a known rate of σ_1. The rate of acoustic intensity per unit area is described by the overall scattering cross section. Therefore Theorem 1.3.6 seems a suitable tool for our investigation. Substituting $\sigma_{\max} = \sigma_{\min} = \sigma_1$ into (1.87) we readily obtain:

$$\sqrt{\frac{\sigma_0}{\sigma_1}} \leq N \tag{3.41}$$

But in the low-frequency region, Theorem 3.1.1 holds. Substituting $\hat{\sigma} = N\sigma_1$ in (3.19) we arrive at:

$$N \leq \sqrt{\frac{\sigma_0}{\sigma_1}\left(1 + \frac{\mathrm{VR}(\boldsymbol{\tau})}{3\rho^2\xi^2}(k_1a_2)^2\right)} \tag{3.42}$$

Given the fact that the components of location vector $\boldsymbol{\tau}$ lie in the interval $(0, 1)$ we can conclude that unless $\rho << 1/\xi$ it will hold

$$\frac{\mathrm{VR}(\boldsymbol{\tau})}{3\rho^2\xi^2}(k_1a_2)^2 \leq \frac{1}{3}$$

Which in return, yields that for the required number of sources, N it holds

$$N \in \left\{ \left[\sqrt{\frac{\sigma_0}{\sigma_1}}\right], \left[\sqrt{\frac{\sigma_0}{\sigma_1}}\right] + 1 \right\}$$

with $[x]$ denoting the integer part of x (floor function).

Remark 3.1.5 *Above analysis was restricted to a 2-layered sphere to avoid mathematically complicated expressions. The qualitative characteristics can be expanded to more than 2 layers, as figures* 3.2 *and* 3.3 *indicate.*

3.1.2 Mixed Excitation

The mixed excitation case, is the case where the interaction cross section ratio depends heavily on the source distribution. In order to demonstrate the diversity in the ISCS ratio behavior, we will use counter-examples. Combining equations (3.7) and (3.16) we understand that the total ISCS ratio $\sigma^{\mathrm{T}}/\sigma$ depends heavily on the value of the fraction $\tilde{\gamma}_1/\gamma_1$. Our intention is to point out the complicated nature of the ISCS ratio. To avoid computationally complicated procedures with minimal insight, we will restrict our analysis to the fraction $\tilde{\gamma}_1/\gamma_1$ since it contains the qualitative characteristics we are interested in. In the first counter-example we suppose that the scatterer is excited by $2N$ sources. N of them are located inside V_1 and lie in a sphere of radius $d \in (a_2, a_1)$ whereas the rest N of them, are located at the exterior V_0 and lie in a sphere of radius $R > a_1$. For the corresponding terms of the overall scattering cross section and the total ISCS holds, respectively:

$$\gamma_1 = 4\pi a_1^2 N^2 d^2 (S_1^0)^2$$
$$\tilde{\gamma}_1 = 4N\pi a_1^2 (S_1^0)^2 (d^2(N-1) + 2(d-1))$$

Then we obtain:

$$\frac{\tilde{\gamma}_1}{\gamma_1} = \frac{N-1}{N} + \frac{2(d-1)}{Nd^2}$$

Let $\mathcal{D}_N(d)$, be the difference from the upper bound $\frac{2N-1}{2N}$ of the inequality (1.87). Then we have:

$$\mathcal{D}_N(d) = \frac{2N-1}{2N} - \frac{\tilde{\gamma}_1}{\gamma_1} = \frac{1}{2N}\left(\frac{d-2}{d}\right)^2 \tag{3.43}$$

Relation (3.43) clearly implies that for a fixed d, as the number $2N$ of sources increases, the total interaction cross section ratio, will tend to the

upper bound $\frac{2N-1}{2N}$, e.g.

$$\lim_{N\to\infty} \mathcal{D}_N(d) = 0$$

On the other hand, for a fixed number of sources $2N$ the interaction cross section ratio decreases as d moves closer to its upper bound ξ (e.g. the sources are closer to the exterior of the sphere) and increases as d moves closer to its lower bound 1 (e.g. the sources are closer to the sphere's core), e.g.

$$\lim_{d\to\xi} \mathcal{D}_N(d) = \frac{1}{2N}\left(\frac{\xi-2}{\xi}\right)^2$$

$$\lim_{d\to 1} \mathcal{D}_N(d) = \frac{1}{2N}$$

Now we proceed, with a different distribution. Let layer V_1 contain $2N-1$ sources that lie on a sphere of radius $d \in (a_2, a_1)$. The sphere's exterior, V_0 contains a solitary source, which is located at distance R from the sphere's center. Following a similar procedure as before, we get for the dominant term of the overall scattering cross section:

$$\tilde{\gamma}_1 = 4\pi a_1^2 (S_1^0)^2 \left[d^2(2N-1)(2N-2) - 2(2N-1)^2 d + 4N^2 - 6N + 4 \right]$$

The key point that highlights the diversity in the ISCS ratio behavior, is not - as before - the behavior of the actual ratio. Instead, it is its sign. In this case, the term $\tilde{\gamma}_1$ of the total ISCS can be negative, which will result in the entire total ISCS being negative. First, we find the roots of $\tilde{\gamma}_1$ with respect to d. These are given by:

$$d^+ = \frac{2N-1+\sqrt{4N-3}}{2N-2}$$

$$d^- = \frac{2N-1-\sqrt{4N-3}}{2N-2}$$

Both roots, are positive for $N \geq 2$. Additionally, it holds that

$$1 < d^+ \leq 2$$

$$0 < d^- \leq 1$$

If the distance d of the point sources located in the interior of V_1, lies in the interval $(1, d^+)$, we conclude that for the leading term of the total ISCS it holds

$$\tilde{\gamma}_1 < 0$$

which results in

$$\sigma^{\mathrm{T}} < 0$$

As we discussed in the energy conservation section of the previous chapter, the physical interpretation for such a case, is that the interaction between the sources will reduce the overall acoustic intensity rate and the sum of individual cross sections in this case, will exceed the overall cross section. However, for $d > d^+$ by similar arguments, we conclude that $\sigma^{\mathrm{T}} > 0$ and the interaction between the sources will amplify the overall acoustic intensity rate.

Remark 3.1.6 *Using the same techniques we can extract similar results hold for the hard and penetrable core cases. According to the discussions of the previous chapter about energy conservation, the mixed excitation case is the case where negative values for the total ISCS is more likely to occur.*

3.2 Inverse Problems in the Low-Frequency Regime

In this section, we state and solve a set of inverse scattering problems. Despite the use of different mathematical procedures, the fundamental mathematical tool when the low-frequency approximation is used, is the isolation of each term of the overall far-field approximation which preceded in equations (3.5a)-(3.5i). This isolation is possible because of the techniques that isolate the terms $\mu_\nu(\theta, \phi)$, see [65]. Some inversion schemes contain mathematical complexity, but this complexity is limited to the analytical procedures and not in the final formulas.

First of all, we note that regardless of the rest of the knowledge we possess about the sphere or the point source distribution, the sphere's

radius a_1 can always be found. From (3.7) we quickly obtain:

$$a_1 = \frac{\sqrt{\gamma_1}}{2\mu_1\sqrt{\pi}} \tag{3.44}$$

So, even if we don't already know the geometrical characteristics of the scatterer, we can always obtain its radius by the preceded formula.

3.2.1 Convergence patterns of the low-frequency far-field approximations

Figures 3.4-3.5 depict representative convergence patterns of the low-frequency far-field approximations to the respective exact far-fields. In each case, the convergence patterns for three different source distributions, namely a "spherical distribution" with sources lying on a sphere, a "line distribution" with sources lying on the z-axis and an "arbitrary distribution", are compared. Particularly, figure 3.4 refers to the soft and hard core cases for external excitation, while figure 3.5 concerns the soft and hard core cases for internal excitation. As the left panel of figure 3.4 demonstrates, in the soft core case for external excitation, the low-frequency approximation matches perfectly the exact far-field for most of the examined frequencies. Even at $k_0a_1 = 1$–a frequency well out of the low-frequency range–the relative error does not exceed 15%. Similar conclusions are drawn for internal excitation in the soft core case as well, where from the left panel of figure 3.5 we see that the relative error does not exceed 10%.

For the hard core, in external excitation the convergence pattern of the right panel of figure 3.4 shows that as we move away from the low-frequency range, the relative error of the approximation increases, but this is caused in part, by the small values of the overall SCS. The situation is similar for internal excitation, depicted in the right panel of figure 3.5; the difference lies in that the deviations start to occur for higher frequencies than in external excitation.

In all examined cases, the sources' distributions do not affect either the sharpness of the low-frequency approximation or the behavior of the far-fields (exact and low-frequency approximations). We note that despite the fact we used $(\pi/2, 0)$ as the direction of observation, quantitatively similar

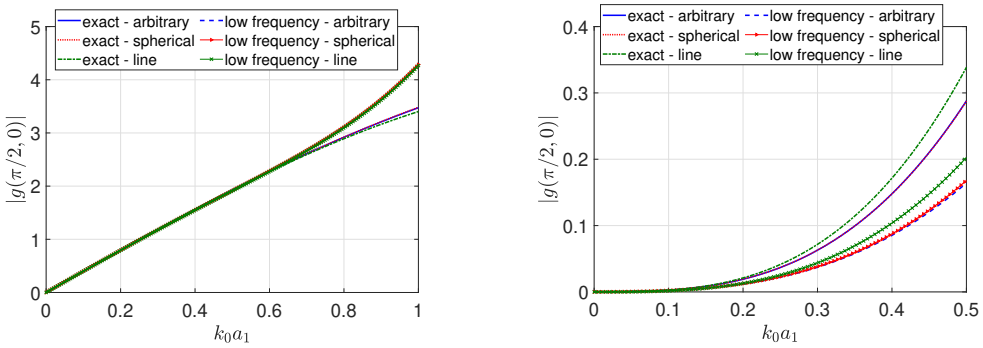

Figure 3.4: Exact and low-frequency far-fields for a 2-layered scatterer with a soft and a hard core, excited by 10 external sources with different distributions. The "arbitrary" distribution is that of figure 3.3, the "line" distribution that of figure 3.2, while the sources of the "spherical" distribution are at distances $r_{0,j} = 2.275a_1$ for $j = 1, \ldots, 10$ with spherical angles $\theta_{0,j} = (j-1)\pi/10$, $\phi_{0,j} = (j-1)\pi/5$. The scatterer's characteristics are as in figure 3.3.

results were obtained for any other direction of observation.

3.2.2 Identification of the Number N of Sources

The first inverse problem we state and solve is a problem which may act as a pre-requisite for more complicated inverse schemes: We seek to identify the number of sources that excite a spherical scatterer. We suppose that the geometrical and physical characteristics of the sphere are known, whereas the only information we have about the point source distribution is that all source lie in the sphere's exterior, V_0. In the soft core case, the number N of sources exciting the scatterer can be swiftly obtained by (3.2a):

$$N = \frac{\mu_1}{S_1^0} \tag{3.45}$$

For the hard core and the penetrable core cases, we replace coefficients S_ν^0 with their corresponding H_ν^0 or P_ν^0, which leads us to obtain:

$$N = \frac{\mathcal{N}_4}{C_1^0} \tag{3.46}$$

with $C_1^0 = H_1^0$ or $C_1^0 = P_1^0$ for a hard core and a penetrable core, respectively.

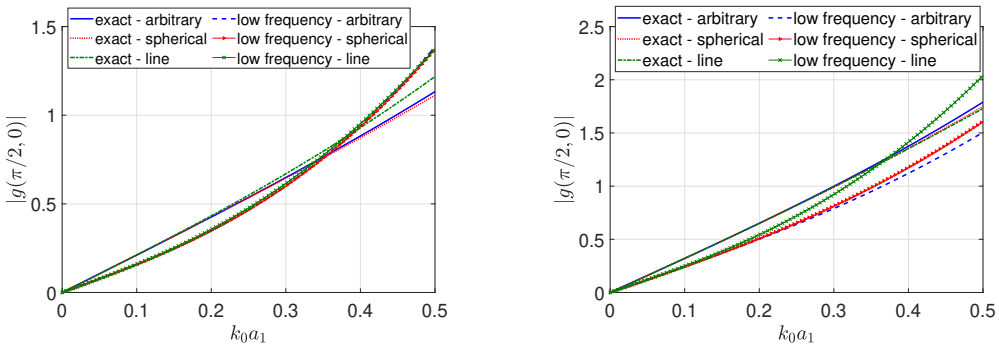

Figure 3.5: Exact and low-frequency far-fields for a 2-layered sphere with a soft and a hard core excited by 6 internal sources for different source distributions. The "arbitrary" distribution is that of figure 3.4, the sources on the "line" distribution lie on the z-axis at distances $r_{1,j} = [0.35 + 0.1(j-1)]a_1$ for $j = 1, \ldots, 6$, while the sources of the "spherical" distribution are at distances $r_{1,j} = 0.6a_1$ for $j = 1, \ldots, 10$ with spherical angles $\theta_{1,j} = \phi_{1,j} = (j-1)\pi/6$. The scatterer's characteristics are as in figure 3.4.

3.2.3 Locating sources

In this part, we provide analytical algorithmic procedures that locate the position vectors of the sources exciting a 2-layered sphere. At first, we suppose that $N = 2$ sources excite our scatterer.

External Excitation

We assume that the sphere's physical and geometrical characteristics are known. The goal is to analytically identify the locations $\mathbf{r}_1, \mathbf{r}_2$ of two the sources exciting the scatterer. Utilizing techniques of [65] we isolate the following terms of the far field:

$$\tau_1 \cos\theta_1 + \tau_2 \cos\theta_2 = X_1 \tag{3.47}$$

$$\cos\theta_1 + \cos\theta_2 = X_2 \tag{3.48}$$

$$\tau_1 \sin\theta_1 \cos\phi_1 + \tau_2 \sin\theta_2 \cos\phi_2 = Y_1 \tag{3.49}$$

$$\sin\theta_1 \cos\phi_1 + \sin\theta_2 \cos\phi_2 = Y_2 \tag{3.50}$$

$$\tau_1 \sin\theta_1 \sin\phi_1 + \tau_2 \sin\theta_2 \sin\phi_2 = Y_3 \tag{3.51}$$

$$\sin\theta_1 \sin\phi_1 + \sin\theta_2 \sin\phi_2 = Y_4 \tag{3.52}$$

with

$$X_1 = \frac{\mu_2(0,\phi) - 2\rho\eta(S_1^0)^2}{S_2^0}, \qquad X_2 = -\frac{\mathcal{N}_1}{S_2^0}$$
$$Y_1 = \frac{\mu_2(\pi/2,0) - 2\rho\eta(S_1^0)^2}{S_2^0}, \qquad Y_2 = \frac{\mathcal{M}_3}{S_2^0}$$
$$Y_3 = \frac{\mu_2(\pi/2,\pi/2) - 2\rho\eta(S_1^0)^2}{S_2^0}, \qquad Y_4 = \frac{\mathcal{M}_4}{S_2^0}$$

The cosine of the angle α between the position vectors of the two sources is given by:

$$\cos\alpha = \cos\theta_1\cos\theta_2 + \sin\theta_1\sin\theta_2\cos(\phi_1 - \phi_2) \tag{3.53}$$

Manipulating equations (3.47)-(3.52) and taking into account (3.53) we obtain:

$$X_2^2 + Y_2^2 + Y_4^2 = 2(1 + \cos\alpha) \tag{3.54}$$
$$X_1^2 + Y_1^2 + Y_3^2 = \gamma_{2,2}^0 \tag{3.55}$$
$$X_1X_2 + Y_1Y_2 + Y_3Y_4 = (\tau_1 + \tau_2)(1 + \cos\alpha) \tag{3.56}$$

Equation (3.54) implies that $\cos\alpha$ can be easily obtained from far-field measurements. If location vectors are not be co-linear it will hold that $X_2^2 + Y_2^2 + Y_4^2 \neq 0, 4$. In this case, by (3.54) and (3.56) we get:

$$\tau_1 + \tau_2 = 2\frac{X_1X_2 + Y_1Y_2 + Y_3Y_4}{X_2^2 + Y_2^2 + Y_4^2} = 2\mathrm{K}_1$$

By means of (3.53), equation (3.15c) yields:

$$\tau_1\tau_2 = \frac{4{\mathrm{K}_1}^2 - \mathrm{L}}{2(1 - \cos\alpha)} = \mathrm{K}_2 \tag{3.57}$$

with

$$\mathrm{L} = \frac{3\gamma_{2,2}^0}{4\pi(a_1S_2^0)^2}$$

Combining equations (3.56) and (3.57), we conclude that the normalized distances τ_1, τ_2 are solutions of the quadratic equation

$$\tau^2 - 2\mathrm{K}_1\tau + \mathrm{K}_2 = 0 \tag{3.58}$$

Therefore τ_1, τ_2 are given by

$$\tau_{1,2} = \mathrm{K}_1 \pm \sqrt{{\mathrm{K}_1}^2 - \mathrm{K}_2} \tag{3.59}$$

Obviously, $\tau_1 = \tau_2 = \mathrm{K}_1$ if and only if $\mathrm{K}_2 = 2{\mathrm{K}_1}^2$. To identify the respective angles, we separate the rest of the procedure, in two cases:

Case I-a: $\tau_1 \neq \tau_2$
At first we suppose that $\tau_1 \neq \tau_2$. Equations (3.47)-(3.52) yield:

$$\cos\theta_1 = \frac{X_1 - \tau_2 X_2}{\tau_1 - \tau_2}, \tag{3.60}$$

$$\cos\theta_2 = -\frac{X_1 - \tau_1 X_2}{\tau_1 - \tau_2} \tag{3.61}$$

$$\sin\theta_1 \cos\phi_1 = \frac{Y_1 - \tau_2 Y_2}{\tau_1 - \tau_2}, \tag{3.62}$$

$$\sin\theta_2 \cos\phi_2 = -\frac{Y_1 - \tau_1 Y_2}{\tau_1 - \tau_2} \tag{3.63}$$

$$\sin\theta_1 \sin\phi_1 = \frac{Y_3 - \tau_2 Y_4}{\tau_1 - \tau_2}, \tag{3.64}$$

$$\sin\theta_2 \sin\phi_2 = -\frac{Y_3 - \tau_1 Y_4}{\tau_1 - \tau_2} \tag{3.65}$$

Since $\cos\theta$ is decreasing in $[0, \pi]$ by (3.60)-(3.61) we obtain θ_1, θ_2. Angles ϕ_1, ϕ_2 are obtained by (3.62),(3.64) and (3.63),(3.65), respectively.

Case I-b: $\tau_1 = \tau_2 = \tau_0$
We isolate the term $\mu_3(0, \phi)$, and we obtain:

$$\tau_0^2 (3\cos^2\theta_1 + 3\cos^2\theta_2 - 2) = X_3 \tag{3.66}$$

with quantity X_3 given by:

$$X_3 = \frac{6\mu_3(0,\phi) + 2S_2^0 X_2 - 2(S_1^0)^2 \beta(\rho, \eta, \xi)}{S_3^0}$$

Utilizing the identity $a^2 + b^2 = (a+b)^2 - 2ab$ for $a = \cos\theta_1, b = \cos\theta_2$ in

equation (3.66) leads to:

$$\cos\theta_1\cos\theta_2 = \frac{X_2^2}{2} - \frac{X_3}{6\tau_0^2} + \frac{1}{3} = \mathrm{K}_3$$

Therefore, the unknown cosines $\cos\theta_1, \cos\theta_2$ are the solutions of the quadratic equation:

$$C^2 - X_2 C + \mathrm{K}_3 = 0 \tag{3.67}$$

On the other hand, it holds:

$$\sin^2\theta_1 + \sin^2\theta_2 + 2\sin\theta_1\sin\theta_2\cos(\phi_1 - \phi_2) = Y_2^2 + Y_4^2 \tag{3.68a}$$

$$\sin^2\theta_1\cos(2\phi_1) + \sin^2\theta_2\cos(2\phi_2) + 2\sin\theta_1\sin\theta_2\cos(\phi_1 + \phi_2) = Y_2^2 - Y_4^2 \tag{3.68b}$$

$$\sin^2\theta_1\cos(2\phi_1) + \sin^2\theta_2\cos(2\phi_2) + \frac{2}{3} - \cos^2\theta_1 - \cos^2\theta_2 = \mathrm{K}_4 \tag{3.68c}$$

with

$$\mathrm{K}_4 = \frac{\mu_3(\pi/2, 0) - S_2^0 Y_2 - N(S_1^0)^3\beta(\rho, \eta, \xi)}{\tau_0^2}$$

When it holds $\sin\theta_1\sin\theta_2 \neq 0$, e.g. there is no source in the z-axis, we obtain the following system:

$$\cos(\phi_1 - \phi_2) = \mathrm{K}_5 \tag{3.69a}$$

$$\cos(\phi_1 + \phi_2) = \mathrm{K}_6 \tag{3.69b}$$

where

$$\mathrm{K}_5 = \frac{Y_2^2 + Y_4^2 - \sin^2\theta_1 - \sin^2\theta_2}{2\sin\theta_1\sin\theta_2}$$

$$\mathrm{K}_6 = \frac{Y_2^2 - Y_4^2 - \mathrm{K}_2}{2\sin\theta_1\sin\theta_2}$$

The solutions of the system are as follows:

$$\phi_1 = 2\pi - \frac{\mathrm{arccos}(\mathrm{K}_5) + \mathrm{arccos}(\mathrm{K}_6)}{2} \tag{3.70a}$$

$$\phi_2 = \frac{\mathrm{arccos}(\mathrm{K}_5) - \mathrm{arccos}(\mathrm{K}_6)}{2} \tag{3.70b}$$

or

$$\phi_1 = \frac{\text{arcccos}(\text{K}_5) + \text{arcccos}(\text{K}_6)}{2} \tag{3.71a}$$

$$\phi_2 = 2\pi - \frac{\text{arcccos}(\text{K}_5) - \text{arcccos}(\text{K}_6)}{2} \tag{3.71b}$$

The choice for the right pair of solutions is made with the help of equations (3.50) and (3.52).

Now, let's suppose that there is a point source lying on the z-axis. Without loss of generality we make the assumption $\sin\theta_1 = 0$. Since $\cos\alpha \neq \pm 1$, then the other point source will not lie in the z-axis. Combining equations (3.50),(3.52) we swiftly recover the angle ϕ_2.

Case II-a: Location vectors have the same direction. We note that in this case we cannot have $\tau_1 = \tau_2$ - since our sources cannot coincide. Furthermore, in this case it will hold $\cos\alpha = 1$ which results in $\theta_1 = \theta_2 = \theta_0, \phi_1 = \phi_2 = \phi_0$. Angles θ_0, ϕ_0 are readily recovered by relations (3.48),(3.50) and (3.52). Under the conditions for this case, equation (3.57) is reduced to:

$$\tau_1 + \tau_2 = \sqrt{\text{L}} \tag{3.72}$$

On the other hand, a measuring of the term $\mu_3(0, \phi)$ yields:

$$(3\cos^2\theta_0 - 1)(\tau_1^2 + \tau_2^2) = X_3$$

Last relation, for $\cos^2\theta_0 \neq 1/3$, can be written as

$$\tau_1\tau_2 = \frac{X_3}{2(3\cos^2\theta_0 - 1)} - \frac{\text{L}}{2} = \text{K}_7$$

which enables us to conclude that the locations τ_1, τ_2 are the solutions of the quadratic equation

$$\tau^2 - \tau\sqrt{\text{L}} + \text{K}_7 = 0 \tag{3.73}$$

For the case where $\cos^2\theta_0 = 1/3$, we will measure the term $\mu_3(\theta, \phi)$. Doing so, we get:

$$\tau_1\tau_2 = \frac{\text{L} - X_4}{2}$$

where

$$X_4 = \begin{cases} 6\frac{\mu_3(\pi/2,0)-(S_1^0)^3\beta(\rho,\eta,\xi)+\sqrt{\frac{2}{3}}S_2^0\cos\phi_0}{S_3^0\cos 2\phi_0}, & if \quad \cos 2\phi_0 \neq 0 \\ 4\frac{\mu_3(\pi/4,0)-(S_1^0)^3\beta(\rho,\eta,\xi)+\sqrt{2}S_2^0(\cos\theta_0+\sin\theta_0\cos\phi_0)}{S_3^0\sin 2\theta_0\cos\phi_0}, & if \quad \cos 2\phi_0 = 0 \end{cases}$$

The desired locations τ_1, τ_2 will be the solutions of the quadratic equation:

$$\tau^2 - \sqrt{\mathrm{L}}\tau + \frac{\mathrm{L} - X_4}{2} = 0 \tag{3.74}$$

Case II-b: Location vectors are in opposite directions
In this case the cosine of the angle between location vectors takes its lowest value, i.e. $\cos\alpha = -1$. Then, it follows that $\theta_2 = \pi - \theta_1, \phi_2 = \pi + \phi_1$ and $\cos\theta_1 = -\cos\theta_2$, $\sin\theta_1 = \sin\theta_2$ and $\cos\phi_1 = -\cos\phi_2$, $\sin\phi_1 = -\sin\phi_2$.

This case, has significant differences from the previously discussed procedures. This is due to the fact that in this case, it holds $X_2 = Y_2 = Y_4 = 0$. To facilitate our procedures, we will divide this case in two occasions: First, we address the occasion where $\tau_1 \neq \tau_2$; this is valid, however, if and only if $X_1^2 + Y_1^2 + Y_3^2 \neq 0$. The second separate occasion is the one where it holds $\tau_1 = \tau_2 = \tau_0$ which will be valid if and only if $X_1 = Y_1 = Y_3 = 0$. For the first occasion, equation (3.57) takes the form:

$$\tau_1 - \tau_2 = \sqrt{\mathrm{L}}$$

In conjunction with equations (3.49) and (3.51) last relation derives:

$$\sin\theta_j = \sqrt{\frac{Y_1^2 + Y_3^2}{L}}$$

for $j = 1, 2$. The angles ϕ_1, ϕ_2 are readily obtained by (3.49) and (3.51). On the other hand, the angles θ_1, θ_2 are obtained by means of (3.47). Finally, locations τ_1, τ_2 can be recovered by either (3.73) or (3.74). It is worth noting the if $Y_1 = Y_3 = 0$, then it will hold $\theta_1 = 0, \theta_2 = \pi$ and both our point sources, will be lying on the z-axis.

Case II-c: Sources locations are symmetric with respect to the scatterer's centre.

Before we proceed, we point out that this case can be easily identified. This happens because in this case it will hold $X_1 = Y_1 = Y_3 = 0$ and subsequently $\gamma^0_{2,2} = 0$. This can be interpreted by the fact that the total ISCS in this case, will depend only on the physical and geometrical characteristics of the scatterer. Furthermore, this can be easily generalized to the case where $N > 2$. As it is evident, in this case, equations (3.47)-(3.52) cannot be used to extract $\theta_{1,2}, \phi_{1,2}$. Thus, we need a different set of measurements to proceed. The following quantities will prove useful:

$$Z_1 = \frac{\mu_3(\pi/2, \pi/4) - \mu_3(\pi/2, 3\pi/4)}{S_3^0}$$
$$Z_2 = \frac{\mu_3(\pi/2, \pi/4) + \mu_3(\pi/2, 3\pi/4) - 2\mu_3(\pi/2, 0)}{S_3^0}$$

Using the measurements mentioned above we arrive at:

$$\tau_0^2 \cos^2\theta_j - \frac{\tau_0^2}{3} = X_3 \tag{3.75a}$$
$$\tau_0^2 \sin^2\theta_j \sin 2\phi_j = Z_1 \tag{3.75b}$$
$$\tau_0^2 \sin^2\theta_j \cos 2\phi_j = Z_2 \tag{3.75c}$$

A combination of (3.75a)-(3.75c) yields the following:

$$\tau_0 = \sqrt{\frac{3}{2}\left(X_3 + \sqrt{Z_1^2 + Z_2^2}\right)} \tag{3.76}$$

Then, equation (3.75a) can be used to extract θ_1, θ_2. We point out that formula (3.76) holds even when $X_3 = 0$. Finally, the angles ϕ_1, ϕ_2 can be readily recovered by relations (3.75b) and (3.75c).

Internal and Mixed Excitation

When all sources lie in the interior of the scatterer, the distances d_1, d_2 of the point sources from the sphere's center, can always be obtained without

knowing the angle between location vectors. For convenience, we denote:

$$I_1 = \frac{\mu_1}{S_1^0} + 1 \tag{3.77}$$

$$I_2 = \frac{\xi \mathcal{M}_2}{\eta S_1^0} \tag{3.78}$$

Measuring the far-field term $\mu_2(\theta, \phi)$ for an arbitrary pair (θ, ϕ) yields:

$$d_1 + d_2 = I_1 \tag{3.79}$$

Taking into account that for internal excitation it holds $\tau_j = \xi/d_j$ and combining (3.79) with (3.78) we arrive at:

$$d_1^2 - I_1 d_1 + \mathrm{B}_1 = 0 \tag{3.80}$$

where

$$\mathrm{B}_1 = \frac{I_2 + I_1^2 - S_1^0(\rho(I_1 + 2\xi) - I_1)}{2} \tag{3.81}$$

Evidently, d_1, d_2 are the solutions of the equation (3.80). The identification of the angles $\theta_1, \theta_2, \phi_1, \phi_2$ is accomplished with the same procedures as in the external excitation case.

For the mixed excitation has again locations τ_1, τ_2 can also be obtained without any knowledge about the angle between location vectors. Furthermore, in this case our sources lie in different excitation layers and thus, we cannot have $\tau_1 = \tau_2$. The location $\tau_1 = \xi/d_1$ of the internal source, can be readily obtained by measuring the term $\mu_1(\theta, \phi)$ for any pair of angles (θ, ϕ). In particular, it holds:

$$d_1 = \frac{\mu_1}{S_1^0} \tag{3.82}$$

The other location is obtained through (3.56).

Remark. The procedures for a hard core and a penetrable are very similar; the only difference is that $C_1^{0,j} = C_2^{0,j} = 0$ for external excitation.

Locating three sources

Now, we address the case where the spherical scatterer is excited by three sources. We suppose that they all lie on the same line, at unknown locations $\mathbf{r}_j = (r_j, \theta_j, \phi_j)$ and let $\hat{\mathbf{r}}_0 = (1, \theta_0, \phi_0)$ be a vector with the same direction as the line. We assume, finally, that the spherical scatterer has a hard core. From the initial measurements, we obtain:

$$\sum_{j=1}^{3} d_j = -\xi\rho\mu_1 = u_1, \tag{3.83}$$

$$\sum_{j=1}^{3} d_j^2 = \frac{\mathcal{M}_1\rho\xi^2}{\eta} \tag{3.84}$$

$$\sum_{j=1}^{3} d_j^3 = \xi(\rho-1)\mu_1 + \frac{3\rho\xi^3}{\eta^2}\mathcal{N}_4 - 3 \tag{3.85}$$

But for any given n it holds:

$$\left(\sum_{j=1}^{n} d_j\right)^2 = \sum_{j=1}^{n} d_j^2 + 2\sum_{j=1}^{n-1}\sum_{\nu=j+1}^{n} d_j d_\nu$$

Setting in the last identity $n = 3$, by means of (3.83),(3.84) we arrive at:

$$\sum_{j=1}^{2}\sum_{\nu=j+1}^{3} d_j d_\nu = \frac{\xi^2\rho^2\mu_1^2}{2} - \frac{\mathcal{M}_1\rho\xi^2}{2\eta} = u_2 \tag{3.86}$$

On the other hand, for any given n it holds:

$$\left(\sum_{j=1}^{n} d_j\right)^3 = \sum_{j=1}^{n} d_j^3 + 3\sum_{j=1}^{n-1}\sum_{\nu=j+1}^{n} d_j^2 d_\nu + 3\sum_{j=1}^{n-2}\sum_{\nu=j+1}^{n-1}\sum_{k=\nu+1}^{n} d_j d_\nu d_k \tag{3.87}$$

For $n = 3$ last relation combined with (3.83)-(3.86), yields:

$$\prod_{j=1}^{3} d_j = \frac{\xi(\rho-1)\mu_1}{3} + \frac{\rho\xi^3}{\eta^2}\mathcal{N}_4 - 1 - \xi\rho\mu_1\left(\frac{\mathcal{M}_1\rho\xi^2}{6\eta} + \frac{\xi^2\rho^2\mu_1^2}{6}\right) = u_3$$

Then, the locations d_j are the roots of the cubic equation

$$d^3 + u_1 d^2 + u_2 d + u_3 = 0 \tag{3.88}$$

which has 3 real roots, since its discriminant is positive. Utilizing the trigonometric solution of the cubic equation for three real roots, we get the locations of the three sources:

$$d_j = 2\sqrt{\frac{p}{3}}\cos\left[\frac{1}{3}\arccos\left(\frac{3q}{2p}\sqrt{\frac{3}{p}}\right) + \frac{2j\pi}{3}\right] \tag{3.89}$$

where

$$p = \frac{3u_2 - u_1^2}{3}$$
$$q = \frac{2u_1^3 - 9u_1u_2 + 27u_3}{27} = \frac{p}{3} + u_3 - \left(\frac{u_1}{3}\right)^3$$

It is worth noting that the procedure and its final outcome is valid, even if our sources do not lie in a line. Therefore, the distances of the point sources from the scatterer are always retrievable. Another conclusion easily drawn is that in case where all sources lie in the z-axis, we can always locate them. This case is easily identified, since it will hold $\mathcal{N}_2 = \mathcal{N}_3 = \mathcal{M}_3 = \mathcal{M}_4 = 0$.

Now, we suppose that our sources don't lie on the z-axis. Then it holds:

$$\sum_{j=1}^{3} C_3^{1,j}\cos\theta_j = -\frac{\mathcal{N}_1}{\eta} \tag{3.90a}$$

$$\sum_{j=1}^{3} \tau_j C_3^{1,j}\cos\theta_j = \mathcal{M}_2 \tag{3.90b}$$

$$\sum_{j=1}^{3} \tau_j^2 C_6^{1,j}\cos^2\theta_j = \mathcal{L}_1 \tag{3.90c}$$

$$\sum_{j=1}^{3} C_3^{1,j}\sin\theta_j\cos\phi_j = -\frac{\mathcal{N}_2}{\eta} \tag{3.90d}$$

$$\sum_{j=1}^{3} \tau_j C_3^{1,j} \sin\theta_j \cos\phi_j = \mathcal{M}_3 \tag{3.90e}$$

$$\sum_{j=1}^{3} \tau_j^2 C_6^{1,j} \sin^2\theta_j \cos^2\phi_j = \mathcal{L}_2 \tag{3.90f}$$

$$\sum_{j=1}^{3} C_3^{1,j} \sin\theta_j \sin\phi_j = -\frac{\mathcal{N}_3}{\eta} \tag{3.90g}$$

$$\sum_{j=1}^{3} \tau_j C_3^{1,j} \sin\theta_j \sin\phi_j = \mathcal{M}_4 \tag{3.90h}$$

$$\sum_{j=1}^{3} \tau_j^2 C_6^{1,j} \sin^2\theta_j \cos\phi_j \sin\phi_j = \mathcal{L}_3 \tag{3.90i}$$

where

$$\mathcal{L}_1 = \sum_{j=1}^{3} C_6^{1,j} \frac{\tau_j^2}{3} + \mathcal{N}_5$$

$$\mathcal{L}_2 = 2\left(\mu_3(0,0) - \mathcal{N}_1 - \mathcal{N}_4 - \frac{2}{3}\mathcal{N}_5 + \frac{1}{4}\sum_{j=1}^{3} \tau_j^2 C_6^{1,j} \sin^2\theta_j\right)$$

$$\mathcal{L}_3 = 4\left(\mu_3(0,\frac{\pi}{4}) - \mathcal{N}_1 - \mathcal{N}_4 - \frac{2}{3}\mathcal{N}_5\right)$$

The equations above constitute a set of 3 systems. In particular, equations (3.90a)-(3.90c) constitute a non-linear system for $\cos\theta_j$, equations (3.90d)-(3.90f) constitute a non-linear system for $\sin\theta_j\cos\phi_j$ and finally, equations (3.90g)-(3.90i) constitute a non-linear system for $\sin\theta_j\sin\phi_j$.

In the case where all sources lie in a line, equations (3.90b), (3.90e) and (3.90h) suffice to obtain (θ_0, ϕ_0). Something similar applies in the case where all sources lie on a plane described by two unit vectors $\hat{\mathbf{r}}_1 = (1, \theta_1, \phi_1)$ and $\hat{\mathbf{r}}_2 = (1, \theta_2, \phi_2)$. Azimuths θ_1, θ_2 can be obtained through (3.90a)-(3.90b) and angles ϕ_1, ϕ_2 can be obtained through equations (3.90d)-(3.90e) and (3.90g)-(3.90i).

Finally, we note that in the case where the three sources do not lie on a line or a plane, the above system might not be analytically solvable. In the case, it is solvable - which can be easily checked by the determinants of both systems - the solution can be obtained as follows: Equations (3.90a)-(3.90b) lead to the following:

$$\cos\theta_2 = A_2 + B_2\cos\theta_1, \qquad \cos\theta_3 = A_3 + B_3\cos\theta_1 \tag{3.91}$$

where

$$A_2 = \frac{\eta\mathcal{M}_2 + \mathcal{N}_1\tau_3}{\eta C_3^{1,2}(\tau_2 - \tau_3)}, \qquad B_2 = -\frac{C_3^{1,1}(\tau_1 - \tau_3)}{C_3^{1,2}(\tau_2 - \tau_3)}$$
$$A_3 = -\frac{\eta\mathcal{M}_2 + \mathcal{N}_1\tau_2}{\eta C_3^{1,3}(\tau_2 - \tau_3)}, \qquad B_3 = \frac{C_3^{1,1}(\tau_1 - \tau_2)}{C_3^{1,3}(\tau_2 - \tau_3)}$$

Substituting in (3.90c) recovers the desired azimuths.

The system for the $\cos\phi_j$ is solved like the corresponding system for the $\cos\theta_j$. Then, we substitute and we obtain a linear system for the $\sin\phi_j$. Combining the solutions, we obtain ϕ_j. We note, however that the above systems are not solvable if any pair of their equations are linearly dependent, i.e. if any of the systems' discriminant is 0. This is due to the fact that the low-frequency approximations are constituted by 10 linearly independent factors. These 10 factors are utilized to obtain the above systems. Therefore, if a need for an "extra" linearly independent equation occurs, it cannot be satisfied.

3.2.4 Identification of the Core and the Excitation Type

Discrimination of the core, with unknown source distribution

Now we address a combined problem. We know that there is a 2-layered scatterer with known physical parameters and geometrical characteristics except the mass density and the wavenumber of its core. Also, we know that $N = 2$ sources excite the scatterer. However, we do not know their location or the scatterer's core type. Our objective, is to develop a set of conditions that will allow us to determine the core and the excitation type.

We note that from the previous section, if we identify the core type and the excitation type, then we can proceed with identifying their locations.

The key for the discrimination are the following quantities:

$$D_1 = \mu_1 - 2S_1^0 \tag{3.92}$$

$$D_2 = \mathcal{M}_1 - 2\rho\eta\mu_1^2 \tag{3.93}$$

$$D_3 = \mathcal{M}_1 - \rho\eta\mu_1^2 \tag{3.94}$$

$$D_4 = \mathcal{N}_4 + \rho\eta\mu_1^2 \tag{3.95}$$

$$D_5 = \mathcal{M}_1 + \frac{\mu_1\eta}{S_1^0\xi}\left(\mu_1 - (\rho-1)(S_1^0)^2\right) \tag{3.96}$$

First, we prove that external excitation holds if and only if $D_1 = D_2 = 0$. Let's suppose that $D_1 = 0$ and that there are two internal sources at distances d_1, d_2 from the sphere's origin. Then, measuring of the far-field term $\mu_2(\theta, \phi)$ leads to:

$$d_1 + d_2 = 4 \tag{3.97}$$

On the other hand, for D_2 holds:

$$D_2 = \frac{\eta}{\xi}S_1^0(-d_1^2 - d_2^2) + 4\frac{\eta}{\xi}(S_1^0)^2(\rho-1) - 4\rho\eta(S_1^0)^2$$

Utilizing (3.97), last equation yields:

$$D_2 = \frac{2\eta}{\xi}S_1^0(d_1d_2 - 6) \tag{3.98}$$

Suppose that $D_2 = 0$. Then it holds $d_1d_2 = 6$ and the distances d_1, d_2 from the sphere's center will be solutions to the quadratic equation $d^2 - 4d + 6 = 0$. This equation however, has complex solutions, which cannot happen. Thus, if we have internal excitation, then $D_2 \neq 0$. Following the same procedure for the mixed excitation case we obtain that $d_1 = 2$, while for D_2 we get:

$$D_2 = -2S_1^0\frac{\eta}{\xi} > 0 \tag{3.99}$$

From the last relation we conclude that $D_2 > 0$ on the mixed excitation case. Therefore, external excitation and a soft core can be identified by the

condition $D_1 = D_2 = 0$. In contrast, external excitation combined with a hard core is a case identified by the order of the terms in the far-field.

On the other hand, we can verify that $D_5 = 0$ in the mixed excitation case, whereas $D_5 < 0$ in the internal excitation case. Specifically, in the internal excitation case, we get:

$$D_5 = \frac{2\eta}{\xi} S_1^0 (d_1 d_2 + 2) < 0 \tag{3.100}$$

In the hard core case, is readily verified that $D_3 = 0$ for mixed excitation and $D_3 < 0$ for internal excitation. We note that the case where $D_3 = D_5 = 0$ cannot occur, since in such a case, it must hold that:

$$\mu_1 = S_1^0$$

Obviously, this can't hold for external excitation. For mixed excitation we readily observe that this leads to $d = 1$, which also, cannot occur. The procedures related to the penetrable core cases resemble the hard core case procedures. Now, we summarize our results in the form of an identification procedure.

Step 1 If the far-field is of order $\mathcal{O}(\kappa^2)$, we have external excitation and a hard or a penetrable core. If $C_4^{q,j} = 0$ we have a penetrable core, otherwise we have a hard core.
Step 2 If $D_1 = D_2 = 0$ we have external excitation and a soft core.
Step 3 If $D_3 = 0$ we have mixed excitation and a hard core.
Step 5 If $D_3 < 0$ we have internal excitation and a hard core.
Step 4 If $D_4 = 0$ we have mixed excitation and a penetrable core.
step 6 If $D_4 < 0$ we have internal excitation and a penetrable core.
Step 7 If $D_5 = 0$ we have mixed excitation and a soft core.
Step 8 If $D_5 < 0$ we have internal excitation and a soft core.

Remark. In the case of a penetrable core, we can determine the relative mass density of the core, by utilizing the procedures of 3.2.3.

Discrimination of the core, with unknown physical parameters

Now, we proceed with another combination problem. In this case, we have full knowledge of the point source distribution that stimulate the sphere but the geometrical and physical characteristics of the scatterer are unknown. The goal is to retrieve the physical and geometrical characteristics of the sphere.

First, we recover the sphere's radius a_1 from equation (3.44). If the source are placed in the sphere's exterior (external excitation), we readily determine the type of the core: If the far-field is of order $\mathcal{O}(\kappa)$ we have soft core; if the far-field is of order $\mathcal{O}(\kappa^2)$ we have a hard core.

Soft Core

If the sphere has a soft core, we swiftly arrive at:

$$\rho = \frac{N + \mu_1(\theta, \phi)}{\mu_1(1-\xi)}, \tag{3.101}$$

$$\eta = \frac{(1-\xi)N^2\mathcal{M}_1}{\mu_1(N + \mu_1(\theta, \phi))} \tag{3.102}$$

$$\beta(\rho, \eta, \xi) = \frac{N^3\mathcal{N}_4}{\mu_1^3} \tag{3.103}$$

Utilizing function's $\beta(\rho, \eta, \xi)$ form and taking into consideration equations (3.101)-(3.103), the last relation takes the form:

$$\xi = \frac{\mathcal{M}_1^2\mu_1^2}{3\mathcal{N}_4\mu_1 + \mathcal{M}_1^2(\mu_1^2 - 3)} \tag{3.104}$$

The relative mass density index and the refractive index can be obtained through (3.101)-(3.103). The parameters ρ_1, k_1 of layer V_1 can be obtained, since the parameters k_0, ρ_0 of the exterior V_0 are known, whereas equation (3.104) delivers the core's radius a_2.

The internal and mixed excitation cases can be dealt with the same techniques.

Hard Core

For the internal excitation case, a combination of relations (3.2a), (3.5a)

and (3.5h) leads to:

$$\rho = -\frac{\sum_{j=1}^{N} d_j}{\xi \mu_1}, \tag{3.105}$$

$$\eta = \xi \frac{\mathcal{M}_1 \sum_{j=1}^{N} d_j}{\mu_1 \sum_{j=1}^{N} d_j^2} \tag{3.106}$$

$$\xi = -\frac{1}{\mu_1} \left(2 \sum_{j=1}^{N} d_j^3 + \frac{N}{\sum_{j=1}^{N} d_j^2} \right) - \frac{\mathcal{N}_4}{\sum_{j=1}^{N} d_j \mathcal{M}_1^2} \tag{3.107}$$

For the external and the mixed excitation cases a similar procedure is required.

3.2.5 Location of a source and determination of the sphere's physical parameters

The final problem is another combination problem. This time, the sphere's geometrical parameters a_1, a_2, ξ and the core's type are known. Its physical parameters η, ρ are unknown. We have knowledge that the sphere is excited by two sources: one is located at a known location $\mathbf{r}_1 = (r, \theta_1, \phi_1)$ and other is located at an unknown location $\mathbf{r}_2 = (r_2, \theta_2, \phi_2)$ inside the sphere. Our objective, is to recover the sphere's physical parameters ρ, η and the type of the sphere's core. Measurement of $\mu_1(\theta, \phi)$ in the hard core case, yields

$$\frac{d_2}{\rho} = -\xi \mu_1, \tag{3.108}$$

$$\rho\eta = \frac{\mathcal{M}_1}{\mu_1^2} \tag{3.109}$$

The coefficient $\mathcal{N}_4$ takes the form:

$$\mathcal{N}_4 = -\frac{(\rho\eta)^2}{3(\xi\rho)^3} \left(2d_2^3 - d_2 + 1 + \frac{d_2}{\rho} \right) \tag{3.110}$$

Combining equations (3.108), (3.109) and (3.110) yields:

$$\left(\rho^{-1}\right)^3 (1-\xi\mu_1) + \left(\rho^{-1}\right)^2 \xi\mu_1 = \xi^3\mu_1^3 \left(2 + \frac{3\mu_1\mathcal{N}_4}{\mathcal{M}_1^2}\right)$$

We denote $u = \xi\mu_1$, $w = 2 + 3\mu_1\mathcal{N}_4/\mathcal{M}^2$ and last equation takes the form:

$$\left(\rho^{-1}\right)^3 (1-u) + \left(\rho^{-1}\right)^2 u - u^3 w = 0 \tag{3.111}$$

Equation (3.111) is a cubic equation with respect to ρ^{-1}. If we utilize the formula for the non-reduced form of the cubic equation, we get for the equation's discriminant Δ_3:

$$\Delta_3 = u^6 w^2 \left(\frac{4}{w} - 27(1-u)^2\right)$$

In the following, we prove that $\Delta_3 < 0$. We observe, that the sign of Δ_3 depends on the sign of the term $f_w(u) = \left(\frac{4}{w} - 27(1-u)^2\right)$. This quantity constitutes a quadratic polynomial with respect to u. From its definition, see appendix, it holds that $\mu_1 < 0$, and in return, $u < 0$. On the other hand, the roots u_1, u_2 of $f(u)$ are given by:

$$u_{1,2} = 1 \pm \frac{2}{\sqrt{27w}}$$

Since d_2, ξ, ρ, η are positive, we conclude that $\mathcal{N}_4$ is negative which results in $w > 0$.

On the other hand, u_1 is obviously positive, whereas for u_2 we have:

$$u_2 = \frac{27w - 4}{\sqrt{27w}(\sqrt{27w} + 2)} = \frac{50\mathcal{M}_1^2 + 3\mu_1\mathcal{N}_4}{\mathcal{M}_1^2\sqrt{27w}(\sqrt{27w} + 2)} > 0$$

We note that $f_w(u)$ will be negative if and only if $u \notin (u_2, u_1)$. Since it holds $u_2, u_1 > 0$ we conclude that $f_w(u) < 0$ and therefore $\Delta_3 < 0$.

Therefore, equation (3.111) has a negative discriminant and thus, it has only one real solution. This solution is the desired parameter ρ^{-1}. Utilizing the hyperbolic solutions of the cubic equations for the case of one real solution and after lengthy calculations, we arrive at:

$$\rho = \frac{2\xi\mu_1}{3\xi\mu_1 - 3}\left(\cosh\left[\frac{1}{3}\text{arccosh}\left(\frac{2 - 27(1-\xi\mu_1)^2(2\mathcal{M}_1^2 + 3\mu_1\mathcal{N}_4)}{2\xi\mu_1\mathcal{M}_1^2}\right)\right]\right)^{-1}$$

Equations (3.108), (3.109) and (3.110) are used to recover η, d_2. Angles θ_2, ϕ_2 can be determined through the procedures of 3.2.3.
For a soft or a penetrable core, the procedure is similar; only difference is the exact form of $\mathcal{M}_1, \mathcal{N}_4$.

Part II:
Electromagnetic Waves

Chapter 4

Energy Transfer Process

4.1 Mathematical Formulation

The layered scatterer V is identified as a bounded and open subset of $\mathbb{R}^3$ with $\mathcal{C}^2$ boundary S_1. The interior of V is divided by $P-1$ $\mathcal{C}^2$ surfaces S_p $(p=2,\ldots,P)$ into P nested, annuli-like layers V_p $(p=1,\ldots,P)$, see Fig. 4.1. Each surface S_p encloses the surface S_{p+1}, for $p=1,\ldots,P-1$ with $\mathrm{dist}(S_p,S_{p+1})>0$, and is oriented by the outward normal unit vector $\hat{\mathbf{n}}$. The scatterer's layers V_p, for $p=1,\ldots,P-1$, are lossless, homogeneous and isotropic and are characterized by wavenumbers k_p, magnetic permeabilities μ_p, and dielectric permittivities ϵ_p. The scatterer's core V_P can be a perfect electric conductor (PEC), perfect magnetic conductor (PMC) or isotropic dielectric with wavenumber k_P, permeability μ_P, and permittivity ϵ_P. The exterior V_0 of V has wavenumber k_0, permeability μ_0, and permittivity ϵ_0. A distribution of N magnetic dipoles - which can be internal or external - excite the scatterer V. Each dipole is located at $\mathbf{r}^i$ and possesses dipole moment $\hat{\mathbf{p}}^i$, with $i=1,\ldots,N$. These dipoles, are distributed in arbitrary fashion, inside Q of the scatterer's layers, which will be called *excitation layers* and when necessary, will be denoted by V_q^{ex}, with $q=1,\ldots,Q$ and $Q\leq P+1$. In the case where the exterior V_0 of the scatterer contains dipoles, then V_1^{ex} coincides with V_0. If no dipoles are contained in V_0, then V_1^{ex} is the outermost layer containing dipoles. Excitation layer V_q^{ex} contains n_q dipoles each one of strength $A_{q,j}$, position vector $\mathbf{r}_{q,j}$, and dipole moment $\hat{\mathbf{p}}_{q,j}$, for $j=1,\ldots,n_q$, while it holds that $n_1+n_2+\cdots+n_Q=N$. Each

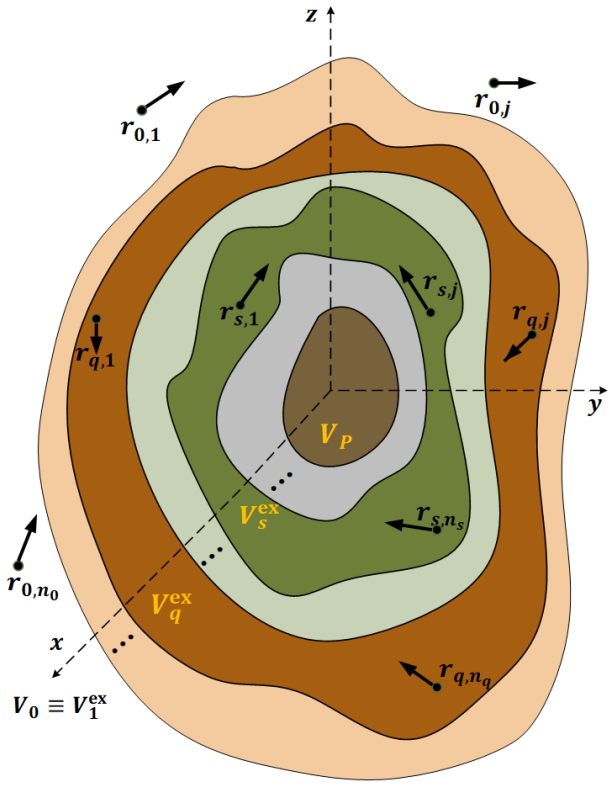

Figure 4.1: The considered layered scatterer V excited by multiple external and internal magnetic dipoles

magnetic dipole radiates primary electric and magnetic fields, respectively, given by [97]

$$\mathbf{E}^{\mathrm{pr}}_{q,j}(\mathbf{r}) = A_{q,j}\nabla \times \left(\frac{\exp(\mathrm{i}k_q|\mathbf{r}-\mathbf{r}_{q,j}|)}{|\mathbf{r}-\mathbf{r}_{q,j}|}\hat{\mathbf{p}}_{q,j} \right), \tag{4.1}$$

$$\mathbf{H}^{\mathrm{pr}}_{q,j}(\mathbf{r}) = \frac{1}{\mathrm{i}\omega\mu_q}\nabla \times \mathbf{E}^{\mathrm{pr}}_{q,j}(\mathbf{r}) \tag{4.2}$$

for $\mathbf{r} \neq \mathbf{r}_{q,j}$ with $j = 1, \ldots, n_q$ and $q = 1, \ldots, Q$. From this point on, we will focus on the definitions of the participating electric fields, since the corresponding magnetic fields can be obtained by means of the Maxwell-Faraday equation, as in (4.2).

If V_p is a non-excitation layer, the secondary electric field generated in V_p by a dipole at $\mathbf{r}_{q,j}$ coincides with the total field in V_p and will be

denoted by $\mathbf{E}^p_{q,j}$. The total electric field induced in an excitation layer V_q due to a single dipole at $\mathbf{r}_{q,j} \in V_q^{\text{ex}}$, according to Sommerfeld's method [81] (referred also as scattering superposition method in [98]), has the following decomposition

$$\mathbf{E}^q_{q,j}(\mathbf{r}) = \mathbf{E}^{\text{pr}}_{q,j}(\mathbf{r}) + \mathbf{E}^{\text{sec}}_{q,j}(\mathbf{r}), \quad \mathbf{r} \in V_q^{\text{ex}} \setminus \{\mathbf{r}_{q,j}\}. \tag{4.3}$$

The fields due to a single dipole, will be called *individual fields*, while the *total q-excitation field* $\mathbf{E}^p_q$ of V_p is the superposition of the total individual fields in V_p due to all dipoles in V_q^{ex}, i.e.

$$\mathbf{E}^p_q(\mathbf{r}) = \sum_{j=1}^{n_q} \mathbf{E}^p_{q,j}(\mathbf{r}). \tag{4.4}$$

In an excitation layer V_q, the *primary q-excitation field* $\mathbf{E}^{\text{pr}}_q$ and the *secondary q-excitation field* $\mathbf{E}^{\text{sec}}_q$ are defined as the superpositions of the corresponding individual fields due to all dipoles in V_q^{ex}, i.e.

$$\mathbf{E}^\ell_q(\mathbf{r}) = \sum_{j=1}^{n_q} \mathbf{E}^\ell_{q,j}(\mathbf{r}), \tag{4.5}$$

where $\ell \in \{\text{pr}, \text{sec}\}$. Thus, the *total q-excitation field* of V_q will be given by

$$\mathbf{E}^q_q(\mathbf{r}) = \mathbf{E}^{\text{pr}}_q(\mathbf{r}) + \mathbf{E}^{\text{sec}}_q(\mathbf{r}), \quad \mathbf{r} \in V_q^{\text{ex}} \setminus \{\mathbf{r}_{q,1}, \ldots, \mathbf{r}_{q,n_q}\}. \tag{4.6}$$

In the same spirit, the *overall field* $\mathbf{E}^p$ of V_p is defined as the superposition of all individual fields of V_p, i.e.

$$\mathbf{E}^p(\mathbf{r}) = \sum_{q=1}^{Q} \sum_{j=1}^{n_q} \mathbf{E}^p_{q,j}(\mathbf{r}) = \sum_{q=1}^{Q} \mathbf{E}^p_q(\mathbf{r}). \tag{4.7}$$

If V_q is an excitation layer, then the *overall secondary field* of V_q is the superposition of all individual secondary fields of V_q, whereas the *overall field* of V_q is defined as

$$\mathbf{E}^q(\mathbf{r}) = \mathbf{E}^{\text{pr}}_q(\mathbf{r}) + \mathbf{E}^{\text{sec}}_q(\mathbf{r}) + \sum_{s \neq q} \mathbf{E}^q_s(\mathbf{r}). \tag{4.8}$$

Individual, q-excitation, and overall fields satisfy the vector Helmholtz equations; e.g. for the total field of V_p, it holds

$$\nabla^2 \mathbf{E}^p(\mathbf{r}) + k_p^2 \mathbf{E}^p(\mathbf{r}) = \mathbf{0}, \tag{4.9}$$

in V_p, if V_p is a non-excitation layer, and in $V_q^{\text{ex}} \setminus \{\mathbf{r}_{q,1}, \ldots, \mathbf{r}_{q,n_q}\}$ if V_p coincides with an excitation layer V_q^{ex}. On the boundaries of each layer V_p ($p = 1, \ldots, P-1$), the (total) individual, q-excitation and overall fields satisfy the transmission conditions

$$\hat{\mathbf{n}} \times \mathbf{E}^{p-1}(\mathbf{r}) = \hat{\mathbf{n}} \times \mathbf{E}^p(\mathbf{r}), \tag{4.10}$$

$$\hat{\mathbf{n}} \times \mathbf{H}^{p-1}(\mathbf{r}) = \hat{\mathbf{n}} \times \mathbf{H}^p(\mathbf{r}), \tag{4.11}$$

We note that for a magneto-dielectric core V_P, conditions (4.10) and (4.11) hold for $p = P$, as well, while for a PEC or a PMC core, the following conditions hold on its boundary S_P [79]

$$\hat{\mathbf{n}} \times \mathbf{E}^{P-1}(\mathbf{r}) = \mathbf{0}, \tag{4.12}$$

$$\hat{\mathbf{n}} \times \mathbf{H}^{P-1}(\mathbf{r}) = \mathbf{0}. \tag{4.13}$$

The total individual fields in V_0 satisfy the Silver-Müller radiation condition [79]

$$\lim_{r \to \infty} \left(Z_0 \mathbf{r} \times \mathbf{H}_{q,j}^0(\mathbf{r}) + r \mathbf{E}_{q,j}^0(\mathbf{r}) \right) = \mathbf{0}, \tag{4.14}$$

uniformly over all directions $\hat{\mathbf{r}} = \mathbf{r}/r$, with $Z_0 = \sqrt{\mu_0/\epsilon_0}$ being the impedance of the exterior, V_0. Subsequently, q-excitation and overall electromagnetic fields satisfy condition (4.14) as well. Being solutions of the vector Helmholtz equation, the individual electric fields in V_0 have the following asymptotic expression, [80]

$$\mathbf{E}_{q,j}^0(\mathbf{r}) = \mathbf{g}_{q,j}(\hat{\mathbf{r}}) h_0(k_0 r) + \mathcal{O}(r^{-2}), \quad r = |\mathbf{r}| \to \infty, \tag{4.15}$$

where h_0 is the spherical Hankel function of the first kind of order 0. Function $\mathbf{g}_{q,j}(\hat{\mathbf{r}})$ constitutes the *individual far-field* in the direction of observation $\hat{\mathbf{r}}$ due to the dipole at $\mathbf{r}_{q,j} \in V_q^{\text{ex}}$. The superposition of the individual far-fields due to all dipoles within V_q^{ex} will be called *q-excitation far-field* and is denoted by $\mathbf{g}_q(\hat{\mathbf{r}})$, while the superposition of the individual far-fields

due to all and due to all N dipoles will be called *overall far-field* and is denoted by $\mathbf{g}(\hat{\mathbf{r}})$. Both fields are respectively defined as follows:

$$\mathbf{g}_q(\hat{\mathbf{r}}) = \sum_{j=1}^{n_q} \mathbf{g}_{q,j}(\hat{\mathbf{r}}), \tag{4.16}$$

$$\mathbf{g}(\hat{\mathbf{r}}) = \sum_{q=1}^{Q} \mathbf{g}_q(\hat{\mathbf{r}}). \tag{4.17}$$

In the same spirit, the *individual cross section* $\sigma_{q,j}$, *q-excitation cross section* σ_q, and *overall cross section* σ are the scattering cross sections due to a dipole at $\mathbf{r}_{q,j} \in V_q^{\text{ex}}$, all dipoles in V_q^{ex}, and all N dipoles, and are, respectively, given by

$$\sigma_{q,j} = \frac{1}{k_0^2} \int_{S^2} |\mathbf{g}_{q,j}(\hat{\mathbf{r}})|^2 \mathrm{d}s(\hat{\mathbf{r}}), \tag{4.18}$$

$$\sigma_q = \frac{1}{k_0^2} \int_{S^2} |\mathbf{g}_q(\hat{\mathbf{r}})|^2 \mathrm{d}s(\hat{\mathbf{r}}), \tag{4.19}$$

$$\sigma = \frac{1}{k_0^2} \int_{S^2} |\mathbf{g}(\hat{\mathbf{r}})|^2 \mathrm{d}s(\hat{\mathbf{r}}), \tag{4.20}$$

where S^2 is the unit sphere of $\mathbb{R}^3$.

Remark 4.1.1 *The definitions and results for excitation by N electric dipoles can be obtained from the respective ones presented here for the case of N magnetic dipoles by using the well-known interchanges between the fields and material parameters (see, e.g., [98], [99]).*

As we discussed in the acoustic waves, the sum of the individual scattering cross sections due to the excitation by all dipoles and the overall scattering cross section are (in general) different. This was thoroughly discussed in [63], whereas in [100] conditions providing that the sum of the individual-particle cross sections is equal to the overall scattering cross section were proven for plane electromagnetic waves impinging on a fixed tenuous group of particles. Therefore, the ISCS for electromagnetic waves and there properties where defined and analyzed in [63] and are in complete accordance

with the ISCS for acoustic waves. For convenience we will re-state them here; for further analysis we refer to section 1 of part II.

Definition 4.1.2 *The q-ISCS, $\tilde{\sigma}_q$, is the difference between the q-excitation cross section σ_q and the sum of the individual cross sections due to all dipoles in V_q^{ex}*

$$\tilde{\sigma}_q = \sigma_q - \sum_{j=1}^{n_q} \sigma_{q,j}. \tag{4.21}$$

The indirect ISCS, σ^{I}, is the difference between the overall cross section σ and the sum of the q-excitation cross sections

$$\sigma^{\mathrm{I}} = \sigma - \sum_{q=1}^{Q} \sigma_q. \tag{4.22}$$

The total ISCS, σ^{T}, is the difference between the overall cross section σ and the sum of the individual cross sections due to all N dipoles

$$\sigma^{\mathrm{T}} = \sigma - \sum_{q=1}^{Q} \sum_{j=1}^{n_q} \sigma_{q,j}. \tag{4.23}$$

By taking into account (4.18)-(4.20), we also derive the following expressions of the above-defined ISCS

$$\tilde{\sigma}_q = \frac{2}{k_0^2} \mathrm{Re} \left[\sum_{j=1}^{n_q - 1} \sum_{\nu=j+1}^{n_q} \int_{S^2} \mathbf{g}_{q,j}(\hat{\mathbf{r}}) \cdot \overline{\mathbf{g}_{q,\nu}(\hat{\mathbf{r}})} \mathrm{d}s(\hat{\mathbf{r}}) \right], \tag{4.24}$$

$$\sigma^{\mathrm{I}} = \frac{2}{k_0^2} \mathrm{Re} \left[\sum_{q=1}^{Q-1} \sum_{s=q+1}^{Q} \int_{S^2} \mathbf{g}_{q}(\hat{\mathbf{r}}) \cdot \overline{\mathbf{g}_{s}(\hat{\mathbf{r}})} \mathrm{d}s(\hat{\mathbf{r}}) \right], \tag{4.25}$$

$$\sigma^{\mathrm{T}} = \frac{2}{k_0^2} \mathrm{Re} \left[\sum_{\nu=1}^{N-1} \sum_{j=\nu+1}^{N} \int_{S^2} \mathbf{g}^{\nu}(\hat{\mathbf{r}}) \cdot \overline{\mathbf{g}^{j}(\hat{\mathbf{r}})} \mathrm{d}s(\hat{\mathbf{r}}) \right], \tag{4.26}$$

where $g^{\nu}(\hat{\mathbf{r}})$ is the individual far field due to a dipole at $\mathbf{r}^{\nu}$. By means of (4.21)-(4.23), we derive the following theorem, which concerns a decomposition of the total ISCS into the direct (sum of the q-interaction cross sections) and indirect ISCS.

Theorem 4.1.3 *Interaction cross sections σ^{T}, σ^{I}, and $\tilde{\sigma}_q$ are related as follows*

$$\sigma^{\mathrm{T}} = \sigma^{\mathrm{D}} + \sigma^{\mathrm{I}}, \tag{4.27}$$

where

$$\sigma^{\mathrm{D}} = \sum_{q=1}^{Q} \tilde{\sigma}_q \tag{4.28}$$

is the direct interaction cross section.

4.2 Scattering Relations and Physical Bounds

4.2.1 Scattering Relations

In the following, we state and prove scattering relations that relate the individual, the q-excitation fields with their corresponding far-fields and their respective individual and total cross sections. Relations that connect the participating fields with the energy functionals enable a better understanding of the physics involved, in various scattering configurations [101] as well as in open-waveguide scattering [102]. The first relation is a reciprocity theorem, that relates the total magnetic fields stemming from two different excitation layers: excitation layer V_q and excitation layer V_s.

Theorem 4.2.1 *The s-excitation field of V_q and the q-excitation field of V_s are related by*

$$\sum_{j=1}^{n_q} A_{q,j} \mathbf{H}_s^q(\mathbf{r}_{q,j}) \cdot \hat{\mathbf{p}}_{q,j} = \sum_{\nu=1}^{n_s} A_{s,\nu} \mathbf{H}_q^s(\mathbf{r}_{s,\nu}) \cdot \hat{\mathbf{p}}_{s,\nu}. \tag{4.29}$$

Proof. Adapting Theorem 3.1 of [58] to the present formulation, and by means of Maxwell's equations, we conclude that for any pair of dipoles it holds

$$A_{q,j} \mathbf{H}_{s,\nu}^q(\mathbf{r}_{q,j}) \cdot \hat{\mathbf{p}}_{q,j} = A_{s,\nu} \mathbf{H}_{q,j}^s(\mathbf{r}_{s,\nu}) \cdot \hat{\mathbf{p}}_{s,\nu}. \tag{4.30}$$

Relation (4.30) is valid for all locations $\mathbf{r}_{s,\nu}$. Fixing $\mathbf{r}_{q,j}$ and summing for $\nu = 1, \ldots, n_s$, we get

$$A_{q,j}\mathbf{H}_s^q(\mathbf{r}_{q,j}) \cdot \hat{\mathbf{p}}_{q,j} = \sum_{\nu=1}^{n_s} A_{s,\nu}\mathbf{H}_{q,j}^s(\mathbf{r}_{s,\nu}) \cdot \hat{\mathbf{p}}_{s,\nu},$$

which, summing for all $j = 1 \ldots, n_q$, yields

$$\sum_{j=1}^{n_q} A_{q,j}\mathbf{H}_s^q(\mathbf{r}_{q,j}) \cdot \hat{\mathbf{p}}_{q,j} = \sum_{j=1}^{n_q}\sum_{\nu=1}^{n_s} A_{s,\nu}\mathbf{H}_{q,j}^s(\mathbf{r}_{s,\nu}) \cdot \hat{\mathbf{p}}_{s,\nu}. \tag{4.31}$$

Changing the summation order in (4.31) and taking into account (4.4), we arrive at (4.29).

□

Remark 4.2.2 For $Q = 2$ and $n_1 = n_2 = 1$ (i.e. $N = 2$ dipoles located in two different excitation layers), Theorem 4.2.1 reduces to Theorem 3.1 of [58]. For $Q = 1$ with $V_1^{\text{ex}} \equiv V_0$ and $N = 2$, Theorem 4.2.1 recovers Theorem 10 of [56].

Next, we define the *individual primary cross section* $\sigma_{q,j}^{\text{pr}}$, the *q-primary cross section* σ_q^{pr} and the *primary interaction cross section*, $\tilde{\sigma}_q^{\text{pr}}$. The first two quantify the average power flux per unit area over all directions that would be radiated if V_q was the scatterer's exterior, while $\tilde{\sigma}_{q,j,\nu}^{\text{pr}}$ quantifies the energy flux average rate per surface unit area, that is attributed to the interaction between fields generated by the dipoles at $\mathbf{r}_{q,j}$ and $\mathbf{r}_{q,\nu}$. They are defined as follows:

$$\sigma_{q,j}^{\text{pr}} = \frac{1}{k_q^2}\int_{S^2} |\mathbf{g}_{q,j}^{\text{pr}}(\hat{\mathbf{r}})|^2 \mathrm{d}s(\hat{\mathbf{r}}) = 4\pi|A_{q,j}|^2, \tag{4.32}$$

$$\sigma_q^{\text{pr}} = \frac{1}{k_q^2}\int_{S^2} |\mathbf{g}_q^{\text{pr}}(\hat{\mathbf{r}})|^2 \mathrm{d}s(\hat{\mathbf{r}}), \tag{4.33}$$

$$\tilde{\sigma}_q^{\text{pr}} = \frac{2}{k_q^2}\sum_{j=1}^{n_q-1}\sum_{\nu=j+1}^{n_q} \mathrm{Re}\left(\int_{S^2} \overline{\mathbf{g}_{q,j}^{\text{pr}}(\hat{\mathbf{r}})} \cdot \mathbf{g}_{q,\nu}^{\text{pr}}(\hat{\mathbf{r}})\mathrm{d}s(\hat{\mathbf{r}})\right), \tag{4.34}$$

where $\mathbf{g}_{q,j}^{\mathrm{pr}}$ is the primary far-field pattern (for a dipole at $\mathbf{r}_{q,j}$) defined by

$$\mathbf{E}_{q,j}^{\mathrm{pr}}(\mathbf{r}) = \mathbf{g}_{q,j}^{\mathrm{pr}}(\hat{\mathbf{r}})h_0(k_q r) + \mathcal{O}(r^{-2}), \quad r \to \infty. \tag{4.35}$$

For the primary field, given by (4.2), the primary far-field pattern is given by

$$\mathbf{g}_{q,j}^{\mathrm{pr}}(\hat{\mathbf{r}}) = \mathrm{i}k_q A_{q,j} \exp\left(-\mathrm{i}k_q \mathbf{r}_{q,j} \cdot \hat{\mathbf{r}}\right)(\hat{\mathbf{r}} \times \mathbf{p}_{q,j}). \tag{4.36}$$

We stress the fact that unless there exist dipoles in the exterior V_0, the primary cross sections are not part of the overall scattering cross section. In the following, we state and prove optical theorems for the overall scattering cross section and the direct and indirect ISCS.

Theorem 4.2.3 *The overall scattering cross section σ due to the excitation of the layered scatterer V by N dipoles is given by*

$$\sigma = 4\pi Z_0 \mathrm{Re}\left(\sum_{q=1}^{Q}\sum_{j=1}^{n_q} \overline{A_{q,j}}\mathbf{H}_q^{\mathrm{sec}}(\mathbf{r}_{q,j}) \cdot \hat{\mathbf{p}}_{q,j}\right) + \frac{Z_0}{Z_q}\sum_{q=1}^{Q}\sigma_q^{\mathrm{pr}}. \tag{4.37}$$

The direct ISCS σ^{D} and indirect ISCS σ^{I} are expressed, respectively, by

$$\sigma^{\mathrm{D}} = 4\pi Z_0 \mathrm{Re}\left(\sum_{q=1}^{Q}\sum_{j=1}^{n_q} \overline{A_{q,j}}\tilde{\mathbf{H}}_{q,j}^{\mathrm{sec}}(\mathbf{r}_{q,j}) \cdot \hat{\mathbf{p}}_{q,j}\right) + \frac{Z_0}{Z_q}\sum_{q=1}^{Q}\tilde{\sigma}_q^{\mathrm{pr}} \tag{4.38}$$

and

$$\sigma^{\mathrm{I}} = 4\pi Z_0 \mathrm{Re}\left(\sum_{q=1}^{Q}\sum_{j=1}^{n_q} \overline{A_{q,j}}\tilde{\mathbf{H}}_q^{\mathrm{sec}}(\mathbf{r}_{q,j}) \cdot \hat{\mathbf{p}}_{q,j}\right), \tag{4.39}$$

where $\tilde{\mathbf{H}}_{q,j}^{\mathrm{sec}}$ denotes the sum of all individual secondary fields of excitation layer V_q except the field induced by the dipole at $\mathbf{r}_{q,j}$, and $\tilde{\mathbf{H}}_q^{\mathrm{sec}}$ denotes the sum of all q-excitation secondary fields radiating in excitation layer V_q, except the fields induced by the dipoles of V_q.

Proof. Utilizing the present formulation in conjunction with Maxwell's equations, the Theorem 4.1 of [58], states that for any two dipoles $\mathbf{r}_{q,j}$ and

$\mathbf{r}_{s,\nu}$ lying in excitation layers V_q, V_s respectively, it holds

$$k_0^2 Z_0 \left(\overline{A_{q,j}} \mathbf{H}_{s,\nu}^q(\mathbf{r}_{q,j}) \cdot \hat{\mathbf{p}}_{q,j} + A_{s,\nu} \overline{\mathbf{H}_{q,j}^s(\mathbf{r}_{s,\nu})} \cdot \hat{\mathbf{p}}_{s,\nu} \right) = \frac{1}{2\pi} \int_{S^2} \overline{\mathbf{g}_{q,j}(\hat{\mathbf{r}})} \cdot \mathbf{g}_{s,\nu}(\hat{\mathbf{r}}) \mathrm{d}s(\hat{\mathbf{r}}). \tag{4.40}$$

Summing for all dipoles inside excitation layer V_s, and then with for all dipoles in excitation layer V_q, by means of (4.4), we find that the magnetic fields in any two excitation layers V_q and V_s are connected as follows:

$$k_0^2 Z_0 \left(\sum_{j=1}^{n_q} \overline{A_{q,j}} \mathbf{H}_s^q(\mathbf{r}_{q,j}) \cdot \hat{\mathbf{p}}_{q,j} + \sum_{\nu=1}^{n_s} A_{s,\nu} \overline{\mathbf{H}_q^s(\mathbf{r}_{s,\nu})} \cdot \hat{\mathbf{p}}_{s,\nu} \right) = \frac{1}{2\pi} \int_{S^2} \overline{\mathbf{g}_q(\hat{\mathbf{r}})} \cdot \mathbf{g}_s(\hat{\mathbf{r}}) \mathrm{d}s(\hat{\mathbf{r}}). \tag{4.41}$$

On the other hand, by Theorem 4.3 of [58], we find that for every two individual secondary fields of V_q, due to dipoles at $\mathbf{r}_{q,j}$ and $\mathbf{r}_{q,\nu}$, holds

$$k_0^2 Z_0 \left(\overline{A_{q,j}} \mathbf{H}_{q,\nu}^{\mathrm{sec}}(\mathbf{r}_{q,j}) \cdot \hat{\mathbf{p}}_{q,j} + A_{q,\nu} \overline{\mathbf{H}_{q,j}^{\mathrm{sec}}(\mathbf{r}_{q,\nu})} \cdot \hat{\mathbf{p}}_{q,\nu} \right) + \frac{k_0 \mu_0}{2\pi k_q \mu_q} \int_{S^2} \overline{\mathbf{g}_{q,j}^{\mathrm{pr}}(\hat{\mathbf{r}})} \cdot \mathbf{g}_{q,\nu}^{\mathrm{pr}}(\hat{\mathbf{r}}) \mathrm{d}s(\hat{\mathbf{r}}) = \frac{1}{2\pi} \int_{S^2} \overline{\mathbf{g}_{q,j}(\hat{\mathbf{r}})} \cdot \mathbf{g}_{q,\nu}(\hat{\mathbf{r}}) \mathrm{d}s(\hat{\mathbf{r}}). \tag{4.42}$$

Using the definition (4.19) of σ_q, and summing (4.42) for all $\nu, j = 1, \ldots, n_q$, we obtain

$$\sigma_q = 4\pi Z_0 \mathrm{Re} \left(\sum_{j=1}^{n_q} \overline{A_{q,j}} \mathbf{H}_q^{\mathrm{sec}}(\mathbf{r}_{q,j}) \cdot \hat{\mathbf{p}}_{q,j} \right) + \frac{Z_0}{Z_q} \sigma_q^{\mathrm{pr}}. \tag{4.43}$$

Relation (4.37) is derived by summing (4.41) for both indices q, s and applying (4.43) for $V_q \equiv V_s$ and taking into account definition (4.20) of σ. Then, adapting Theorem 5 of [58] to the present formulation, we obtain

$$\sigma_{q,j} = 4\pi Z_0 \mathrm{Re} \left(\overline{A_{q,j}} \mathbf{H}_{q,j}^{\mathrm{sec}}(\mathbf{r}_{q,j}) \cdot \hat{\mathbf{p}}_{q,j} \right) + \frac{Z_0}{Z_q} \sigma_{q,j}^{\mathrm{pr}}. \tag{4.44}$$

Equation (4.38) is derived by (4.43) and (4.44) after considering the definitions (4.21) and (4.28). Besides, (4.39) is obtained by summing (4.43) for all excitation layers, and using (4.37) and the definition (4.22).

□

Remark 4.2.4 *The corresponding formula for* σ^{T} *can be obtained by (4.27), (4.38), and (4.39).*

Remark 4.2.5 *We note that for* $N = 2$ *theorem 4.2.3 recovers the well-known* General Scattering Theorem *discussed by various authors, [56], [58], [79].*

For plane-wave light scattering by a small number N of particles, the additivity of the scattering cross sections was investigated in [100] under the condition of sufficiently large distance between each particle. Non-additive properties of the cross sections in conjunction with validity conditions of the Discrete Dipole Approximation (DDA) were studied in [44].

4.2.2 Physical Bounds on Interaction Scattering Cross Sections

In this section, we establish physical bounds for the ratios of ISCS over the corresponding scattering cross sections, which are important in determining the additivity of the cross sections. Then, we investigate the behaviors of these ratios, especially, for large numbers N of exciting dipoles. Since the proving procedures are identical with the corresponding ones for acoustic waves, we will present the statement of these relations without proof. We notice that in theorem 4.2.3, the primary cross sections appear in the overall cross section's expression, despite the fact that the dipoles are not necessarily located at the scatterer's exterior. In the next, we provide an explanation for this puzzling, yet expected, appearance.

Theorem 4.2.6 *The q-ISCS, the indirect ISCS and the total ISCS,* σ^{T},

satisfy, respectively

$$1-n_q\frac{\sigma_q^{\max}}{\sigma_q}\leq\frac{\tilde{\sigma}}{\sigma_q}\leq\min\left\{1-n_q\frac{\sigma_q^{\min}}{\sigma_q},1-\frac{1}{n_q}\right\},\tag{4.45}$$

$$1-Q\frac{\sigma_{\rm ex}^{\max}}{\sigma}\leq\frac{\sigma^{\rm I}}{\sigma}\leq\min\left\{1-Q\frac{\sigma_{\rm ex}^{\min}}{\sigma},1-\frac{1}{Q}\right\},\tag{4.46}$$

$$1-N\frac{\sigma^{\max}}{\sigma}\leq\frac{\sigma^{\rm T}}{\sigma}\leq\min\left\{1-N\frac{\sigma^{\min}}{\sigma},1-\frac{1}{N}\right\},\tag{4.47}$$

where $\sigma_q^{\min}$ *and* $\sigma_q^{\max}$ *denote the minimum and maximum individual cross sections in* V_q, $\sigma_{\rm ex}^{\min}$ *and* $\sigma_{\rm ex}^{\max}$ *denote the minimum and maximum* q*-excitation cross sections and finally,* $\sigma^{\min}$ *and* $\sigma^{\max}$ *denote the minimum and maximum individual cross sections of all dipoles. For*

$$n_q^2\sigma^{\min}\leq\sigma_q,\quad Q^2\sigma_{\rm ex}^{\min}\leq\sigma,\quad N^2\sigma^{\min}\leq\sigma,\tag{4.48}$$

the minima involved in (4.45)-(4.47) are $1-\frac{1}{n_q}$, $1-\frac{1}{Q}$ *and* $1-\frac{1}{N}$, *respectively.*

Corollary 4.2.7 *Conditions (4.48) hold respectively, if and only if*

$$\sqrt{\frac{\sigma_q}{\sigma_q^{\max}}}\leq n_q\leq\sqrt{\frac{\sigma_q}{\sigma_q^{\min}}}\tag{4.49}$$

$$\sqrt{\frac{\sigma}{\sigma_{\rm ex}^{\max}}}\leq Q\leq\sqrt{\frac{\sigma}{\sigma_{\rm ex}^{\min}}}\tag{4.50}$$

$$\sqrt{\frac{\sigma}{\sigma^{\max}}}\leq N\leq\sqrt{\frac{\sigma}{\sigma^{\min}}}\tag{4.51}$$

4.2.3 Large-N Behavior of Scattering Cross-Sections Ratios

The large-N behavior of the cross section ratios follows the same pattern with the corresponding behavior in acoustic waves. Thus, we provide the statement of our findings without further proofs or comments.

Corollary 4.2.8 *If* $\sigma_N^{\rm T}>0$, *for* $N\geq N_0$, *with* N_0 *a certain number of dipoles, then*

$$R_N^{\min}\to 0,\quad for\quad N\to\infty.\tag{4.52}$$

If $\sigma_N^{\mathrm{T}} < 0$ for a fixed number N of dipoles, then

$$R_N^{\max} > \frac{1}{N}. \tag{4.53}$$

If $R_N^{\min} > \frac{1}{N}$ for a fixed number N of dipoles, then

$$\sigma_N^{\mathrm{T}} < 0. \tag{4.54}$$

If $1 - R_{N(\delta)}^{\mathrm{T}} = \delta$, for a fixed $\delta > 0$ and a number $N(\delta)$ of dipoles, then

$$N(\delta) > \frac{1}{\delta}. \tag{4.55}$$

□

Theorem 4.2.9 *If there is a number N_0 of dipoles such that $R_N^{\max}$ increases for all $N \geq N_0$, and $\sigma_N^{\mathrm{T}} > 0$ for all $N \geq N_0$, then*

$$R_N^{\max} \to a R_{N_0}^{\max}, \quad for \quad N \to \infty, \tag{4.56}$$

where $a \in [1, N_0^2]$, and $R_{N_0}^{\max}$ is the maximum cross section ratio for N_0 dipoles.

Corollary 4.2.10 ***Condition 1*** *If for the maximum individual cross section ratio there exists an N_0, such that*

$$R_N^{\max} < \frac{1}{N} \tag{4.57}$$

for all N with $N \geq N_0$, then

$$R_N^{\mathrm{T}} \to 1, \quad as \quad N \to \infty. \tag{4.58}$$

Condition 2 *The following assertions are equivalent*

$$R_N^{\mathrm{T}} \to 1, \quad \text{for} \quad N \to \infty \tag{4.59}$$

$$R_N^j \to 0, \quad \text{for} \quad N \to \infty, \quad \text{with} \quad j = 1, \ldots, N. \tag{4.60}$$

□

4.3 Energy Conservation

4.3.1 Conservation of Energy for a Layered Medium

when an excitation layer contains more than two dipoles in its interior, various interactions and energy exchanges take place simultaneously. For plane-wave scattering of light by a particle, M.I. Mishchenko introduced in [46] the concept of a power flux induced by the interaction between an incident field and the corresponding scattered field that "operate" in the same volume.

The complex Poynting vector $\mathbf{S}$ for the electromagnetic field radiating in a volume V is defined as $\mathbf{S} = \mathbf{E} \times \overline{\mathbf{H}}$. Its real part accounts for the power flux induced in volume V due to excitation by the current distribution in V and its imaginary part accounts for the reactive power or alternating flow, induced in volume V [50]. Two other fundamental quantities in the energy transfer process, are the electric and magnetic energy densities denoted respectively, by $W_{\mathrm{E}}(\mathbf{r}) = \frac{\epsilon}{2}|\mathbf{E}(\mathbf{r})|^2$ and $W_{\mathrm{M}}(\mathbf{r}) = \frac{\mu}{2}|\mathbf{H}(\mathbf{r})|^2$ with ϵ, μ the physical parameters of volume V. The choice of the complex Poynting vector instead of its (more custom for time-harmonic fields) real part was made in order to obtain a global view of the various energy exchanges that take place. In the following, *Lagrangian density* refers to the difference between the magnetic and electric densities

$$L(\mathbf{r}) = \frac{\mu}{2}\left|\mathbf{H}(\mathbf{r})\right|^2 - \frac{\epsilon}{2}\left|\mathbf{E}(\mathbf{r})\right|^2. \tag{4.61}$$

In general, the Lagrangian density is related with conservation laws that describe physical phenomena through the famous Noether's theorem; for mechanical waves (such as acoustic waves) it refers to the difference between the kinetic and potential energies. For electromagnetic waves, however, it coincides with the difference between the electric and magnetic energies [48], [50]. The law of energy conservation in an isotropic space V for time-harmonic fields states that the real part of the Poynting vector is irrotational, i.e. $\mathrm{Re}(\nabla \cdot \mathbf{S}) = 0$ in V and is readily extracted after some minor manipulation of the corresponding Maxwell's equations for time-harmonic fields. Under the assumption that V is smooth, an integration

over ∂V of the real part of the power flux, leads to the following physical interpretation: No *active power flux* is elicited through the boundary of V. By adopting the complex form of the Poynting vector, we can deduce another straight-forward consequence of the Maxwell equations, which would remain hidden, otherwise: The relation between *reactive power* and the Lagrangian density of V, which takes the form

$$\mathrm{Im}(\nabla \cdot \mathbf{S}) = 2\omega L$$

In the next, we present and prove a theorem that relates the q-excitation scattering cross section with its corresponding Lagrangian density and the power flux through an excitation layer's surface. This relation constitutes the energy conservation law for the scattering problem we consider, when all dipoles lie in a single excitation layer V_q.

Theorem 4.3.1 *The q-excitation scattering cross section σ_q, the Lagrangian densities L_q^p of a distribution of magnetic dipoles within a single-excitation layer V_q and the power flux $\mathbf{S}_q^q$ of V_q due to all dipoles in V_q are connected as follows:*

$$\sigma_q = 2\mathrm{i}\omega Z_0 \sum_{p=0}^{q-1} \int_{V_p} L_q^p(\mathbf{r})\mathrm{d}v(\mathbf{r}) + Z_0 \int_{S_q} \hat{\mathbf{n}} \cdot \mathbf{S}_q^q(\mathbf{r})\mathrm{d}s(\mathbf{r}). \tag{4.62}$$

Proof. By Ω we denote the domain of $\mathbb{R}^3$ that is bounded by the scatterer's external surface S_1 and a sphere S_R of radius R; see Fig. 4.2. Applying the divergence theorem in Ω for the power flux $\mathbf{S}_q^0$ of V_0 induced by the dipoles of excitation layer V_q, yields

$$\int_{S_R} \hat{\mathbf{r}} \cdot \mathbf{S}_q^0(\mathbf{r})\mathrm{d}s(\mathbf{r}) - \int_{S_1} \hat{\mathbf{n}} \cdot \mathbf{S}_q^0(\mathbf{r})\mathrm{d}s(\mathbf{r}) =$$
$$\int_\Omega \Big((\nabla \times \mathbf{E}_q^0(\mathbf{r})) \cdot \overline{\mathbf{H}_q^0(\mathbf{r})} - (\nabla \times \overline{\mathbf{H}_q^0(\mathbf{r})}) \cdot \mathbf{E}_q^0(\mathbf{r}) \Big) \mathrm{d}v(\mathbf{r}), \tag{4.63}$$

Taking into account Faraday's and Ampère's laws we arrive at

$$\int_{S_R} \hat{\mathbf{r}} \cdot \mathbf{S}_q^0(\mathbf{r})\mathrm{d}s(\mathbf{r}) = \int_{S_1} \hat{\mathbf{n}} \cdot \mathbf{S}_q^0(\mathbf{r})\mathrm{d}s(\mathbf{r}) + 2\mathrm{i}\omega \int_\Omega L_q^0(\mathbf{r})\mathrm{d}v(\mathbf{r}), \tag{4.64}$$

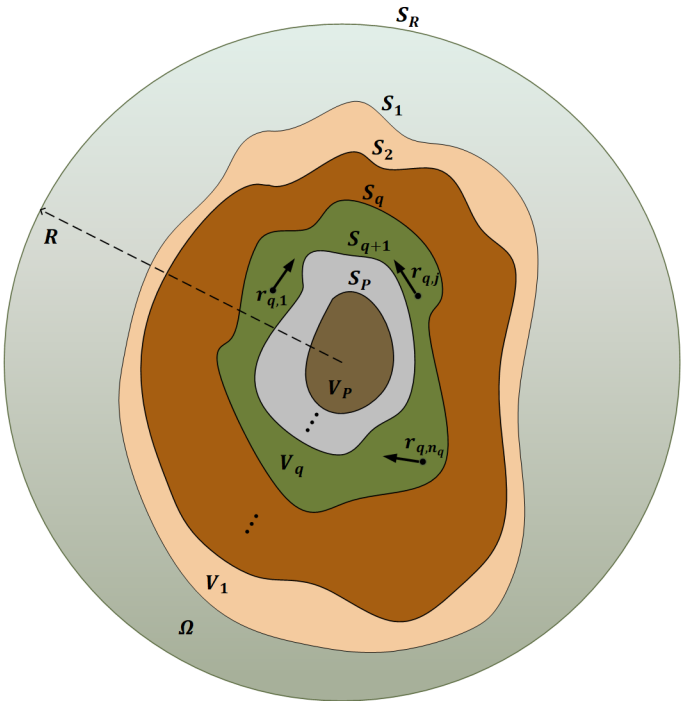

Figure 4.2: A layered scatterer V containing a single excitation layer V_q and surrounded by a sphere of radius R.

with L_q^0 denoting the Lagrangian density in V_0 due to the dipoles of V_q. Letting $r \to \infty$, and using the Silver-Müller radiation condition (4.14), we get

$$\hat{\mathbf{r}} \cdot \mathbf{S}_q^0(\mathbf{r}) = \frac{1}{Z_0 k_0^2 r^2} |\mathbf{g}_q(\hat{\mathbf{r}})|^2 + \mathcal{O}(r^{-3}), \tag{4.65}$$

from which, (4.64), for $R \to \infty$, gives

$$\lim_{R\to\infty} \left(\frac{1}{Z_0 k_0^2} \int_{S_R} \frac{|\mathbf{g}_q(\hat{\mathbf{r}})|^2}{R^2} \mathrm{d}s(\mathbf{r}) \right) = \int_{S_1} \hat{\mathbf{n}} \cdot \mathbf{S}_q^0(\mathbf{r}) \mathrm{d}s(\mathbf{r}) + 2\mathrm{i}\omega \int_{V_0} L_q^0(\mathbf{r}) \mathrm{d}v(\mathbf{r}). \tag{4.66}$$

But it holds

$$\lim_{R\to\infty} \left(\int_{S_R} \frac{|\mathbf{g}_q(\hat{\mathbf{r}})|^2}{R^2} \mathrm{d}s(\mathbf{r}) \right) = \int_{S^2} |\mathbf{g}_q(\hat{\mathbf{r}})|^2 \mathrm{d}s(\hat{\mathbf{r}}) \tag{4.67}$$

Considering the definition (4.19) and the fact that for $R \to \infty$ the domain

Ω coincides with V_0, we derive the following

$$\frac{\sigma_q}{Z_0} = \int_{S_1} \hat{\mathbf{n}} \cdot \mathbf{S}_q^0(\mathbf{r}) \mathrm{d}s(\mathbf{r}) + 2\mathrm{i}\omega \int_{V_0} L_q^0(\mathbf{r}) \mathrm{d}v(\mathbf{r}). \tag{4.68}$$

Applying the divergence theorem in layers V_p, for $p = 1, \ldots, q-1$, we obtain

$$\int_{S_p} \hat{\mathbf{n}} \cdot \mathbf{S}_q^p(\mathbf{r}) \mathrm{d}s(\mathbf{r}) = \int_{S_{p+1}} \hat{\mathbf{n}} \cdot \mathbf{S}_q^p(\mathbf{r}) \mathrm{d}s(\mathbf{r}) + 2\mathrm{i}\omega \int_{V_p} L_q^p(\mathbf{r}) \mathrm{d}v(\mathbf{r}). \tag{4.69}$$

Imposing transmission boundary conditions on surfce S_{p+1}, we get

$$\hat{\mathbf{n}} \cdot \mathbf{S}_q^p(\mathbf{r}) = \overline{\mathbf{H}_q^p}(\mathbf{r}) \cdot (\hat{\mathbf{n}} \times \mathbf{E}_q^p(\mathbf{r})) = \overline{\mathbf{H}_q^{p+1}}(\mathbf{r}) \cdot (\hat{\mathbf{n}} \times \mathbf{E}_q^{p+1}(\mathbf{r})) = \hat{\mathbf{n}} \cdot \mathbf{S}_q^{p+1}(\mathbf{r}). \tag{4.70}$$

Now, successive applications of the divergence theorem, for $p = 1, \ldots, q-1$, in conjunction with (4.69) and (4.70) lead to

$$\int_{S_1} \hat{\mathbf{n}} \cdot \mathbf{S}_q^0(\mathbf{r}) \mathrm{d}s(\mathbf{r}) = 2\mathrm{i}\omega \sum_{p=1}^{q-1} \int_{V_p} L_q^p(\mathbf{r}) \mathrm{d}v(\mathbf{r}) + \int_{S_q} \hat{\mathbf{n}} \cdot \mathbf{S}_q^q(\mathbf{r}) \mathrm{d}s(\mathbf{r}). \tag{4.71}$$

Relation (4.62) is obtained by combining (4.68) and (4.71).

□

Taking the real part of (4.62) yields the following

Corollary 4.3.2 *The individual scattering cross section and the average power flux per unit area out of the excitation layer V_q, are connected as follows:*

$$\sigma_q = Z_0 \mathrm{Re} \left(\int_{S_q} \hat{\mathbf{n}} \cdot \mathbf{S}_q^q(\mathbf{r}) \mathrm{d}s(\mathbf{r}) \right). \tag{4.72}$$

Relation (4.72), is similar to the optical theorem. A way of interpreting it from a physical standpoint is that the active power flux rate that radiates in the far-field (which is quantified by the q-excitation cross section) is proportional to the average power flux through an excitation layer's surface (which is quantified by the integral of the Poynting vector).

Taking the imaginary part of (4.62) we obtain the following:

Corollary 4.3.3 *The reactive power directed into the excitation layer V_q is related with stored energy in all layers of the scatterer prior to V_q by the relation:*

$$2\omega \sum_{p=0}^{q-1} L_q^p(\mathbf{r})\mathrm{d}v(\mathbf{r}) = -\mathrm{Im}\left(\int_{S_q} \hat{\mathbf{n}} \cdot \mathbf{S}_q^q(\mathbf{r})\mathrm{d}s(\mathbf{r})\right). \tag{4.73}$$

Relation (4.73) on the other hand, reveals that the presence of the reactive power in V_q is manifested by the difference between the magnetic energy and electric energy in the scatterer's layers that contain the excitation layer. We note that the minus sign in the integral of the right-hand side in (4.73) is an indication of the direction of the reactive power. In particular, it shows that the reactive power is directed "inwards", i.e. towards the interior of the excitation layer V_q.

Remark 4.3.4 *For $n_q = 1$, we obtain the corresponding results for the individual quantities.*

Now, we steer our focus towards the contribution of the secondary fields in the energy transfer process. For single-layer excitation, by successively implementing the divergence theorem for $p = q+1, q+2, \ldots, P$ we obtain

$$\int_{S_{q+1}} \hat{\mathbf{n}} \cdot \mathbf{S}_q^q(\mathbf{r})\mathrm{d}s(\mathbf{r}) = 2\mathrm{i}\omega \sum_{p=q+1}^{P} \int_{V_p} L_q^p(\mathbf{r})\mathrm{d}v(\mathbf{r}), \tag{4.74}$$

We readily observe that the right-hand side of (4.74) is an imaginary quantity. Thus, we deduce that in the layers layers enclosed by V_q, no active power flux is induced. Furthermore, the reactive power is proportional to the cumulative Lagrangian density in the enclosed by V_q. Relation (4.74) on the other hand, combined with (4.73) implies that the (secondary) fields in the non-excitation layers seem to produce no power flux, while their contribution to the energy transfer process seems to be limited. In particular, they constitute the pool of reactive power.

On the other hand, the divergence theorem under this concept, describes the process of "transforming" the reactive power into energy stored in the scatterer's layers; this sort of "transformation" indicates a similarity with

an absorption mechanism. However, the scatterer types we consider are lossless and therefore there is no power flux absorbed by the scatterer. This seemingly ambiguous behavior, stems from the presence of more than one dipoles in the excitation layer and the inevitable interaction between spherical waves "operating" in the same volume.

In order to delve deeper into the understanding of these interactions, we will press on with (4.62). In particular, we make use of the power fluxes introduced in [46] and we will expand them to better fit the problem of excitation by N dipoles. The ISCS which where the focus of the previous section are a significant part of this expansion. In [46], the *individual power flux* of a dipole radiating in a volume V was decomposed in three parts, as follows:

$$\mathbf{S} = \mathbf{S}^{\mathrm{pr}} + \mathbf{S}^{\mathrm{ext}} + \mathbf{S}^{\mathrm{sec}}, \tag{4.75}$$

Vectors $\mathbf{S}^{\mathrm{pr}}$ and $\mathbf{S}^{\mathrm{sec}}$ constitute the power fluxes induced by the primary and the secondary field, respectively. The third term in (4.75), $\mathbf{S}^{\mathrm{ext}}$, denotes the power flux induced by the interaction between the primary and its own secondary field. Specifically, $\mathbf{S}^{\mathrm{ext}}$ is given by

$$\mathbf{S}^{\mathrm{ext}} = \mathbf{E}^{\mathrm{pr}} \times \overline{\mathbf{H}}^{\mathrm{sec}} + \mathbf{E}^{\mathrm{sec}} \times \overline{\mathbf{H}}^{\mathrm{pr}}. \tag{4.76}$$

In the following, we address the complicated interaction mechanism that takes place, when more than one dipoles are contained in an excitation layer V_q. Each of the primary fields of V_q interacts with its own secondary field, as well as with all the secondary fields induced by the rest of the primary fields of V_q. Even more, this occurs for all primary fields and all secondary fields.

To group these interactions and their corresponding power fluxes - which we will call *interaction power fluxes* (IPF) - we distinguish these interactions in the following manner: Vector quantities $\mathbf{S}_q^{\mathrm{pr}}$ and $\mathbf{S}_q^{\mathrm{sec}}$ will constitute the *primary power flux* and the *secondary power flux*, respectively. These are the power fluxes induced by the interactions between all primary fields and all secondary fields of V_q, respectively. On the other hand, vector quantity $\mathbf{S}_q^{\mathrm{ext}}$ will denote the power flux induced by the interaction between primary and secondary fields of V_q.

The definitions of [46], can be extended to describe in general the power fluxes induced by interaction between two electromagnetic fields. In particular, if $(\mathbf{E}_1, \mathbf{H}_1)$ and $(\mathbf{E}_2, \mathbf{H}_2)$ are two electromagnetic fields that radiate in the same volume, the power flux induced by their interaction is defined as

$$\tilde{\mathbf{S}} = \mathbf{E}_1 \times \overline{\mathbf{H}}_2 + \mathbf{E}_2 \times \overline{\mathbf{H}}_1. \tag{4.77}$$

The following theorem describes in detail the energy process inside an excitation layer.

Theorem 4.3.5 *The power flux induced through the surface S_q is connected with the interaction power fluxes of V_q as follows:*

$$\int_{S_q} \hat{\mathbf{n}} \cdot \mathbf{S}_q^q(\mathbf{r}) \mathrm{d}s(\mathbf{r}) = 2\mathrm{i}\omega \sum_{p=q}^{P} \int_{V_p} L_q^p(\mathbf{r}) \mathrm{d}v(\mathbf{r}) + \int_{\partial V_q} \hat{\mathbf{n}} \cdot \left(\mathbf{S}_q^{\mathrm{pr}}(\mathbf{r}) + \mathbf{S}_q^{\mathrm{ext}}(\mathbf{r}) \right) \mathrm{d}s(\mathbf{r}). \tag{4.78}$$

Proof. Applying the divergence theorem in V_q for the q-excitation secondary power flux, yields

$$\int_{S_q} \hat{\mathbf{n}} \cdot \mathbf{S}_q^{\mathrm{sec}}(\mathbf{r}) \mathrm{d}s(\mathbf{r}) = 2\mathrm{i}\omega \int_{V_q} L_q^{\mathrm{sec}}(\mathbf{r}) \mathrm{d}v(\mathbf{r}) + \int_{S_{q+1}} \hat{\mathbf{n}} \cdot \mathbf{S}_q^{\mathrm{sec}}(\mathbf{r}) \mathrm{d}s(\mathbf{r}), \tag{4.79}$$

with L_q^{sec} being the Lagrangian density of the secondary fields in V_q. Imposing the boundary conditions on S_{q+1} for $\mathbf{E}_q^q, \overline{\mathbf{H}}_q^q$, leads to

$$\begin{aligned} \int_{S_{q+1}} \hat{\mathbf{n}} \cdot \mathbf{S}_q^{\mathrm{sec}}(\mathbf{r}) \mathrm{d}s(\mathbf{r}) = \\ - \int_{S_{q+1}} \hat{\mathbf{n}} \cdot \left(\mathbf{E}_q^{\mathrm{pr}}(\mathbf{r}) \times \overline{\mathbf{H}}_q^{q+1}(\mathbf{r}) \right) \mathrm{d}s(\mathbf{r}) - \\ \int_{S_{q+1}} \hat{\mathbf{n}} \cdot \left(\mathbf{E}_q^{q+1}(\mathbf{r}) \times \overline{\mathbf{H}}_q^{\mathrm{pr}}(\mathbf{r}) \right) \mathrm{d}s(\mathbf{r}) + \\ \int_{S_{q+1}} \hat{\mathbf{n}} \cdot \mathbf{S}_q^{q+1}(\mathbf{r}) \mathrm{d}s(\mathbf{r}) + \int_{S_{q+1}} \hat{\mathbf{n}} \cdot \mathbf{S}_q^{\mathrm{pr}}(\mathbf{r}) \mathrm{d}s(\mathbf{r}). \end{aligned} \tag{4.80}$$

We impose again the boundary conditions on S_{q+1} for the fields $\mathbf{E}_q^{q+1}, \overline{\mathbf{H}}_q^{q+1}$ and by means of (4.80), we obtain

$$\int_{S_{q+1}} \hat{\mathbf{n}} \cdot \mathbf{S}_q^{\text{sec}}(\mathbf{r}) \mathrm{d}s(\mathbf{r}) = \int_{S_{q+1}} \hat{\mathbf{n}} \cdot \mathbf{S}_q^{q+1}(\mathbf{r}) \mathrm{d}s(\mathbf{r})$$
$$- \int_{S_{q+1}} \hat{\mathbf{n}} \cdot \mathbf{S}_q^{\text{pr}}(\mathbf{r}) \mathrm{d}s(\mathbf{r}) - \int_{S_{q+1}} \hat{\mathbf{n}} \cdot \mathbf{S}_q^{\text{ext}}(\mathbf{r}) \mathrm{d}s(\mathbf{r}). \tag{4.81}$$

A combination of (4.81), (4.74), (4.75) and (4.79), derives (4.78).

□

Equation (4.78) combined with (4.62) yields an alternative form of Theorem 4.3.1

$$\sigma_q = 2\mathrm{i}\omega Z_0 \sum_{p=0}^{P} \int_{V_p} L_q^p(\mathbf{r}) \mathrm{d}v(\mathbf{r}) +$$
$$Z_0 \int_{\partial V_q} \hat{\mathbf{n}} \cdot \left(\mathbf{S}_q^{\text{pr}}(\mathbf{r}) + \mathbf{S}_q^{\text{ext}}(\mathbf{r}) \right) \mathrm{d}s(\mathbf{r}), \tag{4.82}$$

This form, implies that the induced power flux is a result of interactions related with the primary fields of an excitation layer. This fact can be traced back to Theorem 4.3.5: Taking the real parts of (4.78) we get a similar result for the active power flux directed out of excitation layer V_q.

Even more, equation (4.82) implies that the interaction between secondary fields is strictly related with the reactive power. Reactive power itself, seems to operate as a "flux-carrier", that “transfers” the induced energy flow from the excitation layer, through the scatterer’s layers, to the far-field zone. The quantity $\mathbf{S}_q^{\text{pr}} + \mathbf{S}_q^{\text{ext}}$ will be called *qprimary interaction power flux* (q-primary IPF).

Finally, we note that the overall difference between the magnetic and electric energy that are stored in the scatterer’s layers, is induced by both the secondary IPF in all layers and the q-primary IPF in excitation layer V_q.

4.3.2 Cross Sections and the Optical Theorem

In this section, we revisit the optical theorem taking into account the previous analysis. In particular, we investigate the connection between the ISCS and the interactions between the corresponding fields in the excitation layer and we highlight the connection between the various IPF with the optical theorem.

The first, we provide calculation formulas for both components of the q-primary IPF in the form of a theorem.

Theorem 4.3.6 *The power fluxes* $\mathbf{S}_q^{\mathrm{pr}}$ *and* $\mathbf{S}_q^{\mathrm{ext}}$ *satisfy the relations*

$$Z_q \mathrm{Re}\left(\int_{\partial V_q} \hat{\mathbf{n}} \cdot \mathbf{S}_q^{\mathrm{pr}}(\mathbf{r}) \mathrm{d}s(\mathbf{r})\right) = \sigma_q^{\mathrm{pr}} \tag{4.83}$$

$$\mathrm{Re}\left(\int_{\partial V_q} \hat{\mathbf{n}} \cdot \mathbf{S}_q^{\mathrm{ext}}(\mathbf{r}) \mathrm{d}s(\mathbf{r})\right) = 4\pi \sum_{j=1}^{n_q} \mathrm{Re}\left(\overline{A}_{q,j} \mathbf{H}_q^{\mathrm{sec}}(\mathbf{r}_{q,j}) \cdot \hat{\mathbf{p}}_{q,j}\right). \tag{4.84}$$

Proof. Taking the real parts of (4.82), we obtain

$$\sigma_q = Z_0 \mathrm{Re}\left(\int_{\partial V_q} \hat{\mathbf{n}} \cdot \left(\mathbf{S}_q^{\mathrm{pr}}(\mathbf{r}) + \mathbf{S}_q^{\mathrm{ext}}(\mathbf{r})\right) \mathrm{d}s(\mathbf{r})\right), \tag{4.85}$$

Equation (4.85) combined with (4.43), takes the form

$$4\pi \sum_{j=1}^{n_q} \mathrm{Re}\left(\overline{A_{q,j}} \mathbf{H}_q^{\mathrm{sec}}(\mathbf{r}_{q,j}) \cdot \hat{\mathbf{p}}_{q,j}\right) + \frac{\sigma_q^{\mathrm{pr}}}{Z_q} = \mathrm{Re}\left(\int_{\partial V_q} \hat{\mathbf{n}} \cdot \left(\mathbf{S}_q^{\mathrm{pr}}(\mathbf{r}) + \mathbf{S}_q^{\mathrm{ext}}(\mathbf{r})\right) \mathrm{d}s(\mathbf{r})\right). \tag{4.86}$$

Applying Green's second theorem for $\overline{\mathbf{E}}_{q,j}^{\mathrm{pr}}, \mathbf{E}_{q,\nu}^{\mathrm{sec}}$ in the domain $\Omega_q = V_q \setminus S_\epsilon$, with S_ϵ denoting a "small" sphere of radius ϵ enclosing the point source

$\mathbf{r}_{q,j}$, we arrive at

$$\int_{\partial V_q} \hat{\mathbf{n}} \cdot \left(\overline{\mathbf{E}}^{\mathrm{pr}}_{q,j}(\mathbf{r}) \times \mathbf{H}^{\mathrm{sec}}_{q,\nu}(\mathbf{r}) + \mathbf{E}^{\mathrm{sec}}_{q,\nu}(\mathbf{r}) \times \overline{\mathbf{H}}^{\mathrm{pr}}_{q,j}(\mathbf{r}) \right) \mathrm{d}s(\mathbf{r}) =$$
$$\int_{S_\epsilon} \hat{\mathbf{n}} \cdot \left(\overline{\mathbf{E}}^{\mathrm{pr}}_{q,j}(\mathbf{r}) \times \mathbf{H}^{\mathrm{sec}}_{q,\nu}(\mathbf{r}) + \mathbf{E}^{\mathrm{sec}}_{q,\nu}(\mathbf{r}) \times \overline{\mathbf{H}}^{\mathrm{pr}}_{q,j}(\mathbf{r}) \right) \mathrm{d}s(\mathbf{r}). \tag{4.87}$$

Implementing the mean value theorem in the last two relations for the integrals over the surface S_ϵ and by letting $\epsilon \to 0$, we obtain

$$\int_{\partial V_q} \hat{\mathbf{n}} \cdot \left(\overline{\mathbf{E}}^{\mathrm{pr}}_{q,j}(\mathbf{r}) \times \mathbf{H}^{\mathrm{sec}}_{q,\nu}(\mathbf{r}) + \mathbf{E}^{\mathrm{sec}}_{q,\nu}(\mathbf{r}) \times \overline{\mathbf{H}}^{\mathrm{pr}}_{q,j}(\mathbf{r}) \right) \mathrm{d}s(\mathbf{r}) =$$
$$4\pi \overline{A}_{q,j} \mathbf{H}^{\mathrm{sec}}_{q,\nu}(\mathbf{r}_{q,j}) \cdot \hat{\mathbf{p}}_{q,j},$$

Repetition of the preceded process for the fields $\mathbf{E}^{\mathrm{pr}}_{q,j}, \overline{\mathbf{E}}^{\mathrm{sec}}_{q,\nu}$ combined with the definition of $\mathbf{S}^{\mathrm{ext}}_{q,j}$, yields

$$\mathrm{Re}\left(\int_{\partial V_q} \hat{\mathbf{n}} \cdot \mathbf{S}^{\mathrm{ext}}_{q,j}(\mathbf{r}) \mathrm{d}s(\mathbf{r}) \right) =$$
$$4\pi \mathrm{Re}\left(\overline{A}_{q,j} \mathbf{H}^{\mathrm{sec}}_{q,\nu}(\mathbf{r}_{q,j}) \cdot \hat{\mathbf{p}}_{q,j} \right). \tag{4.88}$$

Summing the latter for all $j = 1, \ldots, n_q$ yields (4.84). Equation (4.83) is derived by combining (4.84) with (4.86).

□

It is worth noting that the individual fields interact with each other, additionally to the above-discussed IPF. Therefore, another way of discriminating the power fluxes is to categorize them according to whether they stem from interactions between the same fields or from interactions between different fields. We define the *qindividual power flux* and the *qinteraction power flux*, respectively, as follows:

$$\hat{\mathbf{S}}_q(\mathbf{r}) = \sum_{j=1}^{n_q} \left(\mathbf{E}^q_{q,j}(\mathbf{r}) \times \overline{\mathbf{H}}^q_{q,j}(\mathbf{r}) \right) \tag{4.89}$$

$$\tilde{\mathbf{S}}_q(\mathbf{r}) = \sum_{j=1}^{n_q - 1} \sum_{\nu=j+1}^{n_q} \left(\mathbf{E}^q_{q,j}(\mathbf{r}) \times \overline{\mathbf{H}}^q_{q,\nu}(\mathbf{r}) \right), \tag{4.90}$$

A straight-forward implementation of the definitions for all the IPF yields the relation connecting them:

$$\mathbf{S}_q^{\mathrm{pr}} + \mathbf{S}_q^{\mathrm{ext}} + \mathbf{S}_q^{\mathrm{sec}} = \hat{\mathbf{S}}_q + \tilde{\mathbf{S}}_q \tag{4.91}$$

Taking under consideration definition (4.24) and combined it with equation (4.82), we derive the following relation that links the q-ISCS with its corresponding power flux

$$\begin{aligned}\tilde{\sigma}_q = 2\mathrm{i}\omega Z_0 \sum_{p=0}^{P} \int_{V_p} \tilde{L}_q^p(\mathbf{r})\mathrm{d}v(\mathbf{r}) + \\ Z_0 \int_{\partial V_q} \hat{\mathbf{n}} \cdot \tilde{\mathbf{S}}_q(\mathbf{r})\mathrm{d}s(\mathbf{r}),\end{aligned} \tag{4.92}$$

with $\tilde{L}_q^p$ denoting the part of the Lagrangian density that is induced by the interaction between different individual fields radiating in V_p; note that in the above equation, $\tilde{L}_q^q$ refers to $\tilde{L}_q^{\mathrm{sec}}$.

Remark 4.3.7 *For a PEC or a PMC core, relations (4.82) and (4.92) are valid, as well by considering that $L_q^P = 0$. On the other hand, relations (4.82) and (4.92) hold even if the dipole distribution contains dipoles in scatterer's exterior, V_0.*

Now we would like to discuss more about the physical interpretation of (4.92). We focus our attention to the fact that the q-ISCS can be negative. If the q-ISCS is negative, by means of (4.92), we extract the conclusion that in such a case the active power flux will be directed inwards. Thus in this case, the power flux induced by the interaction between individual fields follows a path "returning to the source", i.e. to the excitation layer. This results in a reduction of the pace of the overall energy flow towards the scatterer's exterior. Subsequently, this will lead to a proportional reduction in the active power flux rate which is manifested by the negative sign of the q-ISCS [63], [103]. Finally, we stress that the power fluxes of (4.92) do not include individual power fluxes; only those induced by the interactions between individual fields are included.

Until now, the various energy exchanges and the energy transfer process in the case of a single excitation layer, e.g. all dipoles lie in one of the scatterer's layers (without excluding the scatterer's exterior) were investigated. The general case, however, is the case where the dipoles lie in more than one layers. When that occurs, interactions between participating fields result in different types of power fluxes are encountered.

Specifically, in each excitation layer V_q, the q-primary field $\mathbf{S}_q^{\mathrm{pr}}$ has the exact same meaning with the case of $Q = 1$ excitation layer: it is the power flux induced in V_q by all the dipoles of V_q. Nevertheless, $\mathbf{S}_q^{\mathrm{pr}}$ is only a part of the overall power flux $\mathbf{S}_q^{\mathrm{ov}}$ induced in V_q. This happens because the overall power flux in layer V_q, will contain the IPFs induced by the interaction between the q-primary field and the secondary q-excitation field, which is quantified by $\mathbf{S}_q^{\mathrm{ext}}$. Additionally, there is the IPF induced by the interactions between the q-primary field and the (secondary) fields that stem from the rest of the excitation layers and they radiate in the interior of V_q. The latter IPF in particular, is quantified by the second term in the expression

$$\mathbf{S}_q^{\mathrm{ov}}(\mathbf{r}) = \mathbf{S}_q^{\mathrm{ext}}(\mathbf{r}) + \sum_{s\neq q}\left(\mathbf{E}_q^{\mathrm{pr}}(\mathbf{r})\times\overline{\mathbf{H}}_s^q(\mathbf{r}) + \mathbf{E}_s^q(\mathbf{r})\times\overline{\mathbf{H}}_q^{\mathrm{pr}}(\mathbf{r})\right). \tag{4.93}$$

Remark 4.3.8 *We note that in the single-layer excitation case, it holds* $\mathbf{S}_q^{\mathrm{ov}} = \mathbf{S}_q^{\mathrm{ext}}$.

Now, we will present the form of the energy conservation law in the - more general - case of mixed excitation. The following theorem is proved by a procedure similar to the one of Theorem 4.3.1.

Theorem 4.3.9 *The overall scattering cross section, the overall Lagrangian*

density and the q-excitation fluxes are connected as follows:

$$\sigma = 2\mathrm{i}\omega Z_0 \sum_{p=0}^{P} \int_{V_p} L^p(\mathbf{r})\mathrm{d}v(\mathbf{r}) + Z_0 \sum_{q=1}^{Q} \int_{\partial V_q^{\mathrm{ex}}} \hat{\mathbf{n}} \cdot \left(\mathbf{S}_q^{\mathrm{pr}}(\mathbf{r}) + \mathbf{S}_q^{\mathrm{ov}}(\mathbf{r})\right) \mathrm{d}s(\mathbf{r}). \tag{4.94}$$

When V_p coincides with an excitation layer V_q^{ex}, then L^p refers to L_p^{sec}. If we take into account definition (4.26), we obtain

$$\sigma^{\mathrm{T}} = 2\mathrm{i}\omega Z_0 \sum_{p=0}^{P} \int_{V_p} L_p^{\mathrm{T}}(\mathbf{r})\mathrm{d}v(\mathbf{r}) + Z_0 \sum_{q=1}^{Q} \int_{\partial V_q^{\mathrm{ex}}} \hat{\mathbf{n}} \cdot \tilde{\mathbf{S}}_q^{\mathrm{T}}(\mathbf{r})\mathrm{d}s(\mathbf{r}), \tag{4.95}$$

where L_p^{T} and $\tilde{\mathbf{S}}_q^{\mathrm{T}}$ denote the parts of the Lagrangian density and the power flux, respectively, induced by the interactions between fields generated by different dipoles. On the other hand, definition (4.25) implies

$$\sigma^{\mathrm{I}} = 2\mathrm{i}\omega Z_0 \sum_{p=0}^{P} \int_{V_p} L_p^{\mathrm{I}}(\mathbf{r})\mathrm{d}v(\mathbf{r}) + Z_0 \sum_{q=1}^{Q} \int_{\partial V_q^{\mathrm{ex}}} \hat{\mathbf{n}} \cdot \tilde{\mathbf{S}}_q^{\mathrm{I}}(\mathbf{r})\mathrm{d}s(\mathbf{r}), \tag{4.96}$$

where L_p^{I} and $\tilde{\mathbf{S}}_q^{\mathrm{I}}$ denote the parts of the Lagrangian density and the power flux, respectively, induced by the interactions between fields generated in different layers. If we look closely at relation (4.96), we will observe that the IPF attributed to the primary fields is absent. This is not unexpected - quite the contrary, given the fact that the indirect ISCS quantifies the interaction between fields excited in different layers.

Remark 4.3.10 *We to note that the case of $N > 2$ dipoles is not a mere generalization of the case of $N = 2$. When the scatterer is excited by $N = 2$ dipoles, these dipoles will lie either in the same layer or in a different one. Therefore, only one type of IPF–and subsequently ISCS–can occur. However, when the scatterer is excited by $N > 2$ dipoles, there*

is a chance to have both types of IPF (direct and indirect). When that occurs, the behavior of the overall scattering cross section [103] might be significantly affected. Furthermore, in the case where $N = 2$*, the partial fields coincide with the individual fields and the only IPF present is the one quantifying the power flux induced by the interaction between the* $N = 2$ *dipoles. Evidently, for a multitude of* $N > 2$ *dipoles, this can never occur.*

Chapter 5

The Layered Sphere Excited by N Dipoles

5.1 Geometry Setting

We consider a spherical scatterer of radius a_1, divided into P nested, concentric spherical shells V_p $(p = 1, \ldots, P)$, by $P-1$ spherical surfaces S_p, each characterized by radius a_p with $(p = 2, \ldots, P)$, see figure 5.1. Each layer V_p, geometrically defined by $a_{p+1} \leq r \leq a_p$, is characterized by real wavenumbers k_p, electric permitivities ϵ_p and magnetic permeabilities μ_p with $p = 1, \ldots, P-1$. The exterior V_0 of the scatterer is characterized by wavenumber k_0, electric permitivity ϵ_0 and magnetic permeability μ_0. Of all P layers, Q of them with $Q \leq P+1$, contain n_q magnetic dipoles distributed in their interior, in arbitrary fashion. Each dipole contained in an *excitation layer* V_q, has a location vector $\mathbf{r}_{q,j}$ with respect to the sphere's center, and possesses dipole moment $\hat{\mathbf{p}}_{q,j}$ for $j = 1, \ldots, n_q$ and $q = 1, \ldots, Q$. These dipoles generate spherical waves, with the corresponding *individual primary fields* given by

$$\mathbf{E}^{\mathrm{pr}}_{q,j}(\mathbf{r}) = \mathrm{i}\omega\mu_q \widetilde{\mathbf{G}}(\mathbf{r}, \mathbf{r}_{q,j}) \cdot \mathbf{p}_{q,j}. \tag{5.1}$$

with $\widetilde{\mathbf{G}}(\mathbf{r}, \mathbf{r}_{q,j})$ denoting the dyadic Green's function. Vector $\mathbf{p}_{q,j}$ denotes the *polarized strength* of the dipole, which is given by

$$\mathbf{p}_{q,j} = A_{q,j}\hat{\mathbf{p}}_{q,j} \tag{5.2}$$

with $A_{q,j}$ being the dipole's strength constant.

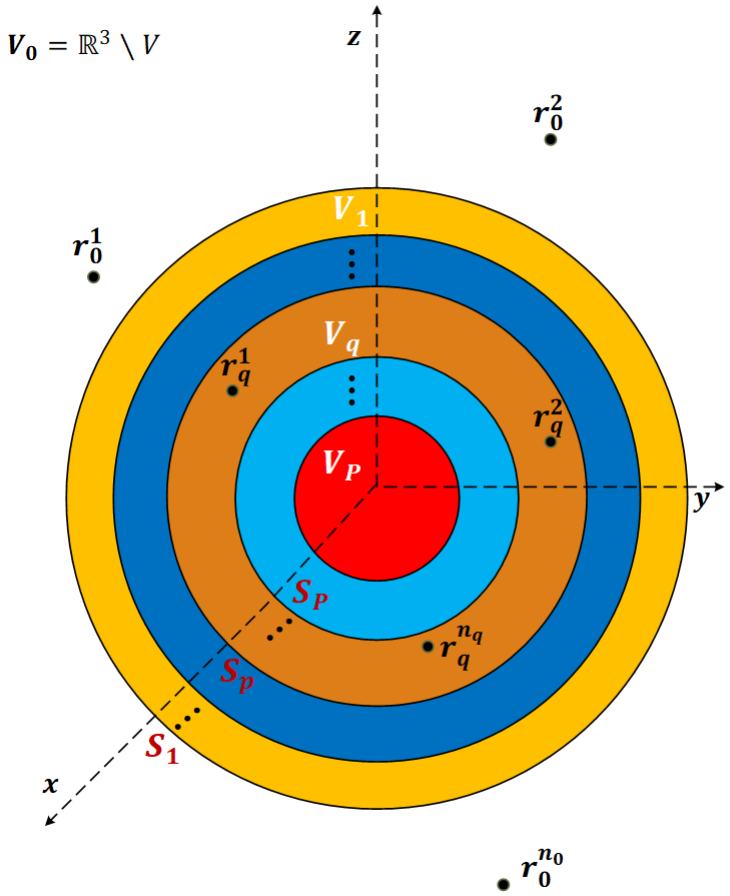

Figure 5.1: Layered spherical medium excited by N arbitrarily located point sources

On each of the spherical surfaces, S_p, the overall fields satisfy for $p = 1, \ldots, P-1$ the *dielectric boundary conditions*

$$\hat{\mathbf{r}} \times \mathbf{E}^{p-1}(\mathbf{r}) = \hat{\mathbf{r}} \times \mathbf{E}^{p}(\mathbf{r}), \quad r = a_p \tag{5.3}$$

$$\hat{\mathbf{r}} \times \mathbf{H}^{p-1}(\mathbf{r}) = \hat{\mathbf{r}} \times \mathbf{H}^{p}(\mathbf{r}), \quad r = a_p. \tag{5.4}$$

The medium's core V_P can be a PEC, a PMC or lossless dielectric. For a PEC core or a PMC core, the respective boundary conditions will read

$$\hat{\mathbf{r}} \times \mathbf{E}^{P-1}(\mathbf{r}) = 0, \quad r = a_P \tag{5.5}$$

$$\hat{\mathbf{r}} \times \mathbf{H}^{P-1}(\mathbf{r}) = 0, \quad r = a_P, \tag{5.6}$$

while for a dielectric core, conditions (5.3)-(5.4) are valid for V_P as well.

5.2 Excitation Operators and Fields' Expansions

We chose a spherical coordinate system (r, θ, ϕ) so that the sphere's center O coincides with the system's origin. Then, each dipole is identified by its location vector $\mathbf{r}_{q,j} = (r_{q,j}, \theta_{q,j}, \phi_{q,j})$ with $a_{q+1} < r_{q,j} < a_q$, for $j = 1, \ldots, n_q$. Utilizing the spherical vector wave functions (SVWF) to expand the primary electric fields, we arrive at [69]

$$\mathbf{E}^{\mathrm{pr}}_{q,j}(\mathbf{r}) = \frac{\mathrm{i}k_q}{4\pi} \sum_{n,m,s} c_{nm} \times \begin{cases} \left(\mathbf{M}^3_{snm}(\mathbf{r}, k_q) \mathbf{M}^1_{snm}(\mathbf{r}_{q,j}, k_q) + \mathbf{N}^3_{snm}(\mathbf{r}, k_q) \mathbf{N}^1_{snm}(\mathbf{r}_{q,j}, k_q) \right) \cdot \mathbf{p}_{q,j}, & r > r_{q,j} \\ \left(\mathbf{M}^1_{snm}(\mathbf{r}, k_q) \mathbf{M}^3_{snm}(\mathbf{r}_{q,j}, k_q) + \mathbf{N}^1_{snm}(\mathbf{r}, k_q) \mathbf{N}^3_{snm}(\mathbf{r}_{q,j}, k_q) \right) \cdot \mathbf{p}_{q,j}, & r < r_{q,j} \end{cases} \tag{5.7}$$

with $\sum_{n,m,s}$ denoting the triple sum with respect to n, m, s, i.e.

$$\sum_{n,m,s} a_{nms} = \sum_{n=1}^{\infty} \sum_{m=0}^{n} \sum_{s=e}^{o} a_{nms}$$

We note that the subscript $s \in \{e, o\}$ refers to whether the involved SVWF are even or odd, see (B.19)-(B.23) of [98]; The coefficient c_{nm} is given by

$$c_{nm} = \frac{2n+1}{n(n+1)} \frac{(n-m)!}{(n+m)!} \epsilon_m$$

with ϵ_m denoting the Neumann factor

$$\epsilon_m = \begin{cases} 1, & m = 0 \\ 2, & m > 0 \end{cases} \tag{5.8}$$

The individual secondary fields in V_p are expanded as

$$\begin{aligned}\mathbf{E}^p_{q,j}(\mathbf{r}) = \frac{\mathrm{i}k_q}{4\pi}\sum_{n,m,s} c_{nm}\times \\ \Bigg[\mathbf{M}^1_{snm}(\mathbf{r},k_q)\left(a^{q,j}_{n,p}\mathbf{M}^1_{snm}(\mathbf{r}_{q,j},k_q)+b^{q,j}_{n,p}\mathbf{M}^3_{snm}(\mathbf{r}_{q,j},k_q)\right) \\ +\mathbf{N}^1_{snm}(\mathbf{r},k_q)\left(c^{q,j}_{n,p}\mathbf{N}^1_{snm}(\mathbf{r}_{q,j},k_q)+d^{q,j}_{n,p}\mathbf{N}^3_{snm}(\mathbf{r}_{q,j},k_q)\right) \\ +\mathbf{M}^3_{snm}(\mathbf{r},k_q)\left(\tilde{a}^{q,j}_{n,p}\mathbf{M}^1_{snm}(\mathbf{r}_{q,j},k_q)+\tilde{b}^{q,j}_{n,p}\mathbf{M}^3_{snm}(\mathbf{r}_{q,j},k_q)\right) \\ +\mathbf{N}^3_{snm}(\mathbf{r},k_q)\left(\tilde{c}^{q,j}_{n,p}\mathbf{N}^1_{snm}(\mathbf{r}_{q,j},k_q)+\tilde{d}^{q,j}_{n,p}\mathbf{N}^3_{snm}(\mathbf{r}_{q,j},k_q)\right)\Bigg]\cdot\mathbf{p}_{q,j} \quad (5.9)\end{aligned}$$

where $\mathbf{X}^\ell_{snm}$ with $\mathbf{X}\in\{\mathbf{M},\mathbf{N}\}, s\in\{e,o\}, \ell\in\{1,3\}$ denote the spherical vector wave functions (SVWF).

Now, we define the following *q-excitation operators*

$$\mathcal{M}^1_{snm}(\mathbf{x}_q) = \frac{\mathrm{i}k_q}{4\pi}c_{nm}\sum_{j=1}^{n_q} x_{q,j}\mathbf{M}^1_{snm}(\mathbf{r}_{q,j},k_q)\cdot\mathbf{p}_{q,j} \quad (5.10)$$

$$\mathcal{M}^3_{snm}(\mathbf{x}_q) = \frac{\mathrm{i}k_q}{4\pi}c_{nm}\sum_{j=1}^{n_q} x_{q,j}\mathbf{M}^3_{snm}(\mathbf{r}_{q,j},k_q)\cdot\mathbf{p}_{q,j}, \quad (5.11)$$

$$\mathcal{N}^1_{snm}(\mathbf{x}_q) = \frac{\mathrm{i}k_q}{4\pi}c_{nm}\sum_{j=1}^{n_q} x_{q,j}\mathbf{N}^1_{snm}(\mathbf{r}_{q,j},k_q)\cdot\mathbf{p}_{q,j} \quad (5.12)$$

$$\mathcal{N}^3_{snm}(\mathbf{x}_q) = \frac{\mathrm{i}k_q}{4\pi}c_{nm}\sum_{j=1}^{n_q} x_{q,j}\mathbf{N}^3_{snm}(\mathbf{r}_{q,j},k_q)\cdot\mathbf{p}_{q,j}, \quad (5.13)$$

where $\mathbf{x_q} = (\mathrm{x}^1_q,\ldots,\mathrm{x}^{n_q}_q)$ arbitrary vectors of $\mathbb{R}^{n_q}$. By denoting

$$\begin{aligned}\mathcal{A}^p_{s,n,m,q} &= \mathcal{M}^1_{snm}(\mathbf{a}^p_{n,q}), \quad \tilde{\mathcal{A}}^p_{s,n,m,q} = \mathcal{M}^1_{snm}(\tilde{\mathbf{a}}^p_{n,q}) \\ \mathcal{B}^p_{s,n,m,q} &= \mathcal{M}^3_{snm}(\mathbf{b}^p_{n,q}), \quad \tilde{\mathcal{B}}^p_{s,n,m,q} = \mathcal{M}^3_{snm}(\tilde{\mathbf{b}}^p_{n,q}) \\ \mathcal{C}^p_{s,n,m,q} &= \mathcal{N}^1_{snm}(\mathbf{c}^p_{n,q}), \quad \tilde{\mathcal{C}}^p_{s,n,m,q} = \mathcal{N}^1_{snm}(\tilde{\mathbf{c}}^p_{n,q}) \\ \mathcal{D}^p_{s,n,m,q} &= \mathcal{N}^3_{snm}(\mathbf{d}^p_{n,q}), \quad \tilde{\mathcal{D}}^p_{s,n,m,q} = \mathcal{M}^3_{snm}(\tilde{\mathbf{d}}^p_{n,q})\end{aligned}$$

where $\mathbf{x}_{n,q}^{p} = (x_{1,n,q}^{p}, \ldots, x_{N,n,q}^{p})$ with $x \in \{a, b, c, d\}$ are the vectors with components the unknown coefficients of the individual secondary fields. Taking under consideration the expansions (5.7), (5.9), and utilize the definitions of overall primary and secondary fields, we obtain the following expansions for the q-excitation primary fields

$$\mathbf{E}_{q}^{\mathrm{pr}}(\mathbf{r}) = \sum_{n,m,s} \begin{cases} \mathbf{M}_{snm}^{3}(\mathbf{r}, k_q)\mathcal{M}_{snm}^{1}(\mathbf{u}_q) + \mathbf{N}_{snm}^{3}(\mathbf{r}, k_q)\mathcal{N}_{snm}^{1}(\mathbf{u}_q), & r > r_{q,j} \\ \mathbf{M}_{snm}^{1}(\mathbf{r}, k_q)\mathcal{M}_{snm}^{3}(\mathbf{u}_q) + \mathbf{N}_{snm}^{1}(\mathbf{r}, k_q)\mathcal{N}_{snm}^{3}(\mathbf{u}_q), & r < r_{q,j}, \end{cases}$$

where $\mathbf{u_q}$ denotes the n_q-dimensional vector $(1, 1, \ldots, 1)$. In a similar manner, the expansion of the overall secondary field of V_p is derived as follows

$$\begin{aligned} &\mathbf{E}^{p}(\mathbf{r}) = \\ &\sum_{n,m,s} \Bigg[\mathbf{M}_{snm}^{1}(\mathbf{r}, k_q) \left(\mathcal{A}_{s,n,m}^{p} + \mathcal{B}_{s,n,m}^{p} \right) + \mathbf{N}_{snm}^{1}(\mathbf{r}, k_q) \left(\mathcal{C}_{s,n,m}^{p} + \mathcal{D}_{s,n,m}^{p} \right) \\ &\quad + \mathbf{M}_{snm}^{3}(\mathbf{r}, k_q) \left(\tilde{\mathcal{A}}_{s,n,m}^{p} + \tilde{\mathcal{B}}_{s,n,m}^{p} \right) + \mathbf{N}_{snm}^{3}(\mathbf{r}, k_q) \left(\tilde{\mathcal{C}}_{s,n,m}^{p} + \tilde{\mathcal{D}}_{s,n,m}^{p} \right) \Bigg] \end{aligned} \tag{5.14}$$

where $x_{s,n,m}^{p} = \sum_{q=1}^{Q} x_{s,n,m,q}^{p}$, the under-determination coefficients of the overall field of V_p with $x \in \{\mathcal{A}, \mathcal{B}, \mathcal{C}, \mathcal{D}, \tilde{\mathcal{A}}, \tilde{\mathcal{B}}, \tilde{\mathcal{C}}, \tilde{\mathcal{D}}\}$.

5.3 Solution of the Direct Problem

Considering the orthogonality properties of the SVWF and imposing boundary conditions, on the boundaries of layers V_p for $p = 1, \ldots, P-1$, we obtain

$$\begin{bmatrix} \mathcal{A}_{s,n,m}^{p} & \mathcal{B}_{s,n,m}^{p} \\ \tilde{\mathcal{A}}_{s,n,m}^{p} & \tilde{\mathcal{B}}_{s,n,m}^{p} \end{bmatrix} = \mathbf{T}_{n}^{(0 \to p)} \cdot \begin{bmatrix} 0 & 0 \\ \tilde{\mathcal{A}}_{s,n,m}^{0} & \tilde{\mathcal{B}}_{s,n,m}^{0} \end{bmatrix} \tag{5.15}$$

$$\begin{bmatrix} \mathcal{C}_{s,n,m}^{p} & \mathcal{D}_{s,n,m}^{p} \\ \tilde{\mathcal{C}}_{s,n,m}^{p} & \tilde{\mathcal{D}}_{s,n,m}^{p} \end{bmatrix} = \mathbf{S}_{n}^{(0 \to p)} \cdot \begin{bmatrix} 0 & 0 \\ \tilde{\mathcal{C}}_{s,n,m}^{0} & \tilde{\mathcal{D}}_{s,n,m}^{0} \end{bmatrix} \tag{5.16}$$

where $\mathbf{T}_n^p, \mathbf{S}_n^p$ are the *transition matrices* from layer V_{p-1} to layer V_p (see [83]), which can be written in the form

$$\mathbf{T}_n^p = -\mathrm{i}x_p^2 \begin{bmatrix} \mathcal{U}_p(h_n, j_n) & \mathcal{U}_p(h_n, h_n) \\ -\mathcal{U}_p(j_n, j_n) & -\mathcal{U}_p(j_n, h_n) \end{bmatrix}$$

$$\mathbf{S}_n^p = -\mathrm{i}x_p^2 \begin{bmatrix} \mathcal{V}_p(h_n, j_n) & \mathcal{V}_p(h_n, h_n) \\ -\mathcal{V}_p(j_n, j_n) & -\mathcal{V}_p(j_n, h_n) \end{bmatrix}$$

with functionals $\mathcal{U}_p, \mathcal{V}_p$ given by

$$\mathcal{U}_p(f,g)(x_p, y_p) = \tilde{f}(x_p)g(y_p) - \frac{\sqrt{\mu_p \epsilon_{p-1}}}{\sqrt{\mu_{p_1}\epsilon p}} f(x_p)\tilde{g}(y_p)$$

$$\mathcal{V}_p(f,g)(x_p, y_p) = \frac{\sqrt{\mu_p \epsilon_{p-1}}}{\sqrt{\mu_{p_1}\epsilon p}} \tilde{f}(x_p)g(y_p) - f(x_p)\tilde{g}(y_p)$$

and $\mathbf{T}_n^{(0\to p)}, \mathbf{S}_n^{(0\to p)}$ are the transition matrices from the exterior V_0 to layer V_p given by $\mathbf{A}_n^{(0\to p)} = \mathbf{A}_n^p \, \mathbf{A}_n^{p-1} \ldots \mathbf{A}_n^1$ for $\mathbf{A} \in \{\mathbf{T}, \mathbf{S}\}$. Let V_q for $q \in \{1, \ldots, P\}$ be the first layer (closer to the exterior V_0) that contains point sources. Then it holds:

$$\begin{bmatrix} \mathcal{A}_{s,n,m}^q & \mathcal{B}_{s,n,m}^q \\ \tilde{\mathcal{A}}_{s,n,m}^q + \mathcal{M}_{snm}^1(\mathbf{u}_q) & \tilde{\mathcal{B}}_{s,n,m}^q \end{bmatrix} = \mathbf{T}_n^{(0\to q)} \cdot \begin{bmatrix} 0 & 0 \\ \tilde{\mathcal{A}}_{s,n,m}^0 & \tilde{\mathcal{B}}_{s,n,m}^0 \end{bmatrix} \tag{5.17}$$

$$\begin{bmatrix} \mathcal{C}_{s,n,m}^q & \mathcal{D}_{s,n,m}^q \\ \tilde{\mathcal{C}}_{s,n,m}^q + \mathcal{N}_{snm}^1(\mathbf{u}_q) & \tilde{\mathcal{D}}_{s,n,m}^q \end{bmatrix} = \mathbf{S}_n^{(0\to q)} \cdot \begin{bmatrix} 0 & 0 \\ \tilde{\mathcal{C}}_{s,n,m}^0 & \tilde{\mathcal{D}}_{s,n,m}^0 \end{bmatrix} \tag{5.18}$$

Boundary conditions at layer V_{q+1} yield:

$$\begin{bmatrix} \mathcal{A}_{s,n,m}^{q+1} & \mathcal{B}_{s,n,m}^{q+1} \\ \tilde{\mathcal{A}}_{s,n,m}^{q+1} & \tilde{\mathcal{B}}_{s,n,m}^{q+1} \end{bmatrix} = \mathbf{T}_n^{q+1} \cdot \begin{bmatrix} \mathcal{A}_{s,n,m}^q & \mathcal{B}_{s,n,m}^q + \mathcal{M}_{snm}^3(\mathbf{u}_q) \\ \tilde{\mathcal{A}}_{s,n,m}^q & \tilde{\mathcal{B}}_{s,n,m}^q \end{bmatrix} \tag{5.19}$$

$$\begin{bmatrix} \mathcal{C}_{s,n,m}^{q+1} & \mathcal{D}_{s,n,m}^{q+1} \\ \tilde{\mathcal{C}}_{s,n,m}^{q+1} & \tilde{\mathcal{D}}_{s,n,m}^{q+1} \end{bmatrix} = \mathbf{S}_n^{q+1} \cdot \begin{bmatrix} \mathcal{C}_{s,n,m}^q & \mathcal{D}_{s,n,m}^q + \mathcal{N}_{snm}^3(\mathbf{u}_q) \\ \tilde{\mathcal{C}}_{s,n,m}^q & \tilde{\mathcal{D}}_{s,n,m}^q \end{bmatrix} \tag{5.20}$$

Combining (5.17) with (5.19) and (5.18) with (5.20) we obtain:

$$\begin{aligned} \begin{bmatrix} \mathcal{A}_{s,n,m}^{q+1} & \mathcal{B}_{s,n,m}^{q+1} \\ \tilde{\mathcal{A}}_{s,n,m}^{q+1} & \tilde{\mathcal{B}}_{s,n,m}^{q+1} \end{bmatrix} =& \mathbf{T}_n^{(0\to q+1)} \cdot \begin{bmatrix} 0 & 0 \\ \tilde{\mathcal{A}}_{s,n,m}^0 & \tilde{\mathcal{B}}_{s,n,m}^0 \end{bmatrix} + \\ & \mathbf{T}_n^{q+1} \cdot \begin{bmatrix} 0 & \mathcal{M}_{snm}^3(\mathbf{1}_q) \\ -\mathcal{M}_{snm}^1(\mathbf{u}_q) & 0 \end{bmatrix} \end{aligned} \tag{5.21}$$

$$\begin{bmatrix} \mathcal{C}^{q+1}_{s,n,m} & \mathcal{D}^{q+1}_{s,n,m} \\ \tilde{\mathcal{C}}^{q+1}_{s,n,m} & \tilde{\mathcal{D}}^{q+1}_{s,n,m} \end{bmatrix} = \mathbf{S}^{(0\to q+1)}_n \cdot \begin{bmatrix} 0 & 0 \\ \tilde{\mathcal{C}}^{0}_{s,n,m} & \tilde{\mathcal{D}}^{0}_{s,n,m} \end{bmatrix} + \mathbf{S}^{q+1}_n \cdot \begin{bmatrix} 0 & \mathcal{N}^3_{snm}(\mathbf{u}_q) \\ -\mathcal{N}^1_{snm}(\mathbf{u}_q) & 0 \end{bmatrix} \tag{5.22}$$

Let V_ν be the next (closer to V_q) layer that contains sources. Then it will hold:

$$\begin{bmatrix} \mathcal{A}^{\nu}_{s,n,m} & \mathcal{B}^{\nu}_{s,n,m} \\ \tilde{\mathcal{A}}^{\nu}_{s,n,m} + \mathcal{M}^1_{snm}(\mathbf{u}_\nu) & \tilde{\mathcal{A}}^{\nu}_{s,n,m} \end{bmatrix} = \mathbf{T}^{(q\to\nu)}_n \cdot \begin{bmatrix} \mathcal{A}^{q+1}_{s,n,m} & \mathcal{B}^{q+1}_{s,n,m} \\ \tilde{\mathcal{A}}^{q+1}_{s,n,m} & \tilde{\mathcal{B}}^{q+1}_{s,n,m} \end{bmatrix} \tag{5.23}$$

$$\begin{bmatrix} \mathcal{C}^{\nu}_{s,n,m} & \mathcal{D}^{\nu}_{s,n,m} \\ \tilde{\mathcal{C}}^{\nu}_{s,n,m} + \mathcal{N}^1_{snm}(\mathbf{u}_\nu) & \tilde{\mathcal{D}}^{\nu}_{s,n,m} \end{bmatrix} = \mathbf{S}^{(q\to\nu)}_n \cdot \begin{bmatrix} \mathcal{C}^{q+1}_{s,n,m} & \mathcal{D}^{q+1}_{s,n,m} \\ \tilde{\mathcal{C}}^{q+1}_{s,n,m} & \tilde{\mathcal{D}}^{q+1}_{s,n,m} \end{bmatrix}. \tag{5.24}$$

$$\begin{bmatrix} \mathcal{A}^{\nu+1}_{s,n,m} & \mathcal{B}^{\nu+1}_{s,n,m} \\ \tilde{\mathcal{A}}^{\nu+1}_{s,n,m} & \tilde{\mathcal{B}}^{\nu+1}_{s,n,m} \end{bmatrix} = \mathbf{T}^{\nu+1}_n \cdot \begin{bmatrix} \mathcal{A}^{\nu}_{s,n,m} & \mathcal{B}^{\nu}_{s,n,m} + \mathcal{M}^3_{snm}(\mathbf{u}_\nu) \\ \tilde{\mathcal{A}}^{\nu}_{s,n,m} & \tilde{\mathcal{B}}^{\nu}_{s,n,m} \end{bmatrix} \tag{5.25}$$

$$\begin{bmatrix} \mathcal{C}^{\nu+1}_{s,n,m} & \mathcal{D}^{\nu+1}_{s,n,m} \\ \tilde{\mathcal{C}}^{\nu+1}_{s,n,m} & \tilde{\mathcal{D}}^{\nu+1}_{s,n,m} \end{bmatrix} = \mathbf{S}^{\nu+1}_n \cdot \begin{bmatrix} \mathcal{C}^{\nu}_{s,n,m} & \mathcal{D}^{\nu}_{s,n,m} + \mathcal{N}^3_{snm}(\mathbf{u}_\nu) \\ \tilde{\mathcal{C}}^{\nu}_{s,n,m} & \tilde{\mathcal{D}}^{\nu}_{s,n,m} \end{bmatrix}. \tag{5.26}$$

Combining above relations, we arrive at:

$$\begin{aligned} \begin{bmatrix} \mathcal{A}^{\nu+1}_{s,n,m} & \mathcal{B}^{\nu+1}_{s,n,m} \\ \tilde{\mathcal{A}}^{\nu+1}_{s,n,m} & \tilde{\mathcal{B}}^{\nu+1}_{s,n,m} \end{bmatrix} =& \mathbf{T}^{(0\to\nu+1)}_n \cdot \begin{bmatrix} 0 & 0 \\ \tilde{\mathcal{A}}^{0}_{s,n,m} & \tilde{\mathcal{B}}^{0}_{s,n,m} \end{bmatrix} + \\ & \mathbf{T}^{(q\to\nu)}_n \cdot \begin{bmatrix} 0 & \mathcal{M}^3_{snm}(\mathbf{u}_q) \\ -\mathcal{M}^1_{snm}(\mathbf{u}_q) & 0 \end{bmatrix} + \\ & \mathbf{T}^{\nu+1}_n \cdot \begin{bmatrix} 0 & \mathcal{M}^3_{snm}(\mathbf{u}_\nu) \\ -\mathcal{M}^1_{snm}(\mathbf{u}_\nu) & 0 \end{bmatrix} \end{aligned} \tag{5.27}$$

$$\begin{aligned} \begin{bmatrix} \mathcal{C}^{\nu+1}_{s,n,m} & \mathcal{D}^{\nu+1}_{s,n,m} \\ \tilde{\mathcal{C}}^{\nu+1}_{s,n,m} & \tilde{\mathcal{D}}^{\nu+1}_{s,n,m} \end{bmatrix} =& \mathbf{S}^{(0\to\nu+1)}_n \cdot \begin{bmatrix} 0 & 0 \\ \tilde{\mathcal{C}}^{0}_{s,n,m} & \tilde{\mathcal{D}}^{0}_{s,n,m} \end{bmatrix} + \\ & \mathbf{S}^{(q\to\nu)}_n \cdot \begin{bmatrix} 0 & \mathcal{N}^3_{snm}(\mathbf{u}_q) \\ -\mathcal{N}^1_{snm}(\mathbf{u}_q) & 0 \end{bmatrix} + \\ & \mathbf{S}^{\nu+1}_n \cdot \begin{bmatrix} 0 & \mathcal{N}^3_{snm}(\mathbf{u}_\nu) \\ -\mathcal{N}^1_{snm}(\mathbf{u}_\nu) & 0 \end{bmatrix} \end{aligned} \tag{5.28}$$

From successive implementation of the boundary conditions, we conclude that it will finally hold:

$$\begin{bmatrix} \mathcal{A}^{P-1}_{s,n,m} & \mathcal{B}^{P-1}_{s,n,m} \\ \tilde{\mathcal{A}}^{P-1}_{s,n,m} & \tilde{\mathcal{B}}^{P-1}_{s,n,m} \end{bmatrix} = \mathbf{T}_n^{(0\to P-1)} \cdot \begin{bmatrix} 0 & 0 \\ \tilde{\mathcal{A}}^{0}_{s,n,m} & \tilde{\mathcal{B}}^{0}_{s,n,m} \end{bmatrix} + \sum_{q=1}^{Q} \mathbf{T}_n^{(q\to P-1)} \cdot \begin{bmatrix} 0 & \mathcal{M}^{3}_{snm}(\mathbf{u}_q) \\ -\mathcal{M}^{1}_{snm}(\mathbf{u}_q) & 0 \end{bmatrix} \tag{5.29}$$

$$\begin{bmatrix} \mathcal{C}^{P-1}_{s,n,m} & \mathcal{D}^{P-1}_{s,n,m} \\ \tilde{\mathcal{C}}^{P-1}_{s,n,m} & \tilde{\mathcal{D}}^{P-1}_{s,n,m} \end{bmatrix} = \mathbf{S}_n^{(0\to P-1)} \cdot \begin{bmatrix} 0 & 0 \\ \tilde{\mathcal{C}}^{0}_{s,n,m} & \tilde{\mathcal{D}}^{0}_{s,n,m} \end{bmatrix} + \sum_{q=1}^{Q} \mathbf{S}_n^{(q\to P-1)} \cdot \begin{bmatrix} 0 & \mathcal{N}^{3}_{snm}(\mathbf{u}_q) \\ -\mathcal{N}^{1}_{snm}(\mathbf{u}_q) & 0 \end{bmatrix} \tag{5.30}$$

where q is used in reference to excitation layer V_q. For a PEC core we obtain:

$$\tilde{\mathcal{A}}^{0}_{s,n,m} = \sum_{q=1}^{Q} \frac{\Psi^2_{n,q}(k_q a_{q+1})}{\Psi^2_{n,P-1}(k_{P-1}a_P)} \mathcal{M}^{1}_{snm}(\mathbf{u}_q) \tag{5.31}$$

$$\tilde{\mathcal{B}}^{0}_{s,n,m} = -\sum_{q=1}^{Q} \frac{\Psi^1_{n,q}(k_q a_{q+1})}{\Psi^2_{n,P-1}(k_{P-1}a_P)} \mathcal{M}^{3}_{snm}(\mathbf{u}_q) \tag{5.32}$$

$$\tilde{\mathcal{C}}^{0}_{s,n,m} = \sum_{q=1}^{Q} \frac{\Omega^2_{n,q}(k_q a_{q+1})}{\Omega^2_{n,P-1}(k_{P-1}a_P)} \mathcal{N}^{1}_{snm}(\mathbf{u}_q) \tag{5.33}$$

$$\tilde{\mathcal{D}}^{0}_{s,n,m} = -\sum_{q=1}^{Q} \frac{\Omega^1_{n,q}(k_q a_{q+1})}{\Omega^2_{n,P-1}(k_{P-1}a_P)} \mathcal{N}^{3}_{snm}(\mathbf{u}_q) \tag{5.34}$$

where $\Psi^1_{n,p}, \Psi^2_{n,p}$ and $\Omega^1_{n,p}, \Omega^2_{n,p}$ the components of the *boundary transition vectors* $\mathbf{\Psi}_{n,p}(x), \mathbf{\Omega}_{n,p}(x)$ which are defined as follows:

$$\mathbf{\Psi}_{n,p}(x) = (\mathbf{T}_n^{(p\to P-1)})^{\mathrm{T}} \cdot \begin{bmatrix} j_n(x) \\ h_n(x) \end{bmatrix} \tag{5.35}$$

$$\mathbf{\Omega}_{n,p}(x) = (\mathbf{S}_n^{(p\to P-1)})^{\mathrm{T}} \cdot \begin{bmatrix} \hat{j}_n(x) \\ \hat{h}_n(x) \end{bmatrix} \tag{5.36}$$

For a PMC core, corresponding results are:

$$\tilde{\mathcal{A}}^0_{s,n,m} = \sum_{q=1}^{Q} \frac{\Phi^2_{n,q}(k_q a_{q+1})}{\Phi^2_{n,P-1}(k_{P-1} a_P)} \mathcal{M}^1_{snm}(\mathbf{u}_q) \tag{5.37}$$

$$\tilde{\mathcal{B}}^0_{s,n,m} = -\sum_{q=1}^{Q} \frac{\Phi^1_{n,q}(k_q a_{q+1})}{\Phi^2_{n,P-1}(k_{P-1} a_P)} \mathcal{M}^3_{snm}(\mathbf{u}_q) \tag{5.38}$$

$$\tilde{\mathcal{C}}^0_{s,n,m} = \sum_{q=1}^{Q} \frac{X^2_{n,q}(k_q a_{q+1})}{X^2_{n,P-1}(k_{P-1} a_P)} \mathcal{N}^1_{snm}(\mathbf{u}_q) \tag{5.39}$$

$$\tilde{\mathcal{D}}^0_{s,n,m} = -\sum_{q=1}^{Q} \frac{X^1_{n,q}(k_q a_{q+1})}{X^2_{n,P-1}(k_{P-1} a_P)} \mathcal{N}^3_{snm}(\mathbf{u}_q) \tag{5.40}$$

where $\Phi^1_{n,p}, \Phi^2_{n,p}$ and $X^1_{n,p}, X^2_{n,p}$ the components of the *boundary transition vectors* $\mathbf{\Phi}_{n,p}(x), \mathbf{X}_{n,p}(x)$ which are defined as follows:

$$\mathbf{\Phi}_{n,p}(x) = (\mathbf{T}_n^{(p\to P-1)})^{\mathrm{T}} \cdot \begin{bmatrix} j_n'(x) \\ h_n'(x) \end{bmatrix} \tag{5.41}$$

$$\mathbf{X}_{n,p}(x) = (\mathbf{S}_n^{(p\to P-1)})^{\mathrm{T}} \cdot \begin{bmatrix} \hat{j}_n'(x) \\ \hat{h}_n'(x) \end{bmatrix} \tag{5.42}$$

where $\hat{j}_n(x), \hat{h}_n(x)$ denote the Riccatti-Bessel functions. Finally, for a dielectric core we obtain:

$$\tilde{\mathcal{A}}^0_{s,n,m} = \sum_{q=1}^{Q} \frac{T^{(q\to P)}_{n,22}}{T^{(0\to P)}_{n,22}} \mathcal{M}^1_{snm}(\mathbf{u}_q) \tag{5.43}$$

$$\tilde{\mathcal{B}}^0_{s,n,m} = -\sum_{q=1}^{Q} \frac{T^{(q\to P)}_{n,21}}{T^{(0\to P)}_{n,22}} \mathcal{M}^3_{snm}(\mathbf{u}_q) \tag{5.44}$$

$$\tilde{\mathcal{C}}^0_{s,n,m} = \sum_{q=1}^{Q} \frac{S^{(q\to P)}_{n,22}}{S^{(0\to P)}_{n,22}} \mathcal{N}^1_{snm}(\mathbf{u}_q) \tag{5.45}$$

$$\tilde{\mathcal{D}}^0_{s,n,m} = -\sum_{q=1}^{Q} \frac{S^{(q\to P)}_{n,21}}{S^{(0\to P)}_{n,22}} \mathcal{N}^3_{snm}(\mathbf{u}_q) \tag{5.46}$$

where $A_{n,ij}^{(q\to u)}$ denotes the $ij-$ component of matrix $A_n^{(q\to u)}$. Now, we present the formulas for two cases, of special importance,as they are often encountered in real-world applications. First, the external excitation (all dipoles lie in the exterior V_0) and core excitation (all dipoles lie in the sphere's core). For the external excitation it holds

$$\tilde{\mathcal{A}}_{s,n,m}^0 = 0, \quad \tilde{\mathcal{B}}_{s,n,m}^0 = -\frac{\Psi_{n,P-1}^1(k_{P-1}a_P)}{\Psi_{n,P-1}^2(k_{P-1}a_P)}\mathcal{M}_{snm}^3(\mathbf{u}_0) \tag{5.47}$$

$$\tilde{\mathcal{C}}_{s,n,m}^0 = 0, \quad \tilde{\mathcal{D}}_{s,n,m}^0 = -\frac{\Omega_{n,P-1}^1(k_{P-1}a_P)}{\Omega_{n,P-1}^2(k_{P-1}a_P)}\mathcal{N}_{snm}^3(\mathbf{u}_0) \tag{5.48}$$

for a PEC core and

$$\tilde{\mathcal{A}}_{s,n,m}^0 = 0, \quad \tilde{\mathcal{B}}_{s,n,m}^0 = -\frac{\Phi_{n,P-1}^1(k_{P-1}a_P)}{\Phi_{n,P-1}^2(k_{P-1}a_P)}\mathcal{M}_{snm}^3(\mathbf{u}_0) \tag{5.49}$$

$$\tilde{\mathcal{C}}_{s,n,m}^0 = 0, \quad \tilde{\mathcal{D}}_{s,n,m}^0 = -\frac{X_{n,P-1}^1(k_{P-1}a_P)}{X_{n,P-1}^2(k_{P-1}a_P)}\mathcal{N}_{snm}^3(\mathbf{u}_0) \tag{5.50}$$

for a PMC core and

$$\tilde{\mathcal{A}}_{s,n,m}^0 = 0, \quad \tilde{\mathcal{B}}_{s,n,m}^0 = -\frac{T_{n,21}^{(0\to P)}}{T_{n,22}^{(0\to P)}}\mathcal{M}_{snm}^3(\mathbf{u}_0) \tag{5.51}$$

$$\tilde{\mathcal{C}}_{s,n,m}^0 = 0, \quad \tilde{\mathcal{D}}_{s,n,m}^0 = -\frac{S_{n,21}^{(0\to P)}}{S_{n,22}^{(0\to P)}}\mathcal{N}_{snm}^3(\mathbf{u}_0) \tag{5.52}$$

for a dielectric core. For the core excitation case, we get:

$$\tilde{\mathcal{A}}_{s,n,m}^0 = \frac{T_{n,22}^P}{T_{n,22}^{(0\to P)}}\mathcal{M}_{snm}^1(\mathbf{u}_P), \quad \tilde{\mathcal{B}}_{s,n,m}^0 = 0 \tag{5.53}$$

$$\tilde{\mathcal{C}}_{s,n,m}^0 = \frac{S_{n,22}^P}{S_{n,22}^{(0\to P)}}\mathcal{N}_{snm}^1(\mathbf{u}_P), \quad \tilde{\mathcal{D}}_{s,n,m}^0 = 0 \tag{5.54}$$

Now, we describe a generic procedure to obtain without additional calculations the coefficients of an individual field. By the expansion of the dyadic Green's function, we observe that each scattering coefficient is associated

with a dyad $\mathbf{XY}$ induced by two SVWF used in scattering phenomena. Let's suppose we want to extract $a_{n,0}^{q,j}$ which is the coefficient associated with the dyad $\mathbf{M}_{snm}^{1}(\mathbf{r}, k_{q,j})\mathbf{M}_{snm}^{1}(\mathbf{r}_{q,j}, k_{q,j})$ for a sphere with a PEC core. All we have to do is to substitute the vector $\mathbf{u}_q$ in formula (5.31) with the vector $\mathbf{e}_{q,j}$ which is the vector of the standard base of $\mathbb{R}^{n_q}$ with 1 in the jth position. For a dielectric core, coefficients are the same for every dipole and thus, do need separate extraction. Taking into account the definition of the SVWF, (equations (B.19-B.23) of [98] and utilizing asymptotic relations of the spherical Bessel and Hankel functions for $r \to \infty$, see [94] we obtain for the q-excitation far-fields and the overall far-field:

$$\mathbf{g}_q(\hat{\mathbf{r}}) = \frac{\omega\mu_0}{4\pi} \sum_{n,m,s} \sqrt{n(n+1)}(-\mathrm{i})^{n-1} \times \left[\mathbf{C}_{snm}(\theta,\phi) \left(\tilde{\mathcal{A}}_{s,n,m,q}^{0} + \tilde{\mathcal{B}}_{s,n,m,q}^{0} \right) + \mathrm{i}\mathbf{B}_{snm}(\theta,\phi) \left(\tilde{\mathcal{C}}_{s,n,m,q}^{0} + \tilde{\mathcal{D}}_{s,n,m,q}^{0} \right) \right] \tag{5.55}$$

$$\mathbf{g}(\hat{\mathbf{r}}) = \frac{\omega\mu_0}{4\pi} \sum_{n,m,s} \sqrt{n(n+1)}(-\mathrm{i})^{n-1} \times \left[\mathbf{C}_{snm}(\theta,\phi) \left(\tilde{\mathcal{A}}_{s,n,m}^{0} + \tilde{\mathcal{B}}_{s,n,m}^{0} \right) + \mathrm{i}\mathbf{B}_{snm}(\theta,\phi) \left(\tilde{\mathcal{C}}_{s,n,m}^{0} + \tilde{\mathcal{D}}_{s,n,m}^{0} \right) \right] \tag{5.56}$$

The corresponding q-excitation cross section and overall cross section will be given by:

$$\sigma_q = \frac{2\pi}{k_0^2} \sum_{s,n,m} (2n+1) \left[\left| \tilde{\mathcal{A}}_{s,n,m,q}^{0} + \tilde{\mathcal{B}}_{s,n,m,q}^{0} \right|^2 + \left| \tilde{\mathcal{C}}_{s,n,m,q}^{0} + \tilde{\mathcal{D}}_{s,n,m,q}^{0} \right|^2 \right] \tag{5.57}$$

$$\sigma = \frac{2\pi}{k_0^2} \sum_{s,n,m} (2n+1) \left[\left| \tilde{\mathcal{A}}_{s,n,m}^{0} + \tilde{\mathcal{B}}_{s,n,m}^{0} \right|^2 + \left| \tilde{\mathcal{C}}_{s,n,m}^{0} + \tilde{\mathcal{D}}_{s,n,m}^{0} \right|^2 \right] \tag{5.58}$$

5.4 Parametric Analysis

In this chapter, we present a parametric analysis for the behaviour of the ISCS and the corresponding cross section.

5.4.1 Single-Layer Excitation

The numerical results we present in this section, concern the case where a layered spherical scatterer V is excited by a dipole distribution located in the sphere's exterior (*external excitation*) or in a specific layer (*internal excitation*). In particular, we considered the case where a 2-layered spherical scatterer V (i.e. $P = 2$) of external radius a_1 and core's radius a_2, is excited by either a dipole distribution lying in V_0 ($r > a_1$) or a dipole distribution lying in the spherical shell V_1 ($a_2 < r < a_1$). The core V_2 ($0 \leq r < a_2$) can PEC or dielectric. In most cases the dipoles lie on the z-axis; that choice was made since the angle and azimuthial angle do not affet significantly the behaviour of the ISCS ratios, see figures [xxx].

In figure 5.2, the variations of $\sigma^{\mathrm{T}}/\sigma$ versus the electric radius $k_0 a_1$ for a distribution of $N = 4$ external dipoles are depicted for different dipole distributions. In particular, we observe the ISCS behaviour of a dipole distribution that is "moving" far away from the scatterer. Specifically, we considered three dipole distributions with the dipoles' distances are given by: $r_j = (1.3 + 0.2j)a_1$, $r_j = (2.3 + 0.2j)a_1$, and $r_j = (3.3 + 0.2j)a_1$, with $j = 0, 1, 2, 3$. We notice that the ISCS ratios are oscillatory for higher frequencies when the dipoles lie close to the sphere. However, the ratio remains within a 4% and a 5% margin in the PEC and dielectric core case, respectively. As the dipole distribution moves away from the scatterer, we observe that the oscillatory behavior remains, but the variation margin deteriorates to the extend we can safely assume that the ISCS ratios for all examined frequencies achieve the upper bound $1 - \frac{1}{N} = 0.75$ of (4.45).

Similar conclusions are drawn from figure 5.3 where the dipole distributions are sparse compared to those of figure 5.2. Specifically, the distance between successive dipoles is half the sphere's radius, namely $r_j = (1.3 + 0.5j)a_1$, $r_j = (2.3 + 0.5j)a_1$, and $r_j = (3.3 + 0.5j)a_1$ with

$j = 0, 1, 2, 3$. A difference worth noting is the following: When the dipoles lie in close proximity to the sphere's boundary, the ISCS variations grow larger, with the corresponding margin being 17% for the PEC and 20% for the dielectric core.

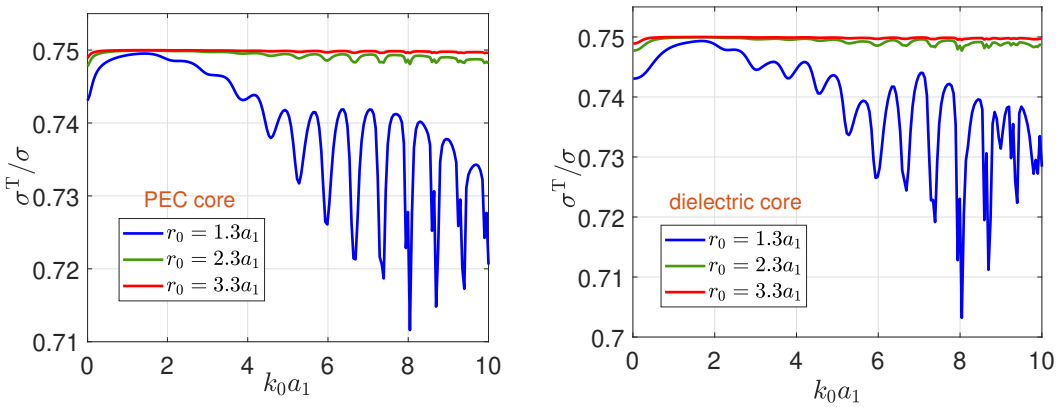

Figure 5.2: ISCS ratios $\sigma^{\mathrm{T}}/\sigma$ versus k_0a_1 for a spherical scatterer with $a_1 = 2a_2, \epsilon_{r1} = 2, \mu_{r1} = 1.5$ and a PEC core (left panel) and dielectric core with $\epsilon_{r2} = 3, \mu_{r2} = 2.5$ (right panel). The scatterer is excited by three sets of $N = 4$ external sources with distance $0.2a_1$ between successive sources.

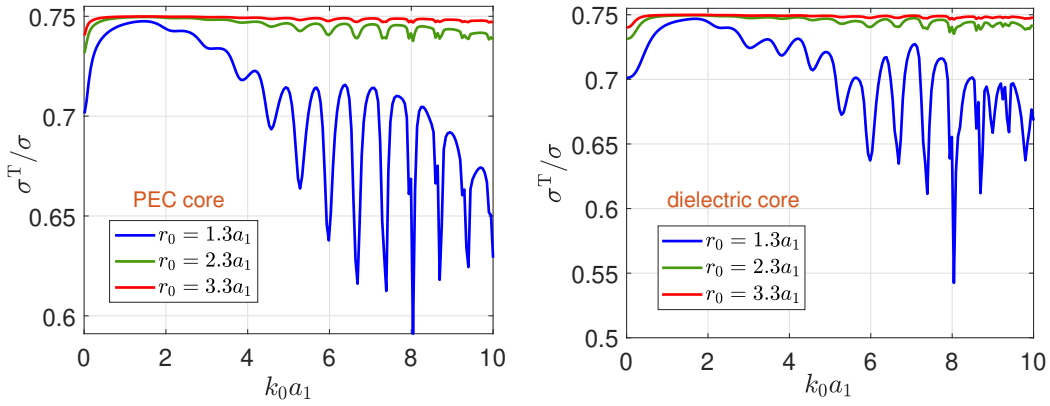

Figure 5.3: As in Fig. 5.2, but for distance $0.5a_1$ between successive sources.

In figure 5.4, we depict the ISCS ratios and their physical bounds indicated by (4.45) for a dipole distribution consisting of $N = 4$ dipoles lying in the exterior V_0 of the sphere, at distances $r_j = (1.25 + 0.25j)a_1$, with $j = 0, 1, 2, 3$ from the sphere's origin. The inset figures depict the same quantities, in the low frequency region, i.e. $k_0a_1 \leq 1$. A first observation is

that for both cores, at lower frequencies - namely, $k_0 a_1 < 3.1$ for the PEC and $k_0 a_1 < 2.1$ for the dielectric core - the upper bound of (4.45) is $1-1/N$, which in turn implies that $\sigma_q^{\min} \leq \sigma/N^2$. Additionally for all examined frequencies and for both core types, the differences between the upper bound and the actual ISCS ratio are less than 1%. On the other hand, the differences between the lower and the upper bounds of (4.45) are less than 4% for $k_0 a_1 \geq 1$, and thus, the upper bound provides a more precise estimation for the actual ISCS ratio. On the other hand, in the low-frequency region we see that the q-ISCS ratios are close to the upper bound, whereas the difference with the lower bounds of (4.45) is substantial. This behaviour can be fully explained if we take a closer look at the minimum and maximum individual cross sections ratios over the q-excitation cross section. In the low-frequency region they differ significantly, e.g. for $k_0 a_1 \leq 0.5$, the difference exceeds 5%, which yields a 20% difference between the corresponding physical bounds, at the very least.

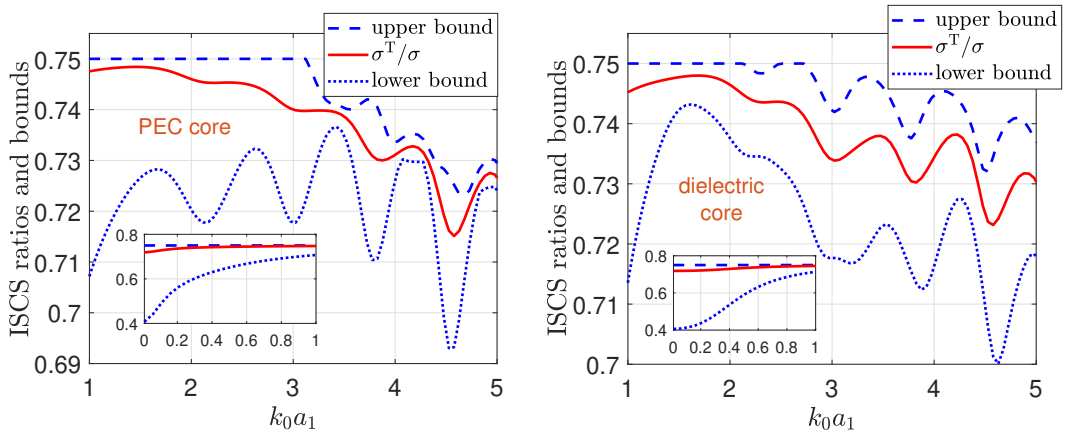

Figure 5.4: ISCS ratios $\sigma^{\mathrm{T}}/\sigma$ and their physical bounds versus $k_0 a_1$ of a 2-layered sphere with $a_1 = 2a_2$, $\epsilon_{r1} = 2$, $\mu_{r1} = 1.5$ and a PEC core (left panel) or a dielectric core (right panel) with $\epsilon_{r2} = 3$ and $\mu_{r2} = 2.5$. The scatterer is excited by $N = 4$ external dipoles.

The ISCS ratios and associated physical bounds from (4.45) are shown in Fig. 5.5 for the case of $N = 4$ internal dipoles located at $r_j = (0.65 + 0.05j)a_1$, with $j = 0, 1, 2, 3$. A steeper descent of the q-excitation ISCS ratio is now observed compared to the external excitation case of Fig. 5.4. For lower frequencies ($k_0 a_1 < 3.5$ for the PEC and $k_0 a_1 < 2.5$ for the

dielectric core), the upper bound of (4.45) is $1 - 1/N$. The differences between the lower and the upper bounds of (4.45) are larger compared to the corresponding differences for external excitation; in some cases they now reach 15%. In the low-frequency region (i.e. $k_0 a_1 \leq 1$), the ISCS ratio almost coincides to its upper bound. Another difference between the behavior of the ISCS ratios for external and internal excitation is that in external excitation, for the frequencies where $\sigma^{\min} \geq \sigma/N^2$, all quantities show a uniform behavior, while in internal excitation, the ISCS ratios seem to act as a "mirror" between the lower and upper bounds.

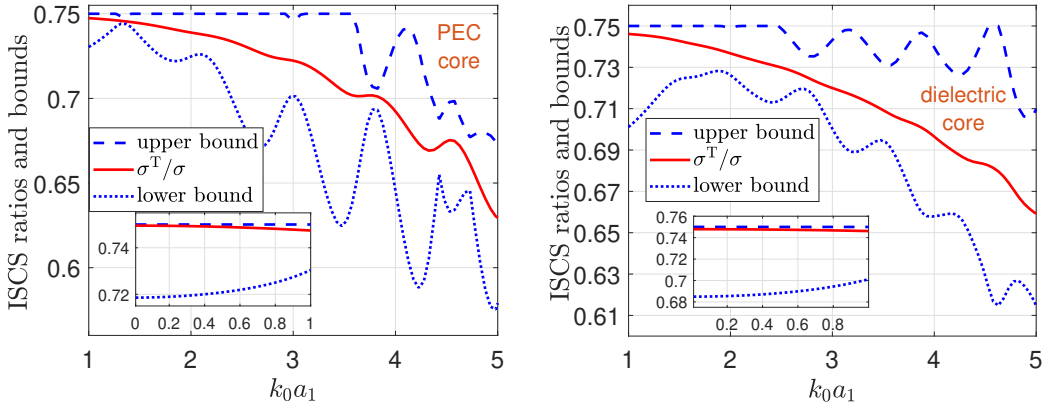

Figure 5.5: As in Fig. 5.4, but for excitation due to $N = 4$ internal dipoles.

In figure 5.6 we demonstrate the accuracy of the physical bounds for the number N of dipoles that excite the spherical scatterer. In this case, the dipole distribution is external, with the dipoles' distance from the sphere's region given by $r_1 = 2.5a_1, r_2 = 2.8a_1, r_3 = 3.1a_1, r_4 = 3.5a_1$. An immediate observation is the identical behavior of the physical bounds for both types of core. Specifically, for $0.2 < k_0 a_1 < 1.5$ (dielectric core) and for $0.1 < k_0 a_1 < 2.5$ (PEC core), the physical bounds are valid and determine accurately the number of dipoles exciting the scatterer. For $k_0 a_1 < 0.2$, (dielectric core) and for $k_0 a_1 < 0.1$, (PEC core) despite the fact that the physical bounds remain valid, they cannot be used to accurately determine the number of dipoles, as the margin of estimation (between 3 and 6) is large. This fact stems from the difference between the minimum and

maximum individual cross sections in the low-frequency region. A very interesting observation - which have been observed in a variety of dipole distributions - is that in the higher frequencies ($k_0 a_1 > 1.5$ for the dielectric core and $k_0 a_1 > 2.5$ for the PEC core) it holds $N = [\sqrt{\sigma/\sigma^{\min}}] + 1$, where $[x]$ denotes the integer part of x. This is caused by the fact that the minimum and maximum individual cross sections do not differ substantially. We would also like to note that similar patterns with respect to the physical bounds and the estimation of the number of dipoles exciting the sphere, have been found to be exhibited by even sparser or denser dipole distributions.

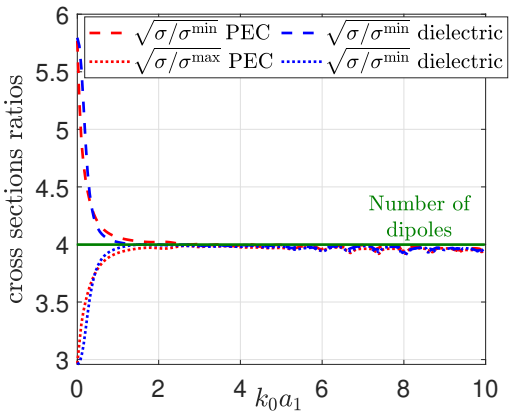

Figure 5.6: Physical bounds for the number N of dipoles exciting a 2-layered sphere with $a_1 = 2a_2$, $\epsilon_{r1} = 2$, $\mu_{r1} = 1.5$. The bounds for a PEC core are depicted with red and the bounds for a dielectric core with blue. For the dielectric core, its parameters are $\epsilon_{r2} = 3$ and $\mu_{r2} = 2.5$. The scatterer is excited by $N = 4$ dipoles, all of them lying in the exterior of the sphere.

In figure 5.7, the variations of the total ISCS $\sigma^{\mathrm{T}}/\sigma$ versus the relative permittivity ϵ_{r1} of the first spherical shell are depicted. The spherical scatterer has a PEC core or a dielectric core and it is excited by a dipole distribution consisting of $N = 4$ dipoles located at $r_1 = 1.3a_1, r_2 = 1.8a_1, r_3 = 2.3a_1, r_4 = 2.8a_1$ on the z-axis of the scatterer's exterior. For the higher frequency, the total ISCS seems to variate slightly with ϵ_{r1}. In particular, less than 2% for the PEC core and less than 3% for the dielectric core. For both types of core, the total ISCS seems to oscillate decreasingly as ϵ_{r1} increases. On the other hand, for the lower frequency, we observe that as ϵ_{r1} increases, the total ISCS increases as well until it stabilizes for $\epsilon_{r1} = 2$ for

the PEC and $\epsilon_{r1} = 3$ for the dielectric core. The margin in the total ISCS ratio are less than 2% and 8% for the PEC and dielectric core, respectively. Similar patterns have been observed at both lower and higher frequencies, for different dipole distributions.

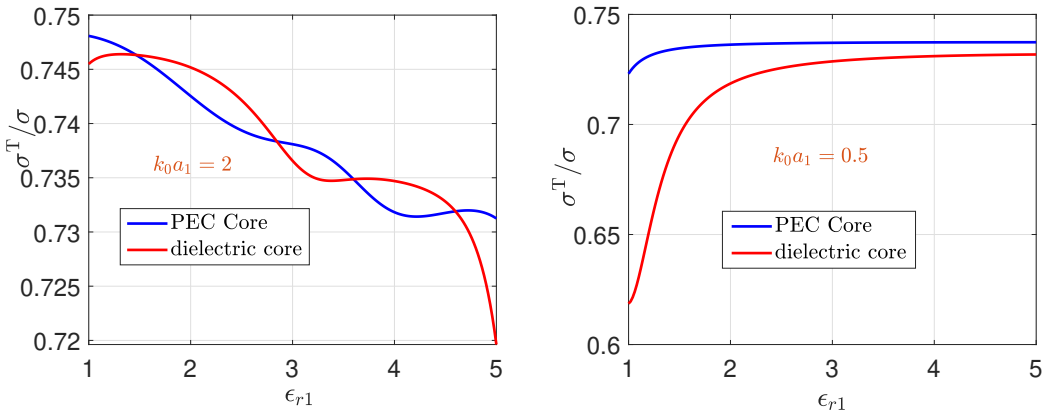

Figure 5.7: ISCS ratios $\sigma^{\mathrm{T}}/\sigma$ versus the relative permittivity ϵ_{r1} of a 2-layered spherical scatterer with $a_1 = 2a_2$, $\mu_{r1} = 1.5$ and $k_0a_1 = 2$ (left panel) or $k_0a_1 = 0.5$ (right panel) with $\epsilon_{r1} = 1.5\epsilon_2$ and $\mu_{r2} = 2.5$. The scatterer is excited by $N = 4$ external dipoles.

In figure 5.8, we demonstrate the behavior of the ratios of the total ISCS, for a dipole distribution consisting of $N = 4$ dipoles located at the first shell V_1 of the sphere, with a PEC core V_2 of radius $a_2 = a_1/5$. We depicted three dipole distributions. In particular, the "core side" distribution refers to the case where the dipoles lie located closer to the core V_2, "middle side" distribution refers to the case where the dipoles lie close to the middle of V_1, and the "boundary side" distribution refers to the case where the dipoles lie close to the sphere's external boundary. Furthermore, the left panel, depicts a denser distribution where the distance between successive dipoles is $0.05a_1$; the right panel depicts a sparser distribution where the corresponding distance is $0.1a_1$. At first, we observe that for $k_0a_1 \leq 5$ the ISCS ratios are smooth and descending for all distributions - regardless of their context. Furthermore, for $k_0a_1 \geq 5$, we notice that oscillations appear for the distributions closer to the boundary, but not for the distribution lying closer to the core. For the sparser distribution, we observe that for higher frequencies rapid oscillations occur for the distribution closer to the scat-

terer's boundary. Specifically, for $k_0 a_1 \geq 7$, we note that the ISCS ratios obtain negative values, which implies the reduction of the energy flux rate. In contrast, for the denser distribution, we observe a much smoother and less oscillatory behavior for all examined distributions. Another interesting point, is that the ranges of the ISCS ratios are smaller for the dense distributions (less than 35%) and larger for the sparser distributions (more than 120%) as far as the excitation frequency is concerned. We note that even sparser dipole distributions, lead to an even less-predictable ISCS ratios behavior; this indicates that the a sparse internal dipole distribution the excitation frequency affects greatly the ISCS behavior.

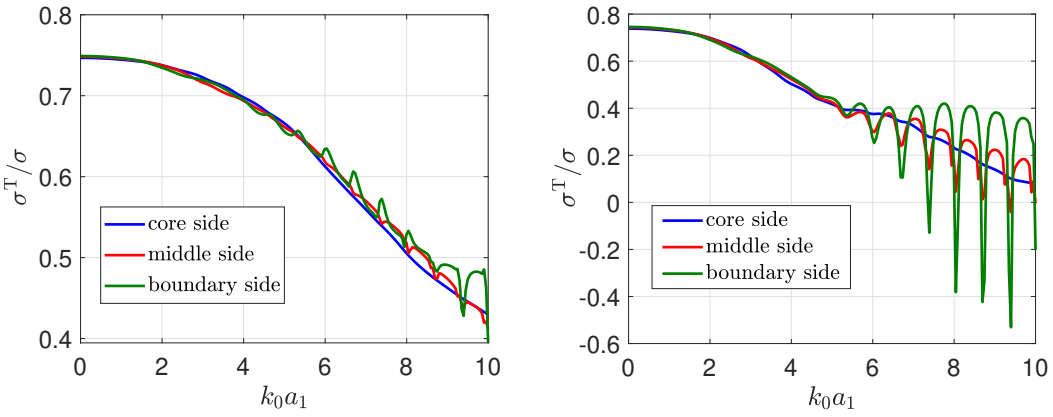

Figure 5.8: ISCS ratios $\sigma^{\mathrm{T}}/\sigma$ for $N = 4$ dipoles lying in the first shell of a 2-layered sphere with $\mu_{r1} = 1.5, \epsilon_{r1} = 2$ and PEC core of radius $a_2 = a_1/5$. Left panel: denser dipole distribution with $r_1^{j+1} - r_1^j = 0.05a_1$ $(j = 1, 2, 3)$ and $r_1^1 = 0.25a_1$ (core), $r_1^1 = 0.55a_1$ (middle), $r_1^1 = 0.8a_1$ (boundary side). Right panel: sparser dipole distribution with $r_1^{j+1} - r_1^j = 0.1a_1$ $(j = 1, 2, 3)$ and $r_1^1 = 0.25a_1$ (core), $r_1^1 = 0.45a_1$ (middle), $r_1^1 = 0.65a_1$ (boundary side).

Figure 5.9 depicts the behavior of the actual values of the ISCS for the same distributions of figure 5.8. An interesting observation can made right away: The values follow a different pattern than their corresponding ratios. In fact, denser distributions lead to greater range in the ISCS values in regard to excitation frequeny $k_0 a_1$, in complete contrast with the small ranges in their corresponding ratios (as we have seen above). Then again, for distributions closer the sphere's core, the ISCS values decrease and approach zero at higher frequencies. Sparser distributions exhibit significantly smaller ISCS values - even negative values at higher frequencies.

Besides, when the distributions lie close to the sphere's core, we notice that the differences in the ISCS values between denser and sparser distributions, demonstrate a similar behavior.

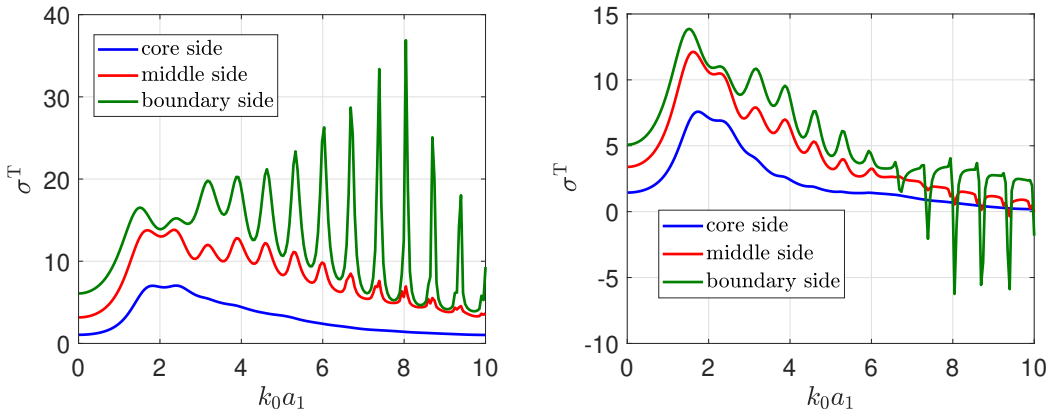

Figure 5.9: Total ISCS σ^{T} values for the same setup of Fig. 5.8

In figure 5.10, we compare the behavior of the overall cross section σ and total ISCS ratio $\sigma^{\mathrm{T}}/\sigma$ versus the radius k_0a_1. The sphere in this case, has a dielectric core of different radii a_2 and it is excited by a dipole distribution consisting of $N = 4$ internal dipoles in shell V_1. For all the examined core's radii, we notice that the values of σ remain fairly unchanged and oscillate rapidly after $k_0a_1 > 1.2$. On the other hand, the total ISCS ratios descent smoothly for $k_0a_1 < 5$ but oscillate rapidly for $k_0a_1 > 5$. Furthermore their behavior does not seem to be significantly affected by changes in the core's radii.

Finally, in figure 5.11 we depict the behavior of the overall cross section σ and the total ISCS values at a fixed frequency $k_0a_1 = 1$ for a spherical scatterer with a PEC core. The focus of the comparison is that we observe the changes in the values of the cross sections variations as one, two, or three dipoles move away from their initial locations. The distance R express the ratio over the sphere's radius a_1. In particular, the initial positions are $r_j = (1.3 + 0.2j)$ with $j = 0, 1, 2, 3$, while the moving dipoles' locations are given by $r_j(R) = r_jR$ with $j = 1, 2, 3$. A similarity can be observed in these figures. We observe that both σ and σ^{T} follow a similar pattern. They

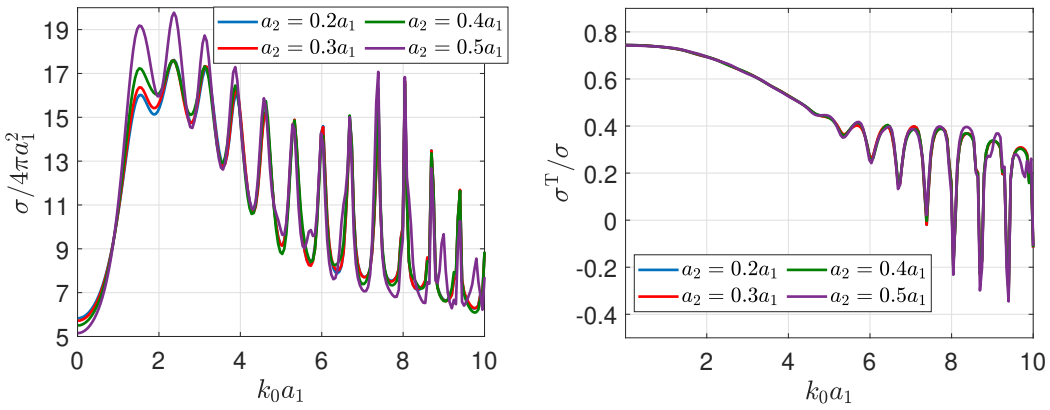

Figure 5.10: Overall cross section σ (left panel) and total ISCS ratios $\sigma^{\mathrm{T}}/\sigma$ (right panel) versus the radius $k_0 a_1$ for $\epsilon_{r1} = 2, \epsilon_{r2} = 3, \mu_{r1} = 1.5, \mu_{r2} = 2.5$, and $N = 4$ internal sources at $r_1^1 = 0.6a_1, r_1^2 = 0.7a_1, r_1^3 = 0.8a_1, r_1^4 = 0.9a_1$. Different radii of the dielectric core are considered.

decrease as more dipoles move away from their initial locations, which leads to a sparser dipole distribution. This implies that the total ISCS ratio will not be significantly affected. Furthermore, the ranges of σ and σ^{T} increase as number of moving dipoles grows. We note that the above conclusions have been found to be qualitatively similar for the dielectric core case; the only notable difference is that the range of σ and σ^{T} is much smaller in the dielectric core case.

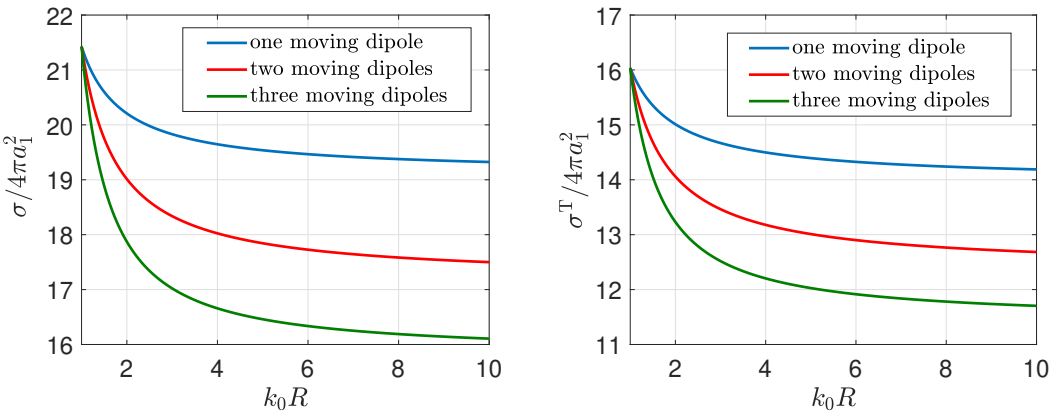

Figure 5.11: Overall cross section σ (left panel) and total ISCS σ^{T} (right panel) of a 2-layered scatterer with $k_0 a_1 = 1$, $\epsilon_{r1} = 2, \mu_{r1} = 1.5$ and a PEC core, excited by $N = 4$ sources at $r_0^1 = 1.3a_1, r_0^2 = 1.5a_1, r_0^3 = 1.7a_1, r_0^4 = 1.9a_1$, as a number of dipoles (one, two and three) move away from the original position by a distance R.

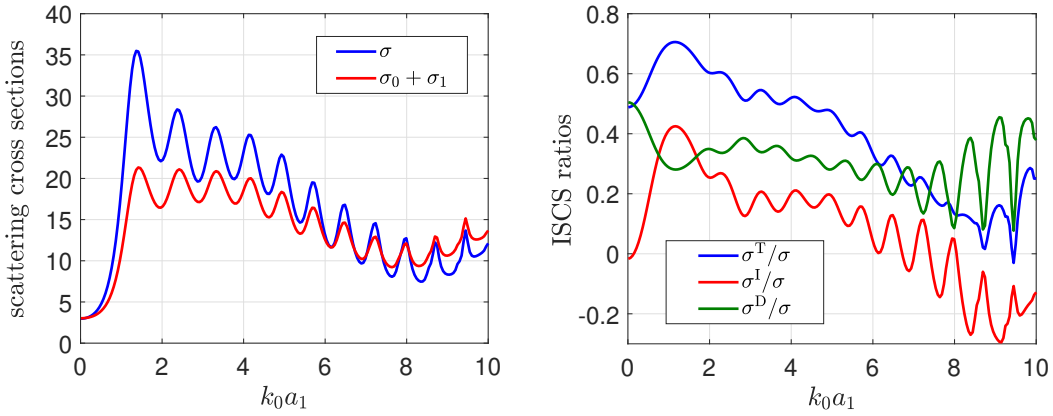

Figure 5.12: Overall cross section σ, 0- and 1-excitation cross sections (top panel) and ISCS ratios (bottom panel) versus radius k_0a_1 of a 2-layered sphere V with $\epsilon_{r1}=2, \mu_{r1}=1.25$ and a PEC core excited by $N=4$ dipoles; $n_1=2$ dipoles lie in the exterior of V at $r_0^1=1.3a_1$, $r_0^2=1.8a_1$, and $n_2=2$ in the first shell of V at $r_1^1=0.7a_1, r_2^1=0.9a_1$.

5.4.2 Mixed Excitation

Now, we consider that the scatterer V is excited by two dipoles in the external region V_0 ($r>a_1$) and two dipoles in the first spherical shell V_1 ($a_2<r<a_1$); hence we have $Q=2$ excitation layers.

In Fig. 5.12, we depict the overall cross section σ and the sum of 0-excitation σ_0 and 1-excitation σ_1 cross sections as well as the total $\sigma^{\mathrm{T}}/\sigma$, indirect $\sigma^{\mathrm{I}}/\sigma$, and direct $\sigma^{\mathrm{D}}/\sigma$ ISCS ratios. We observe that σ gradually converges to the sum $\sigma_0+\sigma_1$, and that $\sigma_0+\sigma_1>\sigma$ for $k_0a_1>8$. This is explained from the behavior of the ISCS ratios, where, for $k_0a_1>8$, we see that $\sigma^{\mathrm{I}}/\sigma<0$, which in turn means that $\sigma^{\mathrm{I}}<0$. In particular, it holds $\sigma=\sigma_0+\sigma_1+\sigma^{\mathrm{I}}$; see (4.22). Hence, larger ratios $\sigma^{\mathrm{I}}/\sigma$ give larger differences between the sum of q-excitation and the overall cross sections.

Fig. 5.13 shows the variations of the total $\sigma^{\mathrm{T}}/\sigma$, the indirect $\sigma^{\mathrm{I}}/\sigma$, and the direct $\sigma^{\mathrm{D}}/\sigma$ ISCS ratios versus the relative electric permittivity ϵ_{r1} of a 2-layered sphere with $k_0a_1=2$ and a PEC core. The ratio $\sigma^{\mathrm{I}}/\sigma$, and hence the indirect ISCS σ^{I}, becomes negative for $\epsilon_{r1}>3.1$. For $\epsilon_{r1}=4$, ratios $\sigma^{\mathrm{T}}/\sigma$ and $\sigma^{\mathrm{I}}/\sigma$ are minimized, while the direct $\sigma^{\mathrm{D}}/\sigma$ ISCS ratio (the sum of the 0- and 1-ISCS) is maximized. Corresponding results for the variations of the ISCS with respect to the magnetic permeability μ_{r1} have been also

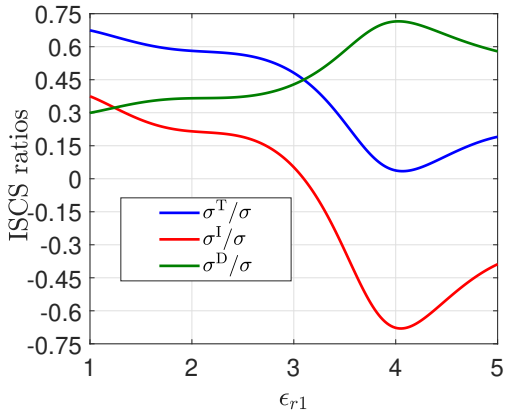

Figure 5.13: Total $\sigma^{\mathrm{T}}/\sigma$, indirect $\sigma^{\mathrm{I}}/\sigma$ and direct $\sigma^{\mathrm{D}}/\sigma$ ISCS ratios versus the relative permittivity ϵ_{r1} of a 2-layered scatterer with $k_0 a_1 = 2$, $\mu_{r1} = 1.5$, and a PEC core, excited by $N = 4$ dipoles; two lie in the exterior of the sphere at $r_0^1 = 1.3a_1$, $r_0^2 = 1.8a_1$ and two in the first shell at $r_1^1 = 0.7a_1, r_1^2 = 0.9a_1$.

derived and the conclusions are the same with the ones drawn above with the only difference being that the range of ISCS variations is now smaller.

In Fig. 5.14, we depict the physical bounds for the number Q of excitation layers indicated by (4.50). The considered number $Q = 2$ is depicted with a straight red line. For $k_0 a_1 > 1$, the physical bounds can be used to determine Q for a wide range of the examined frequencies. The upper physical bound for $k_0 a_1 > 1$ remains very close to the number Q of excitation layers even when the upper bound is not valid. In fact, we see that $Q = [\sqrt{\sigma/\sigma_{\mathrm{ex}}^{\max}}] + 1$. The insets demonstrate the variations in the low-frequency region. For the PEC core, the bounds remain valid, but for $k_0 a_1 \leq 0.5$ cannot be safely used for the determination of Q, since the minimum q-excitation cross section–σ_1 in this case–is significantly smaller than the overall cross section. For the dielectric core, the physical bounds remain valid for $k_0 a_1 < 0.7$. Besides, for both types of cores a change in the minimum and maximum q-excitation cross sections occurs at $k_0 a_1 = 1$. Precisely, for $k_0 a_1 < 1$ it holds $\sigma_0 < \sigma_1$, while for $k_0 a_1 > 1$ it holds $\sigma_0 > \sigma_1$.

Fig. 5.15 depicts the variations of $\sigma^{\mathrm{T}}/\sigma$ and $\sigma^{\mathrm{I}}/\sigma$ for $k_0 a_1 = 1$ and $k_0 a_1 = 2.5$ versus the distance $k_0 R$ between the internal group of $n_1 = 2$

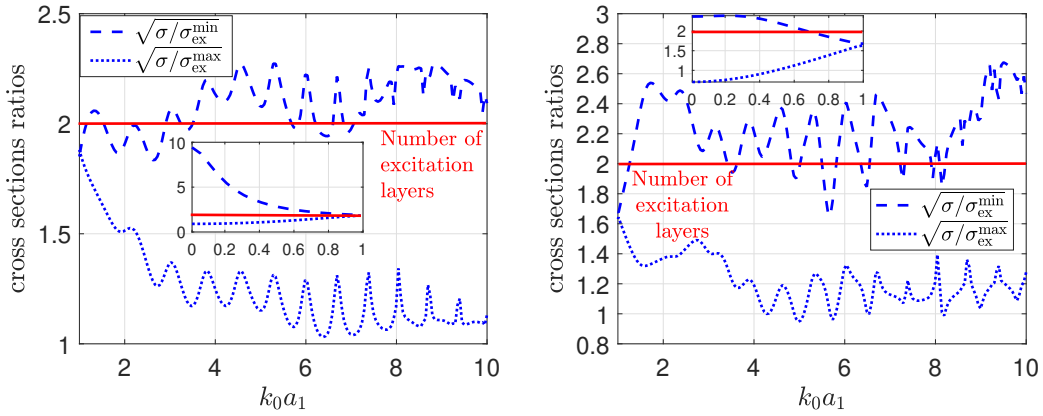

Figure 5.14: Physical bounds for the number Q of excitation layers versus k_0a_1 of a 2-layered sphere with $a_1 = 2a_2$, $\epsilon_{r1} = 2$, $\mu_{r1} = 1.5$ and a PEC core (top panel) or a dielectric core (bottom panel) with $\epsilon_{r2} = 3$ and $\mu_{r2} = 2.5$. The scatterer is excited by $N = 4$ dipoles, two lying in the exterior of the sphere and two in the first spherical shell.

dipoles, initially located at $r_1^1 = 0.8a_1, r_1^2 = 0.9a_1$, and the external group of $n_0 = 2$ dipoles, initially located at $r_0^1 = 1.2a_1, r_0^2 = 1.3a_1$. In the top panel, the internal group moves towards the sphere's core and the external group moves away from the scatterer's boundary with increasing R. Precisely, the moving dipoles' locations are given by $r_0^j(R) = r_0^j R$ for the external group and $r_1^j(R) = r_1^j/R$ for the internal group. The initial setup (before moving the dipoles) corresponds to a negative $\sigma^{\rm I}/\sigma$. We observe that for both frequencies the ISCS ratios $\sigma^{\rm T}/\sigma$ and $\sigma^{\rm I}/\sigma$ follow a similar pattern: they first increase until a certain value of k_0R and then decrease. For the lower frequency, the variations of the ISCS ratios are smaller. In the bottom panel, the meaning of R is slightly different: the initial locations are $r_1^1 = 0.21a_1, r_1^2 = 0.2475a_1$ for the internal group and $r_0^1 = 1.2a_1, r_0^2 = 1.3a_1$ for the external group. The dipoles located at $r_1^1 = 0.21a_1, r_0^1 = 1.2a_1$ remain fixed, while the one at $r_1^2 = 0.2475a_1$ moves towards the scatterer's boundary, and the one at $r_0^2 = 1.3a_1$ moves away from it. The moving dipoles' locations are given by $r_q^2(R) = r_q^2 R$ for $q = 0, 1$. The behavior of the ISCS is different now: for the lower frequency, we see a steeper decrease in $\sigma^{\rm T}/\sigma$ and a sharper increase in $\sigma^{\rm I}/\sigma$. Thus, the direct ISCS will decrease more rapidly than the total ISCS. Furthermore, a crossover is observed at $k_0R = 1.6$ between $\sigma^{\rm T}/\sigma$ and $\sigma^{\rm I}/\sigma$ for the two

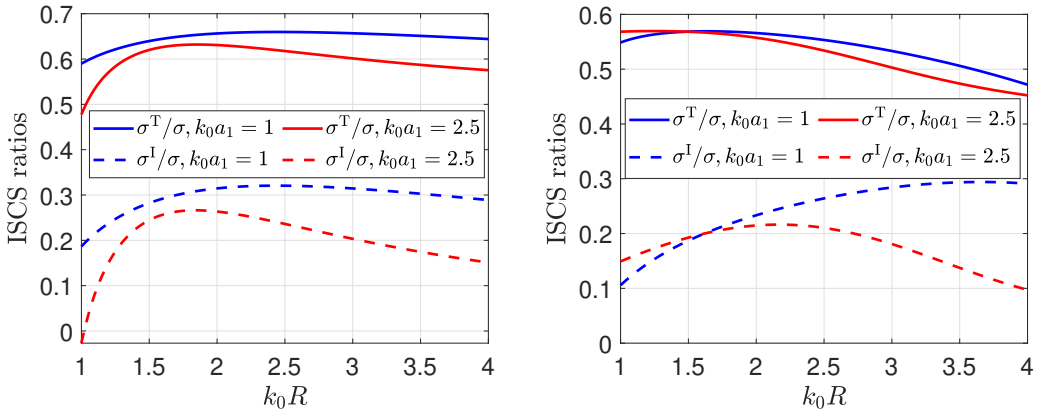

Figure 5.15: Total $\sigma^{\mathrm{T}}/\sigma$ and indirect $\sigma^{\mathrm{I}}/\sigma$ ISCS ratios versus the dipoles distance k_0R for $k_0a_1 = 1$ and k_0a_1=2.5 for a 2-layered scatterer with a dielectric core and parameters $\mu_{r1} = 1.5, \mu_{r2} = 2.5$, $\epsilon_{r1} = 2, \epsilon_{r2} = 3$, $a_2 = a_1/10$. The sphere is excited by $N = 4$ dipoles; two external and two in the first shell, at varying positions.

examined frequencies. This is due to that the decrease in $\sigma^{\mathrm{T}}/\sigma$ is steeper for the higher than the lower frequency. However, for the higher frequency, $\sigma^{\mathrm{I}}/\sigma$ maximizes at $k_0R = 2.2$ and follows a descending behavior after that point. This comes in stark contrast with the ascending behavior of $\sigma^{\mathrm{I}}/\sigma$ for the lower frequency.

In Fig. 5.16, we depict $\sigma^{\mathrm{T}}/\sigma$ and $\sigma^{\mathrm{I}}/\sigma$ versus k_0a_1 for different radii a_2 of the PEC core. A remarkable similarity is observed in the ISCS curves for all examined radii a_2. For $k_0a_1 < 2$, larger radii a_2 yield larger ISCS ratios, while, on the contrary, for $k_0a_1 > 4$, larger a_2 yield smaller ISCS ratios. Larger cores have larger ISCS ranges, e.g. for $a_2 = a_1/5$ we have $\sigma^{\mathrm{T}}/\sigma \in (0.35, 0.61), \sigma^{\mathrm{I}}/\sigma \in (0.1, 0.26)$ whereas for $a_2 = a_1/2$ we have that $\sigma^{\mathrm{T}}/\sigma \in (0.25, 0.7), \sigma^{\mathrm{I}}/\sigma \in (-0.15, 0.41)$. For $2 < k_0a_1 < 4$, a more steady behavior is observed. The ISCS are not significantly affected by the changes in the core's radius, except for the larger core $a_2 = a_1/2$, which yields larger variations. Both $\sigma^{\mathrm{T}}/\sigma$ and $\sigma^{\mathrm{I}}/\sigma$ exhibit more oscillatory behaviors for larger cores.

The variations of the ISCS ratios and values as well as the overall cross section and the sum of individual cross sections (denoted by $\hat{\sigma}$) for different distributions of $N = 4$ dipoles in the high-frequency zone are depicted in Fig. 5.17. The dipoles' distributions are those of the top panel of Fig. 5.15.

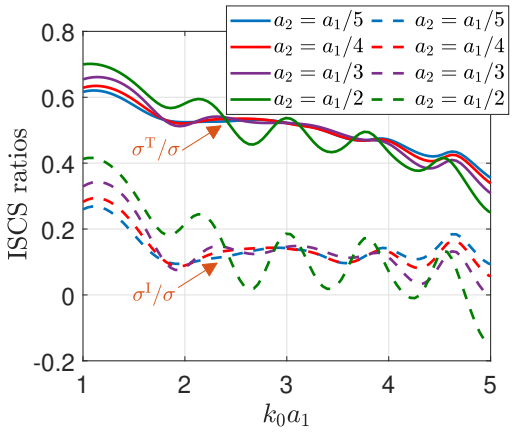

Figure 5.16: ISCS $\sigma^{\mathrm{T}}/\sigma$ and $\sigma^{\mathrm{I}}/\sigma$ versus the radius $k_0 a_1$ of a 2-layered sphere with $\epsilon_{r1} = 2$, $\mu_{r1} = 1.5$ and a PEC core of varying radius a_2, excited by $N = 4$ dipoles; two external ones at $r_0^1 = 1.3a_1$, $r_0^2 = 1.8a_1$ and two internal ones at $r_1^1 = 0.7a_1, r_1^2 = 0.9a_1$.

A notable similarity is observed between the ISCS ratios and the values of all involved cross sections. For $k_0 R > 2$ (i.e. when the distance between the external and the internal dipole groups is larger than the sphere's diameter), the values and ratios begin to stabilize, which implies that the overall cross section σ develops a more stable behavior. Besides, all $\sigma^{\mathrm{T}}/\sigma$ ratios remain positive, except for $k_0 R \in (1.25, 1.35)$ for $k_0 a_1 = 10$. This fact is readily explained by the bottom panel, where we see that for these frequencies, the sum of individual cross sections is greater than the overall cross section.

In Fig. 5.18, we depict the same quantities as in Fig. 5.17, but in the low-frequency regime. The dipoles' distributions are those of the top panel of Fig. 5.15. The ISCS ratios and values remain very close for each of the two examined frequencies. The indirect ISCS remain negative for all $k_0 R$; this fact implies that the interaction between the 0-excitation and 1-excitation fields, reduces the rate of the energy flux. Since the total ISCS remains positive, it is concluded that the sum of the 0- and 1-excitation cross sections is greater than the overall cross section but the sum of individual cross sections remains smaller than the overall cross section, as demonstrated by the bottom panel. Another interesting observation is the ascending behavior of the ISCS ratios as the distance $k_0 R$ between the dipoles groups increases. Indirect ISCS values exhibit an ascending behavior as well–only

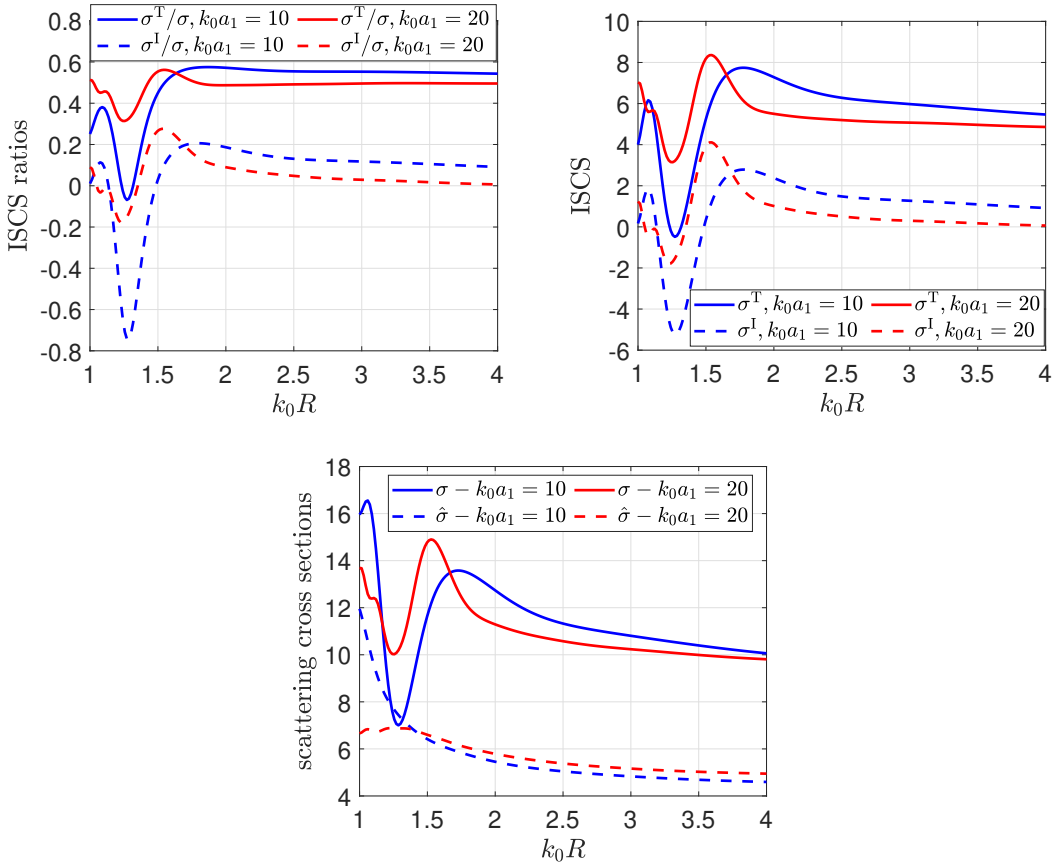

Figure 5.17: ISCS ratios and values versus k_0R for $k_0a_1 = 10$ and $k_0a_1 = 20$ (high-frequency zone) for a 2-layered scatterer with a dielectric core of $a_2 = a_1/10$ and parameters $\epsilon_{r1} = 2, \epsilon_{r2} = 3$, $\mu_{r1} = 1.5, \mu_{r2} = 2.5$. Excitation is due to $N = 4$ dipoles; two external ones and two in the first shell, all at varying distances R.

steeper than their corresponding ratios. This is readily explained by the descending behavior of the total ISCS values with increasing k_0R. The contradiction between the ascending behavior of the indirect ISCS and the descending behavior of the total ISCS is explained from the bottom panel, where we see that the overall scattering cross section approaches zero for large distances R. Additionally, we see that the sum of the individual cross sections is very close to the overall cross section with both quantities following a similar descent pattern.

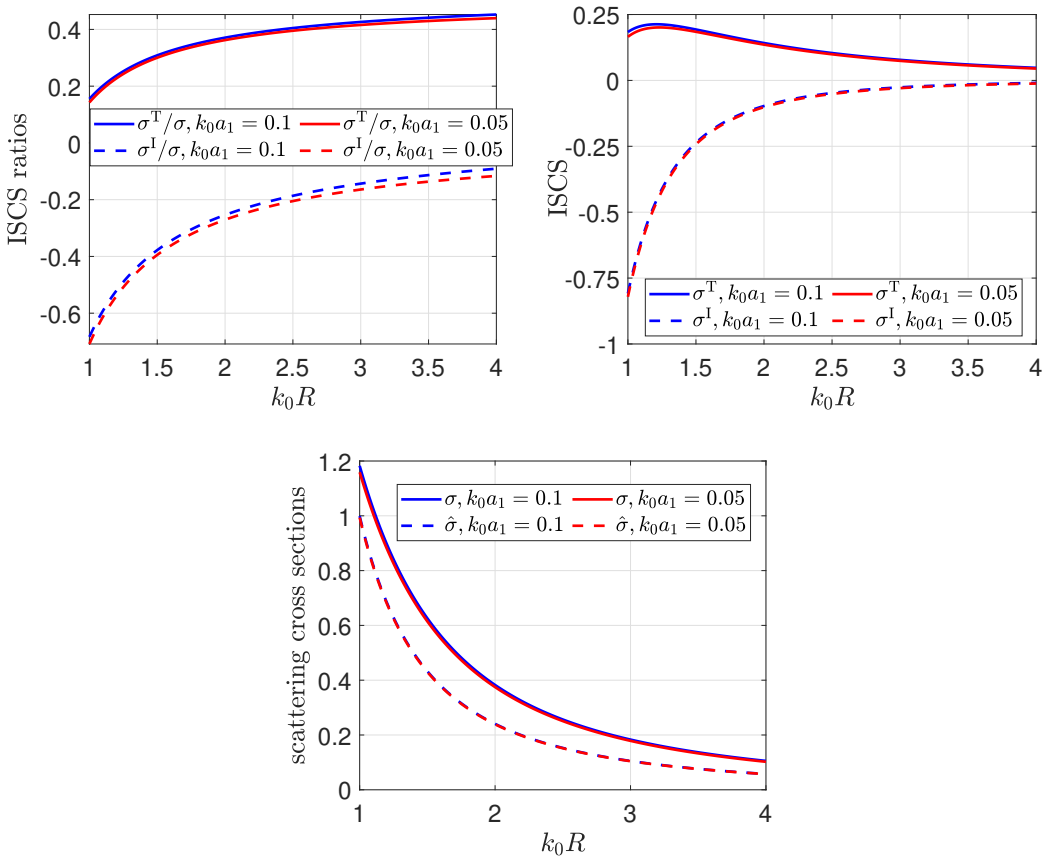

Figure 5.18: ISCS ratios and values versus k_0R for $k_0a_1 = 0.1$ and $k_0a_1 = 0.05$ (low-frequency zone), for a 2-layered scatterer with a dielectric core of $a_2 = a_1/10$ and parameters $\epsilon_{r1} = 2, \epsilon_{r1} = 3$, $\mu_{r1} = 1.5, \mu_{r2} = 2.5$. As in Fig. 5.17, the sphere is excited by $N = 4$ dipoles at varying distances R.

Chapter 6

Inverse Problems

6.1 Low Frequency Approximations

Now, we will further investigate the T-Matrix implementation on the so-called low frequency zone. In other words, we assume that $k_0 a_1 << 1$ which is the case where the wavelength is significantly larger than the scatterer. The low-frequency zone is suitable for analytical solutions of both far-field and near-field inverse problems [57], [104]. We will limit our investigation in the case where a homogeneous, dielectric sphere of radius a_1 is excited by 2 dipoles. We note, that the presence of more than 2 layers does not offer significant differences on the algorithmic procedures, since the extraction of the fields' coefficients follow a recursive rule, see [70]. We will use the following notation:

$$m = \mu_1/\mu_0, \quad \epsilon = \epsilon_1/\epsilon_0, \quad d_j = r_1^j/a_1, \quad \tau_j = a_1/r_0^j \tag{6.1}$$

Additionally, we assume that the power constant for the electric dipoles is of the form

$$A_{q,j} = \frac{r_{q,j}}{\mathrm{i}k_q}\exp(-ik_q r_{q,j}) \tag{6.2}$$

thus the polarized strength will be given by the vector:

$$\mathbf{p}_{q,j} = \frac{r_{q,j}}{\mathrm{i}k_q}\exp(-ik_q r_{q,j})(\hat{p}^j_{(x,q)}, \hat{p}^j_{(y,q)}, \hat{p}^j_{(z,q)}) = (p^j_{(x,q)}, p^j_{(y,q)}, p^j_{(z,q)}) \tag{6.3}$$

In the single-layer excitation case we will use the simpler notations $(\hat{p}^j_x, \hat{p}^j_y, \hat{p}^j_z)$, (p^j_x, p^j_y, p^j_z) for the polarized strength vectors. We additionally utilize the

following parameters to express the individual and overall far-field patterns:

$$\alpha_j = d_j \cos\theta_j, \qquad \beta_j = d_j \sin\theta_j \sin\phi_j, \quad \gamma_j = d_j \sin\theta_j \cos\phi_j \tag{6.4}$$

We divide our results into the different excitation types: external or internal excitation and mixed excitation. From the results of the previous section, it is evident that the far-field is expressed as the superposition of the individual far-fields. The overall far-field for a group of dipoles located at the sphere's interior V_1 is given by:

$$\begin{aligned}\mathbf{g}_1(\theta,\phi) = (g_\theta^0(\theta,\phi) + g_\theta^1(\theta,\phi)\kappa + g_\theta^2(\theta,\phi)\kappa^2)\hat{\boldsymbol{\theta}} + \\ (g_\phi^0(\theta,\phi) + g_\phi^1(\theta,\phi)\kappa + g_\phi^2(\theta,\phi)\kappa^2)\hat{\boldsymbol{\phi}} + \mathcal{O}(\kappa^3)\end{aligned} \tag{6.5}$$

where

$$g_\theta^0(\theta,\phi) = \rho_0 \left[\cos\theta \left(\cos\phi \mathcal{P}_x + \sin\phi \mathcal{P}_y\right) - \sin\theta \mathcal{P}_z\right] \tag{6.6}$$

$$g_\phi^0(\theta,\phi) = \rho_0 \left(-\sin\phi \mathcal{P}_x + \cos\phi \mathcal{P}_y\right) \tag{6.7}$$

$$\begin{aligned}g_\theta^1(\theta,\phi) = (\rho_1 + \rho_2 \cos 2\theta)\left(\mathcal{G}_1^1 \cos\phi + \mathcal{G}_1^2 \sin\phi\right) + \\ \rho_2 \frac{\sin 2\theta}{2}\left[\mathcal{G}_1^5 + \mathcal{G}_1^6 - \cos 2\phi \mathcal{G}_1^3 + \sin 2\phi \mathcal{G}_1^4\right]\end{aligned} \tag{6.8}$$

$$\begin{aligned}g_\phi^1(\theta,\phi) = \cos\theta\Big[(\rho_2 - \rho_1)\cos\phi \mathcal{G}_1^2 + (\rho_1 + \rho_2)\sin\phi \mathcal{G}_1^1\Big] + \\ \rho_2 \sin\theta \left[\mathcal{G}_1^7 - \cos 2\phi \mathcal{G}_1^4 + \sin 2\phi \mathcal{G}_1^3\right]\end{aligned} \tag{6.9}$$

$$\begin{aligned}g_\theta^2(\theta,\phi) = \\ \rho_3 \left[\cos\theta(\mathcal{G}_2^1 \cos\phi + \mathcal{G}_2^2 \sin\phi) + \sin\theta(\mathcal{G}_2^4 \sin 2\phi - \mathcal{G}_2^3 \cos 2\phi)\right]\end{aligned} \tag{6.10}$$

$$\begin{aligned}g_\phi^2(\theta,\phi) = \rho_3[\cos 2\theta(\mathcal{G}_2^2 \cos\phi - \mathcal{G}_2^1 \sin\phi) + \\ \frac{\sin 2\theta}{2}(\mathcal{G}_2^4 \cos 2\phi + \mathcal{G}_2^3 \sin 2\phi + 3\mathcal{G}_2^5)]\end{aligned} \tag{6.11}$$

with the coefficients $\mathcal{G}_1^j, \mathcal{G}_2^\ell$ for $j = 1, ..., 7, \ell = 1, ..., 5$. On the other hand, the overall far-field for a group of dipoles located at the sphere's exterior V_0 is given by:

$$\mathbf{g}_0(\theta,\phi) = (\tilde{g}_\theta^0(\theta,\phi) + \tilde{g}_\theta^1(\theta,\phi)\kappa)\hat{\boldsymbol{\theta}} + (\tilde{g}_\phi^0(\theta,\phi) + \tilde{g}_\phi^1(\theta,\phi)\kappa)\hat{\boldsymbol{\phi}} + \mathcal{O}(\kappa^2) \tag{6.12}$$

with

$$\tilde{g}_\theta^0(\theta,\phi) = 2\chi_0\left[\cos\theta\left(\mathcal{F}_1^1\sin\phi + \mathcal{F}_1^2\cos\phi + \mathcal{F}_1^3\right) - \mathcal{F}_1^4\sin\theta\right] \tag{6.13}$$

$$\tilde{g}_\theta^1 = -\chi_1\left[\mathcal{G}_1^1\cos\phi + \mathcal{G}_1^2\sin\phi\right] \tag{6.14}$$

$$\tilde{g}_\phi^0 = 2\chi_0\left[\mathcal{F}_1^6\cos\phi - \mathcal{F}_1^2\sin\phi\right] \tag{6.15}$$

$$\tilde{g}_\phi^1 = \chi_1\left[\cos\theta\left(\mathcal{A}_x\sin\phi + \mathcal{F}_1^5\cos\phi\right) + \sin\theta\left(\mathcal{G}_1^7 - \sin\phi\mathcal{C}_z\right)\right] \tag{6.16}$$

where the coefficients $\mathcal{F}_1^j$ for $j = 1, ..., 6$ are given in the appendix.

6.2 Inverse Problems in the Low-Frequency Regime

6.2.1 Convergence patterns of the low-frequency far-field approximations

In Fig. 6.1 we depict the variations of the exact far-field patterns for the case of a homogeneous sphere excited by $N = 5$ dipoles located at the sphere's exterior V_0. The sphere is dielectric, with parameters $k_1 = 1.5k_0, \epsilon_1 = 2.25\epsilon_0, \mu_1 = 1.75\mu_0$. The "line" distribution refers to the case where all dipoles lie in the same line at the direction of $(1/2, 1/2, \sqrt{2}/2)$, at distances $r_j^0 = (1 + 0.25j)a_1$ for $j = 1, ..., 5$. The "spherical" distribution refers to the case where all dipoles lie at a constant distance $r_1^0 = ... = r_5^0 = 1.75a_1$ from the sphere's origin, at varying spherical angles $\theta_j = \pi/4 + j\pi/8, \phi_j = \pi/4 + j\pi/6$ for $j = 1, ..., 5$. Finally, in the "arbitrary" distribution the dipole's location don't follow a specific topological pattern; we chose $r_1^0 = 1.15a_1, r_2^0 = 1.5a_1, r_3^0 = 1.6a_1, r_4^0 = 2.05a_1, r_5^0 = 2.35a_1$, with the same spherical angles as in the spherical distribution. The three distributions we chose, have one thing in common, however: the average distance from the sphere's origin is in all distributions the same, i.e. $1.75a_1$. As we observe, in the lower frequencies, i.e. $k_0a_1 < 0.2$ the line and arbitrary distributions follow a similar quantitative behaviour, in contrast with

the spherical distribution which achieves lower values. As the frequency rises however, the arbitrary distribution moves closer to the spherical distribution.

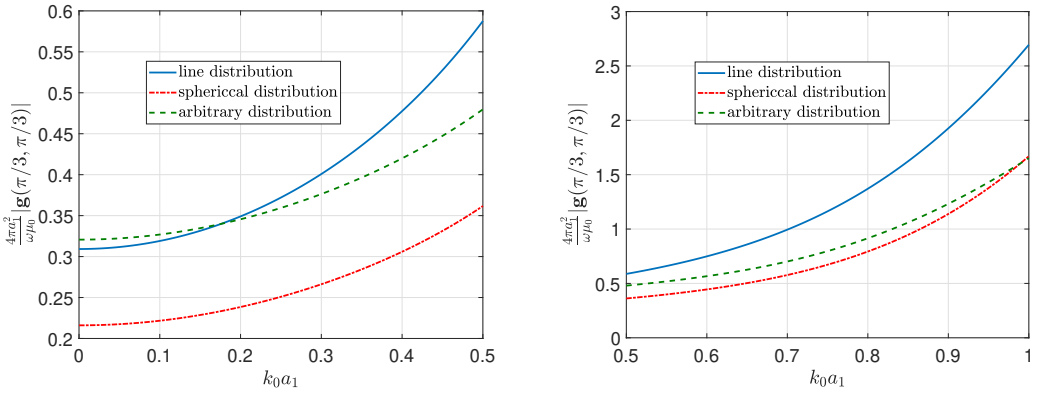

Figure 6.1: Behaviour of the overall far-field, for different dipole distributions. The dielectric sphere is excited by $N = 5$ dipoles, lying in the sphere's exterior at varying distributions.

In Fig. 6.2, we depict the convergence pattern for the spherical distribution for two different placements of the distribution. In the first placement, all the dipoles are located at distances $1.75a_1$ from the sphere's origin, while in the second placement they are located at distances $2.75a_1$ from the sphere's origin. We observe that for both placements, the low-frequency approximation fits well the exact far-field pattern, even at frequencies well beyond the assumption $k_0a_1 << 1$. In particular, the low-frequency approximaton diverges significantly - in both absolute values and error percentage - for $k_0a_1 > 0.85$ for the placement near the sphere and for $k_0a_1 > 0.7$ for the placement far from the sphere. However, the convergence is better for the placement far from the sphere compared to the placement near the sphere.

In Fig. 6.3 we demonstrate the convergence pattern for the spherical distribution of fig. 6.2 with the placement near the sphere, versus the relative electric permittivity $\epsilon_r = \epsilon_1/\epsilon_0$ for $k_0a_1 = 0.1$. The most notable observation is that both the exact far-field and its low-frequency approximation seem to increase as the relative permittivity rises, while for most of the examined values the error percentage is below 20% with the difference in

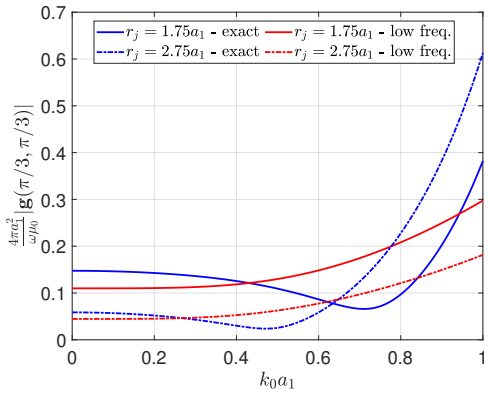

Figure 6.2: Convergence pattern for the overall far-field and its low-frequency approximation, for two different placements of a spherical distribution of dipoles.

absolute numbers not exceeding 10^{-1}. Finally, we observe that for greater permittivities, i.e. for $\epsilon_1 > 5\epsilon_0$ the low-frequency approximation *underestimates* the exact far-field, while it *overestimates* it, for lower permittivities. This pattern appears to be typical for varying placements and different distribution setups. We note that qualitatively similar convergence patterns, were observed for different placements of a spherical distribution and for varying $k_0 a_1$ of the low-frequency regime.

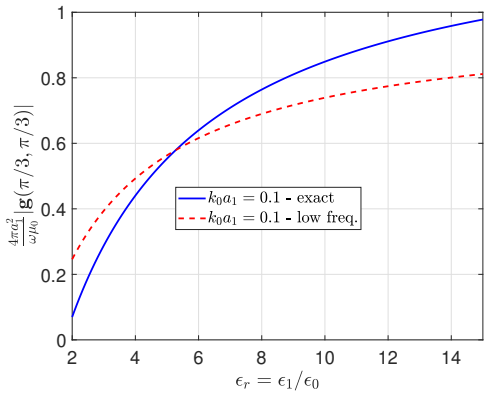

Figure 6.3: Convergence pattern for the overall far-field and its low-frequency approximation for $k_0 a_1 = 0.1$ versus the relative electric permitivitty of the sphere.

6.2.2 A mixed inverse problem

We use the term *mixed inverse problem* to refer to an inverse scattering problem, where the location of at least one dipole and some physical parameters and/or geometrical characteristics of the scatterer are unknown. Here we address two problems of this type. In the first problem we address, the geometrical characteristics of the scatterer are known. An internal dipole inside the sphere emanates a spherical wave, but we don't know the exact dipole's location or the physical parameters ϵ_1, μ_1 of the sphere. To identify the source location and the physical parameters of the scatterer we place an electric dipole at the sphere's exterior in such a way that its polarized strength is vertical with the dipole's position vector. Then, we choose the coordinate system, so that our placed dipole lies on the z-axis and its polarized strength lies on the x-axis. In other words, our placed dipole has the position vector $\mathbf{r}_1 = (0, 0, r_1)$ and its polarized strength will be of the form $\mathbf{p}_1 = (p_1, 0, 0)$. The unknown dipole will be located at $\mathbf{r}_2 = (r_2, \theta_2, \phi_2)$ with unknown polarized strength $\mathbf{p}_2 = (p_x, p_y, p_z)$.

Utilizing the techniques of [65] we isolate the term of order κ of the overall far-field, at the following observation coordinates:

$$g^0_\theta(0,0) = \rho_0 p_x - \frac{2}{3}\tau_1\chi_0 \tag{6.17}$$

$$g^0_\phi(0,0) = \rho_0 p_y \tag{6.18}$$

$$g^0_\theta(\frac{\pi}{2},\frac{\pi}{2}) = -\rho_0 p_z \tag{6.19}$$

$$g^1_\theta(0,0) = (\rho_1+\rho_2)p_x\alpha_2 - (\rho_1-\rho_2)p_z\gamma_2 - \chi_1 \tag{6.20}$$

$$g^1_\theta(\frac{\pi}{2},0) = (\rho_1-\rho_2)p_x\alpha_2 - (\rho_1+\rho_2)p_z\gamma_2 - \chi_1 \tag{6.21}$$

$$g^1_\phi(0,\frac{\pi}{2}) = (\rho_1+\rho_2)p_x\alpha_2 - (\rho_1-\rho_2)p_z\gamma_2 + \chi_1 \tag{6.22}$$

with

$$\chi_0 = \frac{3}{2}\frac{\epsilon-1}{\epsilon+2}, \quad \chi_1 = \frac{3}{2}\frac{\mu-1}{\mu+2} \tag{6.23}$$

Equations (6.20), (6.22) imply

$$\chi_1 = \frac{g^1_\phi(0, \frac{\pi}{2}) - g^1_\theta(0,0)}{2} \tag{6.24}$$

Last relation, combined with (6.23) leads to:

$$\mu = \frac{1+2\chi_1}{1-\chi_1} = \frac{2(1 + g^1_\phi(0, \frac{\pi}{2}) - g^1_\theta(0,0))}{2 - g^1_\phi(0, \frac{\pi}{2}) + g^1_\theta(0,0)} \tag{6.25}$$

Since μ is known, it swiftly follows that ρ_1, ρ_3 are also known. But then again, we obtain:

$$p_x\alpha_2 - p_z\gamma_2 = \frac{\chi_1}{\rho_1} + \frac{g^1_\theta(\frac{\pi}{2}, 0) + g^1_\theta(0,0)}{2\rho_1} = G_1 \tag{6.26}$$

$$p_x\alpha_2 + p_z\gamma_2 = -\frac{\chi_1}{\rho_2} + \frac{g^1_\phi(0, \frac{\pi}{2}) - g^1_\theta(\frac{\pi}{2}, 0)}{2\rho_2} = \frac{G_2}{\rho_2} \tag{6.27}$$

$$p_x\beta_2 - p_y\gamma_2 = \frac{g^1_\phi(\frac{\pi}{2}, \frac{\pi}{2}) + g^1_\phi(\frac{\pi}{2}, 0)}{2\rho_1} = G_3 \tag{6.28}$$

$$p_x\beta_2 + p_y\gamma_2 = \frac{g^1_\phi(\frac{\pi}{2}, \frac{\pi}{2}) + g^1_\phi(\frac{\pi}{2}, 0)}{2\rho_2} = \frac{G_4}{\rho_2} \tag{6.29}$$

Then, we swiftly get:

$$p_z\gamma_2 = G_1 + \frac{G_2}{\rho_2} \tag{6.30}$$

$$p_y\gamma_2 = G_3 + \frac{G_4}{\rho_2} \tag{6.31}$$

But, from the measurements of the terms of order 1, last relations take the form:

$$\gamma_2 = -\frac{\rho_0}{g^0_\theta(\frac{\pi}{2}, \frac{\pi}{2})}\left(G_1 + \frac{G_2}{\rho_2}\right) \tag{6.32}$$

$$\gamma_2 = \frac{\rho_0}{g^0_\phi(0,0)}\left(G_3 + \frac{G_4}{\rho_2}\right) \tag{6.33}$$

which in turn yields:

$$\rho_2 = -\frac{g^0_\phi(0,0)G_2 + g^0_\theta(\frac{\pi}{2}, \frac{\pi}{2})G_4}{g^0_\phi(0,0)G_1 + g^0_\theta(\frac{\pi}{2}, \frac{\pi}{2})G_3} \tag{6.34}$$

The special cases where $g_\phi^0(0,0) = 0$ or $g_\theta^0(\frac{\pi}{2},\frac{\pi}{2}) = 0$ are addressed as follows:

$$\rho_2 = \frac{G_4}{G_3}, \quad for \quad g_\phi^0(0,0) = 0 \tag{6.35}$$

$$\rho_2 = \frac{G_2}{G_1}, \quad for \quad g_\theta^0(\frac{\pi}{2},\frac{\pi}{2}) = 0 \tag{6.36}$$

$$\rho_2 = \frac{G_2}{G_1} = \frac{G_4}{G_3}, \quad for \quad g_\phi^0(0,0) = g_\theta^0(\frac{\pi}{2},\frac{\pi}{2}) = 0 \tag{6.37}$$

In all cases, since ρ_2 becomes known, then ρ_0, χ_0 are also known, which results in p_x, p_y, p_z to be known from the measurements of order $\mathcal{O}(1)$ and thus, $\alpha_2, \beta_2, \gamma_2$ become known. We note that for r_2 it holds $d_2 = \sqrt{\alpha_2^2 + \beta_2^2 + \gamma_2^2}$. In the case were the radius R of the sphere is unknown, we obtain:

$$r_2 = k_1\sqrt{|p_x|^2 + |p_y|^2 + |p_z|^2} \tag{6.38}$$

Which finally yields:

$$R = k_1\sqrt{\frac{|p_x|^2 + |p_y|^2 + |p_z|^2}{\alpha_2^2 + \beta_2^2 + \gamma_2^2}} \tag{6.39}$$

6.2.3 Source Localization Problem

Due to the complexity of the analytical procedure, we will first describe the basic steps of the algorithm.

1. We measure certain terms of the overall far-field for different angles of observation.
2. We manipulate the taken measurements and evaluate a set of quantities which will be necessary for the implementation of the procedure.
3. We perform a series of *procedure tests*.
   (a) If all procedure tests are "negative" the *basic procedure* can be safely implemented.
   (b) Depending on which test is "positive", then we divert to its corresponding *secondary procedure* and continue from there.

4. We use the formulas for extracting the dipoles' location and polarized strengths; the formulas depend on the chosen procedure.

To simplify the procedure, we enlist all the measurements and the quantities involved in the appendix. Under our formulation, the position vectors of the dipoles' locations, will be given by:

$$r_j = R\sqrt{(\alpha_j)^2 + (\beta_j)^2 + (\gamma_j)^2} \tag{6.40}$$

$$\cos\theta_j = \frac{\alpha_j}{\sqrt{(\alpha_j)^2 + (\beta_j)^2 + (\gamma_j)^2}}, \tag{6.41}$$

$$\sin\theta_j = \frac{\sqrt{(\beta_j)^2 + (\gamma_j)^2}}{\sqrt{(\alpha_j)^2 + (\beta_j)^2 + (\gamma_j)^2}} \tag{6.42}$$

$$\cos\phi_j = \frac{\gamma_j}{\sqrt{(\beta_j)^2 + (\gamma_j)^2}} \tag{6.43}$$

$$\sin\phi_j = \frac{(\beta_j)^2}{\sqrt{(\beta_j)^2 + (\gamma_j)^2}} \tag{6.44}$$

As it is evident, the procedure will be centered around the calculation of the parameters $\alpha_j, \beta_j, \gamma_j$. Completion of steps 1 and 2, yields the following equations:

$$\begin{cases} p_x^1 + p_x^2 = M_x, \\ p_y^1 + p_y^2 = M_y, \\ p_z^1 + p_z^2 = M_z \end{cases} \tag{6.45}$$

$$\begin{cases} \alpha_1 p_x^1 + \alpha_2 p_x^2 = A_x, \\ \alpha_1 p_y^1 + \alpha_2 p_y^2 = A_y, \\ \alpha_1 p_z^1 + \alpha_2 p_z^2 = A_z \end{cases} \tag{6.46}$$

$$\begin{cases} \beta_1 p_x^1 + \beta_2 p_x^2 = B_x, \\ \beta_1 p_y^1 + \beta_2 p_y^2 = B_y, \\ \beta_1 p_z^1 + \beta_2 p_z^2 = B_z \end{cases} \tag{6.47}$$

$$\begin{cases} \gamma_1 p_x^1 + \gamma_2 p_x^2 = C_x, \\ \gamma_1 p_y^1 + \gamma_2 p_y^2 = C_y, \\ \gamma_1 p_z^1 + \gamma_2 p_z^2 = C_z \end{cases} \tag{6.48}$$

The above quantities M_j, A_j, B_j, C_j for $j = x, y, z$ depend on the measurements of the far-field for the terms of order $\mathcal{O}(1), \mathcal{O}(\kappa)$ as follows:

$$M_x = \frac{g_\theta^0(0,0)}{\rho_0} \tag{6.49}$$

$$M_y = -\frac{g_\theta^0(0,\pi/2)}{\rho_0} \tag{6.50}$$

$$M_z = \frac{g_\theta^0(\pi/2,0)}{\rho_0} \tag{6.51}$$

$$A_x = \frac{(\rho_1-\rho_2)g_\theta^1(0,0) - (\rho_1+\rho_2)g_\theta^1(\pi/2,0)}{4\rho_1\rho_2} \tag{6.52}$$

$$A_y = \frac{(\rho_1-\rho_2)g_\theta^1(0,\pi/2) - (\rho_1+\rho_2)g_\theta^1(\pi/2,\pi/2)}{4\rho_1\rho_2} \tag{6.53}$$

$$A_z = \frac{g_\theta^1(3\pi/4,\pi/2) - g_\theta^1(\pi/4,\pi/2)}{2\rho_2} - \frac{\rho_1}{\rho_2}B_z \tag{6.54}$$

$$B_x = \frac{(\rho_1-\rho_2)g_\phi^1(\pi/2,0) - (\rho_1+\rho_2)g_\phi^1(\pi/2,\pi/2)}{4\rho_1\rho_2} \tag{6.55}$$

$$B_y = \frac{g_\theta^1(3\pi/4,\pi/2) + g_\theta^1(\pi/4,\pi/2)}{2\rho_2} - \frac{\rho_1}{\rho_2}A_y \tag{6.56}$$

$$B_z = \frac{(\rho_1+\rho_2)g_\theta^1(0,\pi/2) - (\rho_1-\rho_2)g_\theta^1(\pi/2,\pi/2)}{4\rho_1\rho_2} \tag{6.57}$$

$$C_x = \frac{g_\phi^1(\pi/4,\pi/2)}{\rho_2} - \frac{\rho_1}{\rho_2}(B_x - C_y) + B_y \tag{6.58}$$

$$C_y = \frac{(\rho_1+\rho_2)g_\phi^1(\pi/2,0) - (\rho_1-\rho_2)g_\phi^1(\pi/2,\pi/2)}{4\rho_1\rho_2} \tag{6.59}$$

$$C_z = \frac{(\rho_1+\rho_2)g_\theta^1(0,0) - (\rho_1-\rho_2)g_\theta^1(\pi/2,0)}{4\rho_1\rho_2} \tag{6.60}$$

In the following steps we will ellaborate the analytical procedure, under

which formulas (6.40)-(6.44) are extracted.

Primary Procedure

At first we present the *primary procedure*, which is valid if and only if, all procedure tests turn out negative. Combining all equations of (6.45) with their corresponding equation of (6.46), we can derive the components of the polarized strength as expressions of the unknown parameters. In particular it holds:

$$p_x^1 = \frac{M_x\alpha_2 - A_x}{\alpha_2 - \alpha_1}, \qquad p_y^1 = \frac{M_y\alpha_2 - A_y}{\alpha_2 - \alpha_1}, \qquad p_z^1 = \frac{M_z\alpha_2 - A_z}{\alpha_2 - \alpha_1} \tag{6.61}$$

$$p_x^2 = \frac{A_x - M_x\alpha_1}{\alpha_2 - \alpha_1}, \qquad p_y^2 = \frac{A_y - M_y\alpha_1}{\alpha_2 - \alpha_1}, \qquad p_x^2 = \frac{A_z - M_z\alpha_1}{\alpha_2 - \alpha_1} \tag{6.62}$$

Next, from the system of any pair from the equations of (6.47) and (6.48) we obtain the parameters β_j, γ_j as linear expressions of α_j. In particular it holds:

$$\beta_j = N_1 + \alpha_j N_2, \qquad \gamma_j = N_3 + \alpha_j N_4 \tag{6.63}$$

with N_1, N_2, N_3, N_4 being quantities that depend only on the known physical parameters of the scatterer and the measurements of the far-field. Their exact expressions are given in the appendix. Now, we use the measurements of the far-field for the terms of order $\mathcal{O}(\kappa^2)$. We obtain:

$$p_x^1(\alpha_1^2 - \beta_1^2) + p_x^2(\alpha_2^2 - \beta_2^2) + p_y^1\beta_1\gamma_1 + \tag{6.64}$$

$$p_y^2\beta_2\gamma_2 - (p_z^1\alpha_1\gamma_1 + p_z^2\alpha_2\gamma_2) = \frac{g_{\theta,2}(0,0)}{\rho_3}$$

$$p_x^1\beta_1\gamma_1 + p_x^2\beta_2\gamma_2 + p_y^1(\alpha_1^2 - \gamma_1^2) + \tag{6.65}$$

$$p_y^2(\alpha_2^2 - \gamma_2^2) - (p_z^1\alpha_1\beta_1 + p_z^2\alpha_2\beta_2) = \frac{g_{\phi,2}(0,0)}{\rho_3} \tag{6.66}$$

After some minor manipulation, equations (6.46) yield:

$$p_x^1\alpha_1^2 + p_x^2\alpha_2^2 = (\alpha_1 + \alpha_2)A_x - \alpha_1\alpha_2 M_x \tag{6.67}$$

$$p_y^1\alpha_1^2 + p_y^2\alpha_2^2 = (\alpha_1 + \alpha_2)A_y - \alpha_1\alpha_2 M_y \tag{6.68}$$

$$p_z^1\alpha_1^2 + p_z^2\alpha_2^2 = (\alpha_1 + \alpha_2)A_z - \alpha_1\alpha_2 M_z \tag{6.69}$$

Combining equations (6.67)-(6.69) with (6.64),(6.66) and utilizing (6.63) we get the following system:

$$K_1(\alpha_1+\alpha_2)-K_2\alpha_1\alpha_2=K_3, \tag{6.70}$$

$$K_4(\alpha_1+\alpha_2)-K_5\alpha_1\alpha_2=K_6 \tag{6.71}$$

The former system, reveals quantities $\alpha_1+\alpha_2, \alpha_1\alpha_2$. Utilizing Vietta's formulas we conclude that α_1, α_2 are the solutions of the following quadratic equation:

$$\alpha^2-L_1\alpha+L_2=0 \tag{6.72}$$

with

$$L_1=\frac{K_2K_6-K_3K_5}{K_2K_4-K_1K_5}, \qquad L_2=\frac{K_1K_6-K_3K_4}{K_2K_4-K_1K_5} \tag{6.73}$$

The exact expressions of K_m for $m=1,\ldots,6$ are given in the appendix.

Before we continue with the presentation of the procedure tests and the secondary procedures, we proceed with a more careful examination of the determinant of the latter system, e.g. with the quantity $K_2K_4-K_1K_5$. Utilizing the expressions of all involved quantities and the measurements of the far-field, after some lengthy calculations we arrive at the following formula for the expression of this determinant. The importance of this formula is that, in this form the physical interpretation of this determinant is revealed as well as its importance for the algebraic procedure:

$$K_2K_4-K_1K_5=\frac{1}{2}D_\alpha D_p \tag{6.74}$$

with

$$D_\alpha=\begin{vmatrix} \frac{1}{\alpha_1-\alpha_2} & 0 & \frac{1}{\alpha_1-\alpha_2} \\ \gamma_1-\gamma_2 & \beta_1-\beta_2 & 0 \\ 0 & \gamma_1-\gamma_2 & \beta_1-\beta_2 \end{vmatrix} \tag{6.75}$$

$$D_p=\begin{vmatrix} 1 & 1 & 1 \\ p_x^1 & p_y^1 & p_z^1 \\ p_x^2 & p_y^2 & p_z^2 \end{vmatrix} \tag{6.76}$$

The above quantities, include all the procedure tests that are required before we implement any algebraic procedure. Additionally they showcase the

importance of the polarized strength vectors. Another interesting observation, is that the left determinant might have a different form, depending on the choices we made at the beginning of the procedure. Here, we chose to express all quantities as functions of α_1, α_2. If we chose, p.e. to express all quantities as functions of β_1, β_2 or γ_1, γ_2 the left determinant will take, respectively, the form:

$$\begin{vmatrix} \frac{1}{\beta_1-\beta_2} & 0 & \frac{1}{\beta_1-\beta_2} \\ \alpha_1-\alpha_2 & \gamma_1-\gamma_2 & 0 \\ 0 & \alpha_1-\alpha_2 & \gamma_1-\gamma_2 \end{vmatrix} = D_\beta, \qquad \begin{vmatrix} \frac{1}{\gamma_1-\gamma_2} & 0 & \frac{1}{\gamma_1-\gamma_2} \\ \beta_1-\beta_2 & \alpha_1-\alpha_2 & 0 \\ 0 & \beta_1-\beta_2 & \alpha_1-\alpha_2 \end{vmatrix} = D_\gamma \tag{6.77}$$

In other words, depending on the choice between a_j, b_j, c_j the left determinant follows the changes of the transposition $(a_j \quad b_j \quad c_j)$. On the other hand, the right determinant will not change, regardless of the choice between the parameters a_j, b_j, c_j.

Secondary Procedures for the Determinant D_α

Secondary Procedure 1:
The first problem we have to address, is when we have $\alpha_1 = \alpha_2$. This case can be verified through the following test:

$$\frac{A_x}{M_x} = \frac{A_y}{M_y} = \frac{A_z}{M_z}, \quad |M_x|^2 + |M_y|^2 + |M_z|^2 \neq 0 \tag{6.78}$$

In such a case, we only have to express all quantities as functions of β_1, β_2. The rest of the procedure is the same, with only difference the use of D_β. This happens because instead of the measurement of the term $g_{\phi,2}(0,0)$ we must use the measurement $g_{\theta,2}(0,\pi)$ We also note that A_x, A_y can be swiftly obtained, since it will hold $A_x = A_y = A_x/M_x$.

Secondary Procedure 2:
Let's now suppose that it holds $\alpha_1 = \alpha_2$ and $\beta_1 = \beta_2$. This case can be verified through the following test:

$$\frac{A_x}{M_x} = \frac{A_y}{M_y} = \frac{A_z}{M_z}, \quad \frac{B_x}{M_x} = \frac{B_y}{M_y} = \frac{B_z}{M_z}, \quad |M_x|^2 + |M_y|^2 + |M_z|^2 \neq 0 \tag{6.79}$$

Then we use the primary procedure, with the following differences: Terms α_j, β_j can be calculated directly since it will hold $\alpha_1 = \alpha_2 = A_x/M_x, \beta_1 = \beta_2 = B_x/M_x$. Instead of the measurements $g_{\phi,2}(0,0)$ or $g_{\theta,2}(0,\pi)$ we will use the measurement $g_{\theta,2}(\pi/2,0)$ which results in the use of the D_γ determinant. We note, that the case where $\alpha_1 = \alpha_2, \beta_1 = \beta_2, \gamma_1 = \gamma_2$ cannot occur, since we have two distinct dipoles.

Remark 6.2.1 *It is possible to have p.e.* $\alpha_1 = \alpha_2, \gamma_1 = \gamma_2$. *It is obvious that secondary procedure 2, can be implemented only for* β_j.

Secondary Procedure 3:
Now let's suppose that the previous tests are negative, one of the lower 2×2 blocks of the D_p determinant is zero. This doesn't turn our master determinant zero, but we must make a different choice of systems. In particular, quantities N_1, N_2, N_3, N_4 cannot be extracted through the same combination of equations. In particular it holds:

$$\begin{vmatrix} p_w^1 & p_v^1 \\ p_w^2 & p_v^2 \end{vmatrix} = 0 \tag{6.80}$$

if and only if it holds

$$A_w M_v = A_v M_w \tag{6.81}$$

with $w, v \in x, y, z$ and $w \neq v$. The only thing we need change in the primary procedure, is the choice of systems that leads to the N_m quantities for $m = 1, 2, 3, 4$.

Secondary Procedures for the Determinant D_p

The polarization determinant can be zero in three cases: If the polarized strength vectors are parallel, if the polarized strength vectors are antiparallel and finally if at least for one of the polarized vectors holds $p_x^j = p_y^j = p_z^j$. We deal with the latter case, first.

Secondary Procedure 4:
One of the polarized vectors will be of the form $\mathbf{p}_j = (p_j, p_j, p_j)$ if and only if it holds:

$$\frac{A_x - A_y}{M_x - M_y} = \frac{A_y - A_z}{M_y - M_z} = \frac{A_x - A_z}{M_x - M_z} \tag{6.82}$$

and at the same time the test 1 is negative. Without loss of generality, we suppose that $\mathbf{p}_1 = (p_1, p_1, p_1)$. Then we swiftly obtain, $\alpha_2, \beta_2, \gamma_2$ since it will hold:

$$\alpha_2 = \frac{A_x - A_y}{M_x - M_y} \tag{6.83}$$

$$\beta_2 = \frac{B_x - B_y}{M_x - M_y} \tag{6.84}$$

$$\gamma_2 = \frac{C_x - C_y}{M_x - M_y} \tag{6.85}$$

Then, we can readily extract p_x^2, p_y^2, p_z^2 since it will hold:

$$p_x^2 = \frac{(M_x - M_y)(A_x - B_x)}{A_x - A_y - B_x + B_y}, \tag{6.86}$$

$$p_y^2 = \frac{(M_x - M_y)(A_y - B_y)}{A_x - A_y - B_x + B_y}, \tag{6.87}$$

$$p_y^2 = \frac{(M_x - M_y)(A_z - B_z)}{A_x - A_y - B_x + B_y} \tag{6.88}$$

Then p_1 is readily extracted from the measurement of the far-field of order $\mathcal{O}(1)$ and subsequently, from the measurements of the far-field of order $\mathcal{O}(\kappa)$.

So far, the secondary procedures required minor changes to the primary procedure (procedures 1-2-3) or in the case of the procedure 4, they were far easier. The final two secondary procedures, require major changes in the primary procedure.

Secondary Procedure 5:

Here we suppose that $\mathbf{p}_1 = \lambda \mathbf{p}_2$ for $\lambda \neq -1$. From eqs. (6.45) we obtain:

$$p_x^2 = \frac{M_x}{\lambda + 1}, \qquad p_y^2 = \frac{M_y}{\lambda + 1}, \qquad p_z^2 = \frac{M_z}{\lambda + 1} \tag{6.89}$$

Combining the last equations with equations (6.46)-(6.48) we get:

$$\begin{aligned}\frac{M_x}{\lambda+1}(\lambda\alpha_1+\alpha_2)&=A_x,\\ \frac{M_x}{\lambda+1}(\lambda\beta_1+\beta_2)&=B_x,\\ \frac{M_x}{\lambda+1}(\lambda\gamma_1+\gamma_2)&=C_x\end{aligned}\tag{6.90}$$

We introduce the new parameters u_j, v_j, w_j as follows:

$$u_j=\alpha_j\frac{M_x}{A_x},\qquad v_j=\beta_j\frac{M_x}{B_x},\qquad w_j=\gamma_j\frac{M_x}{C_x}\tag{6.91}$$

Then, eqs. (6.90), will respectively take the form:

$$\lambda u_1+u_2=\lambda+1,\qquad \lambda v_1+v_2=\lambda+1,\qquad \lambda w_1+w_2=\lambda+1\tag{6.92}$$

Addtionally, we obtain:

$$\frac{M_x}{\lambda+1}\left(\lambda\alpha_1\beta_1+\alpha_2\beta_2\right)=\frac{A_xB_x}{M_x(\lambda+1)}\left(\lambda(u_1-1)(v_1-1)+1\right)\tag{6.93}$$

$$\frac{M_x}{\lambda+1}\left(\lambda\alpha_1\gamma_1+\alpha_2\gamma_2\right)=\frac{A_xC_x}{M_x(\lambda+1)}\left(\lambda(u_1-1)(w_1-1)+1\right)\tag{6.94}$$

$$\frac{M_x}{\lambda+1}\left(\lambda\gamma_1\beta_1+\gamma_2\beta_2\right)=\frac{B_xC_x}{M_x(\lambda+1)}\left(\lambda(v_1-1)(w_1-1)+1\right)\tag{6.95}$$

Utilizing the measurements of the far-field for the terms of order $\mathcal{O}(\kappa^2)$ we arrive at the following system:

$$\begin{bmatrix}-M_x & 2M_y & -M_z\\ -2M_x & M_y & -M_z\\ -M_y & M_x+M_y & -M_x\end{bmatrix}\cdot\begin{bmatrix}\lambda\alpha_1\beta_1+\alpha_2\beta_2\\ \lambda\alpha_1\gamma_1+\alpha_2\gamma_2\\ \lambda\beta_1\gamma_1+\beta_2\gamma_2\end{bmatrix}=(\lambda+1)\begin{bmatrix}G_1\\ G_2\\ G_3\end{bmatrix}\tag{6.96}$$

The solution, yields:

$$\lambda\alpha_1\beta_1+\alpha_2\beta_2=(\lambda+1)X_1\tag{6.97}$$

$$\lambda\alpha_1\gamma_1+\alpha_2\gamma_2=(\lambda+1)X_2\tag{6.98}$$

$$\lambda\beta_1\gamma_1+\beta_2\gamma_2=(\lambda+1)X_3\tag{6.99}$$

Combining the solution of the previous system with eqs. (6.93)-(6.95) we obtain:

$$X_1 M_x^2 = A_x B_x \left(\lambda(u_1-1)(v_1-1)+1\right) \tag{6.100}$$
$$X_2 M_x^2 = A_x C_x \left(\lambda(u_1-1)(w_1-1)+1\right) \tag{6.101}$$
$$X_3 M_x^2 = B_x C_x \left(\lambda(v_1-1)(w_1-1)+1\right) \tag{6.102}$$

Then, we readily arrive at:

$$u_1 - 1 = N_1(w_1-1) \tag{6.103}$$
$$v_1 - 1 = N_2(w_1-1) \tag{6.104}$$

with

$$N_1 = \frac{X_1 M_x^2 - A_x B_x}{X_3 M_x^2 - B_x C_x}, \qquad N_2 = \frac{X_1 M_x^2 - A_x B_x}{X_2 M_x^2 - A_x C_x} \tag{6.105}$$

This relations also, imply:

$$\lambda(w_1-1)^2 = \frac{X_1 M_x^2 - A_x B_x}{N_1 N_2 A_x B_x} = F_0 \tag{6.106}$$

Then by a far-field measurement we obtain:

$$\frac{g_{\theta,2}(0,0)}{\rho_3} = \frac{M_x}{\lambda+1}(\lambda\alpha_1^2 + \alpha_2^2 - \lambda\beta_1^2 - \beta_2^2) + M_y X_3 - M_z X_2 \tag{6.107}$$

Inserting parameters u_j, v_j into the last equation and expressing in terms of $u_1 - 1$, we arrive at:

$$\frac{g_{\theta,2}(0,0)}{\rho_3} - M_y X_3 + M_z X_2 =$$
$$\frac{1}{M_x}\left(A_x^2((\lambda^2+\lambda)(u_1-1)^2+1) - B_x^2((\lambda^2+\lambda)(v_1-1)^2+1)\right) \tag{6.108}$$

Combining the last relation with (6.103),(6.104) we get:

$$\lambda(\lambda+1)(w_1-1)^2 = \frac{M_x G_4 - A_x^2 + B_x^2}{N_1^2 A_x^2 - N_2^2 B_x^2} = G_0 \tag{6.109}$$

with

$$G_4 = \frac{g_{\theta,2}(0,0)}{\rho_3} - M_y X_3 + M_z X_2 \tag{6.110}$$

Utilizing (6.106) last relation yields:

$$\lambda = \frac{G_0 - F_0}{F_0} \tag{6.111}$$

Since λ we identify the distances r_1, r_2 of the dipoles from the sphere's center:

$$r_1 = \frac{(G_0 - F_0)k_1 M_0}{G_0 a_1} \tag{6.112}$$

$$r_2 = \frac{k_1 M_0 F_0}{G_0 a_1} \tag{6.113}$$

and the polarized stength vectors from eqs. (6.89).
Then, the next step is to extract the value of $w_1 - 1$. If we try to use (6.109) we see that our relations, cannot guarantee the choice of the sign. To bypass that problem, we will use the fact that $\alpha_1^2 + \beta_1^2 + \gamma_1^2 = \tau_1^2$. In particular, if we use the previous "trick" of writing this equation in terms of $w_1 - 1$ we will arrive at:

$$\frac{1}{M_x^2}\left((w_1 - 1)^2 I_1 + 2(w_1 - 1)I_2 + I_3\right) = \tau_1^2 \tag{6.114}$$

where

$$I_1 = N_1^2 A_x^2 + N_2^2 B_x^2 + C_x^2, \tag{6.115}$$

$$I_2 = N_1 A_x^2 + N_2 B_x^2 + C_x^2, \tag{6.116}$$

$$I_3 = A_x^2 + B_x^2 + C_x^2 \tag{6.117}$$

Combining with equation (6.109) we finally arrive at:

$$w_1 - 1 = \frac{1}{2I_2(G_0 - F_0)}\left((G_0 - F_0)(M_x^2 \tau_1^2 - I_3) - F_0^2 I_1\right) = F_1 \tag{6.118}$$

Thus we finally obtain:

$$\alpha_1 = (N_1F_1 + 1)\frac{A_x}{M_x}, \tag{6.119}$$

$$\beta_1 = (N_2F_1 + 1)\frac{B_x}{M_x}, \tag{6.120}$$

$$\gamma_1 = (F_1 + 1)\frac{C_x}{M_x} \tag{6.121}$$

$$\alpha_2 = (\lambda N_1F_1 + 1)\frac{A_x}{M_x}, \tag{6.122}$$

$$\beta_2 = (\lambda N_2F_1 + 1)\frac{B_x}{M_x}, \tag{6.123}$$

$$\gamma_2 = (\lambda F_1 + 1)\frac{C_x}{M_x} \tag{6.124}$$

Utilizing equations (6.41) - (6.44) we determine the exact locations of the dipoles.

Secondary Procedure 6:

The Secondary Procedure 5, cannot be implemented if $\lambda = -1$. A different and rather easier procedure is required, in this case. Let $\mathbf{p}_1 = -\mathbf{p}_2$. Then we swiftly obtain that $r_1 = r_2$ which yields $\tau_1 = \tau_2$. We note, that in such a case, we will have that $M_x = M_y = M_z = 0$. Then, the we have:

$$p_x^1(\alpha_1 - \alpha_2) = A_x, \qquad p_x^1(\beta_1 - \beta_2) = B_x, \qquad p_x^1(\gamma_1 - \gamma_2) = C_x \tag{6.125}$$

Similar equations hold, respectively, for p_y^1, p_z^1. These equations, yield:

$$p_x^1 = \frac{A_x}{\alpha_1 - \alpha_2}, \qquad p_y^1 = \frac{A_y}{\alpha_1 - \alpha_2}, \qquad p_z^1 = \frac{A_z}{\alpha_1 - \alpha_2} \tag{6.126}$$

Utilizing the rest of the equations for the other parameters we obtain

$$\beta_1 - \beta_2 = \frac{B_x}{A_x}(\alpha_1 - \alpha_2), \qquad \gamma_1 - \gamma_2 = \frac{C_x}{A_x}(\alpha_1 - \alpha_2) \tag{6.127}$$

Manipulation of the measurements, yields the following system:

$$\begin{bmatrix} p_x^1 - p_y^1 & p_x^1 - p_y^1 \\ p_x^1 & p_y^1 \end{bmatrix} \cdot \begin{bmatrix} \alpha_1\beta_1 - \alpha_2\beta_2 \\ \alpha_1\gamma_1 - \alpha_2\gamma_2 \end{bmatrix} = \begin{bmatrix} g_1 \\ g_2 \end{bmatrix} \tag{6.128}$$

Solution of the system yields:

$$\alpha_1\beta_1 - \alpha_2\beta_2 = X_1(a_1 - a_2), \qquad \alpha_1\gamma_1 - \alpha_2\gamma_2 = X_2(a_1 - a_2) \tag{6.129}$$

Additionally, it holds:

$$\beta_1\gamma_1 - \beta_2\gamma_2 = X_3 \tag{6.130}$$

where

$$g_1 = \frac{g_\theta^2(\pi/2, 0) - g_\theta^2(\pi/2, \pi/4)}{\rho_3} \tag{6.131}$$

$$g_2 = \frac{g_\phi^2(\pi/4, 0) - g_\phi^2(\pi/4, \pi/2)}{\rho_3} \tag{6.132}$$

$$X_1 = \frac{A_y(g_1 + g_2) - A_x g_2}{(A_x - A_y)^2} \tag{6.133}$$

$$X_2 = \frac{A_x(g_2 - g_1) - A_y g_2}{(A_x - A_y)^2} \tag{6.134}$$

$$X_3 = 2A_y X_2 - A_x X_1 - \frac{g_\phi^2(\pi/4, 0)}{\rho_3} \tag{6.135}$$

After a lengthy manipulation of the measurements for the terms of order $\mathcal{O}(\kappa^2)$ and a series of calculations we arrive at:

$$\alpha_1 - \alpha_2 = I_\alpha^1, \qquad \beta_1 - \beta_2 = I_\beta^1, \qquad \gamma_1 - \gamma_2 = I_\gamma^1 \tag{6.136}$$

where

$$I_\beta^1 = \frac{B_x}{A_x} I_\alpha^1 \tag{6.137}$$

$$I_\gamma^1 = \frac{C_x}{A_x} I_\alpha^1 \tag{6.138}$$

with quantity I_α^1 given by

$$I_\alpha^1 = \frac{X_3(A_y^2 - A_x^2)}{A_y\left(A_z X_2 + \frac{g_\theta^2(0,0)}{\rho_3} - X_4\right) - A_x\left(\frac{g_\phi^2(0,0)}{\rho_3} + A_z X_1\right)} \tag{6.139}$$

This yields the polarized strengths' components which are given by

$$p_u^1 = \frac{A_u}{I_\alpha^1} \tag{6.140}$$

for $u \in \{x, y, z\}$. Utilizing the manipulation of the measurements for the terms of order $\mathcal{O}(\kappa^2)$ we also get the following system:

$$\begin{bmatrix} A_x & -B_x & 0 \\ A_y & 0 & -A_y C_x \\ 0 & -B_x & C_x \end{bmatrix} \cdot \begin{bmatrix} \alpha_1 + \alpha_2 \\ \beta_1 + \beta_2 \\ \gamma_1 + \gamma_2 \end{bmatrix} = \begin{bmatrix} V_1 \\ V_2 \\ V_3 \end{bmatrix} \tag{6.141}$$

where

$$V_1 = \frac{g_\theta^2(0,0)}{\rho_3} - \frac{B_x}{I_\alpha^1} X_3 + A_z X_2 \tag{6.142}$$

$$V_2 = \frac{g_\phi^2(0,0)}{\rho_3} - \frac{A_x}{I_\alpha^1} X_3 + A_z X_1 \tag{6.143}$$

$$V_3 = \frac{A_x}{A_z} \left(\frac{g_\theta^2(\pi/2,0)}{\rho_3} - A_x X_2 + A_y X_1 \right) \tag{6.144}$$

The last system yields the solutions:

$$\alpha_1 + \alpha_2 = I_\alpha^2, \qquad \beta_1 + \beta_2 = I_\beta^2, \qquad \gamma_1 + \gamma_2 = I_\gamma^2 \tag{6.145}$$

Then we readily obtain the desired unknown parameters

$$\alpha_{1,2} = \frac{I_\alpha^1 \pm I_\alpha^2}{2}, \qquad \beta_{1,2} = \frac{I_\beta^1 \pm I_\beta^2}{2}, \qquad \gamma_{1,2} = \frac{I_\gamma^1 \pm I_\gamma^2}{2} \tag{6.146}$$

where

$$I_\alpha^2 = \frac{1}{1 - A_x} \left(\frac{V_2}{A_x} + \frac{C_x}{B_x}(V_3 - V_1) \right) \tag{6.147}$$

$$I_\beta^2 = \frac{1}{B_x(1 - A_x)} \left(\frac{V_2}{A_x} + V_3 - \frac{V_1}{A_x} \right) \tag{6.148}$$

$$I_\gamma^2 = \frac{1}{C_x(1 - A_x)} \left(\frac{V_2}{A_x} + \frac{V_3 - V_1}{A_x} \right) \tag{6.149}$$

6.2.4 Symmetrically Placed Dipoles

Two symmetrically placed dipoles at $\mathbf{r}, \mathbf{r}'$ belong on the same sphere of radius r_0 and their angles and azimuths are related by $\theta' = \pi - \theta$, $\phi' = \phi + \pi$.

For the even and odd spherical harmonics the following relations hold:

$$Y_{\sigma mn}(\theta, \phi') = (-1)^m Y_{\sigma mn}(\theta, \phi) \tag{6.150}$$

$$Y_{\sigma mn}(\theta', \phi') = (-1)^n Y_{\sigma mn}(\theta, \phi) \tag{6.151}$$

Thus, the vector spherical harmonics and the SVWF, satisfy respectively:

$$\mathbf{Y}_{snm}(\mathbf{r}, k_q) = (-1)^n \mathbf{Y}_{snm}(\mathbf{r}', k_q) \tag{6.152}$$

$$\mathbf{X}^{\ell}_{snm}(\mathbf{r}, k_q) = (-1)^n \mathbf{X}^{\ell}_{snm}(\mathbf{r}', k_q) \tag{6.153}$$

for $\mathbf{Y} \in \{\mathbf{B}, \mathbf{C}, \mathbf{P}\}$ denoting the vector spherical harmonics and $\mathbf{X}^{\ell}_{snm}$ denoting the SVWF for $\ell = \{1, 3\}$ and $\mathbf{X} \in \{\mathbf{M}, \mathbf{N}\}$. In particular, for $\mathbf{p} = \pm\mathbf{p}'$, the excitation operator $\mathcal{X}^{\ell}_{snm}$ that corresponds to the SVWF $\mathbf{X}^{\ell}_{snm}$ will be of the form:

$$\mathcal{X}^{\ell}_{snm}(\mathbf{u}_2) = \frac{\mathrm{i}k_q}{4\pi} c_{nm} \mathbf{X}^{\ell}_{snm} \cdot \mathbf{p} \left(1 \pm (-1)^n\right) \tag{6.154}$$

with $\mathbf{u}_2 = (1, 1)$. In particular, the coefficients of the overall far-field for two symmetrically placed dipoles with parallel moments, satisfy:

$$\begin{cases} g^1_{\theta}(\theta, \phi) = g^1_{\phi}(\theta, \phi) = 0 \\ g^{2n}_{\theta}(\theta, \phi) = 2g^{2n}_{\theta,ind}(\theta, \phi) \\ g^{2n}_{\phi}(\theta, \phi) = 2g^{2n}_{\phi,ind}(\theta, \phi) \end{cases} \tag{6.155}$$

for $n = 0, 1$ and $g^k_{\theta,ind}, g^k_{\phi,ind}$ denoting the coefficients of the individual far-field due to the dipole at $\mathbf{r}$. In contrast, the coefficients of the overall far-field for two symmetrically placed dipoles with opposite moments, satisfy:

$$\begin{cases} g^1_{\theta}(\theta, \phi) = 2g^1_{\theta,ind}(\theta, \phi) \\ g^1_{\phi}(\theta, \phi) = 2g^1_{\phi,ind}(\theta, \phi) \\ g^{2n}_{\theta}(\theta, \phi) = g^{2n}_{\phi}(\theta, \phi) = 0 \end{cases} \tag{6.156}$$

The latter case presents a difficulty in inverse schemes, since neither of the secondary procedures is valid. Equations (6.46)-(6.48) take the following form:

$$\begin{cases} \alpha_1 p^1_x = \frac{A_x}{2}, \\ \alpha_1 p^1_y = \frac{A_y}{2}, \\ \alpha_1 p^1_z = \frac{A_z}{2} \end{cases} \tag{6.157}$$

$$\begin{cases} \beta_1 p_x^1 = \frac{B_x}{2}, \\ \beta_1 p_y^1 = \frac{B_y}{2}, \\ \beta_1 p_z^1 = \frac{B_z}{2} \end{cases} \tag{6.158}$$

$$\begin{cases} \gamma_1 p_x^1 = \frac{C_x}{2}, \\ \gamma_1 p_y^1 = \frac{C_y}{2}, \\ \gamma_1 p_z^1 = \frac{C_z}{2} \end{cases} \tag{6.159}$$

A straight-forward manipulation yields:

$$(p_x^1)^2 d_1^2 = \frac{A_x^2 + B_x^2 + C_x^2}{4} \tag{6.160}$$

$$\frac{d_1^2 a_1^2}{k_1^2} = \frac{A_x^2 + A_y^2 + A_z^2}{A_x^2} (p_x^1)^2 \tag{6.161}$$

The last two relations, imply

$$d_1 = \left(\frac{k_1^2}{a_1^2} \frac{(A_x^2 + B_x^2 + C_x^2)(A_x^2 + A_y^2 + A_z^2)}{4A_x^2} \right)^{1/4} \tag{6.162}$$

which in return yields $(p_x^1)^2$. Then again, we obtain:

$$(p_x^1)^2 \sin^2\theta_1 = \frac{B_x^2 + C_x^2}{4} \tag{6.163}$$

Given the fact that $\theta_1 \in [0, \pi]$, last relation yields $\sin\theta_1$:

$$\sin\theta_1 = d_1 \left(\frac{B_x^2 + C_x^2}{A_x^2 + B_x^2 + C_x^2} \right)^{1/2} \tag{6.164}$$

Another manipulation yields

$$\sin(2\phi_1) = \frac{1}{d_1^2} \frac{2B_x C_x}{B_x^2 + C_x^2} \tag{6.165}$$

$$\cos(2\phi_1) = \frac{1}{d_1^2} \frac{C_x^2 - B_x^2}{B_x^2 + C_x^2} \tag{6.166}$$

$$\phi_1 = \frac{B_x}{C_x} \tag{6.167}$$

Last equations reveal $2\phi_1$ and in return ϕ_1. With ϕ_1 known, we readily recover p_x^1, i.e.

$$p_x^1 = \frac{B_x}{2d_1 \sin(\phi_1)\sin(\theta_1)} = \frac{C_x}{2d_1 \cos(\phi_1)\sin(\theta_1)} \tag{6.168}$$

The remaining quantities are easily obtained by the relations:

$$p_y^1 = \frac{A_y}{A_x} p_x^1 \tag{6.169}$$

$$p_z^1 = \frac{A_z}{A_x} p_x^1 \tag{6.170}$$

$$\cos\theta_1 = \frac{A_x}{2p_x^1} \tag{6.171}$$

Next, in the case where the two symmetrically placed dipoles possess the same polarized strengths, i.e. $\mathbf{p} = \mathbf{p}'$ then, the polarized strength components can be easily extracted, from (6.45):

$$p_x^1 = \frac{M_x}{2},$$
$$p_y^1 = \frac{M_y}{2},$$
$$p_z^1 = \frac{M_z}{2}$$

which in return, yields:

$$d_1 = \frac{k_1}{2a_1}\sqrt{M_x^2 + M_y^2 + M_z^2}$$

Manipulation of the measurements of order $\mathcal{O}(\kappa^2)$ leads to the following system:

$$\begin{bmatrix} p_x & 2p_y & -p_z \\ -2p_x & p_y & -p_z \\ 0 & p_1 & p_2 \end{bmatrix} \cdot \begin{bmatrix} \alpha_1\beta_1 \\ \alpha_1\gamma_1 \\ \beta_1\gamma_1 \end{bmatrix} = \begin{bmatrix} g_\phi^2(\pi/4, 0) \\ g_\phi^2(\pi/4, \pi/2) \\ V_4 \end{bmatrix} \tag{6.172}$$

with

$$p_1 = p_x p_z^2 - p_y p_z^2 - p_x p_y^2$$
$$p_2 = p_z p_y^2 + p_y p_x^2 - p_z p_x^2$$
$$V_4 = p_y p_z g_\theta^2(0,0) - p_x p_y g_\theta^2(\pi/2, \pi/2) - p_x p_z g_\phi^2(0,0)$$

The solution of this system yields $\alpha_1\beta_1 = m_1, \alpha_1\gamma_1 = m_2, \beta_1\gamma_1 = m_3$. But it holds:

$$\alpha_1^2 = \frac{m_1 m_2}{m_3} \tag{6.173}$$
$$\beta_1^2 = \frac{m_1 m_3}{m_2} \tag{6.174}$$
$$\gamma_1^2 = \frac{m_2 m_3}{m_1} \tag{6.175}$$

which in return, yields:

$$\cos^2\theta_1 = \frac{m_1 m_2}{d_1^2 m_3} \tag{6.176}$$
$$\sin^2\theta_1 = \frac{m_3(m_1^2 + m_2^2)}{m_1 m_2} \tag{6.177}$$

With $\cos^2\theta_1, \sin^2\theta_1$ known, we readily obtain:

$$\sin(2\phi_1) = \frac{2m_2 m_3^2}{m_1(m_2^2 + m_3^2)} \tag{6.178}$$
$$\cos(2\phi_1) = \frac{d_1^2 m_3^2(m_2^2 - m_1^2)}{m_1^2(m_2^2 + m_3^2)} \tag{6.179}$$
$$\tan\phi_1 = \frac{m_1}{m_2} \tag{6.180}$$

Last three relations, yield ϕ_1. With $\cos\phi_1, \sin\phi_1$ known, we easily extract $\cos\theta_1$ from (6.176) which, in turn, yields θ_1.

Conclusions and Prospect

The subject of this dissertation is the excitation of a layered medium by an arbitrary distribution of point sources (for acoustic waves) or dipoles (for electromagnetic waves). For both types of waves, we devised a mathematical formulation that is based on the locations of the point sources/dipoles in the exterior or the interior of the scatterer (q-partial fields, q-excitation fields), as well as on their multitude (individual fields, partial fields, overall fields).

For the study of the energy transfer process, we adopted the complex form of the energy functionals (acoustic intensity vector - Poynting vector) and by utilizing Green's identities and complex integration techniques we derived acoustic and electromagnetic Energy Conservation Laws. These laws relate the active power (real part of flux vectors) with the corresponding scattering cross sections and the reactive power (imaginary part of flux vectors) with the Lagrangian density in the propagating medium.

We introduced the Interaction Scattering Cross Sections (ISCS) and Interaction Power Fluxes (IPF) that proved to be important in analyzing the energy transfer process in the far-field region and the way the co-existence between point sources/dipoles affects the overall energy flux. In particular, we derived optical theorems and came to the understanding that the *general scattering theorem* is in fact the simplest version of an *interaction theorem*, i.e., an optical theorem that relates the ISCS with the corresponding partial fields. On the other hand, we established physical bounds for the *ISCS ratios*, i.e., the ratios of the total ISCS over the overall scattering cross section, as well as for the determination of the number N of sources/dipoles and the number Q of excitation layers.

For the exact solution of the direct problem in spherical geometry, we devised an *overall superposition method* that combines elements from the T-Matrix approach, Sommerfeld's scattering superposition method and Green's Function methods. In particular, we formulated the superposition of the individual fields that coincides with the overall field, into a single field that is expanded as a series of spherical harmonics (in acoustic waves) or Spherical Vector Wave Functions (in electromagnetic waves). Taking into account the boundary conditions in each of the spherical scatterer's layers, we extracted analytical expressions for

- the coefficients of the overall field in the scatterer's exterior
- the relation between the coefficients of the overall fields in each layer and the coefficients of the overall field in the scatterer's exterior
- the overall far-field pattern, the overall scattering cross section and the total ISCS
- the coefficients for the corresponding individual fields and individual scattering cross sections

Implementing these expressions into a computer code, we were able to investigate numerically our findings and provide an extensive parametric analysis for the behaviour of the energy functionals, the ISCS ratios and the participating fields.

Finally, by employing techniques of asymptotic analysis, we were able to study closer the so-called *low frequency zone* for both types of waves. In particular, we formulated and solved analytically several inverse problems for the spherical geometry that concern the number of sources/dipoles, the physical parameters of the scatterer and/or its geometrical characteristics. We did so, by utilizing techniques that are based on far-field measurements and their analytical manipulation into non-linear systems which were solved analytically.

The current dissertation is part of an ongoing investigation that spans over diverse fields of scattering theory. In particular, future work directions include

- the expansion of the methods proposed here in ellipsoidal geometry, considering and exploiting also the results of previous works on this topic [105], [106]
- the investigation of the energy transfer process and the solution of the direct scattering problem in multiple scattering when the source of incidence is a spherical wave [107]
- the development of inverse numerical schemes, similar to the Discrete Dipole Approximation (DDA), [108], Method of Auxiliary Sources (MAS) [109] or Method of Moments (MoM) [110] for the identification of the sources of excitation.

Appendix

In the appendix we present the exact form of the various quantities (low-frequency coefficients, far-field measurements, etc) we used in the algorithmic procedures of the inverse problems for both acoustic and electromagnetic waves.

Low-frequency coefficients - Acoustics

The exact expressions of the individual coefficients $C_\ell^{q,j}$, for $\ell = 1, \ldots, 6$, used in Chapter 2.

External Excitation

Soft Core	**Hard Core**
$S_1^0 = -\frac{1}{\varrho_1(\xi-1)+1}$	$H_1^0 = 0$
$S_2^0 = \varrho_1\eta_1(S_1^0)^2$	$H_2^0 = 0$
$S_3^0 = \frac{\xi^3(1-\varrho_1)+2+\varrho_1}{\xi^3(1+2\varrho_1)+2-2\varrho_1}$	$H_3^0 = -\frac{2\xi^3(\varrho_1-1)+2+\varrho_1}{2\xi^3(1+2\varrho_1)+2\varrho_1-2}$
$S_4^0 = (2\xi\varrho_1 + \varrho_1 - 1)\frac{\varrho_1\eta_1^2(S_1^0)^3}{3\xi}$	$H_4^0 = \frac{\eta_1^2}{3\xi^3\varrho_1}$
$S_5^0 = -S_3^0$	$H_5^0 = -H_3^0$
$S_6^0 = -\frac{2\xi^5(1-\varrho_1)+3\varrho_1+2}{\xi^5(2+3\varrho_1)+3-3\varrho_1}$	$H_6^0 = \frac{2}{3}\frac{3\xi^5(\varrho_1-1)+2\varrho_1+3}{\xi^5(2+3\varrho_1)+2\varrho_1-2}$

Internal Excitation

Soft Core	**Hard Core**
$S_1^{1,j} = (d_{1,j} - 1)S_1^0$	$H_1^{1,j} = -\frac{d_{1,j}}{\varrho_1 \xi}$
$S_2^{1,j} = \frac{\eta_1}{\xi} S_1^0[-d_{1,j}^2 + d_{1,j} S_1^0(\varrho_1 - 1)] - S_2^0$	$H_2^{1,j} = \frac{d_{1,j}^2 \eta_1}{\varrho_1 \xi^2}$
$S_3^{1,j} = \frac{3(d_{1,j}^3 - 1)}{\xi^3(1+2\varrho_1)+2-2\varrho_1}$	$H_3^{1,j} = \frac{3}{2}\frac{2d_{1,j}^3+1}{-\xi^3(1+2\varrho_1)+1-\varrho_1}$
$S_4^{1,j} = \frac{\eta_1^2}{3\xi^2} S_1^0 \Big[d_j^2(2d_j - 3(\varrho_1 - 1)S_1^0) +$	$H_4^{1,j} = \eta_1^2 \frac{2\varrho_1 d_{1,j}^3 - d_{1,j}(\varrho_1 - 1) + \varrho_1}{3\xi^3 \varrho_1^2}$
$(d_j(\varrho_1 - 1) - \varrho_1 \xi)(S_1^0 + 3\varrho_1 \xi) \Big]$	
$S_5^{1,j} = -\eta_1 S_3^{1,j}$	$H_5^{1,j} = -\eta_1 H_3^{1,j}$
$S_6^{1,j} = -(5d_j^5 - 1)[\xi^5(2 + 3\varrho_1) + 3 - 3\varrho_1]^{-1}$	$H_6^{1,j} = -\frac{5}{3}\frac{3d_{1,j}^5+2}{\xi^5(2+3\varrho_1)+2\varrho_1-2}$

Penetrable Core

External Excitation	**Internal Excitation**
$P_1^0 = 0$	$P_1^{1,j} = \frac{d_{1,j}}{\varrho_1 \xi}$
$P_2^0 = 0$	$P_2^{1,j} = -\frac{d_{1,j}^2 \eta_1}{\varrho_1 \xi^2}$
$P_3^0 = \frac{\xi^3(1-\varrho_1)(\varrho_1+2\varrho_2)+(2+\varrho_1)(\varrho_1-\varrho_2)}{\xi^3(1+2\varrho_1)(\varrho_1+2\varrho_2)+2(\varrho_1-\varrho_2)(1-\varrho_1-\varrho_2)}$	$P_3^{1,j} = \frac{3[d_{1,j}^3(\varrho_1+2\varrho_2)+(\varrho_1-\varrho_2)]}{[\xi^3(1+2\varrho_1)(\varrho_1+2\varrho_2)-2(\varrho_1-1)(\varrho_1-\varrho_2)]}$
$P_4^0 = 0$	$P_4^{1,j} = \frac{2}{3}\frac{d_{1,j}^3 \eta_1^2}{\varrho_1 \xi^3}$
$P_5^0 = -P_3^0$	$P_5^{1,j} = -\eta_1 P_3^{1,j}$
$P_6^0 = \frac{\xi^3(1-\varrho_1)(2\varrho_1+3\varrho_2)+(3+2\varrho_1)(\varrho_1-\varrho_2)}{\xi^3(2+3\varrho_1)(2\varrho_1+3\varrho_2)+6(\varrho_1-\varrho_2)(1-\varrho_1-\varrho_2)}$	$P_6^{1,j} = \frac{5}{3}\frac{d_{1,j}^3(2\varrho_1+3\varrho_2)+2(\varrho_1-\varrho_2)}{\xi^5(2+3\varrho_1)(2\varrho_1+3\varrho_2)-6(\varrho_1-1)(\varrho_1-\varrho_2)}$

Low-frequency coefficients - Electromagnetics

The exact expressions for the coefficients $\mathcal{G}_i^j$ with $i = 1, 2$, $j \in \{1, ..., 7\}$ used in Chapter 5.

$$\mathcal{G}_1^1 = \mathcal{A}_x^1 - \mathcal{C}_z^1, \quad \mathcal{G}_1^2 = \mathcal{A}_y^1 - \mathcal{B}_z^1, \quad \mathcal{G}_1^3 = \mathcal{B}_y^1 - \mathcal{C}_x^1, \quad \mathcal{G}_1^4 = \mathcal{B}_x^1 + \mathcal{C}_y^1$$
$$\mathcal{G}_1^5 = \mathcal{C}_x^1 - \mathcal{A}_z^1, \quad \mathcal{G}_1^6 = \mathcal{B}_y^1 - \mathcal{A}_z^1, \quad \mathcal{G}_1^7 = \mathcal{B}_x^1 - \mathcal{C}_y^1$$
$$\mathcal{G}_2^1 = \mathcal{A}_x^2 - \mathcal{B}_x^2 + (\mathcal{BC})_y - (\mathcal{AC})_z, \quad \mathcal{G}_2^2 = \mathcal{A}_y^2 - \mathcal{C}_y^2 + (\mathcal{BC})_x - (\mathcal{AB})_z$$
$$\mathcal{G}_2^3 = \mathcal{B}_z^2 - \mathcal{C}_z^2 + (\mathcal{AC})_x - (\mathcal{AB})_y, \quad \mathcal{G}_2^4 = (\mathcal{AC})_y + (\mathcal{AB})_x - 2(\mathcal{BC})_z,$$
$$\mathcal{G}_2^5 = (\mathcal{AC})_y - (\mathcal{AB})_x$$

with A_u^ℓ and $\mathcal{P}_u$ for $u \in \{x, y, z\}$ and $\ell \in \{1, 2\}$ given by

$$\mathcal{P}_x = \sum_{j=1}^N p_x^j, \quad \mathcal{P}_y = \sum_{j=1}^N p_y^j, \quad \mathcal{P}_z = \sum_{j=1}^N p_z^j$$
$$\mathcal{A}_u^1 = \sum_{j=1}^N p_u^j \alpha_j, \quad \mathcal{B}_u^1 = \sum_{j=1}^N p_u^j \beta_j, \quad \mathcal{C}_u^1 = \sum_{j=1}^N p_u^j \gamma_j$$
$$\mathcal{A}_u^2 = \sum_{j=1}^N p_u^j \alpha_j^2, \quad \mathcal{B}_u^2 = \sum_{j=1}^N p_u^j \beta_j^2, \quad \mathcal{C}_u^2 = \sum_{j=1}^N p_u^j \gamma_j^2$$
$$(\mathcal{AB})_u = \sum_{j=1}^N p_u^j \alpha_j \beta_j, \quad (\mathcal{AC})_u = \sum_{j=1}^N p_u^j \alpha_j \beta_j, \quad (\mathcal{BC})_u = \sum_{j=1}^N p_u^j \beta_j \gamma_j$$

while coefficients $\mathcal{F}_1^j$ for $j = 1, \ldots, 6$ have the expressions

$$\mathcal{F}_1^1 = (\mathcal{BC})_x + \frac{2}{3}\mathcal{B}_y^2 + (\mathcal{AB})_z - \frac{1}{3}\mathcal{P}_y, \quad \mathcal{F}_1^2 = \mathcal{C}_x^2 + (\mathcal{BC})_y + (\mathcal{AC})_z - \frac{1}{3}\mathcal{P}_x$$
$$\mathcal{F}_1^3 = \mathcal{A}_z^2 + \frac{1}{3}\mathcal{P}_z, \quad \mathcal{F}_1^4 = (\mathcal{AC})_x + (\mathcal{AB})_y, \quad \mathcal{F}_1^5 = \mathcal{B}_z - \mathcal{A}_y$$
$$\mathcal{F}_1^6 = (\mathcal{BC})_x + \frac{1}{3}\mathcal{B}_y^2 + (\mathcal{AB})_z - \frac{1}{3}\mathcal{A}_y^2 - \frac{1}{3}(\mathcal{BC})_y$$

Far-field measurements used in subsection 6.2.3

Quantities N_j for $j = 1, \dots, 4$ are given by

$$N_1 = \frac{B_y A_z - B_z A_y}{M_y A_z - M_z A_y}, \quad N_2 = \frac{M_y B_z - M_z B_y}{M_y A_z - M_z A_y}$$
$$N_3 = \frac{C_y A_z - C_z A_y}{M_y A_z - M_z A_y}, \quad N_4 = \frac{M_y C_z - M_z C_y}{M_y A_z - M_z A_y}$$

Quantites K_j for $j = 1, \dots, 6$ are given by

$$K_1 = \frac{g_{\theta,2}(0,0)}{\rho_3} - (N_3 N_2 + N_1 N_4) A_y + \frac{N_3 A_z}{2} + \\ + N_1 (N_1 M_x + 2 N_2 A_x - N_3 M_y)$$
$$K_2 = (1 - N_2^2) A_x + N_2 N_4 A_y - \frac{N_4 A_z}{2}$$
$$K_3 = (1 - N_2^2) M_x + N_2 N_4 M_y - \frac{N_4 M_z}{2}$$
$$K_4 = \frac{g_{\phi,2}(0,0)}{\rho_3} - (N_3 N_2 + N_1 N_4) A_x + \frac{N_1 A_z}{2} + \\ + N_3 (N_3 M_y + 2 N_4 A_y - N_3 M_x)$$
$$K_5 = (1 - N_4^2) A_x + N_2 N_4 A_x - \frac{N_2 A_z}{2}$$
$$K_6 = (1 - N_4^2) M_x + N_2 N_4 M_x - \frac{N_2 M_z}{2}$$

Bibliography

[1] G. Mie, "Beiträge zur Optik trüber Medien, speziell kolloidaler Metallösungen", *Annalen der Physik* vol 330, pp. 377–445, 1908.

[2] N. A. Logan, "Survey of Some Early Studies of the Scattering of Plane Waves by a Sphere", *Proceeding of the IEEE*, vol. 53, no. 8, pp. 773–785, 1965.

[3] A. Clebsch, "Ueber die Reflexion an einer Kugelflache", *Journal für die reine und angewandte Mathematik*, vol. 61, pp.195–262, 1863.

[4] C. J. Maxwell, "A dynamical theory of the electromagnetic field", *Proceedings of the Royal Society (London)*, vol. 13, pp. 531–536, 1864.

[5] J. W. Nicholson, "Diffraction of short waves by a rigid sphere", *Philosophical Magazine*, vol. 11, pp. 193–205, 1906.

[6] J. W. Nicholson, "A general solution of the electromagnetic relations", *Philosophical Magazine*, vol. 13, pp. 259–265, 1907.

[7] J. W. Nicholson, "The pressure of radiation on a cylindrical obstacle", *Proceedings of the Mathematical Society (London)*, vol. 11, pp. 104–126, 1912.

[8] P. Debye, "Das elektromagnetische Feld um einen Zylinder und die Theorie des Regenbogens", *Physikalische Zeitschrift*, vol. 9, pp. 775–778, 1908.

[9] G. N. Watson, "Bessel functions of large order", *Proceedings of the Cambridge Philosophical Society*, vol. 19, pp. 96–110, 1918.

[10] G. N. Watson, "The diffraction of electric waves by the earth", *Proceedings of the Mathematical Society (London)*, vol. 95, pp. 83–99, 1918.

[11] G. W. Walker, "The shattering of light by small particles", *Quarterly Journal of Mathematics*, vol. 30, pp. 204–220, 1899.

[12] Lord Rayleigh, "On the acoustic shadow of a sphere", *Transactions of the Royal Society*, vol. 203, pp. 97–110, 1904.

[13] Lord Rayleigh, "The incidence of light upon a transparent sphere of dimensions comparable with the wave length", *Proceedings of the Royal Society*, vol. 25, pp. 25–46, 1910.

[14] Lord Rayleigh, "Investigation of the disturbance produced by a spherical obstacle on the waves of sound", *Proceedings of the Mathematical Society (London)*, vol. 4, 253–283, 1872.

[15] L. Lorenz, "Untersuchungen uber die Refractionsconstante", *Annalen der Physik und Chemie*, vol. 11, pp. 70–103, 1880.

[16] L. Lorenz, "Theorie de la dispersion", *Kongelige Danske Videnskabernes Selskabs Skrifter*, vol. 2, pp. 167–182, 1883.

[17] L. Lorenz, "Sur la lumiere reflechie et refractee par une sphere transparente", *Kongelige Danske Videnskabernes Selskabs Skrifter*, vol. 6, pp. 1–62, 1883.

[18] G. Green, "On the reflection and refraction of sound", *Transactions of the Cambridge Philosophical Society*, vol. 6, pp. 457–462, 1838.

[19] G. Green, "On the propagation of light in crystallized media", *Transactions of the Cambridge Philosophical Society*, vol. 7, pp. 121–140, 1839.

[20] N. M. Ferrers, "The Mathematical Papers of the late George Green", *Macmillan Publishers*, 1871.

[21] O. Heaviside, "On Operators in Physical Mathematics Part I", *Proceedings of the Royal Society*, vol. 52, pp. 504–529, 1892.

[22] O. Heaviside, "On Operators in Physical Mathematics Part II", *Proceedings of the Royal Society*, vol. 54, pp. 105–143, 1893.

[23] O. Heaviside, *Electromagnetic Theory, vols 1-3*, The Electrician Printing and Publishing Co, London, 1893-1894.

[24] V. Twersky, "Multiple Scattering by Arbitrary Configurations in Three Dimensions", *Journal of Mathematical Physics*, vol. 3, no. 1, pp. 83–91, 1962.

[25] P. C. Waterman and R. Truell, "Multiple Scattering of Waves", *Journal of Mathematical Physics*, vol. 2, pp. 512–537, 1961.

[26] J. J. Bowman, T. B. Senior, P. L. Uslenghi, *Electromagnetic and Acoustic Scattering by Simple Shapes*, North Holland Publishing Company, 1969.

[27] G. Dassios, "Electric and magnetic activity of the brain in spherical and ellipsoidal geometry", *Mathematical Modeling in Biomedical Imaging*, vol. 1983, pp. 133–202, Springer, 2009.

[28] G. Dassios and A. S. Fokas, "Electro-magneto-encephalography for a three-shell model: dipoles and beyond for the spherical geometry", *Inverse Problems*, vol. 25, no. 3, 035001, 2009.

[29] J. L. Hollmann and L. V. Wang, "Multiple-dipole optical diffusion approximation for a multilayer scattering medium", *Applied Optics*, vol. 46, pp. 6004–6009, 2007.

[30] K. L. Wong, *Design of nonplanar microstrip antennas and transmission lines*, Wiley, Reading, MA, 1999.

[31] C. A. Valagiannopoulos and N. L. Tsitsas, "On the Resonance and Radiation Characteristics of Multi-Layered Spherical Microstrip Antennas," *Electromagnetics*, vol. 28, pp. 243–264, 2008.

[32] B. Xu, M. Gustaffson, S. Shi, K. Zhao, Z. Ying and S. He, "Radio Frequency Exposure Compliance of Multiple Antennas for Cellular Equipment Based on Semidefinite Relaxation", *IEEE Transactions on Electromagnetic Compatibility*, vol. 61, pp. 327–336, 2019.

[33] P. Gas, "Optimization of multi-slot coaxial antennas for microwave thermotherapy based on the S11-parameter analysis", *Biocybernetics and Biomedical Engineering*, vol. 37, pp. 78–93, 2017.

[34] R. Potthast, *Point Sources and Multipoles in Inverse Scattering Theory*, Chapman and Hall/CRC, 2001.

[35] X. Liu, B. Zhang and J. Yang, "The inverse electromagnetic scattering problem in a piecewise homogeneous medium", *Inverse Problems*, vol. 26, no. 12, 125001, 2010.

[36] G. Ping, E. Fernandez-Grande, P. Gerstoft and Z. Chu, "Three-dimensional source localization using sparse Bayesian learning on a spherical microphone array," *Journal of the Acoustic Society of America* vol. 147, pp. 3895–3904, 2020.

[37] H. Ding, Y. Bao, Q. Huang, C. Li and G. Chai, "Three-dimensional localization of point acoustic sources using a planar microphone array combined with beamforming" *Royal Society open science*, vol. 5, 181407, 2018.

[38] L. Zhang, D. Ding, D. Yang, J. Wang and J. Shi, "Sound Source Localization Using Non-Conformal Surface Sound Field Transformation Based on Spherical Harmonic Wave Decomposition" *Sensors*, vol.17, 1087, 2017.

[39] E. Fernandez Grande, "Sound field reconstruction using a spherical microphone array," *Journal of the Acoustical Society of America* vol. 139 1168–78, 2016.

[40] G. Herold and E. Sarradj, "Detection of rotational speeds of sound sources based on array measurements," *Applied Acoustics* ,vol. 157, 107002, 2020.

[41] K. Yamatani, T. Ohe and K. Ohnaka, "An identification method of electric current dipoles in spherically symmetric conductor", *Journal of Computational and Applied Mathematics*, vol. 143, pp. 189–200, 2002.

[42] G. Dassios, A. S. Fokas and F. Kariotou, "On the non-uniqueness of the inverse magnetoencephalography problem," *Inverse Problems*, vol. 21, no. 2, pp. L1–L5, Apr. 2005.

[43] K. Wang, J. -J. Laurin, Q. Zhang, Q. Zhang and K. Wu, "Three-Dimensional Scattering from Uniaxial Objects with a Smooth Boundary Using a Multiple Infinitesimal Dipole Method," *IEEE Access*, vol. 8, pp. 80842-80854, Apr. 2020.

[44] A. E. Moskalensky and M. A. Yurkin, "Energy budget and optical theorem for scattering of source-induced fields," *Physical Review A*, vol. 99, 053824, May 2019.

[45] A. Baptiste, L. D. Brendan and E. C. Le Ru, "Electromagnetic Interactions of Dye Molecules Surrounding a Nanosphere" *Nanoscale*, vol. 11, no. 2, pp. 11, 2019.

[46] M. I. Mishchenko, "The electromagnetic optical theorem revisited," *Journal of Quantitative Spectroscopy and Radiative Transfer*, vol. 101, pp. 404–410, 2006.

[47] A. E. Krasnok, A. E. Miroshnichenko, P. A. Belov and Y. S. Kivshar, "All-dielectric optical nanoantennas," *Optics Express*, vol. 20, no. 18, pp. 20599-20604, 2012.

[48] C. Civelek, T. F. Bechteler, "Lagrangian formulation of electromagnetic fields in nondispersive medium by means of the extended Euler-Lagrange differential equation," *International Journal of Engineering Science*, vol. 46, no. 12, pp. 1218–1227, 2008.

[49] A. Kalogeropoulos and N. L. Tsitsas, "On Interactions Between Spherical Waves in Multiple Scattering by an All-Dielectric Cluster" *Radio Science Letters*, vol. 3, pp. 5, December 2021.

[50] J.D. Jackson, *Classical Electrodynamics*, Wiley, 1998.

[51] F. Jacobsen,"A note on instantaneous and time-averaged active and reactive sound intensity," *Journal of Sound and Vibration*, vol. 147, no. 3, pp. 489–496, 1991.

[52] D. Stanzial, N. Prodi and G. Schiffrer, "it Reactive acoustic intensity for general fields and energy polarization," *Journal of Acoustic Society of America*, vol. 99, no. 4, pp. 1868–1876, 1996.

[53] W. Duan, R. Kirby, J. Prisutova and K. V. Horoshenkov, "Measurement of complex acoustic intensity in an acoustic waveguide," *Journal of Acoustic Society of America*, vol. 134, no. 5, pp. 3674–3685, 2013.

[54] F. Jacobsen and A. R. Molares, "Ensemble statistics of active and reactive sound intensity in reverberation rooms," *Journal of Acoustic Society of America*, vol. 129, no. 1, pp. 211–218, 2011.

[55] D. Stanzial, G. Sacchi and G. Schiffrer, "On the physical meaning of the power factor in acoustics," *Journal of Acoustic Society of America*, vol. 131, no. 1, pp. 269–280, 2012.

[56] C. Athanasiadis, P. A. Martin, A. Spyropoulos and I. G. Stratis, "Scattering relations for point sources: Acoustic and electromagnetic waves," *Journal of Mathematical Physics*, vol. 43, no. 11, pp. 5683-5697, Nov. 2002.

[57] C. Athanasiadis, P. A. Martin, I. G. Stratis, "On the scattering of point-generated electromagnetic waves by a perfectly conducting sphere, and related near-field inverse problems," *Zeitschrift fur die Angewandte Mathematik und Mechanik (ZAMM)*, vol. 83, no. 2, pp. 129–136, 2003.

[58] C. Athanasiadis and N. L. Tsitsas, "Electromagnetic scattering theorems for interior dipole excitation of a layered obstacle," *Mathematical Methods in the Applied Sciences*, vol. 30, pp. 1467–1482, Apr. 2007.

[59] C. Athanasiadis and N. L. Tsitsas, "Scattering Theorems for Acoustic Excitation of a Layered Obstacle By an Interior Point Source," *Studies in Applied Mathematics*, vol. 118, pp. 397–418, 2007.

[60] M. A. Yurkin and M. I. Mishchenko, "Volume integral equation for electromagnetic scattering: Rigorous derivation and analysis for a set

of multilayered particles with piecewise-smooth boundaries in a passive host medium," *Physical Review A*, vol. 97, 043824, 2018.

[61] Y. A. Eremin and T. Wriedt, "Generalization of the Optical Theorem to an Arbitrary Multipole Excitation of a Particle near a Transparent Substrate," *Mathematics*, vol. 9, no. 24, 3244, 2021.

[62] I. Liberal, I. Ederra, R. Gonzalo and R. W. Ziolkowski, "Superbackscattering antenna arrays," *IEEE Transactions on Antennas and Propagation*, vol. 63, no. 5, pp. 2011-2021, Mar. 2015.

[63] A. Kalogeropoulos and N. L. Tsitsas, "Electromagnetic interactions of dipole distributions with a stratified medium: power fluxes and scattering cross sections," *Studies in the Applied Mathematics*, vol. 148, no. 3, pp. 1040–1068, 2021.

[64] A. Kalogeropoulos and N. L. Tsitsas, "Excitation of a Layered Medium by N sources: scattering relations, interaction scattering cross sections and physical bounds," *Quarterly of Applied Mathematics*, vol. 79, no. 2, pp. 335–356.

[65] G. Dassios and G. Kamvyssas, "Point Source Excitation in Direct and Inverse Scattering: The Soft and the Hard Small Sphere" *IMA Journal of Applied Mathematics*, vol. 55 67–84, 1995.

[66] G. Dassios, M. Hadjinicolaou and G. Kamvyssas, "Direct and Inverse Scattering for Point Source Fields. The Penetrable Small Sphere" *Zeitschrift fur Angewandte Mathematik und Mechanik (ZAMM)* vol. 79, 303–316, April 1999.

[67] P. Prokopiou and N. L. Tsitsas, "Direct and Inverse Low-frequency acoustic excitation of a layered sphere by an arbitrarily positioned point source," *Mathematical Methods in the Applied Sciences*, vol. 41, 1040–46, 2016.

[68] N. L. Tsitsas and P. A. Martin, "Finding a source inside a sphere", *Inverse Problems*, vol. 28, 015003, 2012.

[69] P. Prokopiou and N. L. Tsitsas, "Electromagnetic Excitation of a Spherical Medium by an Arbitrary Dipole and Related Inverse Problems," *Studies in Applied Mathematics*, vol. 140, pp. 438–464, 2018.

[70] N. L. Tsitsas, "Direct and inverse dipole electromagnetic scattering by a piecewise homogeneous sphere," *Zeitschrift fur die Angewandte Mathematik und Mechanik (ZAMM)*, vol. 89, pp. 833–849, 2009.

[71] , I. L. Rasskazov, A. Moroz and P. S. Carney, "Electromagnetic energy in multilayered spherical particles," *Journal of the Optical Society of America A*, vol. 36, no. 9, pp. 1591–1601, 2019.

[72] Y. Arnaoudov, G. Dassios and V. Kostopoulos, "The soft and the hard coated sphere within a point source wave field" *Journal of the Acoustical Society of America*, vol. 104, no. 4, pp. 1929–1942, 1998.

[73] G. Dassios, M. Hadjinicolaou and G. Kamvyssas, "The penetrable coated sphere embedded in a point source excitation field" *Wave Motion* vol. 32, 319–338, April 2000.

[74] A. M. Alkhoori and A. Lakhtakia, "Thermally controllable reduction of absorption and extinction of a dielectric sphere by an InSb coating," *Optik - International Journal for Light and Electron Optics*, vol. 260, 168992, 2022.

[75] M. J. Povey, "Ultrasound particle sizing: A review," *Particuology*, vol. 11, pp. 135–147, 2013

[76] V. Pinfield and D. M. Forrester, "Multiple scattering in random dispersions of spherical scatterers: Effects of shear-acoustic interactions," *Journal of the Acoustical Society of America*, vol. 141, pp. 649–660, 2017.

[77] N. S. Grigorieva and G. M. Fridman, "Scattering of Sound by an Elastic Spherical Shell Immersed in a Waveguide with a Fluid Bottom," *Acoustical Physics*, vol. 59, pp. 373–381, 2013.

[78] H. Ammari, J. Chen, Z. Chen, D. Volkov and H. Wang, "Detection and classification from electromagnetic induction data", *Journal of Computational Physics*, vol. 301, pp. 201–217, 2015.

[79] G. Dassios and R. Kleinmann, *Low Frequency Scattering*, Clarendon Press, Oxford, 2000.

[80] D. Colton and R. Kress, *Inverse Acoustic and Electromagnetic Scattering Theory*, 3rd Edition, Springer, New York, 2013.

[81] A. Sommerfeld, *Partial Differential Equations in Physics*, Academic Press, 1949.

[82] D. Colton and R. Kress, *Integral Equation Methods in Scattering Theory*, Society of Industrial and Applied Mathematics, Philadelphia, 2013.

[83] N. L. Tsitsas and C. Athanasiadis, "On the scattering of spherical electromagnetic waves by a layered sphere", *Quarterly Journal of Mechanics and Applied Mathematics*, vol. 59, no. 1, pp. 55–74, 2005.

[84] P. A. Martin, "Multiple Scattering and Scattering Cross Sections", *The Journal of the Acoustic Society of America*, vol. 143, pp. 995–1002, 2018.

[85] P. A. Martin, "Quadratic quantities in acoustics: scattering cross-section and radiation force," *Wave Motion*, vol. 86, pp. 63–78, 2019.

[86] A. D. Pierce, *Acoustics. An Introduction to Its Physical Principles and Applications*, 1st Edition, Mc-Graw Hill Book Company 1980.

[87] P. M. Morse and K. U. Ingard, *Theoretical Acoustics*, McGraw-Hill Book Company, 1968.

[88] R. Aramini, G. Caviglia and G. Giorgi, "The Role of Point Sources and Their Power Fluxes in the Linear Sampling Method," *SIAM Journal of Applied Mathematics*, vol. 71, no. 4, pp. 1044–1069, 2011.

[89] A. Kalogeropoulos and N. L. Tsitsas, "Multiple Scattering by an Impenetrable Cluster: Energy Transfer Process of the Scattered Sound",

Proceedings of the 26th Seminar/Workshop Direct and Inverse Problems in Electromagnetic and Acoustic Wave Theory - DIPED, pp. 7–11, 2021.

[90] C. Athanasiadis, "On the acoustic scattering amplitude for a multilayered scatterer," *Journal of Australian Mathematical Society Series B*, vol. 39, pp. 431–448, 1998.

[91] C. Athanasiadis, P. A. Martin and I. G. Stratis, "On spherical-wave scattering by a spherical scatterer and related near-field inverse problems," *IMA Journal of Applied Mathematics*, vol. 66, pp. 539–549, 2001.

[92] A. Charalambopoulos, "An analytic algorithm for shape reconstruction from low-frequency moments," *Journal of Mathematical Physics*, vol. 52, no. 9, 093795, 2011.

[93] A. Charalambopoulos, "On the reconstruction of low-frequency moments in acoustic scattering," *Quarterly of Applied Mathematics*, vol. 70, no. 2, pp. 311–343, 2012.

[94] M. Abramowitz and I. A. Stegun, *Handbook of Mathematical Functions*, New York: Dover, 1965.

[95] G. Arfken and H. Weber, *Mathematical Methods for Physicists, 7th Edition*, Elsevier/Academic Press, 2013.

[96] P. A. Martin, *Multiple Scattering*, Cambridge University Press, 2006.

[97] J. A. Stratton, *Electromagnetic Theory*, Mc-Graw Hill Book Company, 1941.

[98] C. T. Tai, *Dyadic Green Functions in Electromagnetic Theory*, 2nd Edition, IEEE Press, Piscataway, NJ, 1994.

[99] L. W. Li, P. S. Kooi, M. S. Leong, and T. S. Yeo, "Electromagnetic dyadic Green's function in spherically multilayered media," *IEEE Transactions on Microwave Theory and Technology*, vol. 42, pp. 2302–2310, 1994.

[100] M. I. Mishchenko and M. A. Yurkin, "Additivity of integral optical cross sections for a fixed tenuous multi-particle group," *Optics Letters*, vol. 44, no. 2, pp. 419-422, 2019.

[101] V. Twersky, "Multiple Scattering of Electromagnetic Waves by Arbitrary Configurations," *Journal of Mathematical Physics*, vol. 3, no. 8, pp. 589–610, 1967.

[102] A. I. Nosich, "Radiation conditions, limiting absorption principle, and general relations in open waveguide scattering," *Journal of Electromagnetic Waves and Applications*, vol. 8, no. 3, pp. 329–353, 1994.

[103] A. Kalogeropoulos and N. L. Tsitsas, "Analysis of Interaction Scattering Cross Sections and their Physical Bounds for Multiple-Dipole Stimulation of a Three-Dimensional Layered Medium," *IEEE Open Journal of Antennas and Propagation*, vol. 2, pp. 506–520, 2021.

[104] N. L. Tsitsas, "A Low-Frequency Electromagnetic Near-Field," *Journal of Computational Mathematics*, vol. 31, no. 5, pp. 439–448, 2013.

[105] A. Charalambopoulos and G. Dassios, "Scattering of a spherical wave by a small ellipsoid," *IMA Journal of Applied Mathematics*, vol. 62, no. 2, pp. 117–136, 1999.

[106] F. Kariotou, "Electroencephalogrphy in ellipsoidal geometry," *Journal of Mathematical Analysis and its Applications*, vol. 290, no. 1, pp. 324–342, 2004.

[107] J. H. Wu, A. Q. Liu, H. L. Chen and T. N. Chen, "Multiple scattering of a spherical acoustic wave from fluid spheres," *Journal of Sound and Vibration*, vol. 290, pp. 17–33, 2006.

[108] M. A. Yurkin and A. G. Hoekstra, "The discrete dipole approximation: An overview and recent developments," *Journal of Quantitative Spectroscopy and Radiative Transfer*, vol. 106, pp. 558–589, 2007.

[109] Y. Eremin, N. L. Tsitsas, G. Fikioris, T. Wriedt, "A new method of internal auxiliary source-sinks (MIASS) for two-dimensional interior

Dirichlet acoustic problems," *Journal of Computational and Applied Mathematics*, vol. 386, 113231, 2021.

[110] F. M. Kanhert, "Numerical methods in electromagnetic scattering theory", *Journal of Quantitative Spectroscopy and Radiative Transfer*, vol. 79-80, pp. 775–824, 2003.